Technische Universität Dortmund

Chemistry and Biology of Natural Product-derived Protease Inhibitors

zur Erlangung des akademischen Grades eines Doktors der Naturwissenschaften

(Dr. rer. nat.)

von der Fakultät für Chemie der Technischen Universität Dortmund

angenommene

Dissertation

von

Diplom-Chemikerin

Sara Christina Stolze

aus Dortmund

Dortmund 2012

Dekan: Prof. Dr. Heinz Rehage

1. Gutachter: Prof. Dr. Herbert Waldmann

2. Gutachter: Prof. Dr. Markus Kaiser

Datum der mündichen Prüfung: 09.07.2012

Zusammenfassung

Im Rahmen dieser Dissertation sollten Naturstoffe und davon abgeleitete Derivate synthetisiert und im Hinblick auf ihre biologische Aktivität als Protease-Inhibitoren untersucht werden.

Für die Naturstoffklasse der 3-Amino-6-Hydroxy-2-piperidon(Ahp)-Cyclodepsipeptide, die als nicht-kovalente Serin-Protease-Inhibitoren bekannt sind, konnte eine Festphasensynthese basierend auf einem allgemeinen Ahp-Vorläufermolekül entwickelt werden. Für den Ahp-Vorläufer wurde eine Lösungssynthese entwickelt. Die Festphasenstrategie ermöglicht die Synthese maßgeschneiderter Ahp-Cyclodepsipeptide; sie beinhaltet eine Veresterung an der festen Phase, sowie eine Festphasen-Macrolaktamisierung und etabliert ein neues Protokoll zur Generierung eines Aldehyds bei Abspaltung von der festen Phase. Zur Überprüfung der neu-entwickelten Strategie wurde der Chymotrypsin-Inhibitor Symplocamide A erfolgreich an der festen Phase synthetisiert und im Anschluss auf seine biologische Aktivität hin untersucht.

Mit Symplocamide A als der Leitstruktur wurden vereinfachte Analoga von Ahp-Cyclodepsipeptiden synthetisiert, um zu überprüfen ob diese Analoga, wie die Ahp-Cyclodepsipeptide auch, die sogenannte kanonische Konformation einnehmen. Die kanonische Konformation wurde zuerst in proteinogenen Serinprotease-Inhibitoren beobachtet und studiert. Kürzlich wurden auch peptidische Analoga dieser Inhibitoren untersucht und ein Zusammenhang mit den Ahp-Cyclodepsipeptiden erkannt, welche ebenfalls durch die Einnahme der kanonischen Konformation inhibieren.

Im Rahmen dieser Dissertation war es möglich zu zeigen, dass die Ahp-Einheit unter Retention der biologischen Aktivität durch kommerziell erhältliche Aminosäuren ersetzt werden kann. Mittels Struktur-Wirkungsuntersuchungen konnten zudem die kritischen Determinanten zur Einnahme der kanonischen Konformation bestimmt, sowie ein Einblick in die molekulare Grundlage einer effizienten Inhibition gewonnen werden.

Für den Naturstoff Symplostatin 4 wurde eine konvergente Lösungssynthese entwickelt, die einen flexiblen Zugang zu modifizierten Derivaten ermöglichte. Speziell die Synthese von Sonden für die Untersuchung von Symplostatin 4 mittels aktivitätsbasiertem Proteinprofiling war durch eine 1,3-dipolare Huisgen-Cycloaddition von propargyl-modifizierten Spezies mit Azid-modifizierten Reportermolekülen vereinfacht möglich.

Durch aktivitätsbasiertes Profiling konnten mit den Cystein-Proteasen RD21A und RD21B die Zielenzyme von Symplostatin 4 in der Modellpflanze *Arabidopsis thaliana* identifiziert werden.

Desweiteren wurde die anti-Malaria-Aktivität, die für das chemisch identische Gallinamide A publiziert worden war, für Symplostatin 4 und seine Derivate studiert. Im Rahmen von Untersuchungen mit dem Malariaerreger *Plasmodium falciparum* konnte festgestellt werden, dass Symplostatin 4 ein nanomolarer Inhibitor der Cystein-Proteasen Falcipain 2 und 3 ist, die für den Hemoglobinverdau zuständig sind und als wichtige Zielenzyme einer alternativen Malaria-Chemotherapie betrachtet werden.

Diese Arbeit wurde in der Zeit von Oktober 2007 bis Juni 2011 am Chemical Genomics Centre der Max-Planck-Gesellschaft und in der Zeit von Juni 2011 bis März 2012 am Zentrum für Medizinische Biotechnologie der Universität Duisburg-Essen angefertigt.

Teile dieser Dissertation sind in folgenden Publikationen enthalten:

Solid-Phase Total Synthesis of the 3-Amino-6-Hydroxy-2-Piperidone (Ahp) Cyclodepsipeptide and Protease Inhibitor Symplocamide A, Stolze, S.C.; Meltzer, M.; Ehrmann, M.; Kaiser, M. *Chem. Commun.* **2010**, *46*, 8857-8859.

Development of a Solid-Phase Approach to the Natural Product Class of Ahp-Containing Cyclodepsipeptides, Stolze, S. C.; Meltzer, M.; Ehrmann, M.; Kaiser, M. *Eur. J. Org. Chem.* **2012**, 1616-1625.

Antimalarial activity of Symplostatin 4 is based on nanomolar inhibition of Falcipain 2/3, Stolze, S. C.; Deu, E.; Kaschani, F.; Richau, K. H.; Colby, T.; van der Hoorn, R. A. L.; Bogyo, M.;Kaiser, M., *in preparation.*

Canonical-conformation mimics of Ahp cyclodepsipeptides, Stolze, S. C.; Meltzer, M.; Ehrmann, M.; Kaiser, M., *in preparation*

Wer wagt, selbst zu denken, der wird auch selbst handeln.

Bettina von Arnim

Meiner Familie

1 INTRODUCTION 1

1.1 PROTEASES AND PROTEASE INHIBITORS 1
1.2 SERINE PROTEASES AND THE S1 FAMILY 5
1.3 PROTEINACEOUS SERINE PROTEASE INHIBITORS AND THE CANONICAL CONFORMATION 11
1.3.1 SMALL-MOLECULE ANALOGS OF CANONICAL INHIBITORS 12
1.3.2 THE NATURAL PRODUCT CLASS OF 3-AMINO-6-HYDROXY-2-PIPERIDONE (AHP) CYCLODEPSIPEPTIDES AS PROTEASE INHIBITORS 15
1.4 MALARIA - A PERSISTING GLOBAL BURDEN 22
1.4.1 *PLASMODIUM* SPECIES AS THE CAUSING AGENTS OF MALARIA IN HUMANS 23
1.4.2 ANTIMALARIAL DRUGS AND THEIR MODE OF ACTION 26
1.5 CYSTEINE PROTEASES AND THEIR INHIBITORS 31
1.5.1 FALCIPAINS - POSSIBLE NEW TARGETS FOR MALARIA CHEMOTHERAPY 34
1.6 PROTEOMICS AS A TECHNIQUE FOR ANALYZING THE MODE-OF-ACTION OF SMALL MOLECULES 47
1.6.1 ACTIVITY-BASED PROTEIN PROFILING - ABPP 52
1.7 SYNTHESIS OF PEPTIDIC NATURAL PRODUCTS 58
1.7.1 A TOTAL SYNTHESIS “CLASSIC”: VANCOMYCIN 62

2 AIMS OF THE PHD PROJECT 77

3 RESULTS AND DISCUSSION 82

3.1 CHEMISTRY AND BIOLOGY OF AHP CYCLODEPSIPEPTIDES 82
3.1.1 RETROSYNTHETIC ANALYSIS OF AHP CYCLODEPSIPEPTIDES: DEVELOPMENT OF A SYNTHETIC STRATEGY FOR A GENERAL SOLID-PHASE APPROACH TO THIS NATURAL PRODUCT CLASS 82
3.1.2 SOLID-PHASE TOTAL SYNTHESIS OF SYMPLOCAMIDE A 98
3.1.3 BIOLOGICAL EVALUATION OF SYMPLOCAMIDE A 101
3.2 DEVELOPMENT AND BIOLOGICAL INVESTIGATION OF NATURAL PRODUCT-DERIVED CANONICAL-CONFORMATION PROTEASE INHIBITORS 102
3.2.1 DEVELOPMENT OF A SOLID-PHASE STRATEGY TOWARDS SIMPLIFIED ANALOGS OF AHP CYCLODEPSIPEPTIDES 103
3.2.2 SYNTHESIS OF SAR ANALOGS OF AHP-MIMICKED CYCLODEPSIPEPTIDES 105
3.2.3 BIOLOGICAL EVALUATION OF THE SAR ANALOGS AND ELUCIDATION OF CRITICAL PARAMETERS FOR THE CANONICAL CONFORMATION 107
3.3 SYNTHESIS AND BIOLOGICAL INVESTIGATION OF SYMPLOSTATIN 4 116
3.3.1 DEVELOPMENT OF A SYNTHETIC STRATEGY FOR A CONVERGENT SYNTHESIS OF SYMPLOSTATIN 4 AND DERIVATIVES 116
3.3.2 SYNTHESIS OF SYMPLOSTATIN 4 AND DERIVATIVES FOR THE BIOLOGICAL EVALUATION AND TARGET IDENTIFICATION 121
3.3.3 BIOLOGICAL INVESTIGATION OF SYMPLOSTATIN 4 IN THE MODEL PLANT *ARABIDOPSIS THALIANA* 125
3.3.4 INVESTIGATING THE ANTIMALARIAL ACTIVITY OF SYMPLOSTATIN 4 AND TARGET IDENTIFICATION IN *PLASMODIUM FALCIPARUM* 128

4 SUMMARY AND CONCLUSIONS 135

4.1 DEVELOPMENT OF A GENERAL SOLID-PHASE SYNTHESIS FOR AHP CYCLODEPSIPEPTIDES AND SYNTHESIS OF SYMPLOCAMIDE A 135
4.2 SYNTHESIS AND BIOLOGICAL EVALUATION OF SMALL MOLECULE ANALOGS OF PROTEINACEOUS SERINE PROTEASE INHIBITORS ADOPTING THE CANONICAL CONFORMATION 139
4.3 DEVELOPMENT OF A CONVERGENT SYNTHESIS OF SYMPLOSTATIN 4 AND DERIVATIVES FOR THE TARGET IDENTIFICATION AND BIOLOGICAL EVALUATION 144

5 ZUSAMMENFASSUNG UND AUSBLICK 151

5.1 ENTWICKLUNG EINER ALLGEMEINEN FESTPHASEN-SYNTHESE VON AHP-CYCLODEPSIPEPTIDEN UND SYNTHESE VON SYMPLOCAMIDE A 151
5.2 SYNTHESE UND BIOLOGISCHE EVALUIERUNG VON „SMALL-MOLECULE”-ANALOGA PROTEINOGENER SERINPROTEASEINHIBITOREN MIT KANONISCHER KONFORMATION 155
5.3 ENTWICKLUNG EINER KONVERGENTEN SYNTHESE FÜR SYMPLOSTATIN 4 UND DERIVATEN FÜR DIE TARGET-IDENTIFIZIERUNG UND BIOLOGISCHE EVALUIERUNG 161

6 EXPERIMENTAL 169

6.1 GENERAL METHODS AND INSTRUMENTS 169
6.2 SOLUTION SYNTHESIS OF THE AHP PRECURSORS I AND II 171
6.3 SYNTHESIS OF THE *N,O*-DIMETHYL-3-BROMOTYROSINE BUILDING BLOCK 29 184
6.4 SOLID-PHASE SYNTHESES 186
6.4.1 GENERAL METHODS OF THE SOLID-PHASE SYNTHESES 186
6.4.2 SOLID-PHASE SYNTHESIS OF THE SYMPLOCAMIDE A MODEL AHP CYCLODEPSIPEPTIDE 19 190
6.4.3 SOLID-PHASE SYNTHESIS OF SYMPLOCAMIDE A 195
6.4.4 SYNTHESIS OF STRUCTURE-ACTIVITY ANALOGS OF AHP CYCLODEPSIPEPTIDES 201
6.5 SYNTHESIS OF SYMPLOSTATIN 4 AND ANALOGS 229
6.5.1 SYNTHESIS OF THE BUILDING BLOCKS FOR SYMPLOSTATIN 4 AND ITS DERIVATIVES 229
6.5.2 SYNTHESIS OF SYMPLOSTATIN 4 AND DERIVATIVES FROM THE *C*-TERMINAL AND *N*-TERMINAL PEPTIDES 236
6.5.3 SYNTHESIS OF TAGGED SYMPLOSTATIN 4 DERIVATIVES 239
6.6 ACTIVITY-BASED PROTEIN PROFILING EXPERIMENTS 246
6.6.1 GENERAL METHODS 246
6.6.2 INFILTRATION EXPERIMENTS 247

7 REFERENCES 249

8 APPENDIX 256

1 Introduction

Bioactive substances isolated from natural sources have a long history as therapeutic agents[1] In the search for new pharmacophores, natural products have been and still are a rich inspirational source, contributing to the development of new drugs.[2] Their significance stems from their biologically pre-validated structures owing to their natural origin: during their biosynthesis, natural products are required to interact with different enzymes along an assembly line; the functionalities or molecular structures used for these interactions potentially also address other protein domains regarding the limited number of protein folds. Furthermore, the structures of natural products have evolved to display potent bioactivities either within their originating species or across species.[3,4] Consequently, these properties turn natural products into ideal lead structures for medicinal chemistry research.

In chemical biology, natural products and natural product-derived compounds are valuable tools for the investigation of biomolecules and their biological function. Alternatively, the identification of the molecular basis (*i. e.* elucidation of the direct binding target of a small molecule) for a bioactivity is a challenging question. Both aspects have been addressed in the present dissertation.

1.1 Proteases and protease inhibitors

Proteolytic enzymes, also referred to as peptidases, proteases or proteinases, are important enzymes that are involved in innumerable vital processes. They belong to the superfamily of hydrolases and their biological function is to catalyze the hydrolysis or the formation of peptide bonds. The breakdown of a peptide bond is the major function of proteases, although the reverse reaction, *i. e.* the formation of a peptide bond, is catalyzed as well. The cleavage of a peptide bond is effected by the addition of water to the peptide bond, resulting in the hydrolysis of the peptide or protein into an acid and an amine part.

Although the hydrolysis of a peptide bond is favored thermodynamically, the partial double bond character of a peptide bond lowers the electrophilic character of the carbonyl group and thereby prevents hydrolysis under physiological conditions. Instead, enzyme catalysis is required to achieve peptide bond hydrolysis.[5] The enzyme-mediated cleavage is achieved by a nucleophilic attack on the carbonyl carbon of the scissile bond, either from the active site residue of the protease or from an enzymatically-activated water molecule.[6,7]

The molecular interaction of a protease with a substrate or inhibitor is described by the Schechter-Berger nomenclature[8]. The subsites of the protease *N*-terminal to the scissile bond (non-primed side) are numbered S_1 to S_n; on the *C*-terminal side (primed side) they are numbered S_1' to S_n'. The corresponding amino acid residues of the substrate are numbered P_1 to P_n and P_1' to P_n' respectively (Fig. 1). The specificity as well as the strength of the interaction are different for every protease; they are determined by the interaction of the subsites with the substrate.[9]

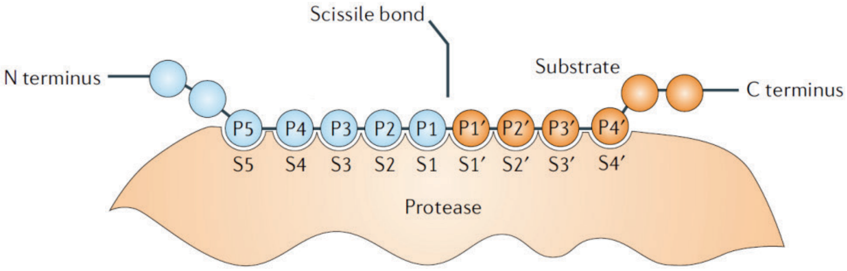

Figure 1 (adapted from [9]): Schematic representation of the interaction of a protease with a peptidic substrate or an inhibitor.

Proteases were initially classified into endopeptidases, targeting internal peptide bonds, and exopeptidases with either carboxypeptidase (*i. e.* cleavage from the *C*-terminus of their substrate) or aminopeptidase (*i. e*. cleavage from the *N*-terminus of their substrate) activity. This classification is complemented by an alternative classification based on structural and mechanistic considerations. As a result, proteases are subdivided by their catalytically active amino acids and nowadays six classes of proteases are known: aspartic, glutamic and metalloproteases as well as cysteine, threonine and serine proteases; glutamic proteases have so far not been found in mammals. In cysteine, threonine and serine proteases, the eponymous active site amino acid is directly involved in the nucleophilic attack on the carbonyl group. Consequently, these proteases act *via* a *covalent catalysis* mechanism. Aspartic, glutamic and metalloproteases on the other hand mediate hydrolysis by a *general acid-base catalysis* mechanism, causing the nucleophilic attack by an activated water molecule (Fig. 2).[7,10]

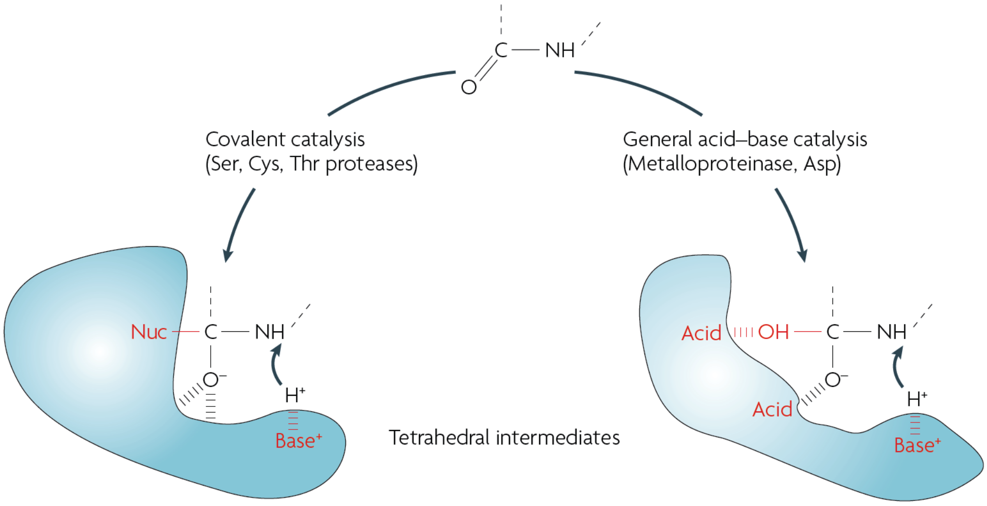

Figure 2[10]: Different tetrahedral intermediates formed during the cleavage of a peptide bond *via* covalent catalysis or general acid-base catalysis.

In the MEROPS classification of proteases, protease classes are further divided into different families on the basis of bioinformatic comparison of their amino acid sequences; this alignment results in a categorization of proteases into clans and families based on similarities in their three-dimensional structure and the order of the catalytic residues as well as phylogenetic similarities.[11]

Originally, research on proteases focused mainly on their digestive function where they act as non-specific protein-degrading enzymes to supply an organism with amino acids.[7] This restricted view has however changed dramatically in the last decades when proteases were recognized as key players in numerous vital processes. For example, protease signaling pathways are crucial elements in various physiological processes and are therefore strictly regulated. Moreover, many pathogenic states have been traced back to the dysfunction or misregulation of proteases, leading to a wide range of diseases such as cardiovascular or inflammatory disorders, osteoporosis, metastasis formation in cancer and even neurological pathologies such as Alzheimer´s disease. Due to the critical role of proteases in these vital processes, proteases have consequently been recognized as important drug targets.[7,9]

The important role of proteases in biology is further emphasized by genomic analyses of various organisms. These studies have revealed that 2-4% of a genome generally encodes proteolytic enzymes. In humans, around 2% of the genome encodes for proteases, corresponding to a total number of 500 to 600 proteases.[9,12] To date, the MEROPS database as the central inventory of known proteases lists 686 different proteases for *Homo sapiens* and 423 homologs that have been characterized biochemically (December 2011).[11] Of note, approximately 14% of the known human proteases were under investigation as drug targets in 2001 and recent estimations testify that 5 to 10% of all pharmaceutical targets pursued for drug discovery are indeed proteases.[10,13]

1.2 Serine proteases and the S1 family

Among the different classes of proteolytic enzymes, the serine proteases play the most prominent role as over one third of all known proteases are serine proteases. To date, over 26000 serine proteases grouped into 13 different clans and 40 families are represented in the MEROPS database (for an overview, see Table 1).

Table 1: general properties of serine proteases (adapted from [12,14])

Clan	Number of families	Representative member	Fold	Catalytic residues
PA(S)	12*	trypsin	Greek-key β-barrels	His, Asp, Ser
SB	2	subtilisin	3-layer sandwich	Asp, His, Ser
SC	2	prolyl oligopeptidase	α/β hydrolase	Ser, Asp, His
SE	6	*D*-Ala-*D*-Ala carboxypeptidase	α-helical bundle	Ser, Lys
SF	3	LexA peptidase	all β	Ser, Lys/His
SH	2	cytomegalovirus assemblin	α/β barrel	His, Ser, His
SJ	1	Lon peptidase	α + β	Ser, Lys
SK	2	Clp peptidase	αβ	Ser, His, Asp
SP	3	nucleoporin	all β	His, Ser
SQ	1	aminopeptidase DmpA	4-layer sandwich	Ser
SR	1	lactoferrin	3-layer sandwich	Lys, Ser
SS	14	*L*,*D*-carboxypeptidase	β-sheet + β-barrel	Ser, Glu, His
ST	5	rhomboid	α-barrel	His, Ser

* 7 additional families of viral origin in clan PA use a catalytic Cys

In serine proteases, the eponymous serine residue acts as nucleophile during the hydrolysis reaction. The nucleophilicity of the catalytically active serine is enhanced by an interaction with one or two additional amino acids. These specific arrangements are known as catalytic triads (in case of two other amino acids) or dyads (if only one other amino acid is directly involved). The most prominent catalytic triad is the Asp, His, Ser combination, which is also referred to as the charge relay system. Four different three-dimensional folds have been found to exhibit this identical arrangement of catalytic residues. Remarkably, these folds have originated from four different evolutionary pathways yielding exactly the same mechanism of catalysis which is an astonishing example for a convergent evolution. The prominent examples for the four different folds are: trypsin, subtilisin, prolyl oligopeptidase and Clp peptidase.[12,14]

The underlying catalysis mechanism of the catalytic triad was first elucidated for chymotrypsin (clan PA, Fig. 3), but could later also be confirmed in other proteases by crystallographic analyses. In the first step of the cleavage reaction the carbonyl carbon of the cleavable peptide bond is attacked by the activated Ser-195 residue, resulting in the formation of a covalent tetrahedral intermediate (1). This instable intermediate then forms an acyl-enzyme intermediate under cleavage of the peptide bond. This reaction is mediated by the Asp-102-polarized His-57, which acts as an acid in this step (2). Subsequently, the amine cleavage product associated with His-57 is exchanged for a water molecule. His-57 now acts as a base and activates the water molecule for the nucleophilic attack of the acyl-Ser-195 intermediate, which results in the formation of a second tetrahedral intermediate (3). The final step of the catalysis cycle is the liberation of the *C*-terminal cleavage product along with the recovery of the active enzyme (4) (Fig. 3). It should be noted that serine proteases not only mediate catalysis *via* the described covalent catalysis mechanism. Moreover, also transition state catalysis plays a major role. To this end, the backbone hydrogens of Ser-195 and the adjacent Gly-193 form an oxyanion hole which stabilizes the tetrahedral intermediate (and thus lowers the corresponding transition state energetically).[15]

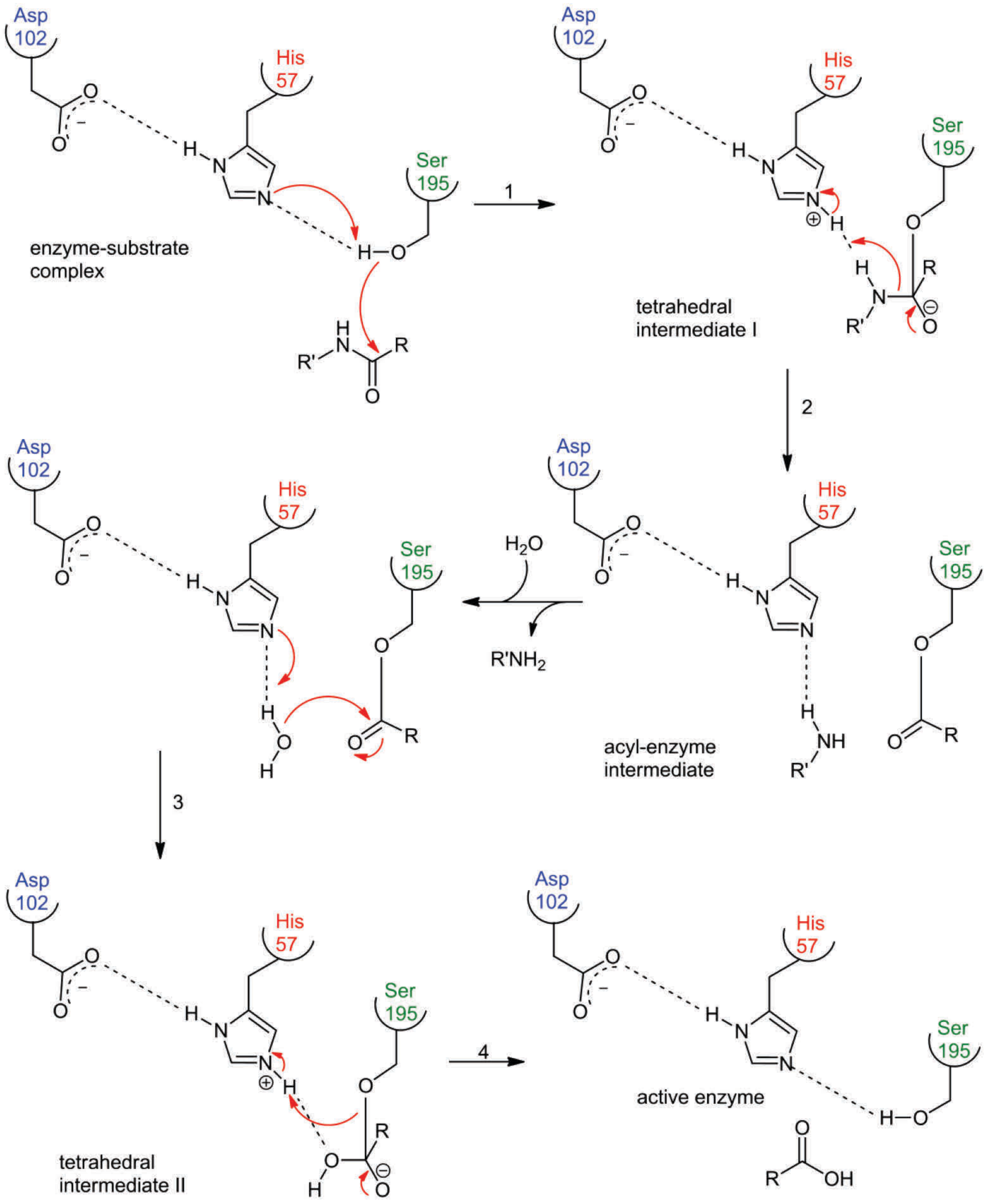
Asp
102
His
57
Ser
195
enzyme-substrate
complex
1
tetrahedral
intermediate I
2
acyl-enzyme
intermediate
H2O
R'NH2
3
tetrahedral
intermediate II
4
active enzyme

Figure 3 (adapted from[15]): Schematic representation of the peptide cleavage mediated by the Asp-His-Ser catalytic triad.

Besides the described catalytic triad, other serine proteases achieve hydrolysis by using simpler catalytic dyad system, in which the active site serine is accompanied by a lysine or a histidine residue. Additionally, recent investigations have identified catalytic triads that feature unconventional arrangements of active site residues. For example, a pair of histidines along with the active site serine has been found as a catalytic triad system in some proteases (Table 1).

Among the serine proteases, the S1 family (serine proteases with the "classical" chymotrypsin fold) of clan PA (MEROPS classification, also sometimes referred to as "S"), plays by far the most prominent role in eukaryotic organisms. In fact, of the 699 known human proteases, 178 are serine proteases and 138 of those are S1 proteases (Fig. 4).[12,14]

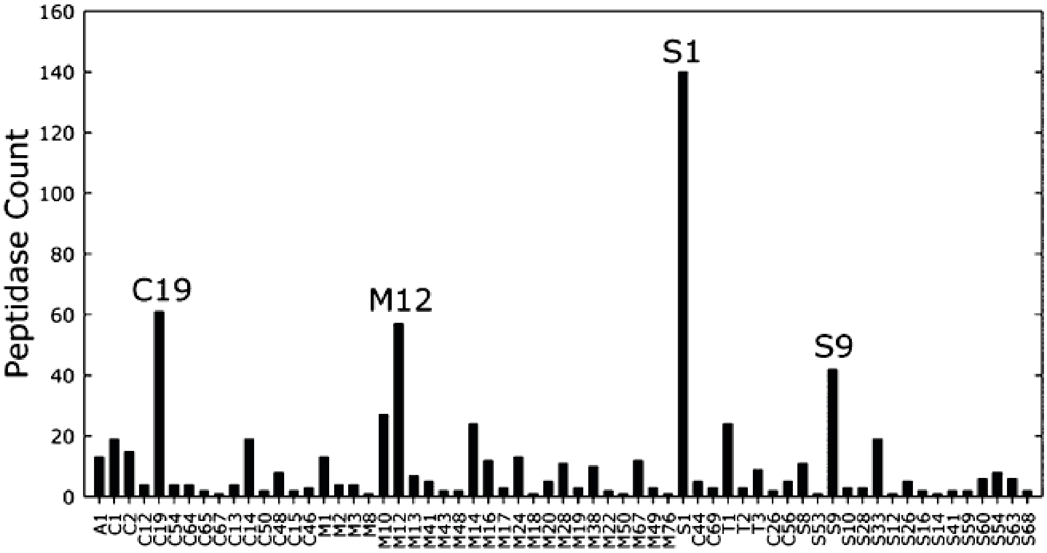

Figure 4[14]: Overview on the diversity of proteases in the human degradome. Only 4 families of proteases underwent a significant gene duplication and diversification. The S1 family represents the largest homologous group.

A comparison of the diversity of proteases from different organisms reveals that the S1 proteases have obviously emerged from the evolutionary selection process to become key players in intra- and extracellular processes as their diversity strongly increases with evolutionary development. While lower organisms seem to have reacted to natural selection by developing novel mechanisms of proteolysis resulting in a wide variety of protease families and novel catalytic mechanisms, this variation is much lower in higher metazoa. Instead, the diversity of proteases increased, in particular for S1 serine proteases. (Fig. 5) This pinpoints that S1 serine proteases are evolutionary validated to overtake a wide range of biological functions. As a consequence, S1 serine proteases display an unusually high proteolytic diversity.[16]

In fact, the high abundance of S1 proteases, alongside with the key roles they have taken in eukaryotic organisms, implies a selective advantage of the chymotrypsin-fold compared to other protease folds. The trypsin-like proteases have emerged from the evolutionary process as chief proteases, most probably due to their efficient catalytic activity, substrate selectivity and the efficient interaction with auxiliary protein modules to achieve a regulation of the proteolytic activity.[12]

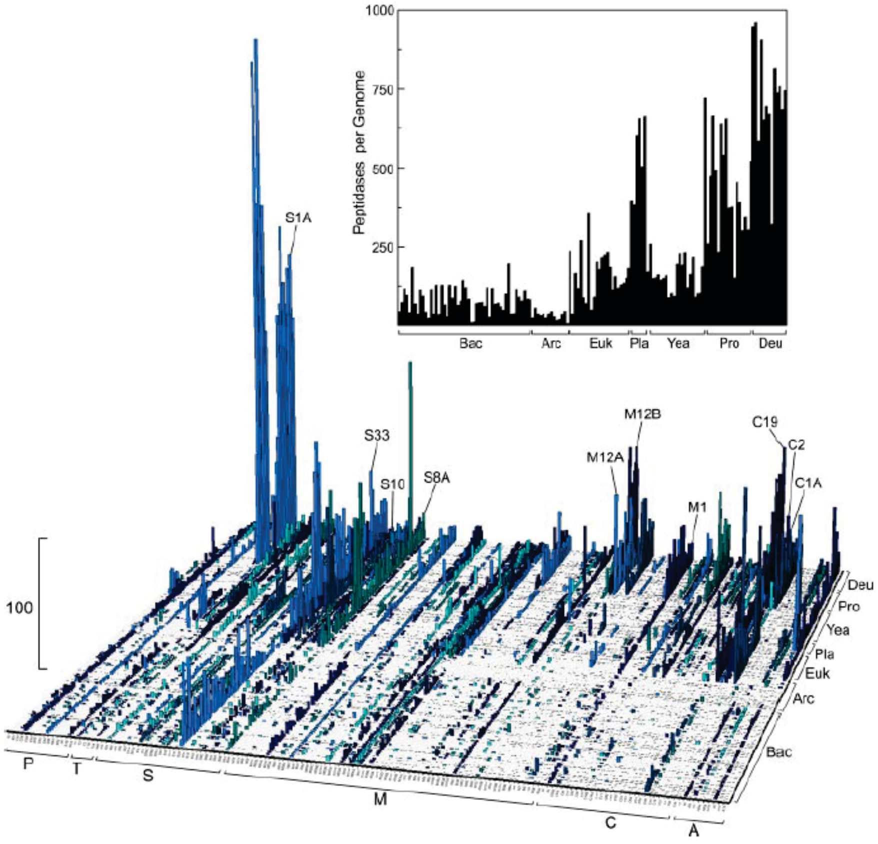

Figure 5[16]: Landscape representation of protease diversity in eukaryotic, eubacterial and archeal genomes. The distribution of 154 peptidase families from the different catalytic classes (aspartic (*A*), cysteine (*C*), metallo (*M*), threonine (*T*), serine (*S*) and mixed (*P*); x-axis)) was quantified for 128 complete genomes. Over 2 million protein sequences from eubacteria (*Bac*), archaea (*Arc*), plants (*Pla*), lower eukarya (*Euk*), yeasts (*Yea*), protostomes (*Pro*) and deuterostomes (*Deu*) (ordered along the z-axis) contained more than 38000 proteases.

On a structural level, all S1 serine proteases adopt the so-called chymotrypsin fold. A remarkable feature of this fold is the even distribution of the catalytically active amino acids over the peptide sequence. The two β-barrels constituting the fold host the active pocket at their interface. Asp-102 and His-57 are located within the *N*-terminal β-barrel, Ser-195 and the oxyanion hole (Ser-195, Gly-193) are found within the *C*-terminal β-barrel.

The substrate specificity of the S1 proteases is determined mainly by the S_1 subsite, other sites do not enhance selectivity in a significant manner. The trypsin-like proteases have a preference for the basic amino acids Lys and Arg in the P_1 position, whereas chymotrypsin preferentially digest substrates with larger hydrophobic residues such as Phe, Trp or Tyr. Although the molecular origin of these different preferences was determined to be a single exchange of amino acids within the primary specificity pocket (Asp-189 in trypsins, Ser-189 in chymotrypsins), attempts to engineer a trypsin into a chymotrypsin protease by carrying out this single exchange did not suffice. To obtain at least the desired selectivity, further alterations in loop regions that are not in contact with the substrate are necessary. However, despite these additional replacements, a full conversion and comparable enzyme efficiency has not been achieved. For the conversions of chymotrypsin to trypsin or of trypsin to elastase this strategy to date even failed completely. Consequently, these results indicate that the structure-function relation of the trypsin selectivity is not as straightforward as often perceived and still requires further investigation.[12]

The proteases of the chymotrypsin fold (S1) are further classified into two subfamilies: S1A (trypsin-like) and S1B: Despite representing two phylogenetically distinct families, both subfamilies nevertheless share the common two β-barrel structure. The S1B proteases are found ubiquitously and their function usually lies in the intracellular protein turnover. In contrast, the S1A proteases often act in the extracellular space, mediating many processes crucial to the persistence of an organism. The genomic distribution of the S1A proteases is uneven as they are underrepresented in plants, prokarya and archaea; in higher eukarya, however, they underwent a significant expansion and overtake innumerous functions. For example, the S1A proteases trypsin, chymotrypsin and elastase are endopeptidases heavily involved in food digestion. In contrast, the tryptases are the main components in the secretory granules of mast cells, being important components of the immune system. The matriptases are a family of membrane-bound enzymes with a substrate specificity similar to that of trypsin. High expression levels of these enzymes are a hallmark in some cancer types, although the biological function of matriptases is still largely unknown. The kallikrein family has attracted interest also due to its overexpression in various cancer types; kallikreins are involved in the blood coagulation, representing essential elements of the kinin system. Finally, granzymes play a role in the defense against viral infection by mediating directed apoptosis through natural killer cells and cytotoxic T cells. As a unique feature, granzymes have a preference for acidic amino acids in the P_1 position.[14]

A unique trait of trypsin-like proteases is that they are biosynthesized as inactive zymogens and are activated by cleavage of a proprotein precursor. Upon cleavage of the propeptide, the active conformation is adopted, thereby resulting in an active protease.[9,12]

1.3 Proteinaceous serine protease inhibitors and the canonical conformation

Serine proteases represent crucial factors in the maintenance and vitality of eukaryotic organisms. Consequently, their enzymatic activity in living organisms is strictly regulated *via* several different control mechanisms. Among them, the secretion of proteinaceous serine protease inhibitors plays an important role and several classes of these factors have been identified so far.

The so-called canonical inhibitors are a subclass of these proteinaceous serine protease inhibitors. They are usually relatively small proteins ranging from 29 to about 180 amino acids in size and their mode of action has been extensively studied in the last decades. Their primary feature is an exposed binding loop that binds to the target protease in a substrate-like manner. The resulting backbone conformation of the binding loop is the eponymous canonical conformation and represents the structural basis for protease inhibition. At least 18 non-homologous families of serine protease inhibitors adopting this conformation have been identified so far, thereby representing an outstanding example of convergent evolution.[17,18]

Besides this common feature, the canonical inhibitors are quite diverse in their structure as they do not rely on a common folding motif. In fact, extensive studies of different canonical-conformation inhibitors have revealed that except for the common conformation of the binding loop, the inhibitors display quite different folding motifs. Additional, distinct structural elements in the vicinity of the binding loops are not required for the interaction with the protease.

On a molecular level, the association of the inhibitor with the protease is effected by binding of the reactive-site loops to the enzyme’s catalytic residues in an analogous manner to the productive binding of a substrate. To this end, the protein portion on the *N*-terminal part of the protein (in relation to the scissile bond) binds to the enzyme in the form of an antiparallel β-strand with main-chain interaction hydrogen bonds forming between the two different proteins. On the *C*-terminal side, other hydrogen bond can be formed (for example on position P_2'). The reactive site of the inhibitor is positioned closely to the catalytically active residues of the protease so that the P_1 carbonyl carbon is fixed to the Ser-195-γ-O and projects into the oxyanion hole formed by Ser-195 and Gly-193. Interestingly, the scissile bond is not cleaved, although for some inhibitor complexes a slight out-of-plane deformation of the carbonyl-carbon was observed.

Although several of the exposed side chains of the loop regions around the active site (P_9 to P_4') also interact with the protease, mainly by hydrophobic interactions, the primary determinant of binding is the interaction of P_1 with the S_1 subsite for chymotrypsin-like proteases. Alongside, the interactions of the P_2, P_1' and P_2' residues with the corresponding, more shallow subsites also contribute to specificity, but to a lesser extent.

The packing at the interface of the complex is very dense, both for the protease as well as for the inhibitor and is comparable to the packing in the inside of a protein. In shape, the contact areas between native inhibitors and their target proteases are highly complementary. Consequently, the formation of the enzyme-inhibitor complex requires only slight changes in the conformation of the inhibitor. The high complementarity furthermore contributes to a fast association of the inhibitor with the protease to form a tight substrate-like complex. Overall, the substrate-like binding structure is defined by intra- and intermolecular interactions between the inhibitor's primary binding loop with its core and with the enzyme's binding site; the mutual stabilization of these interactions results in an extremely tight binding, so that a cleavage of the inhibitor and subsequent decomposition of the complex rarely occurs.[17,19]

1.3.1 Small-molecule analogs of canonical inhibitors

In contrast to the abundant and well-studied proteinaceous serine protease inhibitors, small molecule peptidic inhibitors that act *via* a similar mechanism are rather rare. Some peptidic natural product inhibitors of serine proteases have been elucidated as "canonical inhibitors". Moreover, some synthetic peptides have been designed that also act in a similar manner. Interestingly, all small molecule "canonical inhibitors" described so far are macrocycles.

For example, synthetic peptides derived from the reactive site loop of Bowman-Birk type inhibitors were developed. These compounds are macrocycles with an average of 11 amino acid residues that were arranged *via* an internal disulfide bridge into a fold that resembles a canonical conformation (Fig. 6). Consequently, these synthetic compounds not only retained the three-dimensional structure of the active site loop of Bowman-Birk inhibitors but also the biological potency of the original proteinaceous structure.[18,20] Investigations were able to reveal that the required 9 amino acid core structure (Fig. 6) can be stabilized by introduction of one additional amino acid at each terminus of the peptide; resulting in an increased potency for these 11-mer peptides.[20] Interestingly, a naturally occurring cyclic peptide inhibitor from sunflower seeds known as sunflower trypsin inhibitor 1 (SFTI-1) also incorporates a similar inhibitory motif and has been identified as a canonical inhibitor.

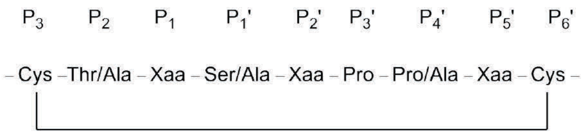
P_3 P_2 P_1 P_1' P_2' P_3' P_4' P_5' P_6'
– Cys – Thr/Ala – Xaa – Ser/Ala – Xaa – Pro – Pro/Ala – Xaa – Cys –

Figure 6 (adapted from[20]): The 9-mer core sequence of disulfide-linked peptidic inhibitors derived from BBI. Xaa represents any amino acid.

The disulfide bridge formed between the cysteines at P_3 and P_6' could also be replaced by a *D*-Pro-*L*-Pro linkage as enclosure of the core loop structure, yet the activity of these derivatives is reduced, due to the loss of potential contacts with the target protease.[20,21]

The variation of single amino acids within the core structure revealed important structure-function relations. As expected, the P_1 amino acid determines the specificity towards a target protease, for instance, inhibitors with a Lys or Arg at this position selectively inhibit trypsin. For the 11-mer sequence SC**X**FSIPPQCY (with F being P_1), Thr was found to be the optimal P_2 amino acid in terms of chymotrypsin inhibition. In a study with trypsin inhibitors of the sequence SCTKS**X**PPQCY (with K being P_1), Ile could be determined as optimal P_2' residue.

In a large, combinatorial synthesis-based approach the same consensus sequence for chymotrypsin inhibitors could be obtained, additionally, Tyr in P_1 position and Nle in the P_2' position were selected.[20]

In conclusion, the P_1 residue is the crucial residue in terms of protease selectivity. In the canonical conformation it is hyper-exposed for the primary interaction with the target protease, this interaction is supposed to be responsible for up to 50% of the total intermolecular contacts. In the P_2 position, Thr is conserved among the peptidic BBI-derived inhibitors, it enhances the stability of the peptide against hydrolysis by forming a hydrogen bond with a backbone amide using its side chain hydroxyl group. In the P_2' position Ile is widely conserved, contributing to the affinity and also to the hydrolytic stability.[18,22]

The location of the putative scissile bond for the peptidic inhibitors described before is yet determined neither by the primary sequence of the inhibitor nor by the enzyme’s selectivity but by the canonical conformation of the backbone which is an inherent feature of this class of inhibitors. The pre-arranged backbone is the part of the peptide that is complementary to the enzyme’s active site and hyper-exposes the P_1 residue to establish the primary contact to the protease. The backbone conformation is enforced by the conserved P_3' Pro and further enhanced by another Pro in P_4' position leading to the formation of a *cis*-amide bond that resembles the native-like structure found in BBIs. Although the P_4' Pro has a *trans* conformation, it enhances the formation of a *cis*-amide bond for the preceding P_3' Pro residue. This hypothesis was verified by replacing the P_4' Pro with Ala, which resulted in the formation of a 1:1 mixture of slowly exchanging and structurally diverse *cis*/*trans* isomers.[18,23] Furthermore, the covalent cyclization by a disulfide bridge is required for a potent inhibition.

Interestingly, Leatherbarrow and coworkers found that despite its stubborn conservation among the BBI-derived inhibitors the P_1' Ser is not an essential element for the integrity of the reactive site loop, although there is an indication from crystal structures, that the side chain hydrogen bond is involved in a transannular hydrogen bond with the backbone. An NMR study, in which either the P_1' Ser or the putative bonding partner, P_5' Gln, was replaced by Ala, indicated clearly that the hydrogen bond formed between P_1' and P_5' is dispensable in terms of the overall structure and that the loss of this bond reduces the inhibitory potency only marginally.[22]

Besides the natural product SFTI-1 and the described small molecule inhibitors, some depsipeptide inhibitors of bacterial origin are another class of small molecule analogs of proteinaceous canonical conformation inhibitors. In these compounds, macrocycles are formed *via* lactonization of the hydroxyl group of the Thr side chain with the acid function of another amino acid residue. The overall fold of results in a canonical conformation and represents another remarkable example of convergent evolution. A comparison of the binding structures of a proteinaceous canonical Bowman-Bork inhibitor (BBI), the designed small molecule Bowman-Birk inhibitor mimics, the sunflower-derived small molecule natural product inhibitor SFTI-1 and the bacterial cyclodepsipeptides scyptolin A and A90720A clearly illustrates the global concept of the canonical conformation as a motif for efficient inhibition of serine proteases. Although the “fixation” of the canonical conformation is realized in different ways, the same three-dimensional structure is adopted by all compound classes (Fig. 7).[18]

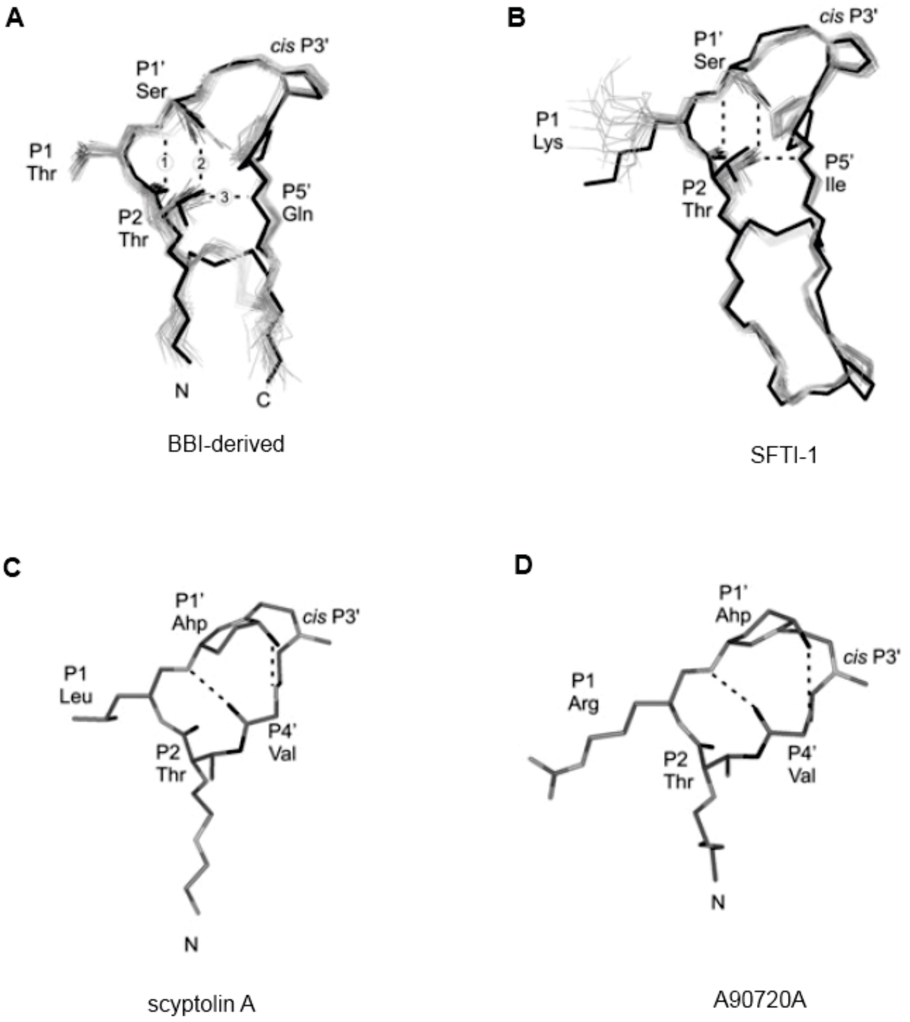
A
P1' Ser
cis P3'
P1 Thr
1
2
3
P2 Thr
P5' Gln
N
C
BBI-derived
B
P1' Ser
cis P3'
P1 Lys
P2 Thr
P5' Ile
SFTI-1
C
P1' Ahp
cis P3'
P1 Leu
P2 Thr
P4' Val
N
scyptolin A
D
P1' Ahp
cis P3'
P1 Arg
P2 Thr
P4' Val
N
A90720A

Figure 7 (adapted from[18]): Structural comparison of plant-derived (**A**, **B**) and bacterial macrocyclic (**C**, **D**) inhibitors isolated from different cyanobacteria.
A: NMR structure of the synthetic BBI-derived cyclic peptidic elastase inhibitor NleCTTSIPPQCY superimposed onto reactive side loop of the Lima bean Bowman-Birk-Inhibitor (black sticks; 1H34); **B**: NMR structure of SFTI-1 superimposed onto its binding structure in complex with bovine trypsin (black sticks; 1SFI, 1JBL); **C**: crystal structure (1OKX) of the elastase inhibitor scyptolin A from *Scytonema hofmanni* in complex with porcine pancreatic elastase; **D**: crystal structure (1TPS) of the trypsin inhibitor A90720A from *Microchaete loktakensis* in complex with bovine trypsin.[18]

1.3.2 The natural product class of 3-amino-6-hydroxy-2-piperidone (Ahp) cyclodepsipeptides as protease inhibitors

The cyanobacterial macrocyclic inhibitors containing the unusual 3-amino-6-hydroxy-2-piperidone (Ahp) unit are a class of natural products that represent potent serine protease inhibition. They comprise a growing class of non-toxic, secondary metabolites isolated from diverse cyanobacteria such as *Microcystis*, *Anabaena*, *Oscillatoria*, *Nostoc*, *Lyngbya*, or *Symploca* spp. and have the remarkable feature of selectively and potently inhibiting S1 serine proteases in a non-covalent mode of action. Regarding these remarkable properties it is not surprising that this class of natural products has been suggested as a lead for serine protease inhibitor design.[24,25]

To date, two x-ray structures of Ahp cyclodepsipeptides with serine proteases are available. In their co-crystallization study of the depsipeptide A90720A with bovine trypsin Clardy and coworkers were able to observe the expected substrate-like binding of the inhibitor molecule to its target protease trypsin. The substrate-like binding is achieved by steric complementarity and hydrophobic interactions; it is further enhanced by the formation of hydrogen bonds. The Ahp residue thereby forms two hydrogen bonds within the macrocycle; one bond is formed between the Ahp-NH and the lactone carbonyl, the other one is formed by the hydroxyl group of the Ahp ring and the valine amide. These two hydrogen bonds are proposed to be responsible for the elliptical shape that enables the molecule to adopt the canonical conformation and the high rigidity of the inhibitor that further enhances binding.[25,26] Rigidity and decreased rotational and conformational degrees of freedom are general strategies for efficient enzyme inhibition: an inhibitor that is already restricted in its binding conformation does not lose as much entropy upon binding as a comparable structure with more degrees of freedom. In these terms, the Ahp unit plays a central role in the efficient inhibition mechanism displayed by the Ahp depsipeptides.

On the non-primed side of the inhibitor, ranging from the P_1 residue Arg to the P_4 residue glyceryl sulfate, several hydrogen bonds are formed with the protease. The P_1 arginine moiety deeply penetrates into the narrow S_1 pocket, where the guanidinium unit forms an ion bond/hydrogen bond with the Asp-189 at the bottom of the catalytic site as well as one hydrogen bond with the hydroxyl group of Ser-190. In a natural substrate, the carbonyl carbon of the arginine that is directly located in the active site would be attacked by the hydroxyl group of the catalytically active Ser-195. In the co-crystal structure, however, the distance of the arginine carbonyl carbon and the Ser-195 hydroxyl group is extended, thereby excluding a nucleophilic attack. The arginine carbonyl oxygen nevertheless is hydrogen-bonded to the backbone amides of Gly-193 and Ser-195, thus creating the oxyanion hole, just as expected for a natural substrate. Finally, the hydrophobic region of A90720A, represented by P_2' Leu and P_3' *N*MeTyr binds into a hydrophobic pocket of the protease.

Overall, these interactions lead to a tight, substrate-like binding of the inhibitor. The binding interactions are so strong that no dissociation of the inhibitor can occur. The highly complementary interaction of the inhibitor and the protease thereby leads to a deep energy minimum for the complex, resulting in an elevated activation barrier for the hydrolysis. Even if a hydrolysis occurred, the inhibitor fragments cannot dissociate and are held in place by the cyclic nature of the molecule and the transannular hydrogen bonds of the Ahp residue. Consequently, a restoration of the macrocyclic structure would occur.[26]

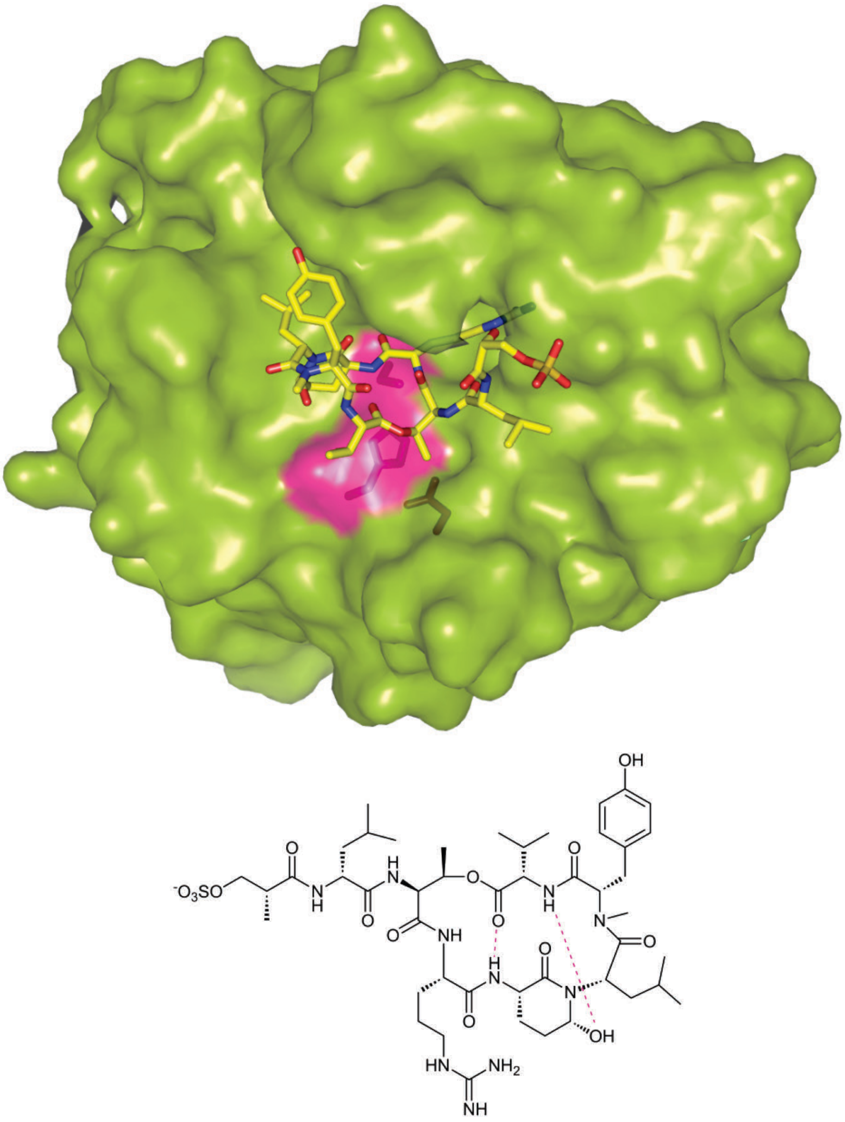

Figure 7: The cyanobacterial inhibitor A90720A in complex with bovine trypsin (1TPS).[26]
Top: Representation of the X-ray structure of A90720A with bovine trypsin, the side chains of the residues forming the catalytic triad are shown in pink. Bottom: chemical structure of A90720A; the transannular hydrogen bonds formed by the Ahp unit are indicated by dashed bonds.

The comparison of the A90720A-trypsin complex with a complex formed by the cyanopeptolin scyptolin A[27,28] with elastase pinpoints that all Ahp cyclodepsipeptides share a universal mode-of-action. In fact, the structure of scyptolin A with its target protease elastase is highly similar and well superimposable to the one observed for the A90720A-trypsin complex. The different specificity is determined by a leucine residue at the P_1 position instead of the arginine found in A90720A. Besides the interactions of the non-primed side of the inhibitor with the S_1 to S_4 subsites of elastase that form an antiparallel β-sheet structure by main chain hydrogen bonds and the interaction of the P_1 leucine carbonyl oxygen with the residues forming the oxyanion hole, further hydrogen bonds of the P_4 alanine carbonyl oxygen as well as the P_2’ threonine hydroxyl with the protease could be observed. In addition, the authors however furthermore noted a conspicuous water molecule bound in a perfect tetrahedral conformation by three residues of the inhibitor (*i. e*. the carbonyl oxygen of the S_2 threonine, the side chain hydroxyl of P_3 threonine and the hydroxyl group of the P_3’ cmTyr) and the guanidinium amide of Gln-200 from elastase. It has been proposed that the binding of this water molecule enhances the overall rigidity of the complex. Finally, a further contribution to the overall binding and complementarity of the inhibitor with the protease is provided by the accommodation of the butyroyl group as well as the chlorine substituent in a hydrophobic environment.

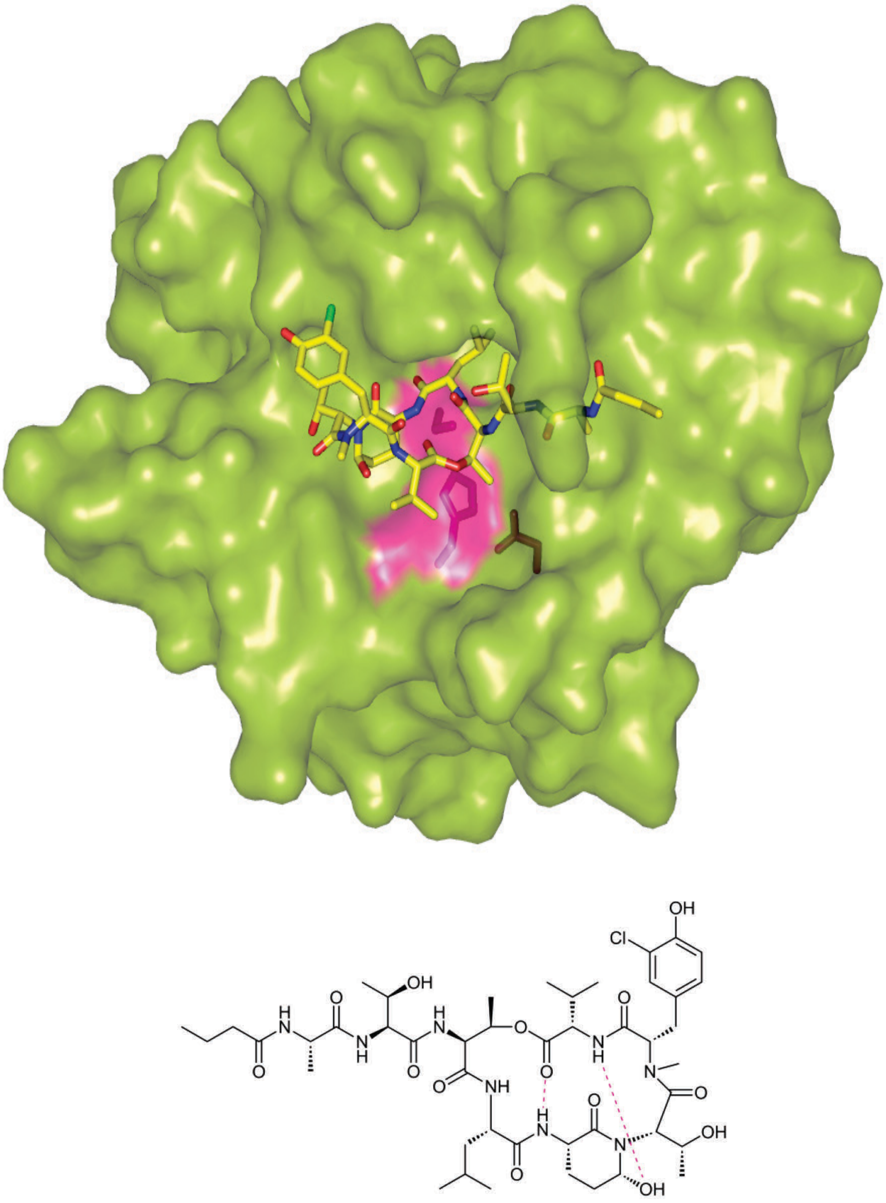

Figure 8: The cyanobacterial inhibitor scyptolin A in complex with porcine pancreatic elastase (1OKX).[28]
Top: Representation of the X-ray structure of scyptolin A with porcine pancreatic elastase, the side chains of the residues forming the catalytic triad are shown in pink. Bottom: chemical structure of scyptolin A; the transannular hydrogen bonds formed by the Ahp unit are indicated by dashed bonds.

After comparing the overall structure of the scyptolin A-elastase complex (Fig. 8) to other inhibitor-elastase complexes, Schulz and coworkers however became aware of another striking feature of Ahp cyclodepsipeptides. They recognized that the Ahp unit occupies the space within the catalytic pocket in which, in other structures, the water molecule required for hydrolysis is located. This emphasizes yet again the crucial contribution of the Ahp residue for the inhibitory potency of the Ahp depsipeptides.[28]

A superimposition of the scyptolin A complex with the A90720A complex reveals highly similar conformations for the 19-membered macrocycles, including the Ahp residue as well as the transannular hydrogen bonds (Fig. 9).[29]

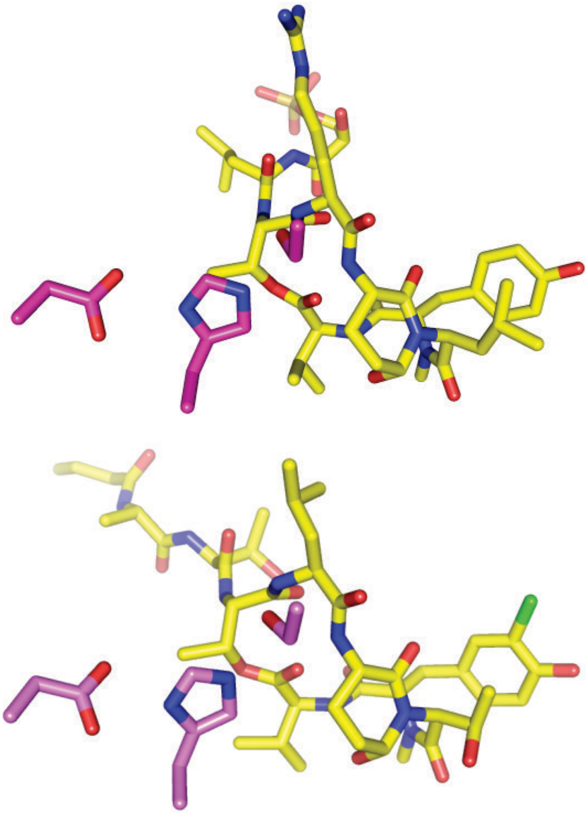

Figure 9: Comparison of the binding structures of A90720A[26] (top) and scyptolin A[28] (bottom) with their target proteases.
The inhibitors as well as the catalytic triad (pink) display a nearly identical conformation for both inhibitor molecules.

In summary, analysis of the mode-of-action of Ahp cyclodepsipeptides has revealed that they act as canonical conformation inhibitors. The Ahp unit is thereby of particular interest and is located in the P_1' position where it overtakes special functions. First, the Ahp residue plays a central role for the bioactivity of this inhibitor class by stabilizing the canonical conformation *via* formation of two stabilizing transannular hydrogen bonds. Second, the Ahp residue also enhances the potency and selectivity towards distinct proteases by accommodation to the S_1' subsite.[18,29] Finally, x-ray analyses have suggested that the Ahp unit might play another interesting role. It seems as this residue occupies the space of the "catalytic" water molecule that during the enzymatic mechanism mediates the hydrolysis of the acyl-enzyme complex. Consequently, the hydrolytic water is excluded from the enzyme which provides an additional protection against a hydrolysis of the inhibitor.[28,29]

As a consequence of their selective and potent inhibition of S1 serine proteases by a remarkable non-covalent mechanism, the Ahp cyclodepsipeptides and have been suggested for further investigations in terms of structure-activity relationships and also the wish to enable access to modifiable templates has been expressed.[29] Both aspects have indeed been part of the work presented in this thesis.

1.4 Malaria - a persisting global burden

The complex and devastating disease malaria is still a heavy burden on global population, affecting especially the weakest members in the poorest countries of the world. In the year 2008, 3.3 billion people in 109 countries and territories worldwide were still threatened by a malaria infection. It is most devastating in Africa, where malaria represents the second most frequent cause of death from an infective disease after HIV/AIDS. In contrast, malaria ranges in fifth place worldwide. After abortion of the Global Malaria Eradication campaign (1950s to 1970s), the interest in this disease has dropped dramatically, despite its enduring presence. Only in 1998, after the numbers of malaria cases and deaths had multiplied, the Roll Back Malaria partnership was initiated by the World Health Organization (WHO), the United Nations Children´s Emergency Fund (UNICEF), the United Nations Development Programme (UNDP) and the World Bank to coordinate malaria control and treatment globally.[30] As a consequence of this concerted action the number of malaria cases worldwide could be reduced from 233 million in 2000 to 225 million (176 million in Africa) in 2009. The number of deaths was also reduced from nearly one million in 2000 to 781000 in 2009.

The primary measure to take control of malaria and in long-term eliminate malaria completely is vector control, *i. e*. elimination of the mosquitos transmitting the parasite, and thereby preventing the infection and reinfection with malaria. The individual protection against mosquito bites is in this circumstance the first line of defense, enforced by distribution of insecticide-treated nets (ITNs) under which, in the ideal case, every individual in high-risk areas should sleep every night. Besides providing these safety measures, it is of course also of great importance to instruct the local population to a correct and most importantly regular use of the provided nets.

The second approach to prevent transmission is indoor residual spraying (IRS) with insecticides, a measure which enables rapid elimination of transmission. The full potential of IRS is achieved when 80% or more of all households and animal shelters within a community are treated.

Another measure that is undertaken to prevent the transmission of malaria is the intermittent preventive treatment of pregnant women at risk in sub-Saharan Africa, as well as preventive treatment of infants at risk in sub-Saharan Africa.[31,32]

Despite these protective measures, an infection with malaria currently cannot be prevented completely. Consequently, chemotherapeutics for treatment of malaria disease represent another important component to reduce the global burden of malaria.

1.4.1 *Plasmodium* species as the causing agents of malaria in humans

Malaria in humans is caused by 5 different species of *Plasmodium* parasites which are transmitted by the bites of female *Anopheles* mosquitos, the so-called malaria vectors. *Plasmodium falciparum*, which is spread in tropical regions, is by far the most common and also most deadly of the five species. It is responsible for the majority of malaria-related fatalities in sub-Saharan Africa and thereby the main target of malaria control. Infections with *Plasmodium vivax*, common in most of Asia, the Eastern Mediterranean and the endemic countries in the Americas, are responsible for 25 to 40% of worldwide malaria cases, although the infection usually does not progress as severe as by *P. falciparum* infection; on the other hand, *P. vivax* infection can cause relapses and a treatment of the infection should therefore also focus on preventing relapses. Additionally, it has been reported that the host inflammatory response upon *P. vivax* infection is higher than upon *P. falciparum* infection at comparable levels of parasitemia.[33] The number of infections caused by *P. malariae* and *P. ovale* are rather small and these infections also progress in an uncomplicated manner, comparable to *P. vivax* in most cases. Only recently a fifth species, *P. knowlesi*, known to cause malaria in monkeys, has also been reported to cause human malaria. [30,32]

All *Plasmodium* species have complex life cycles that differ slightly between the different species. The parasite is transmitted in the sporozoite form to the human blood cycle with the saliva of female *Anopheles* mosquitos. From there, the sporozoites are rapidly taken up by the liver where they infect the hepatocytes. At this stage differences between the different *Plasmodium* species occur. *P. falciparum* and *P. malariae* progress rapidly through the hepatocytes, replicating asexually *via* a schizont state and re-enter the blood cycle after the rupture of the hepatocytes as haploid merozoites. In the case of *P. vivax* or *P. ovale* infections, a certain part of the infected hepatocytes become dormant hypnozoites which can be reactivated without a repeated infection after different time periods ranging from 3 weeks to several years, causing a relapse of the disease. In all cases, the merozoites then infect red blood cells (RBCs), progressing from the ring-stage via the trophozoite stage that exhibits a nucleus and a digestive vacuole and then entering asexual replication within the erythrocytes until the rupture of the schizont. The egress from the schizont sets free a large number of merozoites which can again invade RBCs and increase the parasite´s biomass with every replication cycle (Fig. 10).

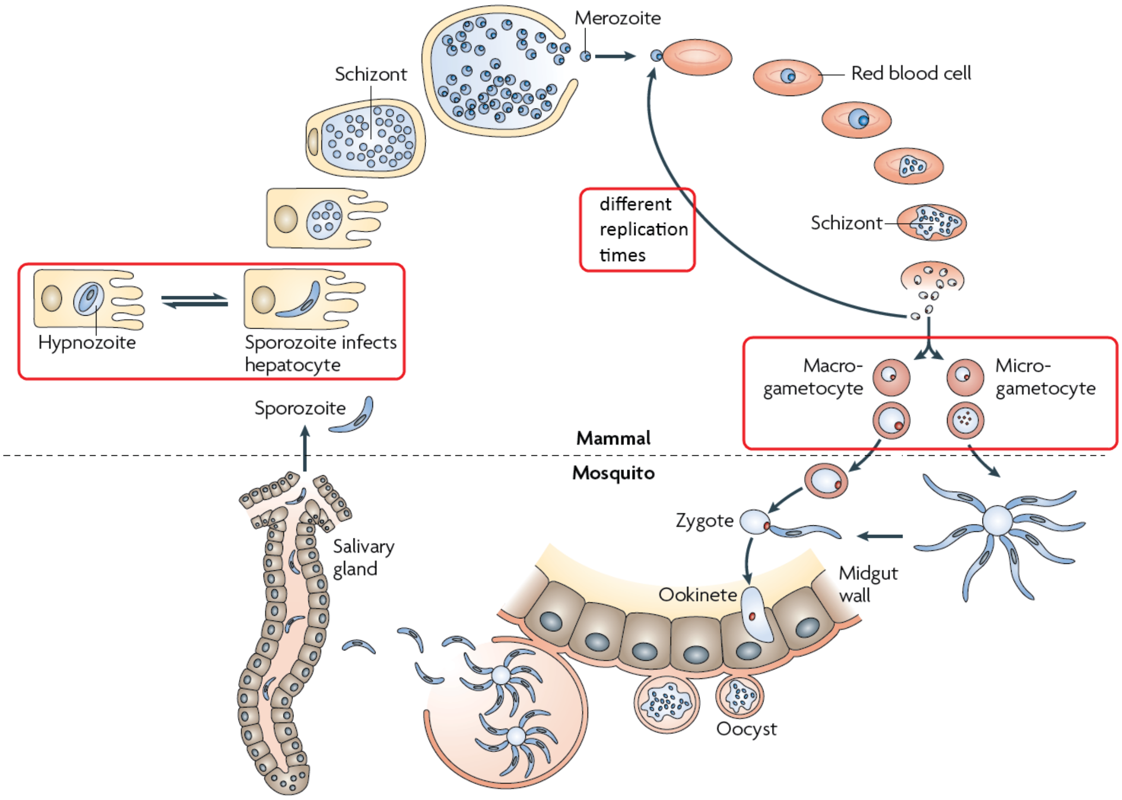
Merozoite
Schizont
Red blood cell
different replication times
Schizont
Hypnozoite
Sporozoite infects hepatocyte
Sporozoite
Macro-gametocyte
Micro-gametocyte
Mammal
Mosquito
Zygote
Salivary gland
Ookinete
Midgut wall
Oocyst

Figure 10 (adapted from[33]): The life cycle of the malaria parasite. The major differences between the different *Plasmodium* spp. are indicated by red boxes.

During the replication in the RBCs, the parasites process hemoglobin in an acidic food vacuole to nurture from the amino acids and peptides originating from this digestion. The digestion of hemoglobin also produces heme, a toxic side product, which is on the one hand related to symptoms caused during a malaria infection, but on the other hand also an entry to the treatment of malaria; this point will be discussed in the following section.

The rupture of the red blood cells and the liberation of parasital toxins and the host's inflammatory response then cause the typical symptoms of malaria such as fever, headache and chills, more severe infections can also result in anemia or cerebral malaria in the case of *P. falciparum* infection. The times between these febrile paroxysms can vary between the *Plasmodium* spp. and represent the replication times of the parasites. The replication time of *P. falciparum* and *P. vivax* is 48 hours, whereas the cycle of *P. malariae* is longer (72 hours).

The newly discovered *P. knowlesi* has a very low replication time of only 24 hours and could progress to a life-threating infection even at low parasitemia rates if it remains untreated.[33]

To progress the parasites' development, some of the merozoites differentiate and develop into male and female gametocytes which are able to undergo a sexual replication cycle once taken up by a mosquito during a blood meal. The point of time at which gametocytes appear is yet another key difference between *P. falciparum* and *P. vivax*. In a *P. vivax* infection, gametocytes can appear simultaneously with the asexual stages or even before those. In contrast to this, for a *P. falciparum* infection gametocytes are observed only at late stages of the infection (Fig. 10).

Once taken up by the mosquito during a blood meal, the male gametocytes are activated to form gametes which then fuse with the female gametocytes thereby forming diploid ookinetes. The ookinetes can then migrate to the midgut of the mosquito and, after passing the cell wall, form into oocysts. By meiotic division sporozoites are formed which, after liberation, migrate to the salivary glands of the mosquito to be transmitted to a host again during a blood meal (Fig.10).[33]

Finally, it should be noted that when treating *P. falciparum* or *P. vivax* infections the differences between the species should be considered. A *P. vivax* infection rather demands for an elimination of the gametocytes rather than an inhibition of differentiation.

Although *P. falciparum* malaria is often accounted for as the form of malaria causing more severe cases of infection; *P. vivax* can also cause severe disease progressions that become life-threatening.[34,35] Severe *P. falciparum* malaria shows various clinical symptoms ranging from an initial high fever, over progressing anemia to multiorgan dysfunction and unconsciousness or coma which is a sign of cerebral malaria. This severe etiopathology is determined by various factors that originate from the parasite itself as well as from the host organism. Overall, a malaria infection is a complex process with many different events cumulating to a severe outcome of the infection.[34,36]

When comparing *P. falciparum* and *P. vivax* malaria infections, a greater inflammatory response is observed for the *P. vivax* infection. This infection has been found to cause higher fevers at comparable levels of parasitemia; *i. e*. the pyrogenic threshold of *P. vivax* is higher than that of *P. falciparum*. In general, a *P. vivax* infection does not lead to as high parasitemia as observed for *P. falciparum*; nevertheless at comparable or even higher levels of *P. falciparum*, a *P. vivax* infection causes a greater inflammatory response, related to a higher level of cytokines.[35]

1.4.2 Antimalarial drugs and their mode of action

The first drug that was used to treat malaria was quinine, which could be isolated from the bark of *Cinchona calisaya* as early as 1632. Until the 19th century it was the only drug known to cure malaria. After World War I, synthetic derivatives of quinine were developed. First, primaquine and quinacrine came to the market and finally chloroquine was introduced in 1934. By 1946, chloroquine had become the preferred anti-malarial drug, overcoming the undesired adverse effects of quinine.[33,37]

Quinine and its derivatives are potent schizonticides, eliminating exclusively the asexual blood stages of the parasite. Their mode of action is the interference in the deposition of the toxic heme to insoluble hemozoin. The parasites dispose of the toxic metabolite formed upon hemoglobin digestion by polymerizing the heme to form crystalline hemozoin, which is also referred to as malaria pigment and can be visualized by simple microscopy. By interfering with this process, the parasite is intoxicated and killed by its own metabolic products. Evidence for the proposed interference in heme detoxification is provided by the finding that chloroquine and related drugs act stage-specific, killing only those parasites that digest hemoglobin. Morphologically, the effect of a quinoline therapy is accompanied by a significant swelling of the food vacuole (food vacuole defect) caused by the hyperconcentration of heme.[38,39] Interestingly, the mechanism of this heme detoxification is still unclear and different polymerization scenarios have been discussed.[40,41]

On the other hand the formation of hemozoin by a crystallization process in a hydrophobic environment by a biomineralization process has been suggested and is accepted today as the most probable mechanism for heme detoxification.[39]

Mutations of the parasite however lead to chloroquine resistance due to reduced take-up of the drug to the digestive food vacuole. The underlying mechanism of resistance is not yet fully understood, although there is strong evidence that mutations in the gene encoding for *Plasmodium falciparum* chloroquine resistance-related transporter protein (PfCRT) as well as mutations in the *Plasmodium falciparum* multidrug resistance (*pfmdr1*) gene are key players.[37] For *P. vivax*, a resistance to chloroquine was reported as late as 1989, compared to the first evidence for resistant *P. falciparum* in 1957.[42]

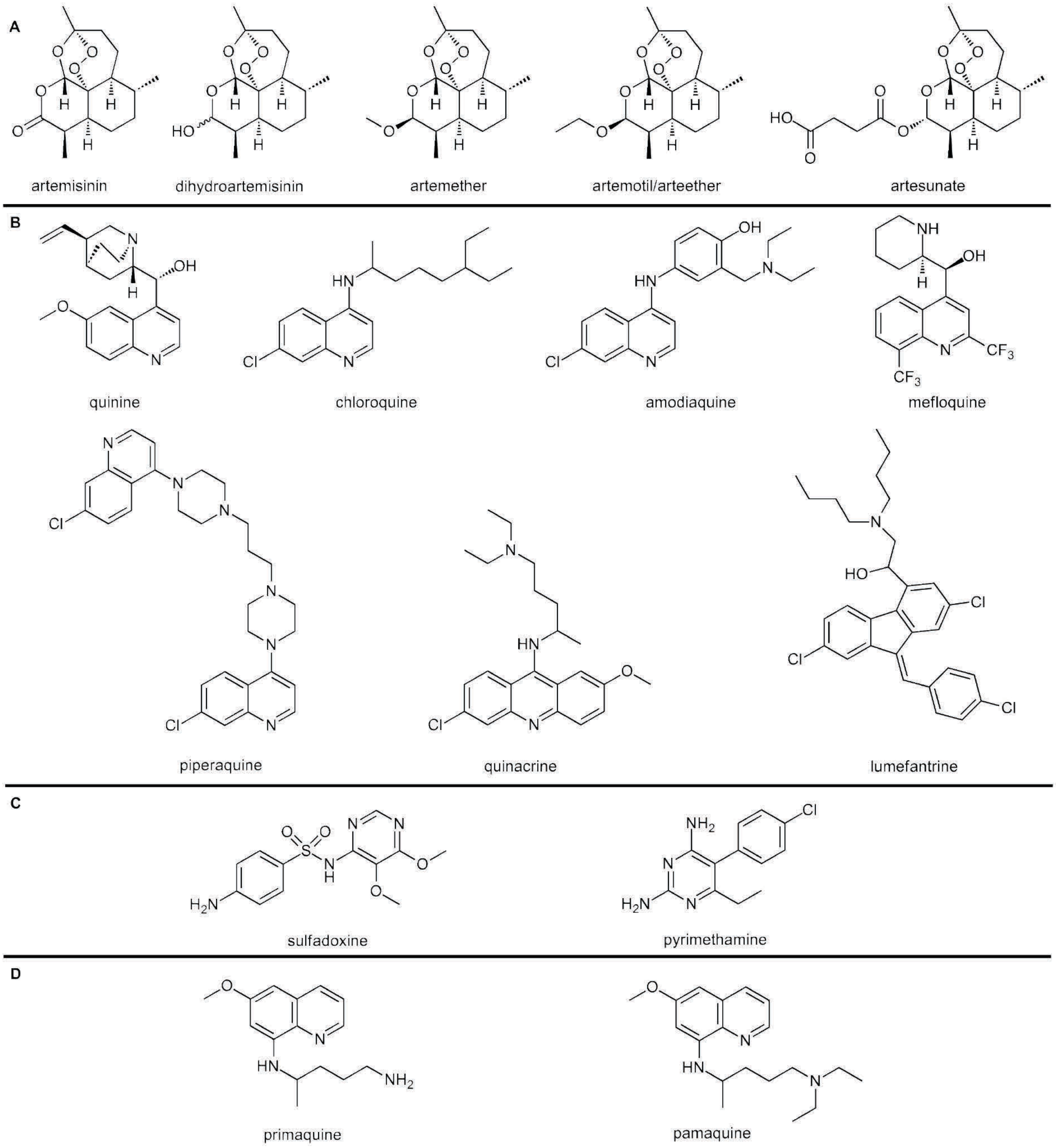
A
artemisinin
dihydroartemisinin
artemether
artemotil/arteether
artesunate
B
quinine
chloroquine
amodiaquine
mefloquine
piperaquine
quinacrine
lumefantrine
C
sulfadoxine
pyrimethamine
D
primaquine
pamaquine

Figure 11: Antimalarial drugs currently in use to treat malaria infections (selection from[33]). **A**: Artemisinin and derivatives; **B**: Quinine and quinine derivatives, some of the drugs are used for ACT; **C**: combination drugs used mostly as preventive therapy; **D**: drugs recommended for treatment of *P. vivax*, effective in hypnozoite elimination.

In another approach, rational design of inhibitors targeting the essential folate production of the parasite is pursued. The malaria parasites are not able to salvage folate and depend on synthesizing it *de novo*, as it is required for the synthesis of tetrahydrofolate, the co-factor needed for methylation reactions. The two drugs emerging from this design were sulfadoxine, inhibiting dihydropteroate synthetase (DHPS) and pyrimethamine which inhibits dihydrofolate reductase (DHFR). Both drugs interfere effectively in the synthesis of dihydrofolate, an important intermediate in the synthesis of tetrahydrofolate. The best effect is achieved when they are used as sulfadoxine-pyrimethamine (SP) combination. In the second half of the 20th century, SP was used as second line treatment following chloroquine treatment for acute, uncomplicated infections caused by all 4 *Plasmodium* spp..[33,40] With evolving chloroquine resistance, SP replaced the former as first-line treatment in Thailand and 10 African countries.[43] Today, SP therapy is used and recommended for intermittent preventive treatment of pregnant women and infants in moderate to high risk regions of sub-Saharan Africa.[31] Unfortunately, SP resistance occurred very quickly after its introduction, the mutations leading to the drug resistance are well described.[43]

Especially the appearance of chloroquine resistant strains was a major drawback in the battle against malaria. Intensive research was conducted to find replacements for chloroquine, which lead to the discovery of the chloroquine-derived drugs such as piperaquine, mefloquine, amodiaquine and lumefantrine that were all active against the chloroquine-resistant strains and acted by the same mechanism as chloroquine. Unfortunately, resistances to these new drugs appeared rapidly after their introduction and their utilization as first line treatment.

A new era of malaria treatment commenced with the (re)discovery of artemisinin (Quinghaosu) by Chinese researchers in 1972. Artemisinin is isolated from the leaves of *Artemisia annua* and has been known to traditional Chinese medicine for over 2000 years; its use as antimalarial agent was described in the fourth century for the first time. Chemically, artemisinin is a sesquiterpene featuring an unusual endoperoxide bridge. The main metabolite of artemisinin is the lactole dihydroartemisinin (DHA); derivatives like arthemether, artemotil and artesunate are esterified derivatives of DHA. Artemisinin as well as its derivatives are active against all drug-resistant strains of *P. falciparum*, killing all blood stages of the parasite, thereby leading to the shortest fever clearance times of all antimalarials. Besides the broad range against all blood stages of the parasite, the synthetic derivatives also possess an excellent safety profile. Furthermore, artemisinins help to reduce transmission as they are also active against the gametocytes, both immature and developing.[33,44]

There is no consensus on the mode of action of artemisinins. It has been reported that the toxicity to the parasite at nanomolar concentrations is based on an enhanced uptake of the metabolite DHA in infected RBCs. Indeed, infected RBCs seem to take up more than 100-fold higher concentrations of DHA than uninfected RBCs. Concerning their mode of action, there is strong evidence that the artemisinins act by generating free radicals that damage the parasite cells. The alkylation of proteins by the electrophilic species generated in artemisinin decomposition most probably accounts for the potency of the drug. Besides the effects in the food vacuole, other cell organelles of the parasites are damaged as well by artemisinins: effects on the mitochondria, rough endoplasmatic reticulum and the nuclear envelope have been observed.[45] The very effective two-way mechanism of artemisinin proceeding *via* an activation within the parasite to free radical species that specifically target parasital enzymes and alkylate them, has rendered the artemisinins the drug of choice for the treatment of uncomplicated *P. falciparum* malaria.

To overcome a potential drug resistance and to retain the desperately required activity of artemisinin derivatives, artemisinin monotherapies have been replaced by artemisinin combination therapies (ACT), in which an artemisinin derivative is combined with a partner antimalarial drug. The artemisinin component of the ACT is supposed to kill off the bulk parasite loading, while the partner drug with a longer half-life eliminates residual parasites. The combination of two drugs minimizes the selective window for either drug, thereby protecting their antimalarial potency and suppressing the emergence of resistant strains.[44]

Despite the efforts undertaken to preserve artemisinin activity, first indications of an emerging artemisinin resistance were reported from the Cambodian side of the Cambodia-Thailand border region in 2004. The region of Western Cambodia had already been in focus after the emergence of chloroquine and SP resistances, underlining the urgency to encounter the newly reported resistance with all measures available.[44]

Consequently, artemisinin resistance has to be monitored constantly, as new cases of reduced efficacy have been reported from the Thailand-Myanmar border region, the China-Myanmar border region as well as from one Vietnamese province.[31]

Unlike *P. falciparum*, *P. vivax* can still be treated with chloroquine, which is recommended by the WHO as first-line treatment in regions with no chloroquine-resistant strains. For the regions in which *P. vivax* has become resistant to chloroquine, an adequate ACT is recommended. For the elimination of hypnozoites pamaquine and primaquine are recommended as oral medication.[31,33]

Currently, the different types of malaria infections can be treated effectively with the drugs described above. Nevertheless, the parasites themselves as well as the malaria vectors quickly adapt to drug pressure which results in the emergence of resistances. This calls for research efforts to identify alternative possible targets for a safe and more specific chemotherapy as well as the rational design of drugs addressing these targets.[40] Although the identification of a molecular target is tedious work, it is advantageous to identify the molecular target and mechanism of a potential drug candidate before entering the clinical phase of drug development.[33]

1.5 Cysteine proteases and their inhibitors

Cysteine proteases, also referred to as thiol proteases, are another large group of proteases that are widely distributed in viruses, bacteria, protozoa, plants, mammals and also fungi.[46] In the MEROPS database, the cysteine proteases are divided into 8 clans and about 60 different families (of which some so far have not been assigned to a protease clan). Furthermore, the four clans of mixed mechanism (P) proteases include cysteine proteases as well. An overview of cysteine protease clans along with prominent family members is given in Table 2 (based on: MEROPS database[11], January, 2012)

Table 2: Representation of the cysteine protease clans and examples for unassigned families currently listed in the MEROPS database (January, 2012).

Clan	Number of families	Representative member(s)	Family
CA	27	papain	C1
		calpain-2	C2
CD	6	clostripain	C11
		caspase-1	C14
CE	6	adenain	C5
CF	1	pyroglutamyl-peptidase I	C15
CL	2	sortase A	C60
CM	1	hepatitis C virus peptidase 2	C18
CN	1	sindbis virus nsP2 peptidase	C9
CO	1	dipeptidyl peptidase VI	C40
unassigned	13	chestnut blight fungus virus p29 peptidase	C7
		RvrRpt2 peptidase	C70
PA	6	poliovirus-type picornain 3C	C3
PB	5	amidophosphoribosyl transferase precursor	C44
PC	2	gamma glutamyl hydrolase	C26
PD	1	hedgehog protein	C46

The clan CA represents the most populated clan of cysteine proteases, followed by the clan CD. A look on the different cysteine protease families reveals that the C1 family of papain-like cysteine proteases is most often found. The most prominent member of this family is the name-giving protease papain isolated from papaya. Other important representatives are the related plant proteases bromelain or chymopain, the lysosomal cathepsins, proteases from parasitic protozoa such as cruzipain from *Trypanosoma cruzi*, the parasite causing Chagas' disease, or the falcipains from the malaria parasite *Plasmodium falciparum*.[47]

In humans, the most important cysteine proteases of the C1 family of papain-like proteases are the cathepsins. They comprise a class of enzymes found in the intracellular space that are mostly localized in the lysosomes. In total, 11 cysteine protease cathepsins (B, H, L, S, C, K O, F, V, X and W) were so far identified in humans. With the exception of cathepsin S, the cathepsins were found to be expressed in various cell types and their major role was believed to be the non-specific degradation of proteins inside the lysosomes. Under special conditions, often related to pathogenic states, cathepsins can also be found outside of the lysosomes. Moreover, the development of new microbiology techniques enabled the identification of tissue-specific cathepsins, cathepsin K for example is expressed almost exclusively in osteoclasts. The lysosomal cysteine proteases require a reducing and slightly acidic environment for optimal function. They are mostly endopeptidases, cathepsin B also acts as a dipeptidyl carboxypeptidase and cathepsin H is an aminopeptidase. Cathepsin C is an exception, being a dipeptidyl aminopeptidase.

Besides their appointed role inside the lysosomes, the cathepsins also degrade proteins outside the lysosomes and are involved in the processing of proteins. Other important cellular processes such as the antigen presentation or bone resorption are closely related to lysosomal proteases. Furthermore, it has been observed that the secretion of lysosomal cysteine proteases can be very harmful and has been related to various disorders. Consequently, their inhibition can represent an important strategy for the development of novel chemotherapeutics. Their unwanted inhibition however can cause serious side effects due to their important role in various cellular processes.

In protozoic parasites, cysteine proteases are also key players, ensuring the “well-being” of the parasital species. Despite the high diversity of pathogenic, protozoan species, the vast majority of proteases isolated from these species are in fact cysteine proteases. Some of these proteases are key players in the parasitic life cycle, ensuring the nutrition of the parasite as well as the invasion of the host cells. A full example for a parasitic protozoan species with a description of its crucial cysteine proteases is given in the following section on the falcipains from the malaria parasite *P. falciparum*.

Additional examples for essential parasital cysteine proteases are cruzipain from *Trypanosoma cruzi*, the pathogen causing Chagas’ disease or cysteine proteases from *Schistosoma mansonia*, the parasite responsible for intestinal bilharzia that, similar to *P. falciparum*, also nourishes on hemoglobin digested by cysteine proteases.[46]

The currently best investigated cysteine protease is papain, for which the full sequence as well as the three-dimensional structure is known.[46] The papain-like proteases consist of two domains, the L and the R domain (**l**eft and **r**ight, the names originate from the orientation of the domains in the common view) that interact through a large, planar interaction surface, opening at one side to form a V-shaped active site cleft. The main feature of the L domain is a helix motif; the catalytically active Cys-25 is located at the *N*-terminus of the helix. The key feature of the R domain is a β-barrel structure incorporating His-159, the second component needed in the mechanism of catalysis.[47] Activation of the active site cysteine is thereby achieved by a catalytic dyad between cysteine and a histidine residue.

The binding of substrates to cysteine proteases has been studied with different proteases and protease inhibitors and showed that the principles observed for the model protease papain can be extended to other papain-like cysteine proteases. In fact, crystallographic analyses of the co-complex structures of papain with different inhibitors revealed that the interaction of papain-like proteases with a substrate or an inhibitor usually only spans the S_2 to S_2' subsites (in contrast to the seven binding subsites (S_4 to S_3') postulated by Schechter and Berger[8]). This has led to the definition of the term “substrate binding site” for binding to the S_2 to S_2' subsites, while the additional sites are termed as “binding area” because the experimental data does enable a clear definition of these binding sites. The individual binding sites are formed by loops originating from the core of the two domains (Fig. 12).[47]

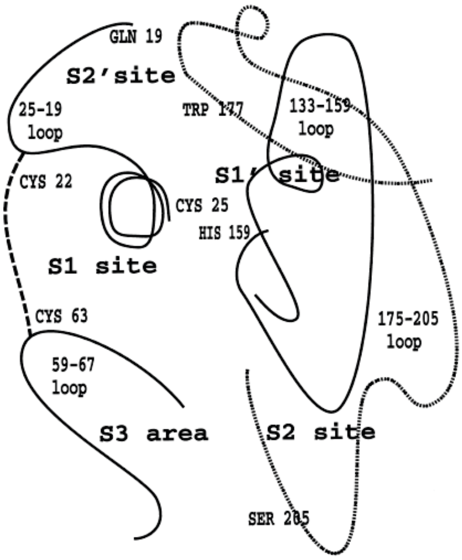

Figure 12[47]: Schematic representation of the substrate binding sites of papain-like cysteine proteases. The different binding sites are formed by various loops and one disulfide bridge. Some key amino acids are represented in the figure.

Just as for all other proteases, a strict control of cysteine protease activity is necessary. One important means of control and regulation of cysteine protease activity are thereby endogenous cysteine protease inhibitors.

To this end, mammals express a number of proteinaceous cysteine protease inhibitors, the cystatin superfamily. This superfamily can be further grouped into three families on the basis of sequence homologies: a) the stefin family, b) the cystatin family and c) the kininogen family.[46,48]

In addition to these proteinaceous cysteine protease inhibitors, also small molecule inhibitors, either derived from natural sources or synthetic compounds, are known. In general, these small molecule inhibitors are based on the incorporation of an electrophilic element in a peptide sequence. The electrophilic warhead is attacked by the nucleophilic thiol, leading to a covalent modification of the target enzyme. A representation of different cysteine protease inhibitors is given in the following section on falcipains. The principles presented for the inhibition of falcipains can also be adapted to other cysteine proteases.

1.5.1 Falcipains - possible new targets for malaria chemotherapy

The completion of the genome sequencing of *P. falciparum* in 2002 lead to the identification of 92 putative proteases encoded within the genome. As already discussed, proteases are excellent drug targets; the inhibition of parasital proteases may provide access to a more specific and effective therapy of malaria infections.[49]

In the search for antimalarial drugs, the parasital proteases have been suggested as very promising drug targets, as they are involved in numerous processes essential to parasite survival. Among them, the cysteine proteases are regarded as most auspicious candidates. The best characterized cysteine proteases in *P. falciparum* are the four falcipains, belonging to the family of papain-like cysteine proteases.

From inhibitory studies, an essential role in hemoglobin digestion was appointed to these cysteine proteases. Inhibitors applied to different life-cycle stages maximally affected the mature trophozoite and schizont stages. Additionally, further roles were suggested on the basis of the observation that all developmental stages of the parasite were affected after a long term treatment with cysteine protease inhibitors.

The best characterized function of cysteine proteases within the parasite is the degradation of hemoglobin, providing the parasite with amino acids for the biosynthesis of proteins. It has been suggested that the hydrolysis of hemoglobin is a cooperative process mediated by cysteine, aspartic and metallo proteases, although the participation of cysteine proteases was found to be the essential element: The distinct food vacuole swelling related to a disturbed hemoglobin hydrolysis could only be observed when cysteine proteases were inhibited by compounds such as leupeptin or E-64, which are well-known inhibitors of cysteine proteases. Besides this direct involvement of falcipain-2 and falcipain-3, they also indirectly influence the hemoglobin hydrolysis in an indirect manner by processing aspartic proteases involved in the hydrolysis process.

Inhibitory studies alongside with gene disruption experiments revealed a certain redundancy among the proteases involved in hemoglobin processing. This allows the parasite to react to a temporary loss of one or more proteases from different classes involved in this essential process. Nevertheless, this redundancy is not complete and so the inhibition of falcipains is detrimental to the parasite. A synergistic effect in antimalarial activity, when inhibiting cysteine as well as aspartic proteases, could also be observed.

The falcipains are four cysteine proteases of *P. falciparum* belonging to the family of papain-like cysteine proteases (clan CA, family C1) and are denoted as falcipain-1 (FP-1), falcipain-2 (FP-2), falcipain-2’ (FP-2’ or -2B), which is 99% homologous to FP-2 in the catalytic domain, and falcipain-3. FP-1 is only 40% homologous to the other falcipains that share 68% of their sequences, so the falcipains are subdivided into FP-1 and the FP-2/3 subfamilies. In *P. vivax* a homolog of FP-1 could be identified, showing 72% homology; for FP-2/3, three homologs with 60 to 70% identity were characterized.[50]

FP-2 and FP-3 are expressed at different points of time in the parasite life-cycle: FP-2 is expressed in early trophozoites, the maximum expression of FP-3 can be found in late trophozoites. FP-2 has been found to be responsible for 90% of the cysteine protease activity with standard peptidyl substrates, whereas FP-3 is relatively unreactive against these peptidyl substrates. Both proteases prefer hydrophobic residues at the P_2 position, characterizing them as cathepsin L-like.[50,51]

From the expression profiles at different points of time as well as from knock-out studies for FP-2 and FP-3 it could be determined that FP-3 is the critical falcipain expressed at a later stage of parasital development.[52,53] These studies attempted the knock-out of all four falcipains in erythrocytic stage parasites using the 3D7 strain. The mutants carrying the FP-1 and FP-2’ knock-outs could not be distinguished from wild-type parasites, indicating that FP-

1 as well as FP-2’ does not play a role in erythrocytic development. The overall role of FP-2’ remains uncertain, taking into account that it shares 99% identity with FP-2 in the catalytic domain but obviously does not seem to play a role in the erythrocytic development of the parasite. The FP-2 knock-out mutants showed the distinct swollen food vacuole, related to a disturbed hemoglobin digestion. The same phenotype was observed when treating the parasite culture with the cysteine protease inhibitor E-64 (Fig. 13).

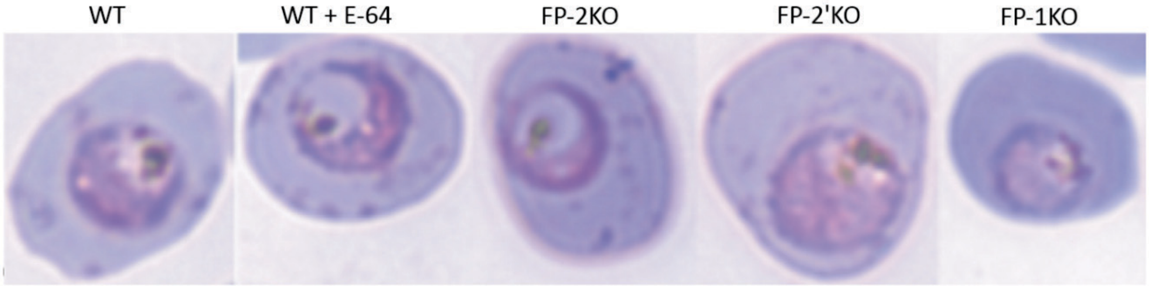

Figure 13[53]: Trophozoite morphologies: WT: synchronized wild-type, WT+E-64: wild-type treated with E-64 (10 µM), FP-2, FP-2’ and FP-1 knock-out. All cells were cultured for 22 h, then the smears were stained with Giemsa and the morphologies were evaluated under a bright field microscope. WT+E-64 and FP-2KO show the distinct swelling of the food vacuole.

Furthermore, the FP-2 knock-out mutants showed a twice increased sensitivity to cysteine protease inhibitors as well as a 1000-fold increase in sensitivity towards an aspartic protease inhibitor. This result resembles well the postulated synergistic effect of cysteine and aspartic proteases in hemoglobin digestion. Nevertheless, FP-2 knock-out mutants remain viable and progress to schizont stage, where the observed altered morphology resolves, leading to a phenotype not distinguishable from the wild-type. The same effect was observed for the FP-1 and FP-2’ knock-out mutants.

All attempts to generate a FP-3 knock-out mutant failed. The mutants were not viable, indicating a crucial role for FP-3 in the erythrocytic development of the parasite. To rule out a mutation-resistance of the FP-3 locus, the gene was replaced readily by a tagged version, affording viable mutants, expressing FP-3. This finding underlines the essential role of FP-3 in the development and progression of the trophozoites.

The results of the knock-out studies were able to emphasize the essential roles of FP-2 and FP-3 in the erythrocytic development of *P. falciparum*. In the early developmental stage of the trophozoites, FP-2 is responsible for the hydrolysis of hemoglobin. In late trophozoites the expression level of FP-2 is lower, here FP-3 expression is maximal and FP-3 ensures hemoglobin hydrolysis and proliferation to the schizont stage. The FP-2 knock-out mutants are most probably rescued by FP-3, which is expressed in the late trophozoite stage and in the schizont stage. The lethality of a FP-3 knockout further supports such a rescue-mechanism. Consequently, FP-2 and FP-3 seem to have very similar roles, but are expressed at different points of time within the erythrocytic development, pinpointing for a stage-dependent activity rather than a redundant activity of these two proteases. For antimalaria research, the results clearly indicate that a focus should be put on FP-2 and FP-3 inhibitors. Furthermore, a combined strategy with cysteine and aspartic protease inhibitors should represent a viable approach as indicated by the increased sensitivity of the FP-2 knock-out mutants.[53]

When compared biochemically, FP-2 and FP-3 show similar but not identical features. Both proteases have a low pH optimum consistent with their location in the acidic food vacuole. Moreover, a reducing environment is required for the maximum activity. Like most members of the papain-family, FP-2 and FP-3 specificity towards a substrate is determined by the P_2 residue and both proteases prefer substrates with leucine at this position. FP-2 shows a high affinity for peptidyl substrates, represented *in vivo* by globin peptides, whereas FP-3 shows a higher affinity for native hemoglobin. In a study with recombinant enzymes, FP-3 was found to hydrolyze native hemoglobin with a greater activity than FP-2. The reaction rate of both enzymes in globin digestion was significantly higher than the digestion rate for native hemoglobin, both enzymes hydrolyzed globin at comparable rates.

The different substrate affinities enable an optimal digestion and recycling of native hemoglobin as well as denatured globin proteins. Another difference between the proteases was found concerning their pH stability: both proteases are stable at acidic pH, but FP-2 is also stable at neutral pH and is additionally able to undergo autohydrolysis to the mature protease at this pH. The different stabilities as well as substrate preferences may stem from different roles of the two enzymes. After expression as membrane-bound preforms both enzymes need to be processed to an active, mature form and relocated to the food vacuole. FP-2 is processed more quickly and undergoes autohydrolysis at neutral pH, which provides evidence for an additional role of FP-2 outside the food vacuole. FP-2 was found to hydrolyze the erythrocyte cytoskeletal proteins band 4.1 and ankyrin at neutral pH, indicating a role in destabilization of the erythrocyte membrane before the rupture and liberation of the merozoites.

FP-3 is on the other hand more stable and active at acidic pH and is most probably located only in the acidic food vacuole, where it is the more potent hemoglobinase, hydrolyzing native hemoglobin as well as denatured globin proteins.[50,54]

Recently, the crystal structures of FP-2 with E-64 and of FP-3 with leupeptin were solved. These studies revealed – as expected – that both proteases are highly homologous to other members of the papain-like cysteine protease family (Fig. 14). They exhibit a clear preference for hydrophobic residues at the P_2 position and the preference of FP-2 and FP-3 for a leucine residue on this position can be explained by the co-complex structure. It has been recognized previously that FP-3 seems to be more difficult to address with peptide-based inhibitors. The co-crystallization of the proteases with small molecule inhibitors revealed subtle differences in the actives sites of the two proteases that may be the molecular basis of the observed different substrate preferences. The overall secondary structure of the two enzyme-inhibitor complexes was found to be highly similar, with no notable movements in the backbone or loop regions. The superimposition of the respective substrate-specificity determining S_2 subsites, however, revealed two amino acid substitutions that slightly alter the nature of the subsite.[51]

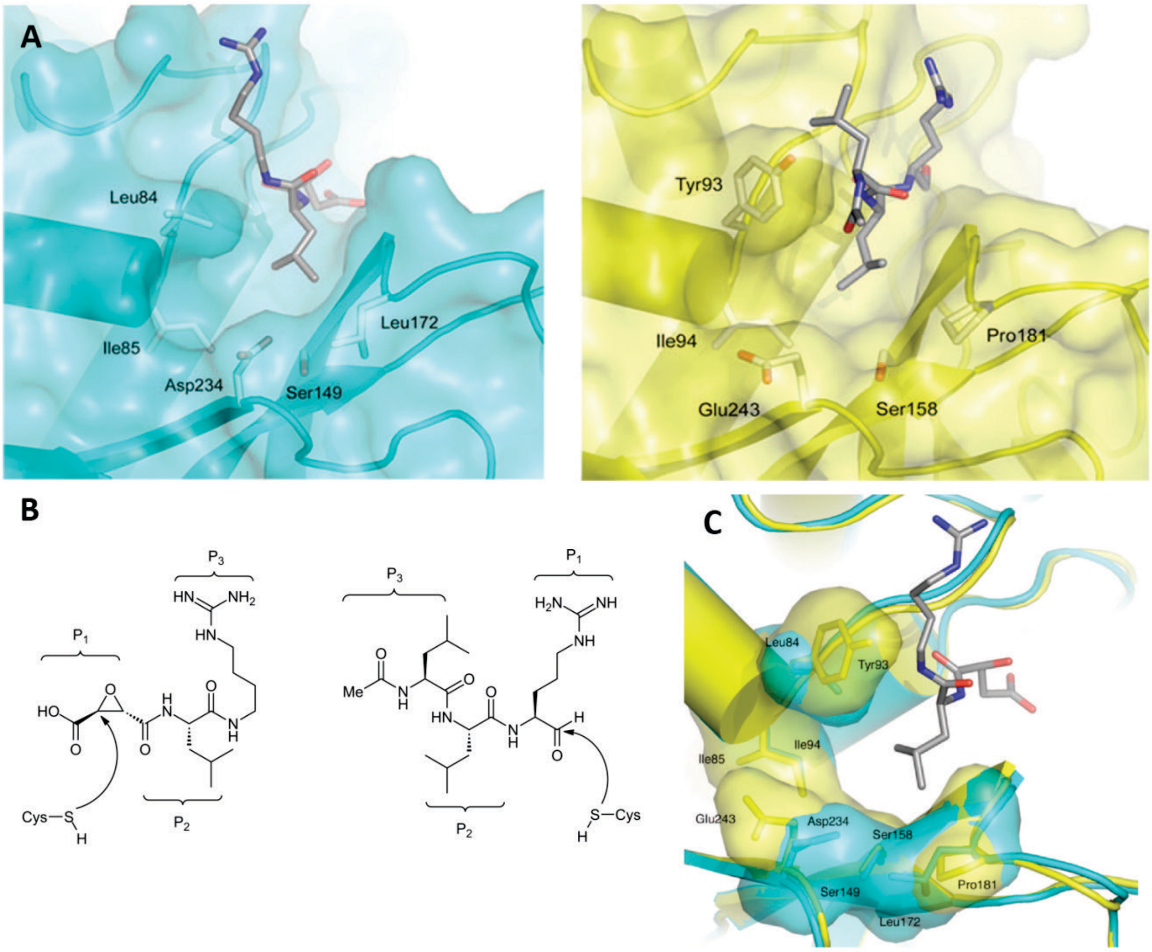
A
Leu84
Ile85
Asp234
Ser149
Leu172
Tyr93
Ile94
Glu243
Ser158
Pro181
B
P1
HN
NH2
HN
HO
O
O
H
N
O
N
H
Cys—S
H
P2
P3
Me
N
H
O
HN
O
N
H
H2N
NH
NH
H
O
S—Cys
H
P2
P1
C
Leu84
Tyr93
Ile85
Ile94
Glu243
Asp234
Ser158
Ser149
Pro181
Leu172

Figure 14 (adapted from[51]): Close-up on the structures of FP-2 and FP-3 active sites in complex with small molecule inhibitors. **A**: left: surface representation of FP-2 in complex with E-64, the inhibitor is shown in gray, right: surface representation of FP-3 with leupeptin, the inhibitor is represented in gray; **B**: chemical structures of E-64 (left) and leupeptin (right), the putative attack of the catalytic cysteine is indicated; **C**: superimposition of the S_2 subsites, color in accordance with **A**.

The first substitution is the replacement of Asp-234 in FP-2 for Glu-243 in FP-3. This position is generally non-conserved throughout the clan CA enzymes. The amino acid is located at the base of the S_2 subsite; but as both inhibitors used in the co-crystallization experiment contain a leucine at the P_2 position, a hydrogen bond with the carboxylic acid functionality can be excluded. In the FP2-E-64 crystal structure, the Asp-234 is rotated away from the inhibitor, but is prevented from pointing toward the solvent. In the FP-3-leupeptin crystal structure, Glu-243 is also rotated away from the inhibitor; in this case, however, it points outward into the solvent and forms an additional hydrogen bond to Tyr-245. Overall, the base of the S_2 subsite in FP-3 is more exposed to the solvent allowing additional stabilization. Glu-243 in comparison to Asp-234 is more bulky and due to the additional carbon-carbon-bond more flexible, thereby altering the base of the subsite. The second amino acid substitution is the replacement of Leu-84 to Tyr-93 in FP-3, resulting in an overall narrowing and thereby restricted accessibility of the S_2 subsite. The position of Tyr-93 has been suggested as one of two gatekeeper residues in a FP-3 homology model, pinpointing that this residue together with the Asp-234 to Glu-243 modification contributes to the different preferences of FP-2 and FP-3.[51]

The similar activities of FP-2 and FP-3 have resulted in the development of compounds that inhibit both proteases, although most inhibitors are developed for FP-2. The peptidic inhibitors developed for FP-2 and FP-3 are based on a leucine or an alternative hydrophobic residue in the P_2 position and incorporate a reactive group in the P_1' position that is known for the interaction with cysteine proteases. Variation can be included in the P_3 position to enhance selectivity and pharmacological parameters.

Fluoromethyl ketone inhibitors (Fig. 15) are known as highly reactive, selective and irreversible inhibitors for cysteine proteases. A number of fluoromethyl ketone-based FP-2 inhibitors was tested, among them, (*Z*)-Phe-Arg-CH_2F was distinguished as the most potent inhibitor of FP-2 (IC_{50} = 0.36 nM). The inhibitor furthermore blocked hemoglobin hydrolysis and inhibited the growth of cultured parasites, both at nanomolar concentrations (IC_{50} = 0.10 μM for hemoglobin hydrolysis; IC_{50} = 64 nM for malaria parasite development) and was active at nanomolar concentrations in four different *P. falciparum* strains while being non-toxic in four human cell lines. Other fluoromethyl ketone inhibitors incorporating a morpholine urea (Mu) moiety at P_3 were able to inhibit FP-2 at nanomolar or even picomolar concentrations. The inhibitor Mu-Phe-HomoPhe-CH_2F was not only an effective inhibitor of FP-2 (IC_{50} = 3 nM), but also inhibited the rodent *P. vinckei* cysteine protease most effectively (IC_{50} = 5.1 nM). The *P. vinckei* cysteine protease is biochemically very similar to FP-2 in terms of molecular weight, pH preferences, substrate specificity and inhibitor sensitivity and can be tested *in vivo* in a murine malaria model. Of the *P. vinckei* infected mice treated parenterally with the inhibitor (four doses / day, four day treatment), 80% were cured by inducing a long-lasting immunity.[55]

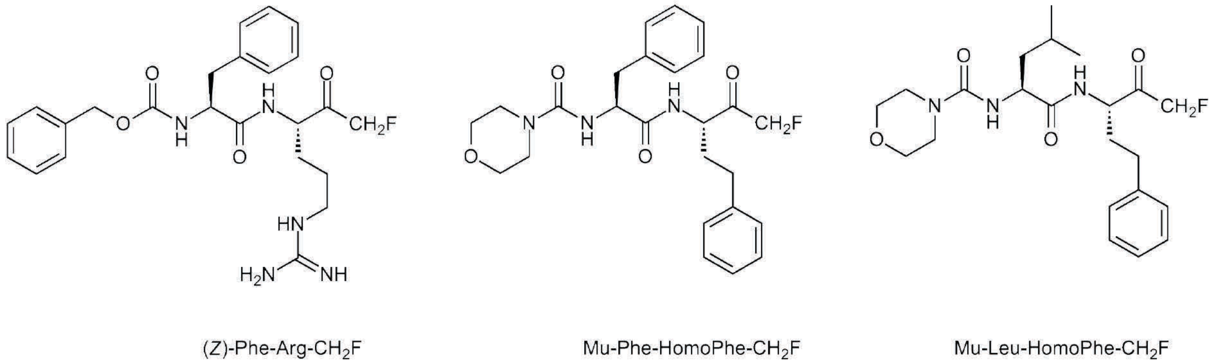

(Z)-Phe-Arg-CH_2F Mu-Phe-HomoPhe-CH_2F Mu-Leu-HomoPhe-CH_2F

Figure 15: Examples of highly effective FP-2 fluoromethyl ketone inhibitors: IC_{50}((*Z*)-Phe-Arg-CH_2F) = 0.36 nM; IC_{50}(Mu-Phe-HomoPhe-CH_2F) = 3 nM; IC_{50}(Mu-Leu-HomoPhe-CH_2F) = 0.42 nM.[55]

Another class of irreversible covalent inhibitors are the peptidyl vinyl sulfones. They act by the addition of the reactive cysteine thiol to the Michael acceptor system. The generally-accepted mechanism includes the polarization of one of the sulfone oxygens by a protonated histidine present in the proximity of the active site which should enhance the nucleophilic attack on the β-carbon. The resulting negative charge on the α-carbon is then eliminated by deprotonation of the participating histidine (Fig. 16).[55]

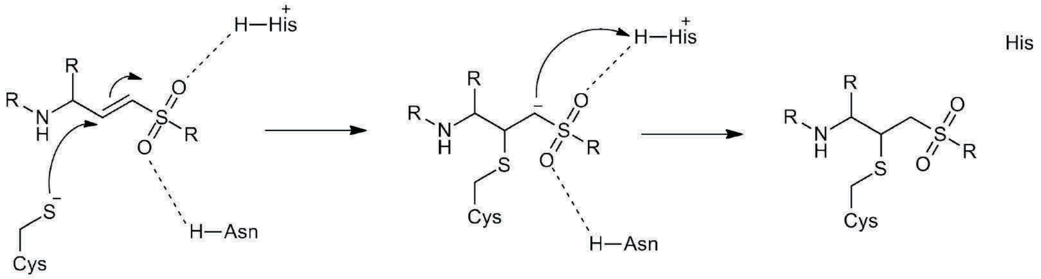

Figure 16 (adapted from[55]): Proposed reaction mechanism for the vinyl sulfone inhibitors.

Vinyl sulfones are highly specific inhibitors of cysteine proteases, being unreactive to other protease classes (despite the proteasome) as well as to non-active site cysteines or free thiols such as glutathione. Extensive SAR studies have been carried out for the vinyl sulfones starting from peptidyl vinyl sulfones analogous to the fluoromethyl ketones described before (Fig. 17).[55]

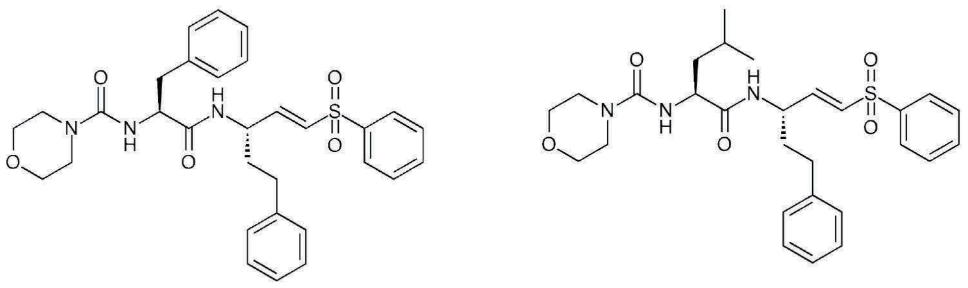

Mu-Phe-HomoPhe-VSPh

Mu-Leu-HomoPhe-VSPh

Figure 17: Vinylsulfone inhibitors incorporating a morpholine urea.[55]

These first inhibitors were tested against FP-2 and its *P. vinckei* analog, showing similar inhibitory effects against both targets. Mu-Phe-HomoPhe-VSPh was evaluated as a mid-nanomolar inhibitor of both proteases (IC$_{50}$ (FP-2) = 0.08 μM; IC$_{50}$ (*P. vinckei*) = 0.1 μM). The homologous Mu-Leu-HomoPhe-VSPh inhibitor however showed an increased activity against FP-2, but a decreased activity against the homologous *P. vinckei* protease (IC$_{50}$ (FP-2) = 0.003 μM; IC$_{50}$ (*P. vinckei*) = 0.2 μM), indicating a critical role of the inhibitor peptide portion for specificity towards the different target enzymes.

To improve the bioavailability as well as the solubility, the morpholine urea was replaced by an *N*-methyl piperazyl urea (*N*-Pipu) (Fig. 18) which resulted in a slightly increased IC$_{50}$ of 8.7 nM, but this new analog showed a decreased IC$_{50}$ against *P. falciparum* (IC$_{50}$(Mu-Leu-HomoPhe-VSPh) = 22 nM *vs.* IC$_{50}$(*N*-Pipu-Leu-HomoPhe-VSPh) = 4.5 nM). A further improvement in the activity against *P. falciparum* could be achieved by replacing the original morpholine urea by a 4-pyrrole-piperidine urea (4-Py-Pipu) moiety. (IC$_{50}$(Mu-Leu-HomoPhe-VSPh) = 22 nM *vs*. IC$_{50}$(4-Py-Pipu-Leu-HomoPhe-VSPh) = 1.6 nM); this compound also inhibited FP-2 at low nanomolar concentrations (IC$_{50}$ = 6.7 nM).[55]

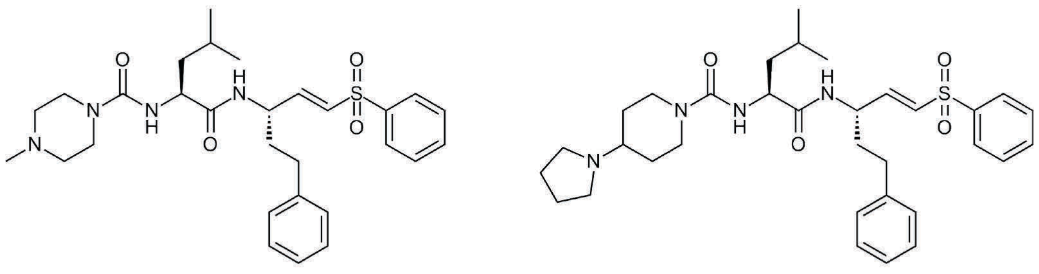

N-Pipu-Leu-HomoPhe-VSPh 4-Py-Pipu-Leu-HomoPhe-VSPh

Figure 18: Improved vinyl sulfone inhibitors. The compounds showed an improved inhibition of *P. falciparum* (IC_{50} = 4.5 nM for *N*-Pipu-Leu-HomoPhe-VSPh and IC_{50} = 1.6 nM for 4-Py-Pipu-Leu-HomoPhe-VSPh) in comparison to the original Mu-Leu-HomoPhe-VSPh (IC_{50} = 22 nM). The inhibition of FP-2 was slightly increased for the new compounds (IC_{50} = 8.7 nM for *N*-Pipu-Leu-HomoPhe-VSPh and IC_{50} = 6.7 nM for 4-Py-Pipu-Leu-HomoPhe-VSPh) compared to Mu-Leu-HomoPhe-VSPh (IC_{50} = 3.0 nM).[55]

In another series of inhibitors, a sulfonamide moiety was used instead of a sulfone residue, resulting in a higher potency (FP-2 inhibition: IC_{50} = 2.3 nM) while the excellent inhibition of *P. falciparum* growth was maintained (IC_{50} = 4.4 nM) (Fig. 19).[55]

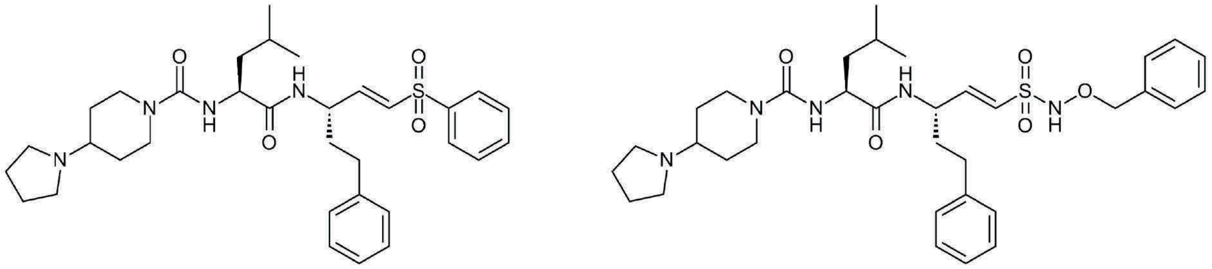

4-Py-Pipu-Leu-HomoPhe-VSPh 4-Py-Pipu-Leu-HomoPhe-VSA-OPh

Figure 19: Comparison of vinyl sulfone and vinyl sulfonamide inhibitors of FP-2. The inhibition of FP-2 was improved (IC_{50} = 8.7 nM for *N*-Pipu-Leu-HomoPhe-VSPh and IC_{50} = 2.3 nM for 4-Py-Pipu-Leu-HomoPhe-VSA-OPh) while the excellent inhibition of *P. falciparum* growth was maintained (IC_{50} = 4.5 nM for *N*-Pipu-Leu-HomoPhe-VSPh and IC_{50} = 4.4 nM for 4-Py-Pipu-Leu-HomoPhe-VSPh).[55]

In contrast to the previously described fluoromethyl ketone and vinylsulfone inhibitors, peptide aldehyde and α-ketoamides inhibit cysteine proteases in a covalent but reversible manner. So far, they are the most potent inhibitors of FP-2 and show also activity against FP-3. Mu-Leu-HomoPhe-al as well as Mu-Leu-HomoPhe-(CO)-Phe-NH_2 exhibit potent inhibitory activity against FP-2 (IC_{50} = 1 nM for both inhibitors) and are potent anti-plasmodial agents against different strains of *P. falciparum* (low nanomolar IC_{50} values) (Fig. 20). However, the inhibitors were less potent in the mouse model of *P. vinckei* malaria, emphasizing once more the difference between the falcipain targets in *P. falciparum* and *P. vinckei* that represents a serious problem in malaria drug research for compound validation in rodent models.[55] This issue might be overcome by the introduction of recombinant rodent parasites expressing the human *P. falciparum* proteases or by the introduction of a *P. falciparum* mouse model.[50]

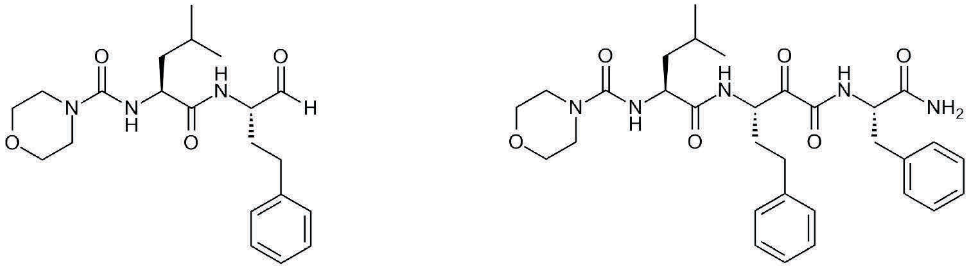

Mu-Leu-HomoPhe-al

Mu-Leu-HomoPhe-(CO)-Phe-NH_2

Figure 20: Peptide aldehyde and α-ketoamide inhibitors based on potent peptidic core structures.[55]

The major drawbacks of peptidic inhibitors in terms of drug development are their low bioavailability as well as their susceptibility towards degradation by endogenous proteases. To overcome this weakness and to improve pharmacokinetic and -dynamic parameters, a common strategy is the replacement of peptidic structures by rigid scaffolds locking a defined conformation and mimicking the secondary structure motif. The β-turn motif has in this context been suggested as for a suitable motif for enhancing bioactivity. 1,4-benzodiazepines have been reported as β-turn mimetics with favorable pharmacodynamics. Consequently, FP-2 inhibitors based on the 1,4-benzodiazepine core in the P_2 position (as replacement for leucine) have been developed. For example, the peptidomimetic 1 (Fig. 21) showed a potent inhibition of FP-2A and B (IC_{50} = 8.7 μM for FP-2A; IC_{50} = 25.9 μM for FP-2B). The peptidomimetic 2 (Fig. 21), in which the masked aspartyl aldehyde functionality from peptidomimetic-1 was replaced by a classical Michael acceptor displayed a low dissociation constant for FP-2 (k_{inac} (min^{-1}) / K_{inac} (μM) = 0.10/0.32)and potent inhibition of *P. falciparum* growth (IC_{50} = 9.1 μM). [49,55]

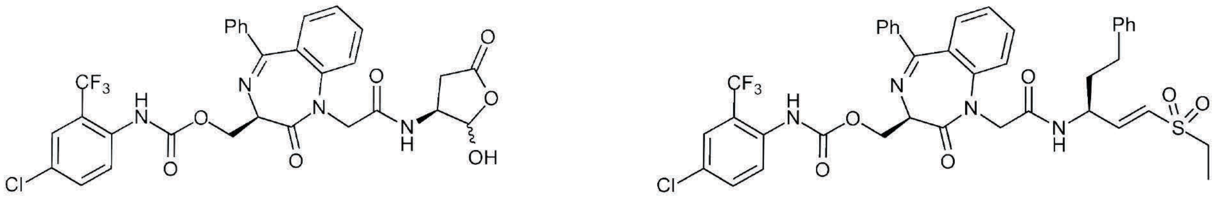

peptidomimetic 1

peptidomimetic 2

Figure 21: Peptidomimetic FP-2 inhibitors based on the 1,4-benzodiazepine scaffold. [49,55]

Besides the 1,4-benzodiazepine core, other peptidomimetic scaffolds that lock the peptide backbone conformation have been examined as potential replacements for the P_2 amino acid. For example the use of the 5-aminopyridone (peptidomimetic 3), a pyridone (peptidomimetic 4) or a pyrrolidone (peptidomimetic 5) motif with different electrophilic warheads (Fig. 22) also resulted in potent anti-plasmodial inhibitors.[49]

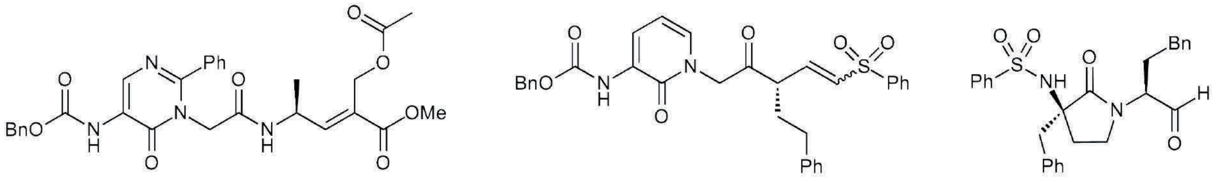

peptidomimetic 3

peptidomimetic 4

peptidomimetic 5

Figure 22: Structurally diverse peptidomimetic inhibitors with potent anti-plasmodial activities against different strains of *P. falciparum* and/or potent FP-2/FP-3 inhibition. Peptidomimetic 3: IC_{50} = 0.016 μM against D6, IC_{50} = 0.018 μM against W2; peptidomimetic 4: IC_{50} = 5.7 μM against 3D7, IC_{50} = 9.0 μM against TM6; peptidomimetic 5: IC_{50} = 0.05 μM against FP-2/FP-3.[49]

Further research has been conducted in the field of non-peptidic inhibitors of falcipains. Several potent inhibitors have been synthesized based on the chalcone natural product licochalcone A, which was the first compound from this class reported to exhibit antimalarial activity. Furthermore, the inhibitory potential of isoquinoline and thiosemicarbazone inhibitors has been investigated (Fig. 23). So far, no enzyme inhibition mechanism for the non-peptidic inhibitors could be determined, only few docking experiments have revealed putative structure-activity relations.[55]

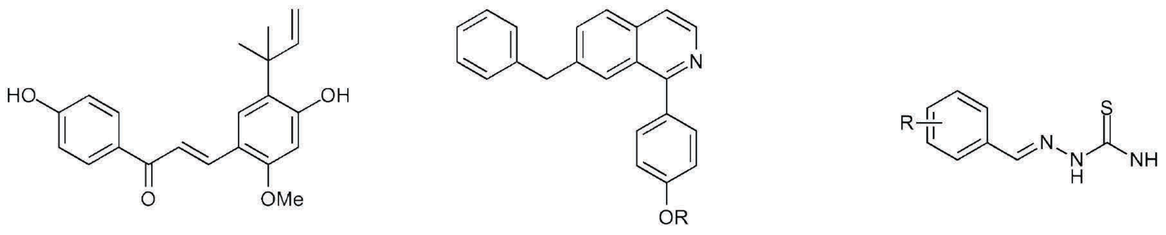

licochalcone A isoquinolines thiosemicarbazones

Figure 23: Structures of non-peptidic falcipain inhibitors.[55]

Considering all potential drug targets in anti-malaria therapy, the falcipains seem to represent an appropriate class of target enzymes. FP-2 and FP-3 are crucial (hemo)globinases of the malaria-causing pathogens, ensuring the nutritious supply of the parasite in the erythrocytic stages as well as the progression of the life cycle. Consequently, FP-3 activity is essential for the survival at late developmental stages. Attempts to disrupt FP-3 expression genetically failed, emphasizing the crucial role of this protease.

Nevertheless, inhibitors targeting falcipains usually are designed to inhibit FP-2. So far, no inhibitor explicitly targeting FP-3 has been reported. In the past decades, resistances against the “classical” antimalarial drugs have evolved, thereby underlining the requirement for new therapeutic targets and new chemotherapeutics. Studies of parasital resistance against a vinylsulfone falcipain inhibitor have revealed a very slow selection of resistant mutants and a complex mechanism of drug resistance, holding the promise that falcipain inhibitors may not be as prone to development of resistances as other substance classes have been. Hence, the falcipains remain an interesting and sensible target for the investigation of antimalarial compounds.[50]

1.6 Proteomics as a technique for analyzing the mode-of-action of small molecules

The term "proteome" was used for the first time in 1995 to describe the total complement of proteins encoded by a genome. [56] The individual proteome expressed in a distinct cell or tissue type is subject to fluctuations that are caused by internal influences such as the developmental stage and mutation or external influences such as stress response, drug perturbation or pathogens. The research area of proteomics is nowadays defined as the systematic study of the many and highly diverse properties of proteins on a large scale. This includes expression levels, post-translational modifications and interactions with other proteins. The goal is to gain comprehensive insights on the structure, function and control of biological systems in healthy and diseased organisms.[57,58]

The proteomics approach emerged originally from the genome sequencing projects that had set out to map and sequence complete genomes and resulted in the finding that many gene products did not have an assigned function.[58] Moreover, the relatively small number of genes identified for the human genome compared to the larger number of proteins expressed in the different cells and tissues emphasizes the need of an alternative technique to mRNA expression level analysis and the requirement to reconsider traditional concepts such as the "one gene - one protein" hypothesis.[59] In both cases, proteomics can serve as a powerful tool to identify proteins, assign them a function and determine their role in a network of protein-protein interactions.

As a consequence of the genome sequencing projects and the advent of proteomics, the systems biology approach has recently emerged aiming at the determination of the spatiotemporal distribution of biomolecules and their organization into networks and pathways. To reach this highly ambitious (and potentially even unattainable) goal, proteomics is regarded as a rich source of information because proteins are involved in almost all biological processes. An understanding of their diverse function will provide access to an elaborate understanding of physiological processes.

In the early days of proteomic research, the goal was to rapidly identify the full set of proteins expressed in an organism which has so far not been achieved for any organism. The goals of proteomics have however shifted nowadays towards a systematic determination of selected processes in which the diverse properties of proteins are studied, including their sequence, structure and state of modification, the quantity and cellular distribution, their activity and the interactions with one another.[58] The ultimate goal of proteomics is not only to reveal all proteins of an organism and assign their individual functions, but also to identify all isoforms and modifications of those proteins, the interactions between the proteins and higher-order complexes; in other words, proteomics studies proteins “post-genomic”.[60] In general, the experimental set-up required for proteomics is by far more complex than the one required for genomics. Nevertheless, proteomics has been impressively successful in a relatively short period of time and has provided insights into the gene expression of different cell and tissue types in healthy and diseased states. Furthermore is has helped to dissect cellular pathways and led to a deeper understanding of molecular physiology. In terms of technological development, proteomics is supplied with mature tools that are, nevertheless, under constant refinement.[58,60] Consequently, proteomics has been provided with elaborate instrumentation and has conceptually become the method of choice for the analysis of biological systems, yet there are still some challenges that have to be met.

As an analytical method for proteomics research, mass spectrometry has become the most essential technique. To be able to analyze a molecule by mass spectrometry, the molecule of interest first needs to be ionized, enabling its transfer to the gas phase, in which it is then analyzed within the mass spectrometer. The mass of the analyte is measured as the mass-to-charge ratio, m/z. Initial attempts to ionize proteins or peptides with the given ionization techniques proved difficult, leading to massive fragmentation of the sensitive molecules. The development of mild ionization techniques for biomolecules was a major breakthrough in the field, enabling a rapid analysis and identification of proteins and pushing forward all research concerned with proteins. The relevance of this advance in technology is demonstrated by the recognition with the Nobel prize in 2002.[61]

The two techniques for mildly ionizing protein molecules and thereby enable their transfer to the high vacuum system of the spectrometer are electrospray ionization (ESI) and matrix-assisted laser desorption ionization (MALDI). Both methodologies quickly penetrated into protein research once they had been combined with commercial mass spectrometers.

The MALDI-type ion sources (Fig. 24) are usually combined with time-of-flight (TOF) analyzers, in which the ionized molecules are accelerated and separated by their different velocities. Since all ions are accelerated with the same energy, the lighter ions reach a higher velocity than heavier ions with the time of flight being proportional to $\sqrt{m/z}$.

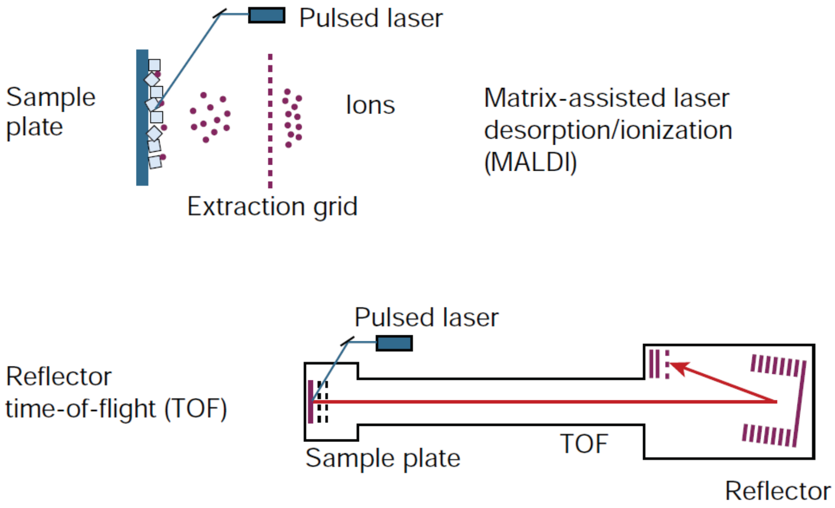
Pulsed laser
Sample plate
Ions
Extraction grid
Matrix-assisted laser desorption/ionization (MALDI)
Pulsed laser
Reflector time-of-flight (TOF)
Sample plate
TOF
Reflector

Figure 24 (adapted from[61]): Set-up of a MALDI ion source (top), MALDI-TOF instrument set-up (bottom)

MALDI allows the determination of the mass of a peptide or protein with high accuracy and a broad spectrum of masses can be addressed. The mass of a protein is, however, not a uniquely identifying feature, so further measurements are necessary to determine the identity of a protein. In the so-called peptide mass fingerprinting a protein of interest is digested with an enzyme with known cleavage specificity to generate smaller peptide fragments that are then analyzed by mass spectrometry. The fragments generated by proteolysis are unique for each protein and can therefore be used to identify the protein by comparison of the fragments identified by mass spectrometry with a sequence database. The accuracy of this method depends on the specificity of the enzyme used in the digest (usually trypsin), on the number of fragments identified and on the accuracy of the mass spectrometer. Owing to the highly increased accuracy of MALDI, the peptide mass fingerprinting using MALDI-TOF has become the method of choice to identify proteins that were separated by 2D electrophoresis and then individually digested to obtain the peptide fragments.[61]

The ESI ion sources (Fig. 25) are usually combined with triple-quadrupole or ion trap instruments, a more recent combination includes hybrid-quadrupole TOF MS/MS spectrometers. All of the instruments mentioned are not only able to measure a peptide mass, they are also able to isolate selected ions according to their *m/z* ratio and fragment the ions in the gas phase for recording of MS/MS spectra.

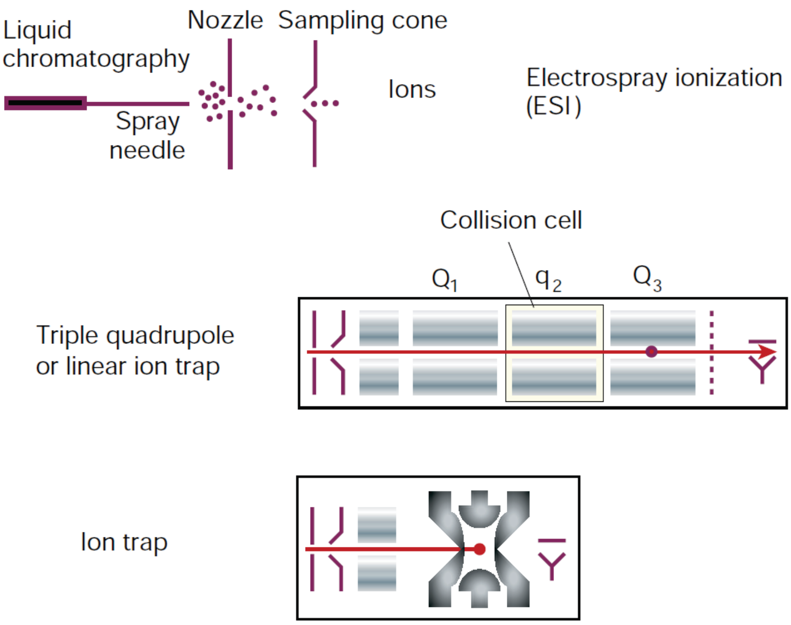

Figure 25 (adapted from[61]): Set-up of an ESI ion source (top), mass analyzers typically combined with ESI: triple-quadrupole/linear ion trap (middle) or ion trap (bottom)

This fragmentation is specific and also sequence-dependent, the MS/MS spectrum of a protein can, in principle, be used to determine the sequence. The MS/MS spectrum can uniquely identify a protein by matching the fragments to a database and the accuracy of this type of identification is often higher than for peptide mass fingerprinting. A further advantage of ESI-MS/MS set-ups is their facile incorporation into existing protein purification systems such as HPLC, as both systems can be operated using the same solvents. Nanospray-ESI allows the direct injection of unseparated peptide mixtures into the mass spectrometer at very low flow rates and is able to reach much higher sensitivity than traditional ESI-MS. This method consumes only very small amounts of sample and owing to the low flow rate, it is possible to record fragment ion spectra of several precursor ions that can be observed. The precursor ions can either be selected manually by an operator or by computer-controlled software that allows the automatic measurement of MS/MS spectra for multiple peptide ions without operator intervention. These automatized analyses are mainly used in systems that are supplied online by an HPLC system and this approach is referred to as LC-MS/MS.[58,61]

A gel-independent alternative is the shotgun proteomics approach based on a LC-MS/MS methodology. This approach uses the combination of LC-MS/MS analysis with sequence database searches and is applied to the analysis of complex mixtures of peptides generated by proteolysis of a sample containing several proteins. It provides the opportunity to catalog hundreds to thousands of compounds from samples obtained from different sources.[58]

Besides the identification of proteins in complex protein mixtures, also the quantification of distinct proteins is of interest. Unfortunately, a regular mass spectrometric analysis does not provide quantitative information for mixtures of proteins because the signal intensity depends on the chemical composition of the peptide and the matrix and not on the abundance of a peptide in the mixture. A loophole to this dilemma is a technique known as isotope-tagging: Two peptides of identical chemical composition that nevertheless differ in their masses due to a different isotopic composition give identical and specific signals in a mass spectrometer based on the theory of stable isotope dilution.[58]

One technique following this methodology involves the use of isotope-coded affinity tags (ICATs). The reagents contain a linker region that incorporates either hydrogens or deuteriums to achieve the isotope dilution, a reactive group that chemically modifies the peptides and a biotin tag for the affinity purification of the tagged peptides. In a typical experiment, two samples are treated with one of the ICAT reagents, combined and digested. The tagged peptides are then selected by affinity purification and submitted to mass analysis. For each peptide two signals will then be obtained corresponding to the light and the heavy version, respectively. The signal intensities can in this case be used to quantify the amount of peptide. Furthermore, the sequences of the individual peptides can be determined from the MS/MS spectra (Fig. 26).[58,62]

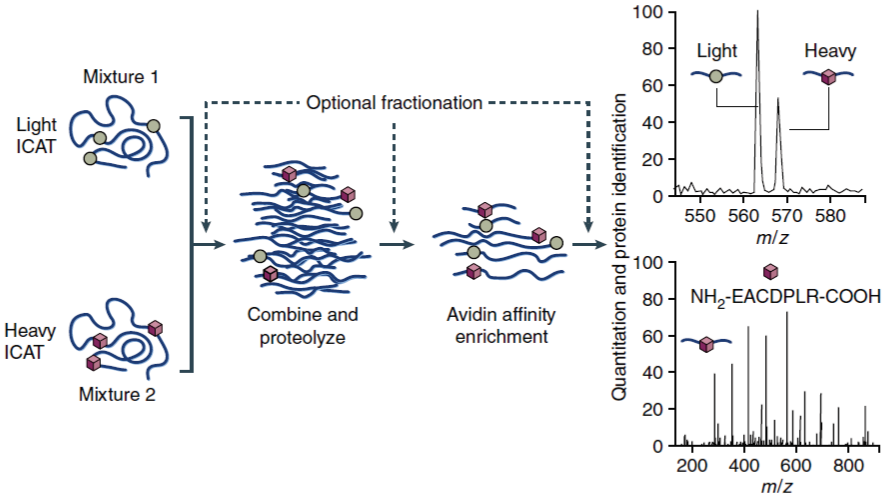
Mixture 1
Light ICAT
Heavy ICAT
Mixture 2
Optional fractionation
Combine and proteolyze
Avidin affinity enrichment
Quantitation and protein identification
100
80
60
40
20
0
Light
Heavy
550 560 570 580
m/z
NH$_2$-EACDPLR-COOH
200 400 600 800
m/z

Figure 26 (adapted from[62]): Schematic representation of the ICAT experimental set-up.

Not surprisingly, proteomics has also become the major tool to investigate the mode-of-action of bioactive small molecules *via* elucidation of their direct protein targets. Moreover, chemical tools have been invented to reduce the data set in proteomics studies. Such approaches belong to the evolving field of chemical proteomics.[60] The most prominent chemical proteomics technology thereby is an approach known as activity-based protein profiling (ABPP). In the present PhD thesis, ABPP has been used to determine the direct target of synthesized bioactive small molecules and will therefore be described explicitly in the next section.

1.6.1 Activity-based protein profiling - ABPP

The assignment of protein functions is one of the central aims of proteomics research. After the completion of numerous sequencing projects it became clear that a large part of the identified gene products did not have an assigned function. Activity-based protein profiling (ABPP) has become the key technology in the field of chemical proteomics that set out to assign the function of active enzymes. It has emerged into a powerful tool for analyzing samples isolated from all types of cells and tissues and recent advances allow an application even in native biological systems.[63]

In ABPP, activity-based probes (ABPs) are used to selectively label active enzymes. To this end, an activity-based probe consists of several subunits: First, an ABP features a reactive group or “warhead” that is supposed to react with the active site of a distinct subset of enzymes. Ideally, the reactive group labels a distinct number of enzymes belonging to the same class and shows little cross-reactivity with enzymes of other classes. Generally, there are two types of reactive groups: one type is represented by electrophilic groups that react with the active center nucleophiles, the second group are photoreactive moieties that react with residues in the proximity of the reactive site upon UV irradiation.

The second part of an activity-based probe is the tag which is connected to the reactive group by a variable linker region. The linker region is not only required to connect the reactive group and the tag, it also ensures an adequate distance between the two groups to prevent an interference of the tag with the reactive group’s reactivity.

Finally, ABPs feature reporter tags. These can for example be fluorescent dyes such as rhodamine for direct visualization. Also biotin can be used that has a dual function: it can be used as a reporter in a Western blot, but it can also be used to purify the labeled proteins by affinity chromatography. A further possibility is the use of alkyne or azide tags that enable the attachment of a reporter group after the actual labeling reaction by a copper-mediated 1,3-dipolar Huisgen cycloaddition (click reaction). The advantage of using activity-based probes with click tags is the reduced size of the tag that does not interfere with the labeling reaction. Due to the bioorthogonality of the click reaction the reaction can even be carried out *in vivo* if desired. The respective tags require different read-out or work-up procedures after the labeling experiment and the used reporter tag dictates the options for the read-out.[63] Enhancements to the "traditional" reporter tags are trifunctional activity-based probes that consist of a reactive group and two tags, for example a biotin for purification and visualization in a Western blot and a rhodamine for the direct in-gel detection by fluorescence.[64]

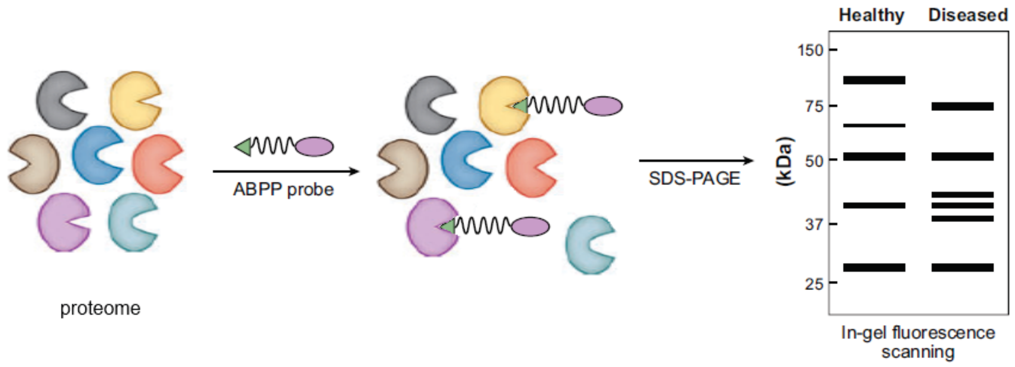

Figure 27 (adapted from[63]): Schematic set-up of a typical ABPP experiment.

As indicated in Figure 27, the most important experimental platform for the analysis of ABPP experiments is in-gel visualization. After the labeling experiment the labeled proteins are separated by gel electrophoresis, in most cases a standard 1D-SDS-PAGE is sufficient. The visualization then depends on the reporter that was used. After having visualized the proteins, their identity can be determined by mass spectrometry. The gel-based methods for ABPP are still the most widely used method for the rapid and comparative analysis of proteomes.[63]

In addition, gel-independent methods based on LC-MS have been developed for ABPP. Such mass spectrometry-based ABPP approaches (Fig. 28) can be performed in two different manners: on the one hand, the target protein of a probe can be determined; on the other hand, peptides derived from the labeled protein can be identified. The first approach represents a combination of ABPP and multidimensional protein identification technology (ABPP-MudPIT) and uses biotin probes. After the labeling with the probe, the labeled enzymes are enriched by using streptavidin beads, followed by on-bead digestion with trypsin and analysis of the resulting peptides by LC-MS. This method has the capacity to identify 50 to 100 enzymes from one proteome (Fig. 28, A).

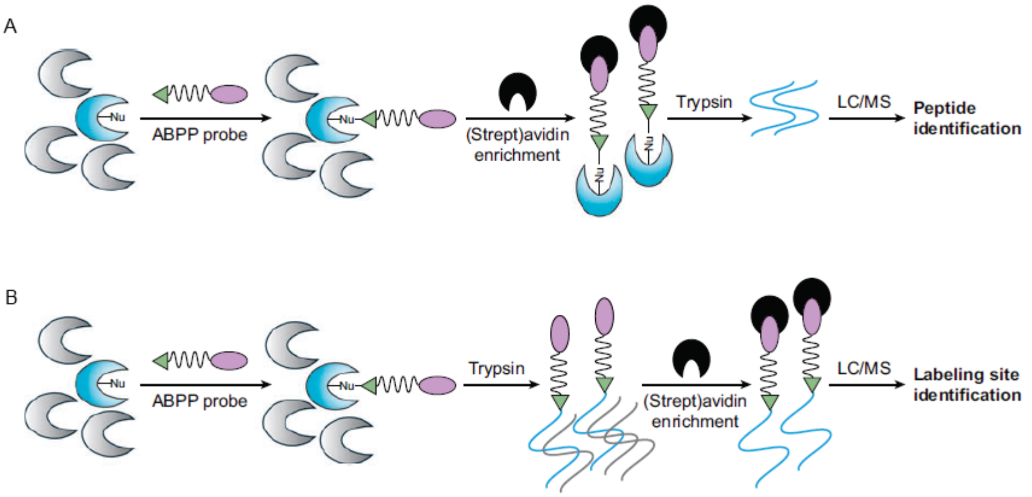
A
Nu
ABPP probe
Nu
(Strept)avidin enrichment
Nu
Trypsin
LC/MS
Peptide identification
B
Nu
ABPP probe
Nu
Trypsin
(Strept)avidin enrichment
LC/MS
Labeling site identification

Figure 28[63]: Gel-independent ABPP experiments based on LC-MS.
A: Experimental set-up for the ABPP-MudPIT approach; **B** experimental set-up for the ASPP approach.

The shortcoming of the ABPP-MudPIT approach is that it cannot directly identify the probe-labeled peptide from each target and therefore the active site of the enzyme. This can however be achieved by the so-called active site peptide profiling(ASPP)-approach in which the labeled proteins are first digested with trypsin and then only the labeled peptides are enriched using streptavidin beads (Fig. 28, B). This allows identification and assignment of only the peptides that are directly labeled by a probe. One has to note that MudPIT and ASPP are complementary methods. MudPIT is however far more sensitive than ASPP because it is able to identify more enzymes as multiple peptides originating from one protein are analyzed in contrast to single peptides in the ASPP approach. On the other hand ASPP provides the possibility to determine if a protein was really targeted at its active site or if the labeling occurred at another site.[63]

In general, two different ABPP approaches can be differentiated. Comparative ABPP is the method of choice to compare differentially perturbed proteomes and to identify the targets of an activity-based probe. In comparison to the more classical genomics-proteomics approaches, ABPP has some advantages. First of all, ABPP addresses active enzymes and is thereby able to enable access to proteins that are just activated by post-translational modifications, making ABPP a method to identify post-translational modifications and to study their functional effect. Moreover, in ABPP, enzymes are labeled in relation to their activity and not due to their abundance. This allows to target enzymes with a low abundance that normally fall through the grid of traditional profiling.

Besides the comparative ABPP, a competitive ABPP set-up is possible as well. This approach enables the identification of enzyme inhibitors and is therefore a powerful tool for drug discovery. In a general set-up, the proteome of interest is pre-incubated with an inhibitor of interest and then treated with the activity-based probe. If an enzyme is inhibited, the protein band visible in an untreated sample decreases in intensity or (in the case of a very potent inhibition) vanishes completely. By treating a proteome with different inhibitors a reactivity profile of the inhibitors for distinct members of the proteome can be established (Fig. 29).[63]

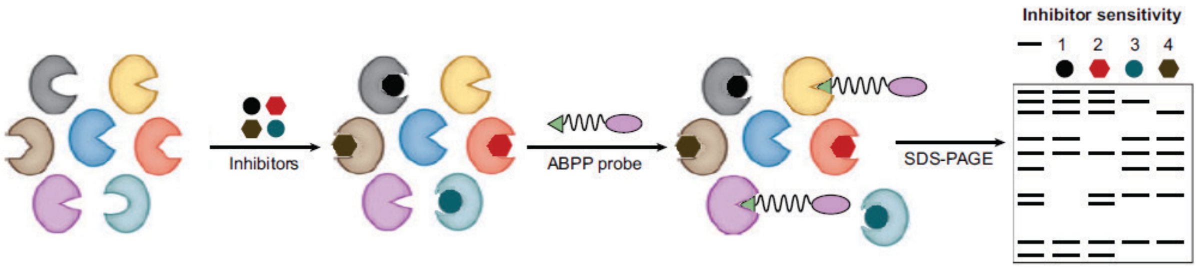

Figure 29 (adapted from[63]): Schematic experimental set-up of a competitive ABPP experiment.

Once an inhibitor for a certain enzyme has been identified, it is also possible to determine the inhibitory potency quantitatively, for example, an IC_{50} can be determined. To achieve this, the comparative assay is repeated using a fixed excess amount of the activity-based probe and different concentrations of the inhibitor. By monitoring the appearance or disappearance of the labeled enzyme in the gel at the different concentrations of inhibitor, its inhibitory potency can be determined. The concentration experiments can be carried out either with the whole proteome sample or with isolated enzymes obtained for example by recombinant expression.

ABPP can address a great variety of different enzymes, depending on the respective activity-based probe. The most prominent examples of enzyme classes that are studied by ABPP are the highly important and ubiquitously abundant serine and cysteine proteases. The most prominent activity-based probes for serine proteases are based on phosphonate residues, such as fluorophosphonates or aryl-phosphonates (Fig. 30). They represent very selective serine protease probes owing to the high oxophily of the phosphorus.[63]

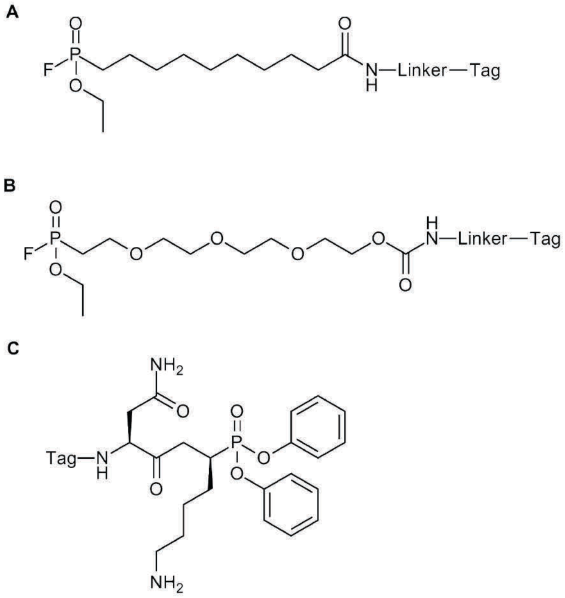

Figure 30 (adapted from[63]): Examples of phosphonate-based activity-based probes for serine proteases. **A**: a fluorophosphonate probe with an alkyl linker; **B**: a fluorophosphonate probe with a polyethylenglycol linker; **C**: an aryl-phosphonate probe.

Activity-based probes directed against cysteine proteases contain highly reactive electrophiles such as epoxides, halomethyl ketones or unsaturated systems that can be attacked by the nucleophilic thiol of the active center cysteine. Many activity-based probes for cysteine proteases are based on the broad band cathepsin inhibitor E-64; modified versions of E-64, for example, a fluorescently-tagged version has found broad applications (Fig. 31).[63]

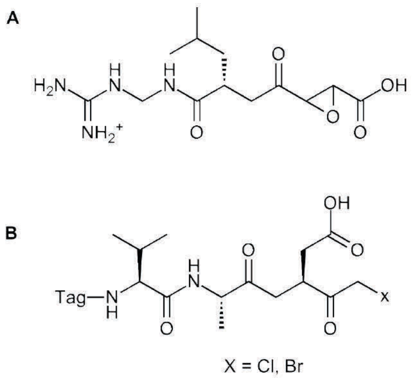

Figure 31 (adapted from[63]): Examples of activity-based probes for cysteine proteases. **A**: the cathepsin inhibitor E-64, a basis for various activity-based probes for cysteine proteases; **B**: a halomethyl ketone-based probe for cysteine proteases.

Besides using well-known probes as a basis for activity-based protein profiling, it is also possible and reasonable to convert putative inhibitors into activity-based probes and investigate their activity. The possibility to incorporate for example an azide or an alkyne tag into an existing inhibitor, derived for example from a natural product, makes the conversion to an activity-based probe a task that can readily be incorporated into an existing synthesis. Such an approach has for example been followed in the present PhD work.

In summary, activity-based protein profiling has evolved to become a fundamental technology platform in proteomics. It enables the rapid and experimentally facile analysis of highly differential proteomic samples in a comparative manner. It can be used to identify targets, determine enzyme functions and activities and help to gain insights into complex biological systems. ABPP is used on a broad basis, its applications range from fundamental research in biology to highly versatile profiling in a clinical environment to applications in drug discovery.[63]

1.7 Synthesis of peptidic natural products

The total synthesis of natural products is until today regarded as the flagship of organic chemistry. Natural products have always been a challenge to be met; their complex nature has inspired, improved and pushed forward efforts towards new or improved synthetic methods or synthesis strategies. The application of new concepts to the total synthesis of a natural product can demonstrate the scopes and limitations of a novel method and bridge the gap between a model reaction and the application on a level of higher molecular complexity.

The motivations for a chemist to enter the field of natural product synthesis can be diverse: the complex molecular structure, representing an intellectual challenge and the prospect of developing novel synthetic strategies may be one. Then again, another motivation could be the wish to synthetically generate a larger amount of a substance so far available only in minute amounts by isolation from natural sources. This motivation is usually accompanied by the wish to gain insight into the biomolecular activity of a natural product and the desire to elucidate its mode-of-action. This can contribute not only to medicinal research, but also to the fields of chemical ecology, biosynthesis studies or chemical biology. The biological investigation of natural products and the evaluation of their bioactivities are closely related to the wish and, in cases of medicinal research, the requirement to modify an existing structure in order to amend desired properties or to eliminate undesired features. An existing total synthesis is a valuable starting point for such investigations. Finally, the total synthesis of a natural product and the comparison of synthetic and natural material is the ultimate means to validate a proposed structure.[65,66]

Peptidic natural products represent a class of natural products of diverging levels of complexity, ranging from linear peptide sequences originating from a simple ribosomal assembly to highly complex architectures that represent a daunting challenge to any organic chemist. Different features of a peptidic natural product can contribute to the molecule’s overall complexity: unusually modified or built up from unnatural amino acids, polyketide fragments, rearranged elements that do not reveal the peptidic origin at first glance or highly complex stereochemical settings are only a few examples.

Peptidic natural products usually present a high density of functionalities and can be regarded as biologically pre-validated structures owing to their natural origin.[1] Just as any given natural product, a peptidic natural product is synthesized in the respective organism by different enzymes and is hence required to interact with different binding partners during the assembly; the functionalities or molecular structures needed for these interactions can serve as tools for the investigation of molecular interactions and biological function. Peptidic natural products may be used as lead structures for medicinal chemistry research, yet they are also important tools in chemical biology, helping to gain in-depth insight into biomolecular mechanisms of action.[3]

In the medicinal chemistry field, peptidic natural products may bridge the gap arising from the limited size of small molecules: some protein-protein interactions that are regarded as potential drug targets cannot be addressed by small molecules because the interaction surface is too large for a small molecule effector.[67]

The desire to use peptidic natural products in research implies the necessity to synthesize the molecule of interest in larger amounts and/or in modified forms. In over 100 years of research on peptide synthesis and on the development of new synthetic strategies, reliable methodologies have been developed for the synthesis of peptides of varying complexities. Different protecting group strategies that enable flexible approaches to a synthetic problem have been developed. Still, the most important protecting groups are the Boc/*t*-Bu groups and the Fmoc group, although the arsenal has been expanded to highly specialized groups meeting different requirements. The development of solid-phase peptide synthesis by Merrifield marks a major breakthrough for the field, enabling a quick and facilitated approach to the assembly of peptides. The use of an insoluble solid support not only enables a quick access to the desired structures, the process can be automated and combinatorial methods open the gate to highly diverse products. In addition to the original Merrifield resin, numerous solid supports have been developed that enable the attachment and the cleavage of diverse functional groups and converting solid-phase synthesis to a general method in organic chemistry beyond the assembly of peptides.[68]

The development of different coupling reagents meeting the requirements of peptide synthesis such as highly efficient and racemization-free coupling of sterically hindered or unreactive building blocks further enhanced the possibilities in peptide synthesis and opened the gateway to the synthesis of more complex molecules. Nowadays, innumerous methods and reagents for the formation of the crucial amide bond are available, guaranteeing high yields for this important reaction step.[69]

Naturally, methods developed for other fields of synthetic organic chemistry have found entrance into the syllabus of peptide synthesis which has evolved from the belittled “just amide bond formation” to a field of highly elaborate chemistry addressing highly complex structures.

Some structures that have until recently failed a proper addressing have now been synthesized successfully and their total syntheses demonstrate beautifully the status-quo of peptide syntheses.

An example for a natural product that includes highly racemization-prone amino acids that are extremely difficult to integrate into in an efficient synthesis is feglymycin. In their total synthesis of feglymycin, Süssmuth and coworkers have demonstrated how to chemically handle such delicate building blocks.[70] Another example are supplementary intramolecular linkages that often contribute to the complexity of the molecule and are another challenge to encounter in a total synthesis. Centers of atropisomerism that are created by certain side chain macrocyclizations represent a significant challenge in a total synthesis. The syntheses of the structurally related [71,72] natural products chloropeptin I and isocomplestatin by Hoveyda and coworkers [73-75] or the synthesis of complestatin by Boger *et. al.*[76,77] illustrate the difficulties provided by strained structures along with the handling of racemization prone phenylglycine derivatives. A very recent example illustrating the high complexity that can be displayed by a natural product with a peptidic core structure is the product class of kapakahines. Total syntheses have now been accomplished by the Baran group [78,79] as well as by Rainier and Espejo.[80,81]

Exemplary for structurally highly elaborate molecules with a peptidic core structure is the antibiotic vancomycin that has kept a number of research groups busy for several years until Evans and coworkers as well as Nicolaou and coworkers were able to present individual total syntheses.[82] The syntheses presented by these two groups have become classics of organic synthesis and will be presented here as examples for the state of the art in the synthesis of highly complex peptidic natural products in solution phase synthesis.

Nowadays, a peptide chemist can revert to a large number of methods to synthesize amino acid building blocks, choose from a wide variety of commercially available coupling reagents and methods, apply different orthogonal protecting group strategies and decide between a solution and a solid-phase strategy. Despite the enormous number of tools available for the synthesis of peptidic natural products, also the synthesis of less complex peptidic natural products can be a challenge, requiring precise synthesis planning and development of new methods. For example, some amino acids seem not to be compatible to the “standard” coupling procedures and require a different handling as demonstrated for example in the synthesis of tubulysin D by Ellman and coworkers.[83] Another challenge also in, on a first sight, less complex architectures are cyclization reactions. The syntheses of FK228 by Simon[84] and Williams[85] that are based on a macrolactonization strategy and the alternative approach by Ganesan[86] who applied a macrolactamization strategy, however, demonstrated how a “simple” condensation can hamper the accomplishment of a total synthesis. Some natural products also call for different ring closing strategies, if for example a double bond is featured in a macrocyclic core. Waldmann and coworkers as well as Kaiser and coworkers have demonstrated the incorporation of a ring closing metathesis in their syntheses of chondramide C[87] and syringolin A[88,89], respectively.

Solid-phase peptide synthesis has indeed revolutionized peptide chemistry and the syntheses of simple linear or also (cyclo)depsipeptides have become routine work. Still, a solid phase approach is only feasible if the reactions can be conducted with high yields and minimized racemization. The incorporation of non-standard amino acids into a solid-phase peptide synthesis is still a challenge that requires a precise strategic planning and preliminary studies in order to establish a fruitful synthesis. The synthesis of oxathiocoraline by Albericio *et. al* [90] is such an example for a solid-phase synthesis that has emerged from tedious preliminary studies.[91] In the present PhD thesis, synthetic methodologies for the synthesis of natural products on solid phase have been developed.

1.7.1 A total synthesis “classic”: vancomycin

Vancomycin was first isolated in 1956 from *Streptomyces orientalis* and is considered as the prototypical member of a family of antibiotics that possess an aryl-glycine rich heptapeptide core (the aglycon) decorated with different sugar residues (Fig. 32).

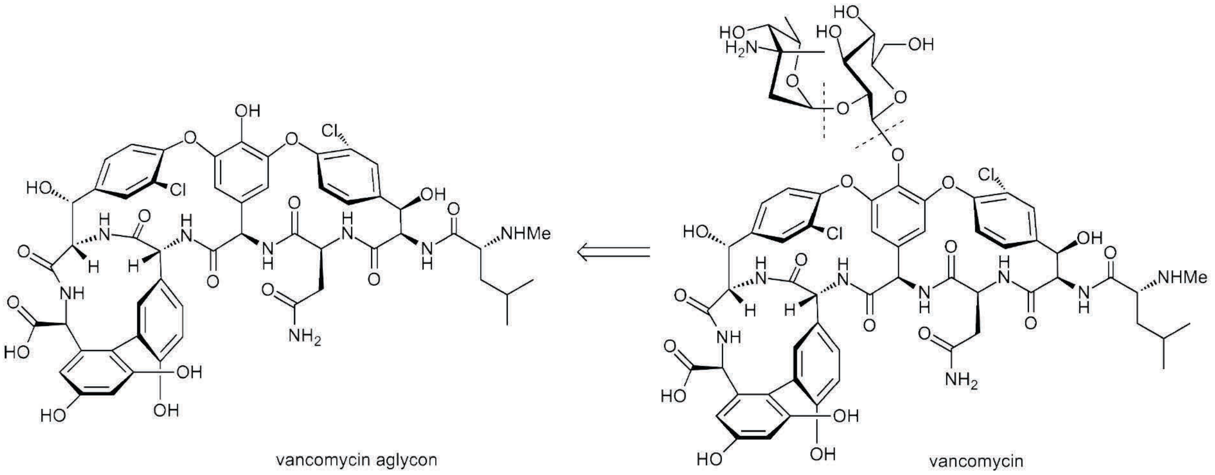

Figure 32: Structure of vancomycin and the vancomycin aglycon.

The structural diversity within this natural product class is created by variation of amino acids in the aglycon as well as by differing positions, numbers and natures of the sugar residues attached to the aglycon. Vancomycin has found a clinical application as a potent antibiotic reagent acting against Gram-positive bacteria. Most importantly, it is also active against methicillin-resistant *Staphylococcus aureus* and has therefore become the antibiotic of last resort against this fatal pathogen.[92]

Vancomycin has long attracted chemists not only because of its potent bioactivity but mainly due to its unusual molecular architecture. Efforts driven towards the total synthesis of vancomycin have resulted in the development of a number of new synthetic methods.[93]

The most daunting synthetic challenge posed by the vancomycin molecular architecture are for sure the three stereochemical elements of atropisomerism occurring due to a hindered rotation within each of the cyclic tripeptide subunits.

1.7.1.1 Evans' synthesis of the vancomycin aglycon

In their considerations towards the synthesis of the vancomycin aglycon, Evans and coworkers envisioned a strategy that would enable them to control the formation of each of these elements of atropisomerism individually during the assembly of the target structure.

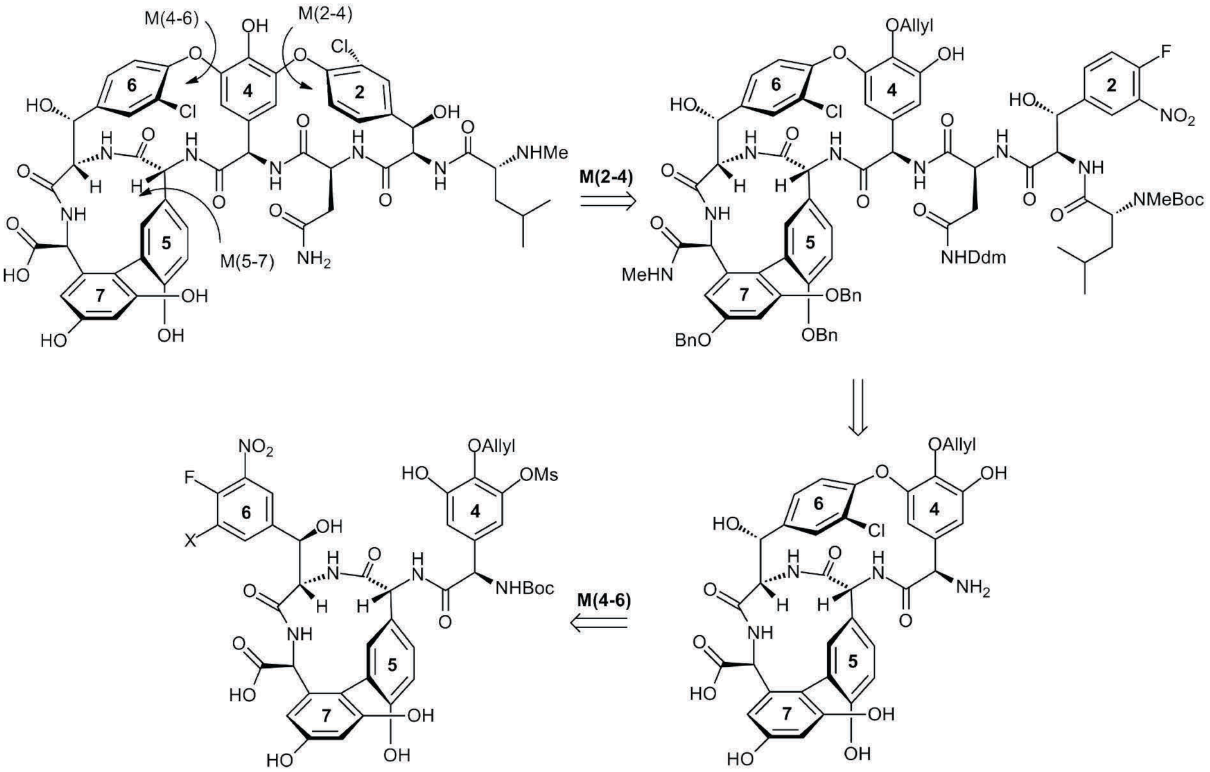

Figure 33: Retrosynthesis for Evans' synthesis of the vancomycin aglycon.[92]

Extensive studies were carried out to achieve conditions that would deliver the desired stereochemistry of these crucial architectural features. Ultimately, the reactions developed dictated the overall synthesis plan and the individual strategy for each of the cyclic tripeptide units that were designated as M(2-4), M(4-6) and M(5-7) (Fig.33). The amino acids required to synthesize the 4-7 tetrapeptide were synthesized using the chiral auxiliary methods developed by the Evans group.

Initially, two analogs of amino acid 6 were envisioned and investigated, a chloro and a dechloro derivative. With these two analogs in hand, the desired M(4-6) chlorine atropisomer would be possible to obtain from either stereochemical outcome of the envisioned S_NAr-based macrocyclization due to the possibilities provided by the Sandmeyer reaction that would enable a $NO_2 \rightarrow H$ as well as an $NO_2 \rightarrow Cl$ transformation. In the end, the chloro analog delivered the desired atropisomer.

The synthesis of amino acid 6 starts with an (isothiocyanoacetyl)oxazolidinone-assisted asymmetric Aldol reaction affording the *syn*-Aldol product. In the following conversions the products had to be handled delicately to prevent S_NAr-type reactions due to a fluoride displacement. After the Boc protection of the thioamide, the directing oxazolidinone was cleaved to afford the carboxylic acid, simultaneously the thiooxazolidinone was converted to the oxazolidinone. In the next step, amino acid 7 could be coupled to the free acid using EDC/HOBt activation and affording the dipeptide. Subsequently, the oxazolidinone was cleaved under mild basic conditions (Li_2CO_3) to afford a Boc-protected amino alcohol element. After removal of this Boc protection, amino acid 5 could be coupled to the resulting amine. The Boc protection on amino acid 5 was then replaced by a trifluoroacetamide, thereby setting the stage for the first macrocyclization reaction. The oxidative biaryl coupling was carried out using VOF_3 and afforded the desired *R* atropisomer with a high diastereoselectivity. The reductive quenching had to be adjusted to prevent the reduction of the nitro group. Simultaneously, the benzyl ether protection on ring 5 was also removed during the coupling reaction.

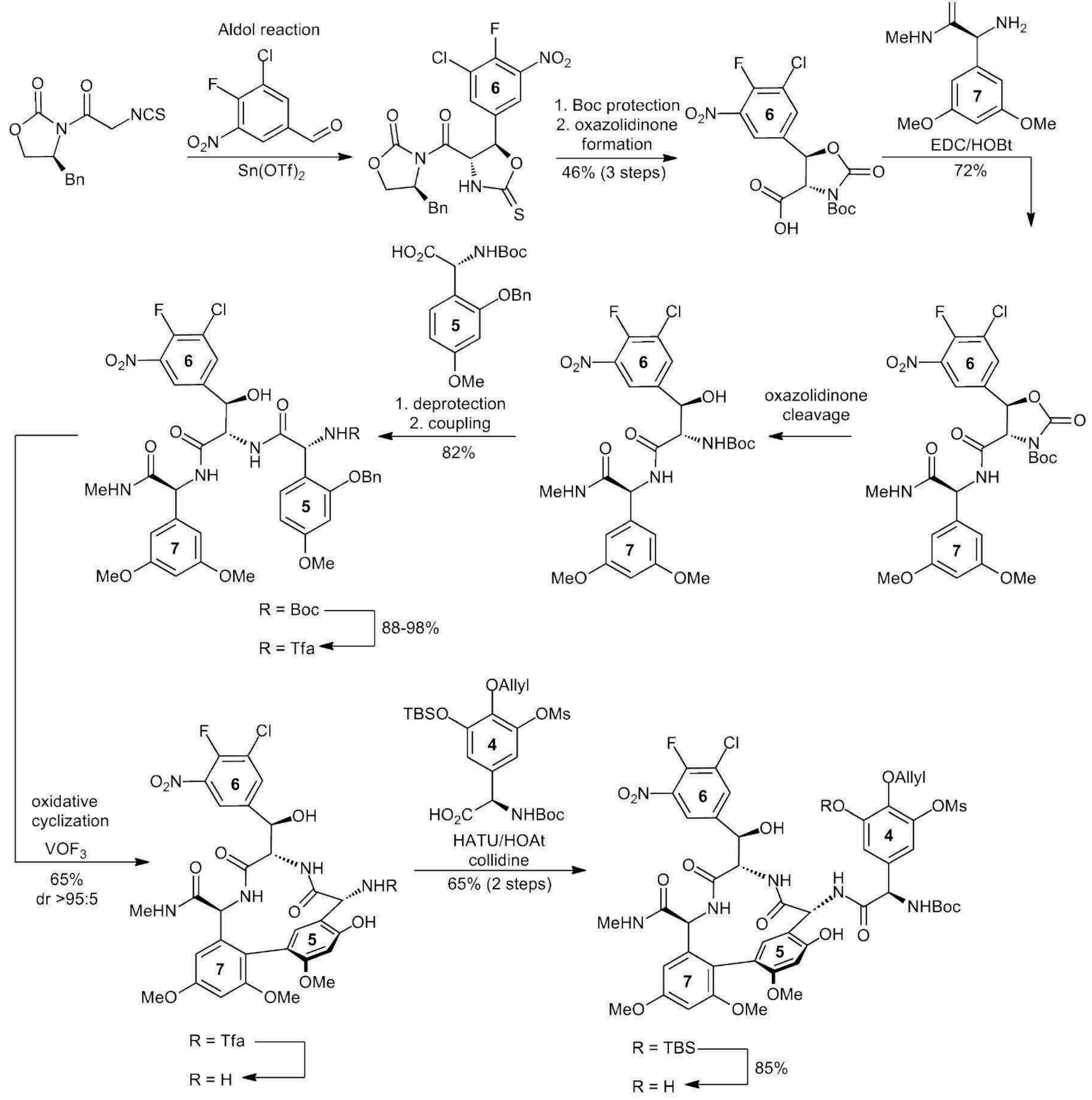
Aldol reaction
Sn(OTf)2
1. Boc protection
2. oxazolidinone formation
46% (3 steps)
EDC/HOBt
72%
oxazolidinone cleavage
1. deprotection
2. coupling
82%
R = Boc
R = Tfa
88-98%
oxidative cyclization
VOF3
65%
dr >95:5
R = Tfa
R = H
HATU/HOAt
collidine
65% (2 steps)
R = TBS
R = H
85%
4
5
6
7

Figure 34: Synthesis of the 4-7 tetrapeptide.[92]

After the removal of the trifluoroacetamide protection, amino acid 4 was coupled with HATU/HOAt activation. The removal of the phenolic TBS ether on ring 4 then set the stage for the second macrocyclization reaction, the M(4-6) biaryl ether coupling (Fig. 34).

At this point, various strategies using the two different amino acid 6 analog-derived tetrapeptides, were examined. The optimal conditions delivering the desired stereochemistry with the chloro analog of amino acid 6 were the application of basic conditions (Na_2CO_3) at room temperature. Due to an enhanced electrophilicity, the reaction of the chloro analog was much quicker compared to the dechloro analog (1.5 h *vs.* 66 h) for a full conversion. The desired atropisomer could be obtained with a dr of 5:1 in a yield of 79%.

After the removal of the nitro group by a two-step reduction/diazotation-reduction process, the monochloride with the desired *R* configuration, as confirmed by NMR, could be obtained. The Pd-mediated removal of the allyl ether on ring 4 and the aryltriflate on ring 5, as well as the adjustment of the protecting groups at the *N*-terminus and on ring 4 then and the cleavage of the methyl ethers on ring 7 set stage for the M(5-7) atropisomerization. The isomerization reaction proceeded under very mild conditions (55 °C, MeOH) to afford the desired *S* biaryl configuration with an excellent selectivity (dr >95:5). For the following final assembly of the vancomycin aglycon, the phenols on ring 5 and 7 were benzylated and the Piv protection on ring 4 was exchanged for an allyl ether again. Additionally, the Ms group on ring 4 was removed as well as the trifluoroacetamide protection. To the free amide, a pre-synthesized tripeptide was coupled using EDC/HOAt activation and affording the heptapeptide in 86% yield with no detectable epimerization (Fig. 35).

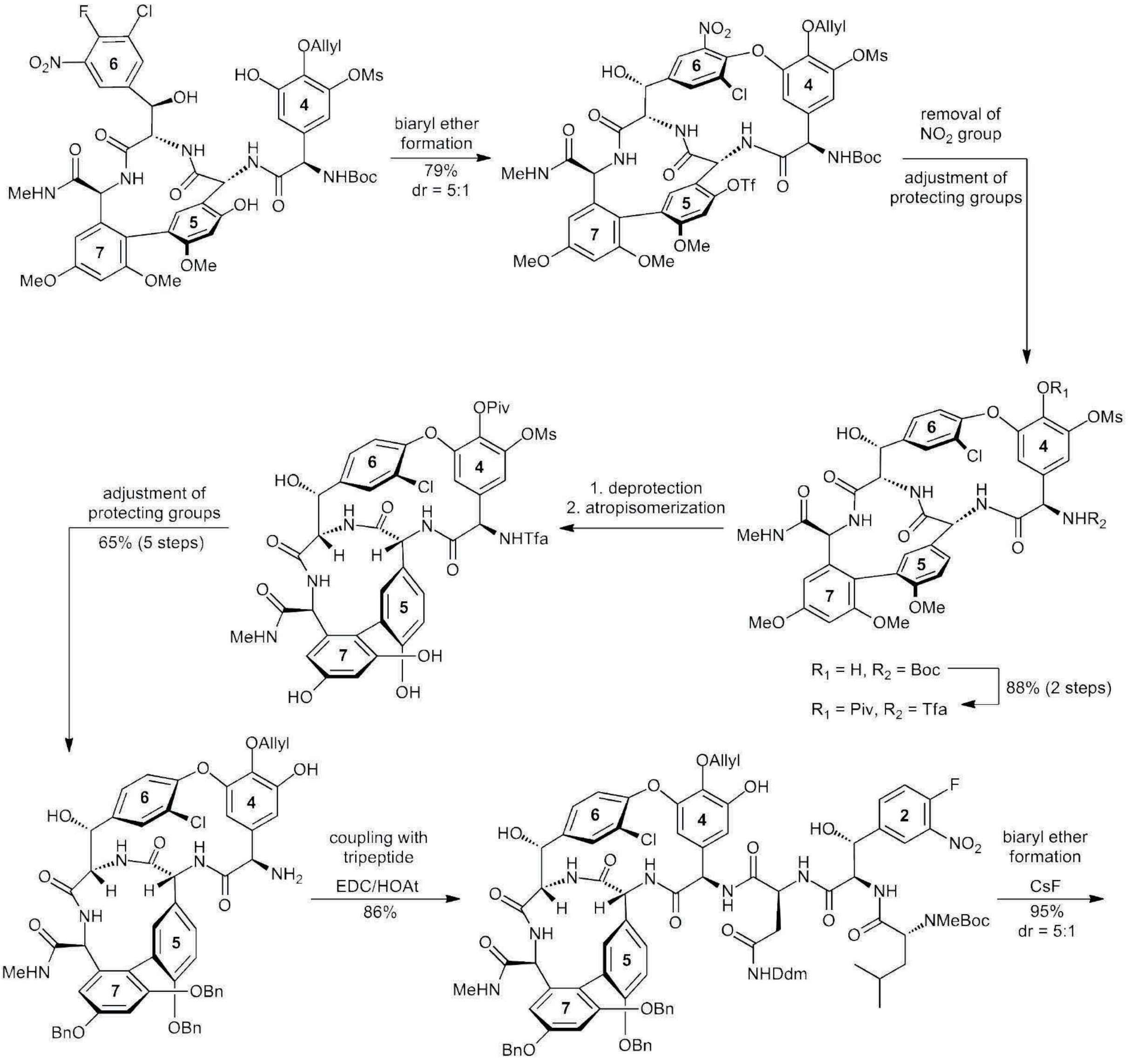
biaryl ether formation
79%
dr = 5:1
removal of NO2 group
adjustment of protecting groups
1. deprotection
2. atropisomerization
R1 = H, R2 = Boc
R1 = Piv, R2 = Tfa
88% (2 steps)
adjustment of protecting groups
65% (5 steps)
coupling with tripeptide
EDC/HOAt
86%
biaryl ether formation
CsF
95%
dr = 5:1

Figure 35: Synthesis of the heptapeptide intermediate and establishment of the M(4-6) and M(5-7) centers of atropisomerism.[92]

The final S_NAr macrocyclization provided the full tricyclic vancomycin core, the M(2-4) atropisomer with the desired *R* stereochemistry was obtained with a dr of 5:1 in an overall yield of 95%. After reduction of the diastereomeric mixture, the resulting diastereomeric anilines could be separated chromatographically. The following Sandmeyer transformation then installed the chlorine on ring 2 and provided the fully assembled protected vancomycin aglycon. Conversion of the methyl amide to the free acid by nitrosation/oxidation and careful removal of the remaining protecting groups finally afforded the vancomycin aglycon from a sequence of 40 steps (longest linear sequence) from 3,5-dimethoxy alcohol, the starting material for amino acid 7 (Fig. 36).[92]

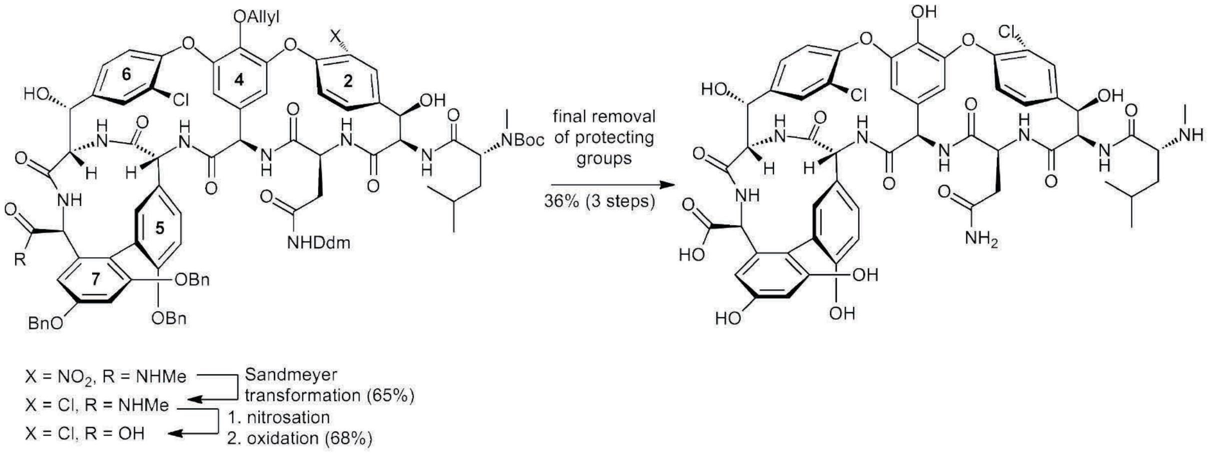
OAllyl
X
6
4
2
HO
Cl
OH
NBoc
NH
R
7
5
OBn
BnO
OBn
NHDdm
final removal
of protecting
groups
36% (3 steps)
OH
Cl
HO
NH
HO
OH
HO
OH
NH
NH₂
X = NO₂, R = NHMe
X = Cl, R = NHMe
X = Cl, R = OH
Sandmeyer
transformation (65%)
1. nitrosation
2. oxidation (68%)

Figure 36: Final transformations yielding the vancomycin aglycon.[92]

1.7.1.2 Nicolaou's total synthesis of vancomycin

When planning the total synthesis of the vancomycin aglycon and subsequently vancomycin, Nicolaou and coworkers envisioned a strategy similar to the one of Evans *et. al.* concerning the order of establishment of the centers of atropisomerism. First the M(5-7) center should be established, followed by the M(4-6) center. Instead of an individual control of the single centers of atropisomerism, the building block of amino acid 4 was designed in a fashion that it would have the intrinsic ability to control the formation of both biaryl ethers (M(4-6) and M(4-2)). To achieve this, a triazene-mediated biaryl coupling method, based on the complexation of copper by triazene, was developed in the course of the efforts towards the synthesis of vancomycin in the Nicolaou group. For the M(5-7) linkage, a Suzuki-coupling approach was envisioned.[93]

The synthesis of the individual amino acids required for the vancomycin framework was established by using well-established methods. Instead of auxiliary methods as used in the Evans approach, Sharpless asymmetric dihydroxylation or aminohydroxylation reactions were preferred. The synthesis of the amino acids 4 to 7 is summarized in Figure 37.

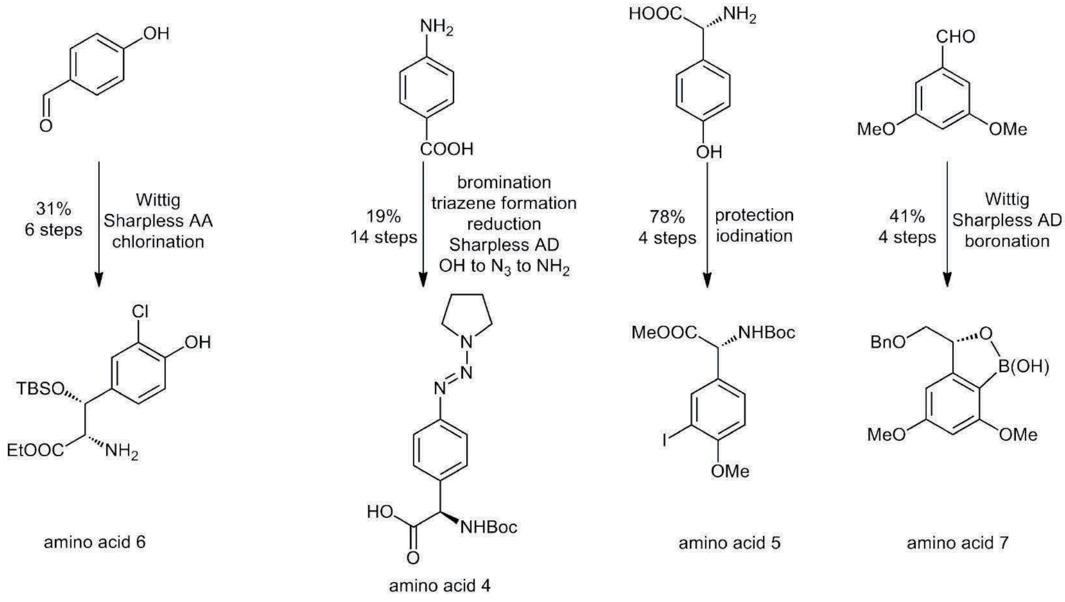
OH
O
31%
6 steps
Wittig
Sharpless AA
chlorination
Cl
OH
TBSO
EtOOC
NH2
amino acid 6
NH2
COOH
19%
14 steps
bromination
triazene formation
reduction
Sharpless AD
OH to N3 to NH2
N
N
N
HO
NHBoc
O
amino acid 4
HOOC
NH2
OH
78%
4 steps
protection
iodination
MeOOC
NHBoc
I
OMe
amino acid 5
CHO
MeO
OMe
41%
4 steps
Wittig
Sharpless AD
boronation
BnO
O
B(OH)
MeO
OMe
amino acid 7

Figure 37: Syntheses of the building blocks for amino acids 4 to 7 (summarized).[93]

To establish the first center of atropisomerism, the amino acids 5 and 7 were coupled in a Suzuki reaction that yielded 84% of a 2:1 mixture of atropisomers. Further investigation proved the major isomer to be one desired for the further synthesis.

After conversion of the hydroxyl group to the azide as well as the hydrolysis of the methyl ester, the dipeptide was coupled with amino acid 6 using EDC/HOAt activation, affording the tripeptide in 85% yield (dr = 13:1). After removal of the Boc protection, the central amino acid 4 was coupled, yielding the tetrapeptide in 76% yield. The tetrapeptide was then subjected to the first triazene-based biaryl coupling that was carried out using CuBr·SMe_2 for the coupling and yielded the two possible atropisomers in an equal mixture with an overall yield of 60%. (Figure. 38 shows only the atropisomer relevant for the further synthesis.) The two atropisomers were easily be distinguished by their distinct NMR spectra. To establish the bicyclic 4-7 vancomycin framework, a macrolactamization reaction was carried out after the desilylation of the TBS ether, the conversion of the azide to the amine and the hydrolysis of the ethyl ester. An FDPP-mediated coupling reaction then provided the bicyclic system; the correct stereochemistry could be assigned by NMR analysis.[93]

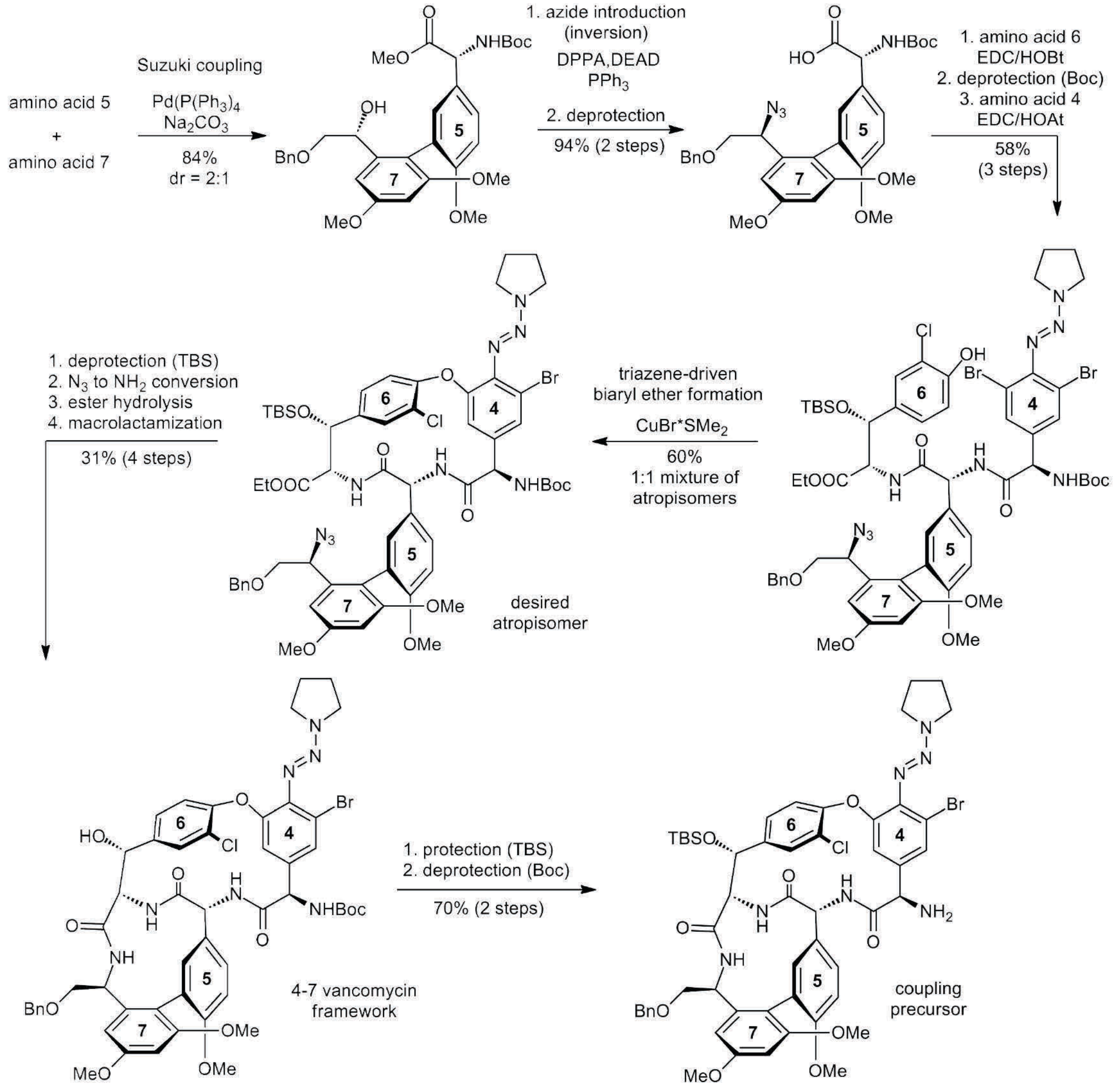
amino acid 5
+
amino acid 7
Suzuki coupling
Pd(P(Ph3)4
Na2CO3
84%
dr = 2:1
1. azide introduction (inversion)
DPPA,DEAD
PPh3
2. deprotection
94% (2 steps)
1. amino acid 6
EDC/HOBt
2. deprotection (Boc)
3. amino acid 4
EDC/HOAt
58%
(3 steps)
triazene-driven
biaryl ether formation
CuBr*SMe2
60%
1:1 mixture of
atropisomers
desired
atropisomer
1. deprotection (TBS)
2. N3 to NH2 conversion
3. ester hydrolysis
4. macrolactamization
31% (4 steps)
1. protection (TBS)
2. deprotection (Boc)
70% (2 steps)
4-7 vancomycin
framework
coupling
precursor

Figure 38: Establishment of the 4-7 vancomycin framework.[93,94]

The synthesis was then continued by preparing the molecule for the attachment of the *N*-terminal tripeptide portion. First, the free hydroxyl function of amino acid 6 was reprotected as a silyl ether, and then the *N*-terminal Boc group was removed (Fig. 38).

The *N*-terminal tripeptide was pre-synthesized from amino acids prepared by well-established methods. The heptapeptide was obtained by an EDC/HOAt-mediated coupling in a yield of 81%. This set the stage for the second triazene-mediated biaryl ether coupling, which was carried out using the previously established conditions, yielding a 1:3 mixture of atropisomers in an overall yield of 72%. Unfortunately, the minor isomer was required for further synthesis but the yield could be enhanced by heating the chromatographically separated atropisomers in 1,2-dichlorobenzene which resulted in the formation of a 1:1 mixture of separable atropisomers (Fig. 39).[94]

The final steps for the total synthesis of the vancomycin aglycon required the removal of the triazene, the oxidation of the homobenzylic alcohol as well as the removal of the remaining protecting groups.

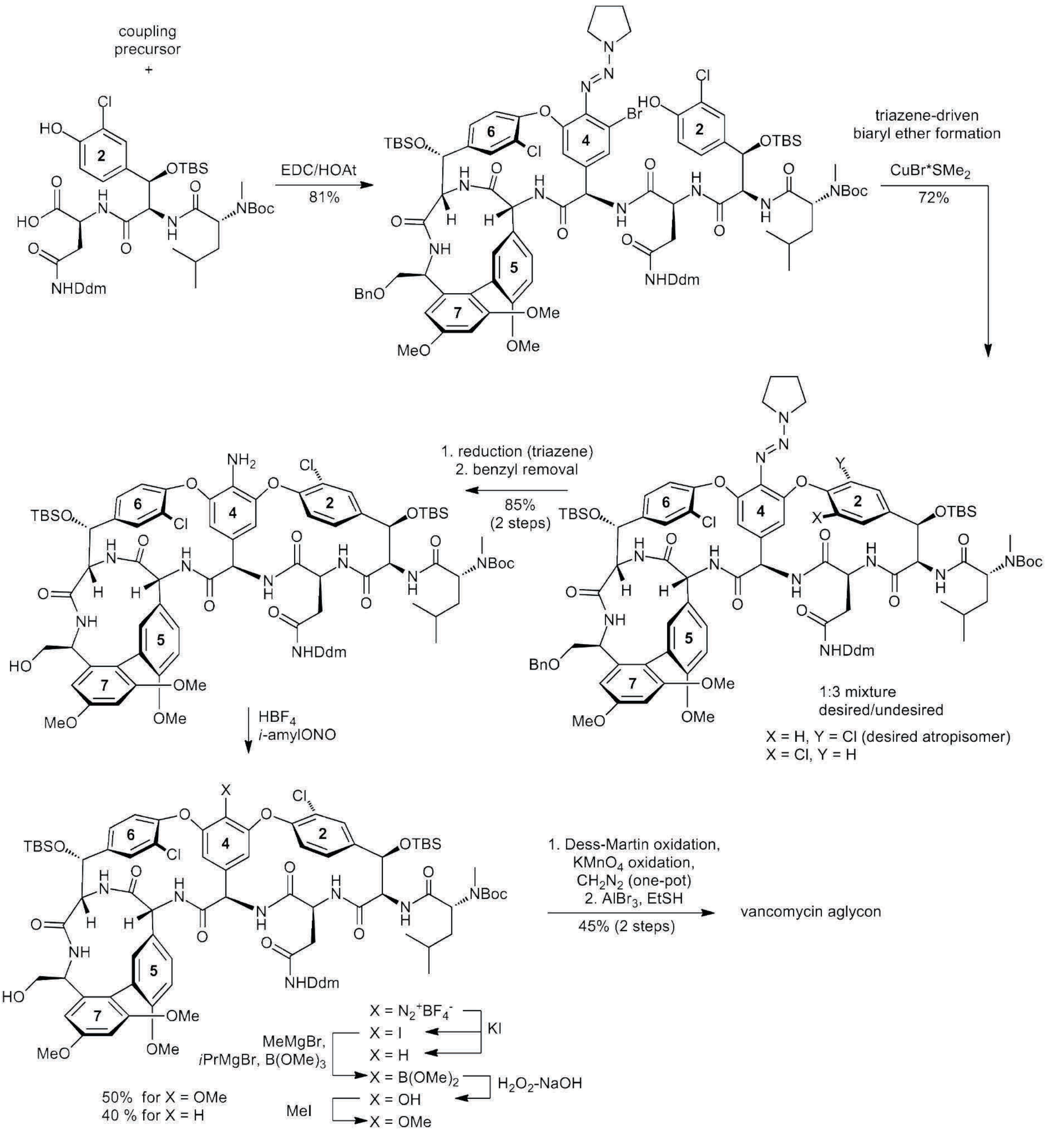
coupling precursor
+
EDC/HOAt
81%
triazene-driven biaryl ether formation
CuBr*SMe2
72%
1:3 mixture desired/undesired
X = H, Y = Cl (desired atropisomer)
X = Cl, Y = H
1. reduction (triazene)
2. benzyl removal
85% (2 steps)
HBF4
i-amylONO
1. Dess-Martin oxidation, KMnO4 oxidation, CH2N2 (one-pot)
2. AlBr3, EtSH
45% (2 steps)
vancomycin aglycon
X = N2+BF4-
X = I
X = H
X = B(OMe)2
X = OH
X = OMe
KI
MeMgBr, iPrMgBr, B(OMe)3
H2O2-NaOH
MeI
50% for X = OMe
40 % for X = H

Figure 39: Final steps in the synthesis of the vancomycin aglycon.[94,95]

Especially the removal of the triazene residue proved to be a greater challenge than expected. Initial attempts using standard conditions for the removal could not provide the desired phenol but resulted in a fully reduced product (X = H, refer to Figure 39). The successful sequence leading finally to the desired phenol started with the conversion to an aniline by a Raney-Ni reduction. This also effected a partial cleavage of the benzyl ether, which was completed by a $Pd(OH)_2$/C-reduction. Next, the aniline was converted to the diazonium salt, which was treated with potassium iodide to establish the iodide, this reductive procedure also resulted in the formation of the previously observed reduction product (X = H) which could not be separated from the iodide at this stage. Instead, the mixture was subjected to boronation conditions and on the boronate stage the reduced product could be removed by chromatography. The boronate was formed by deprotonation of all NH groups followed by metal-halogen-exchange with MeMgBr and *i*PrMgBr and quenching of the aryl-Grignard species with an excess of $B(OMe)_3$. The peroxide-mediated oxidation of the boronate then finally provided the desired phenol derivative along with a reduced product which could be separated by preparative thin layer chromatography. Consequently, the overall yield for the phenol was only 50% from the aniline. Surprisingly, all of these manipulations did not affect the stereochemistry in the natural product. In preparation of the final oxidation, the phenol was protected with a methyl group. A sequential treatment with Dess-Martin periodinane, potassium permanganate and finally diazomethane established the methyl ester. Removal of the remaining protection groups with $AlBr_3$/EtSH finally provided the desired vancomycin aglycon (Fig. 39).[95]

To complete the synthesis of vancomycin, the sugar moieties still had to be coupled to the aglycon. First the aglycon had to be protected properly: persilylation and methyl ester formation followed by a selective desilylation of the central phenol provided the desired glycosyl acceptor. The development of a proper strategy for the glycosyl donors was again tedious work and resulted in the use of a trichloroacetimidate as the glucosyl donor and a fluoridated vancosamine donor. To complete the synthesis, the glucosyl building block was coupled to the deprotected vancomycin aglycon, providing a mono-glycosylated intermediate. After removal of the Alloc protection, the second sugar moiety was introduced, providing a protected vancomycin derivative. A sequential removal of the silyl groups and the acetate groups followed by the hydrolysis of the methyl ester and the reductive cleavage of the Cbz groups then finally yielded the complete natural product vancomycin (Fig. 40).[96]

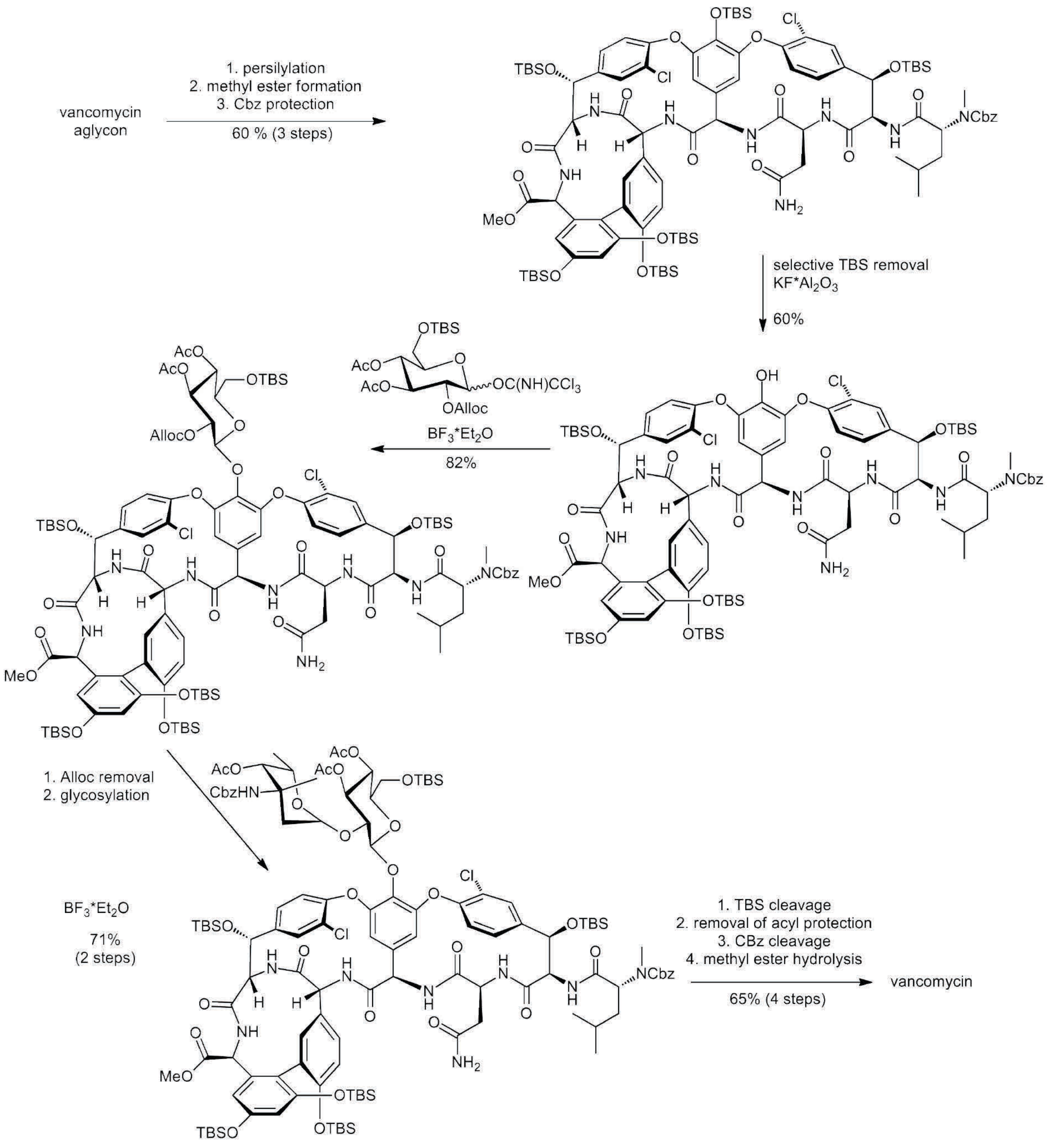
vancomycin aglycon
1. persilylation
2. methyl ester formation
3. Cbz protection
60 % (3 steps)
selective TBS removal
KF*Al$_2$O$_3$
60%
BF$_3$*Et$_2$O
82%
1. Alloc removal
2. glycosylation
BF$_3$*Et$_2$O
71%
(2 steps)
1. TBS cleavage
2. removal of acyl protection
3. CBz cleavage
4. methyl ester hydrolysis
65% (4 steps)
vancomycin

Figure 40: Synthesis of vancomycin from the vancomycin aglycon.[96]

1.7.1.3 Synthesis planning, solid-phase peptide synthesis: oxathiocoraline

Although solid-phase strategies are highly elaborated and offer solutions to a great number of synthetic problems, contributions to this field are still to be made. An alternative cleavage strategy meeting the requirements of a total synthesis is one innovation to solid-phase peptide chemistry that was investigated throughout the project presented in this dissertation. Another contribution to the field is represented by the synthesis of oxathiocoraline by Albericio and coworkers that is an example of efficient synthesis planning and development [90,91]. It also pinpoints that the transfer of synthetic strategies to the solid support requires complex considerations, a wise choice of protecting groups, the will to use a higher number of protecting groups and carefully planned transformations. Then, a successful and robust solid-phase strategy paves the road to a quick and simplified access to analogs and derivatives of the original compound.

Oxathiocoraline is a C_2-symmetrical compound belonging to a family of anti-tumoral bicyclic peptide antibiotics that are known bisintercalators to DNA.[97] Oxathiocoraline itself is not a natural product, it is a pharmacokinetically more stable derivative of the potent natural product thiocoraline[98,99] It contains a high density of non-proteinogenic amino acids, in this case *N*-methylated and *D*-amino acids, in addition it features a central disulfide bridge that is flanked by two ester bonds that establish the bicyclic core structure of the molecule (Fig. 41).

The total synthesis presented by Albericio and coworkers is highly elaborated and extensive preliminary studies were carried out to optimize the conditions for this challenging synthesis. The studies included the evaluation of the optimal starting amino acid, the investigation of alternative resins, coupling reagents and optimization of the protecting group strategy. One of the major difficulties to encounter in this synthesis is the lower reactivity of a hydroxyl group compared to an amine which is accompanied by a lower stability of the resulting ester bond and the formation of diketopiperazines. Cysteines are a challenge in the assembly of peptides as they are prone to racemization when they are part of an ester, additionally *N*-methylated cysteines are also known to eliminate under basic conditions and can easily undergo oxidation. This stands of course in stark contrast to the harsh conditions that are required for the coupling to *N*-methylated amino acids.

In the successful synthesis route, glycine was chosen as the anchoring point to the solid phase, as no racemization can occur with this amino acid during the attachment to the resin and further racemization is also suppressed. After removal of the Fmoc protection, Fmoc-Ser(Trt)-OH was coupled to glycine using HATU/HOAt activation. The *N*-terminal Fmoc protection was then replaced by a *p*-nitrobenzyloxycarbonyl (*p*NZ) group that showed a better compatibility with the ester bond and serves on the other hand as a placeholder for the aromatic heterocyclic moiety. After removal of the trityl protection, the hydroxyl group was esterified with Alloc-*N*Me-Cys(Acm)-OH using DIPCDI and DMAP for the activation. The Alloc protection was then removed in a Pd-mediated isomerization and Boc-*N*Me-Cys(Acm)-OH was coupled using HATU/HOAt activation and a reduced amount of base to minimize side reactions. By using this strategy the tetradepsipeptide could be obtained in 89% purity. The next step was the on-resin formation of the central disulfide bridge which was achieved by oxidation with iodine in methanol. The subsequent cleavage from the resin was performed in the presence of water to prevent the formation of sulfoxides. The cleavage conditions also removed the remaining Boc groups, providing the precursor for the final cyclizations. Without a purification step, the lyophilized crude peptide was pre-activated with HOAt at a slightly basic pH and PyBOP was used as the coupling reagent to establish the bicyclic structure. In this manner, the bicycle could be obtained without notable diketopiperazine formation. After a reductive removal of the *p*NZ groups, 3-hydroxyquinaldic acid was coupled using mild EDC/HOSu activation to finally yield oxathiocoraline in an overall yield of 7%. This synthesis is an example of a highly optimized solid-phase approach; the optimization nevertheless holds promise for a quick access to modified analogs of oxathiocoraline.[90]

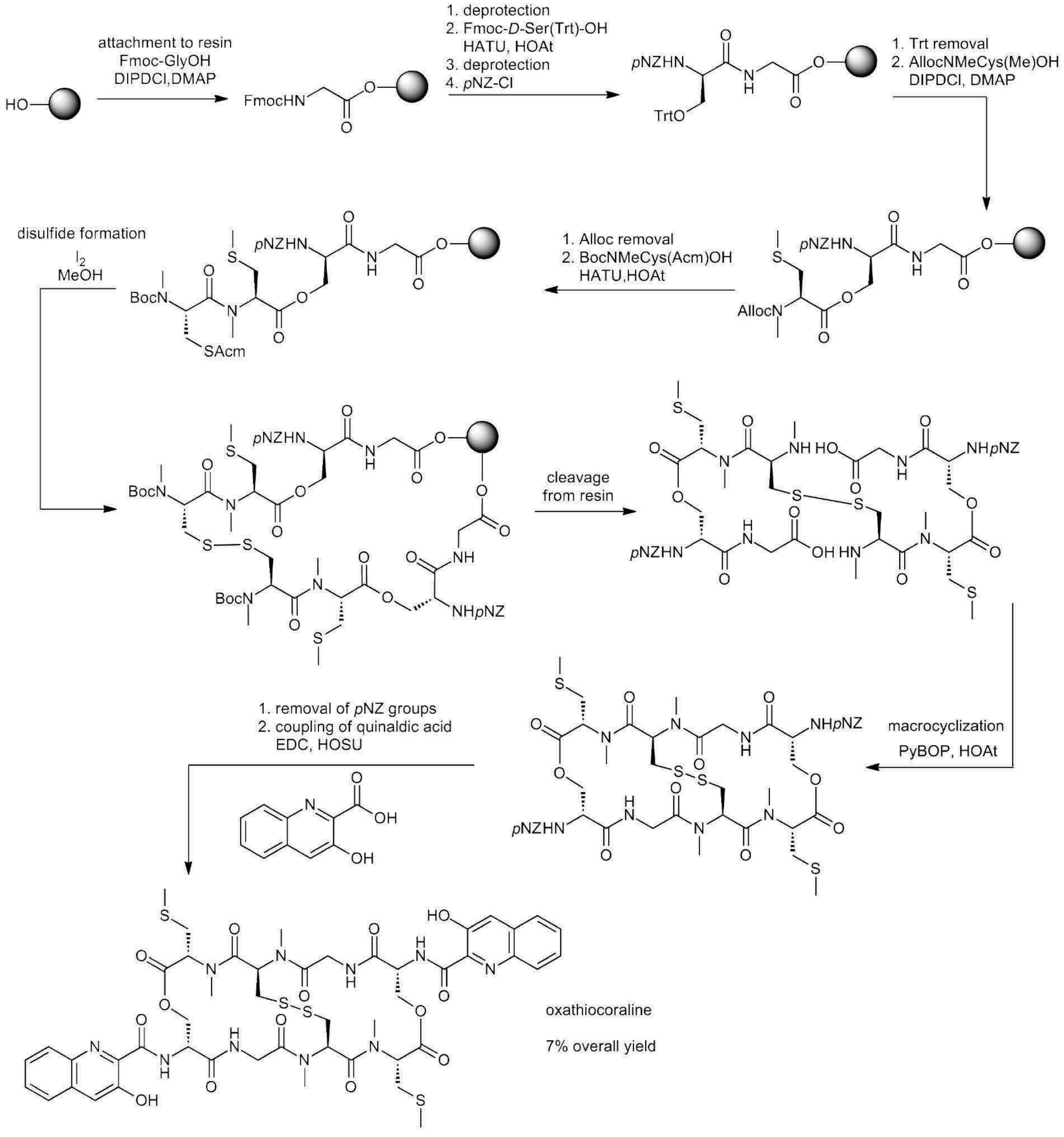
HO
attachment to resin
Fmoc-GlyOH
DIPDCl,DMAP
FmocHN
1. deprotection
2. Fmoc-D-Ser(Trt)-OH
HATU, HOAt
3. deprotection
4. pNZ-Cl
pNZHN
TrtO
1. Trt removal
2. AllocNMeCys(Me)OH
DIPDCl, DMAP
AllocN
1. Alloc removal
2. BocNMeCys(Acm)OH
HATU,HOAt
BocN
SAcm
disulfide formation
I2
MeOH
NHpNZ
cleavage
from resin
macrocyclization
PyBOP, HOAt
1. removal of pNZ groups
2. coupling of quinaldic acid
EDC, HOSU
oxathiocoraline
7% overall yield

Figure 41: Solid-phase synthesis of oxathiocoraline.[90]

2 Aims of the PhD project

The main focus of this dissertation was set on the development of a general solid-phase approach to the natural product class of 3-amino-6-hydroxy-2-piperidone (Ahp) containing cyclodepsipeptides. This natural product class is, as described already, known for its potent and most intriguingly non-covalent inhibition of S1 serine proteases. The potent inhibition is achieved by adapting the so-called canonical conformation which has been recognized as a structural motif in proteins and peptides of natural and synthetic sources mediating a non-covalent inhibition of serine proteases. [17-20] At the beginning of the project, solution-phase syntheses of two Ahp containing cyclodepsipeptides, micropeptin T-20 and somamide A, had been published.[100-102] Although these syntheses finally attained the synthesis of the respective natural product, they are highly specialized and require multi-step solution phase syntheses. Nevertheless, Yokokawa *et. al.* could prove in their syntheses that the crucial Ahp hemiaminal residue can readily be generated from a precursor aldehyde macrolactam at a late stage of the peptide synthesis. In fact, the Ahp hemiaminal forms spontaneously from the precursor aldehyde.[100-102]

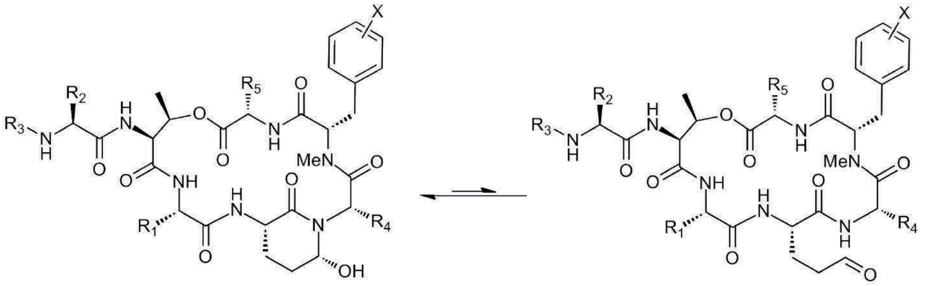

Figure 42: General structure of the Ahp containing depsipeptides. The Ahp hemiaminal is formed spontaneously from a precursor aldehyde macrocycle, with the equilibrium being on the side of the hemiaminal structure.

Accordingly, the synthetic outline for a solid-phase approach to the class of Ahp containing cyclodepsipeptides envisioned the development a suitable precursor unit that can be coupled to solid support and, after the assembly of the peptide sequence, can be converted to an aldehyde residue (and thus ultimately to the Ahp unit). This approach was envisaged to pave the way to tailor-made Ahp cyclodepsipeptides because the unifying element of the substance class (*i. e.* the Ahp unit) was chosen as the anchoring point to the solid phase. As a proof of principle for this approach, a solid phase synthesis of the natural product Ahp cyclodepsipeptide symplocamide A was chosen. Symplocamide A was only discovered recently[24] and no synthesis of this natural product had been reported before this PhD project.

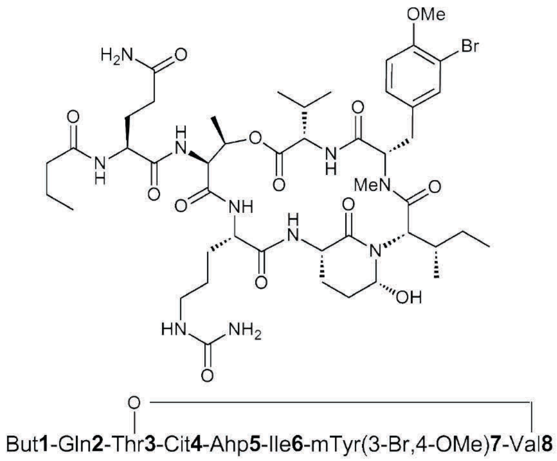

Figure 43: Symplocamide A, an Ahp cyclodepsipeptide isolated from a *Symploca* sp. from Papua New Guinea.[24] The natural product was chosen as the synthetic target for the validation of the newly developed solid-phase strategy.

In a second step after its synthesis, a validation of its reported biological activity and investigation of further bioactivities were planned.

After the successful development of a solid phase-based synthesis of Ahp containing cyclodepsipeptides, the follow-up question of the significance of the Ahp moiety in Ahp cyclodepsipeptides was to be addressed. The contribution of the Ahp moiety to the induction of a canonical conformation in the cyclodepsipeptide is well-described in literature. As the synthesis of such Ahp-containing cyclodepsipeptides is however rather laborious, the development of peptidic analogs of the Ahp containing cyclodepsipeptides that could retain the canonical conformation and thereby the biological activity was an aim in this PhD thesis.

To this end, analogs in which the Ahp unit was replaced by other amino acids were investigated for their biological activity. The elucidation of suitable Ahp mimics would enable a quick and if necessary combinatorial access to canonical conformation inhibitors and therefore represent valuable tools for chemical biology investigations of serine proteases.

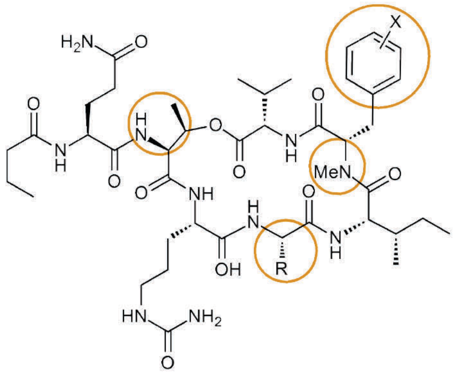

Figure 44: General structure of structure-activity analogs derived from symplocamide A. The amino acids envisioned to be investigated are indicated.

In a second project, the synthesis of the natural product symplostatin 4 and derivatives that would enable the biological investigation as well as the identification of the molecular target of symplostatin 4 by the means of an activity-based approach was planned.

Symplostatin 4 is a linear peptide isolated from a cyanobacterium of the *Symploca* genus and shows a structural similarity to the potent cytotoxic agents dolastatin 10 and 15 which are lead compounds in cancer therapy. As dolastatin 10 and 15 are potent disruptors of microtubule polymers, symplostatin was also tested on microtubule interaction, displaying an effect significantly lower than dolastatins 10 and 15, but leading to the same cellular phenotypes.[103]

Interestingly, the natural product gallinamide A isolated from a *Schyzothryx* sp., was published just shortly before symplostatin 4 was disclosed and later studies demonstrated that both natural products have the same structure.[103,104] However, gallinamide A emerged from a screen of compounds isolated from marine cyanobacteria and displayed a promising antimalarial activity.[104] Symplostatin 4 initially attracted interest as a target structure for this dissertation owing to the prominent Michael acceptor system that is accompanied by the rather unusual methyl-methoxypyrrolinone. In an activity-based approach, a probe generated on the basis of symplostatin 4 could be a valuable tool for the investigation of proteases that are known targets of α,β-unsaturated carbonyls. Moreover, the methyl-methoxypyrrolinone unit could be studied in terms of its influence on the activity and selectivity of the natural product once a target is identified.

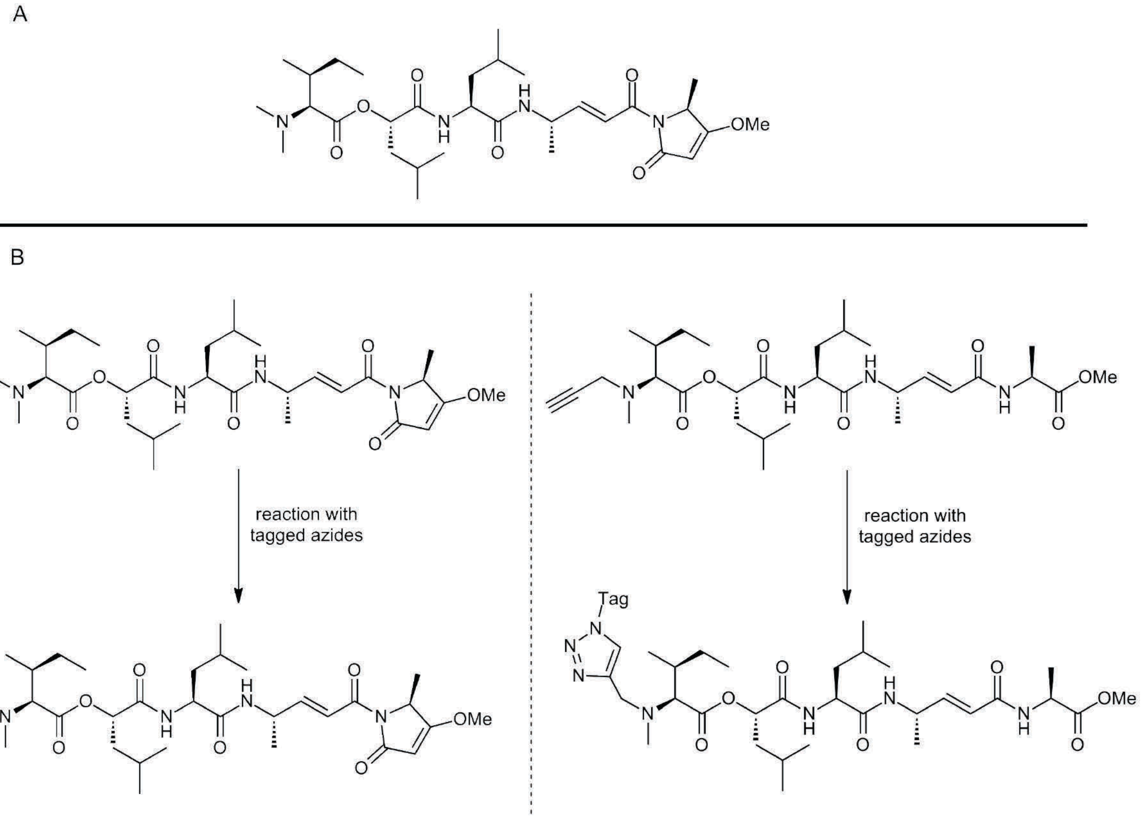

Figure 45: Symplostatin 4 and derivatives for biological studies. **A**: The natural product symplostatin 4, a natural product isolated from a *Symploca sp.* from Key Largo.[103] **B**: Derivatives of symplostatin 4 for biological studies. Differentially tagged derivatives should be accessible by the reaction of alkyne-modified analogs with differentially tagged azides using click chemistry.

In addition, some chemical biology studies with symplostatin 4 such as a target identification in different organisms were envisaged. To this end, two collaborations with groups from different research fields were established. First, in collaboration with the van der Hoorn group (MPI Cologne), the effect of symplostatin 4 in the model plant *Arabidopsis thaliana* was to be investigated and the targets of symplostatin 4 and its analogs were to be identified. In addition, the molecular basis of the antimalarial activity of Symplostatin 4 should be investigated. To this end, a collaboration with the Bogyo group (Stanford University) was initiated; this studies aimed at the determination of the potency of the antimalarial effect of symplostatin 4 as well as the target identification of this compound in *Plasmodium falciparum* using the newly generated derivatives of symplostatin 4.

3 Results and Discussion

3.1 Chemistry and Biology of Ahp cyclodepsipeptides

3.1.1 Retrosynthetic analysis of Ahp cyclodepsipeptides: Development of a synthetic strategy for a general solid-phase approach to this natural product class

The Ahp cyclodepsipeptides are an interesting natural product class due to their potent biological activity directed against S1 serine proteases and their non-covalent mode of inhibition. Consequently, the substance class has been suggested as a potential lead for the rational design of drugs.[25]

For investigating the interaction of an inhibitor with its target, a certain amount of inhibitor is required for the biological experiments. The isolation from natural sources, however, is usually laborious and yields mostly only minute amounts of the pure natural substance. Often, this amount does not suffice to initiate an elaborate evaluation of the biological activities of a natural substance. Moreover, for in-depth insights into the mode-of-action of a natural product, as well as for the development of new natural product-derived drugs, derivatives or analogs of the original substances are desired. The modified compounds can be used as tools in chemical biology approaches to investigate the structural determinants of inhibition. For the development of a bioactive small molecule into a drug, a derivatization of a lead structure is often required to enhance its efficacy and to minimize potential side effects as well pharmacological parameters such as the solubility or the uptake of a drug. The chemical synthesis of natural products and derivatives therefore provides a powerful platform that enables researchers to overcome the limited material supply and also offers a multitude of possibilities to the modification of natural products for different applications.

So far, no general approach to the synthesis of Ahp cyclodepsipeptides has been established. Yokokawa and coworkers however reported the synthesis of the Ahp containing cyclodepsipeptides somamide A and micropeptin T-20. In these syntheses, they demonstrated that the crucial hemiaminal constituting the Ahp unit can be formed from a precursor aldehyde macrocycle at a late stage of the peptide synthesis. Both syntheses were based on a tedious multi-step solution-phase assembly of different peptide fragments to finally obtain the desired natural products.[100-102]

In contrast to this laborious solution synthesis, a more straightforward solid-phase strategy that could be applied to the synthesis of various Ahp cyclodepsipeptides was envisioned. To this end, the development of a general Ahp precursor molecule that could be used in solid phase synthesis was envisaged. Consequently, the whole Ahp cyclodepsipeptide could be assembled on solid phase, using standard peptide couplings as well as an *on-resin* esterification to the depsipeptide residue.

To achieve this aim, the following retrosynthetic strategy was pursued (Fig. 46): The target Ahp cyclodepsipeptide structure should form spontaneously from a precursor aldehyde that could be generated upon liberation from the solid phase (**A**). To this end, the aldehyde functionality could be introduced *via* oxidative cleavage of a suitable masked glutamic aldehyde equivalent. The ring closure to the macrocycle from a linear precursor was planned as an *on-resin* macrolactamization. Prior to the macrolactamization, the attachment of the final amino acid to the sterically hindered and less reactive methylated amino acid needed to be achieved in an efficient manner. The esterification of the unreactive threonine side chain hydroxyl group was regarded as another crucial step in the synthesis, due to the low reaction rates of an esterification reaction compared to the formation of an amide bond (**B**). A further breakdown of the peptidic structure then leads to the Ahp precursor coupled to the solid phase (**C**). Finally, a synthesis of the Ahp precursor is required which could be achieved by solution-phase chemistry.

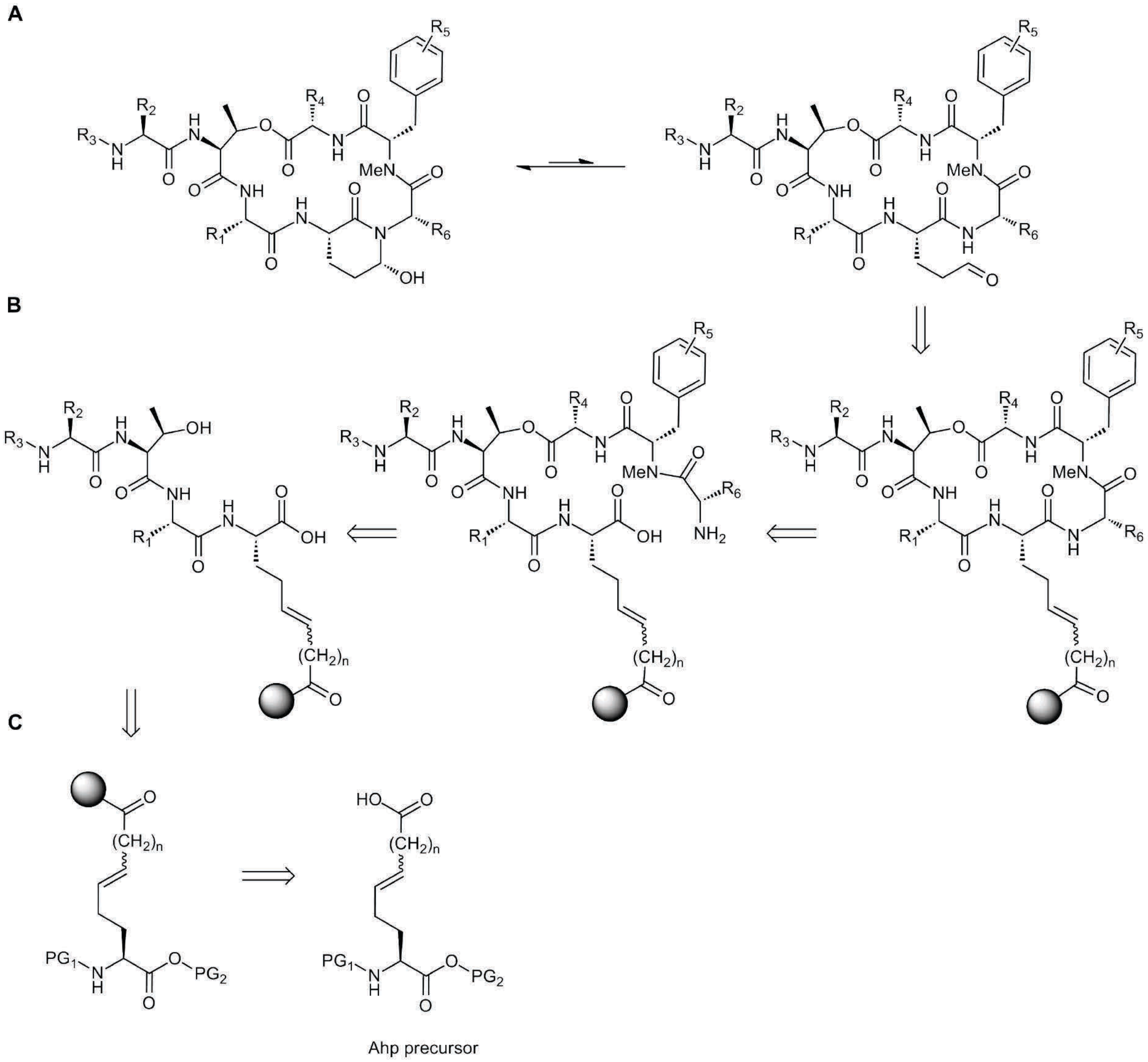

Figure 46: Retrosynthetic analysis for a solid-phase approach towards Ahp cyclodepsipeptides.

Besides the incorporation of the masked glutamic aldehyde equivalent, the Ahp precursor needs to be equipped with adequate protection groups at both termini. Especially the protection of the *C*-terminus is critical for the synthesis strategy as it has to be stable under the different peptide synthesis conditions that are required for the assembly but also has to be removed under mild conditions at a late stage of the peptide synthesis. Consequently, an allyl ester protection seems to be a wise choice in this place because it is stable under the peptide synthesis conditions and can be cleaved under very mild conditions on the solid phase using palladium catalysis.[105]

The choice of a double bond as the masked glutamic aldehyde equivalent was based on previous works by the Meldal group. This group has demonstrated that the oxidative cleavage of double bonds by a dihydroxylation-glycol cleavage protocol cleanly generates aldehydes on solid phase.[105-108] Accordingly, an adapted dihydroxylation-glycol cleavage protocol should represent a feasible method to generate an aldehyde upon cleavage from the solid phase.

3.1.1.1 Development of a suitable Ahp precursor - Synthesis of the Ahp precursor in solution

The first Ahp precursor (**1**, Ahp precursor I) that was tested for the development of a solid-phase approach featured a Fmoc protecting group for the *N*-terminus as well as an allyl ester protection of the *C*-terminus. The allyl ester represents an orthogonal protecting group that can be removed prior to the cyclization. As a masked glutamic aldehyde, an α,β-unsaturated carboxylic acid moiety was envisaged as the acid function can be coupled to the solid phase – for example onto a 2-chlorotrityl chloride resin.

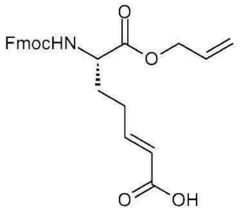

1
(Ahp precursor I)

Figure 47: Ahp precursor I

The synthesis of **1** started from the commercially available Boc-protected glutamic acid benzyl ester (Fig. 48). First, the glutamic acid side chain was reduced to the alcohol using Shioiri's protocol from the synthesis of micropeptin T-20.[101] In this procedure, the acid functionality was first converted to a more reactive mixed anhydride which is then reduced to the alcohol using sodium borohydride. A subsequent Dess-Martin oxidation to the aldehyde however resulted in the preferential formation of a hemiaminal and only a small amount of the aldehyde was formed. However, due to the equilibrium between the aldehyde and hemiaminal form, a subsequent conversion of the mixture of hemiaminal and aldehyde to the corresponding α,β-unsaturated acid derivative was attempted. Despite several trials for example *via* Wittig reactions, all attempts to obtain this derivative failed, The formation of such undesired hemiaminals that represent intramolecular traps has been described in literature.[109] The formation of these unwanted hemiaminals can however be prevented by the introduction of a second Boc protecting group on the amine.[110,111]

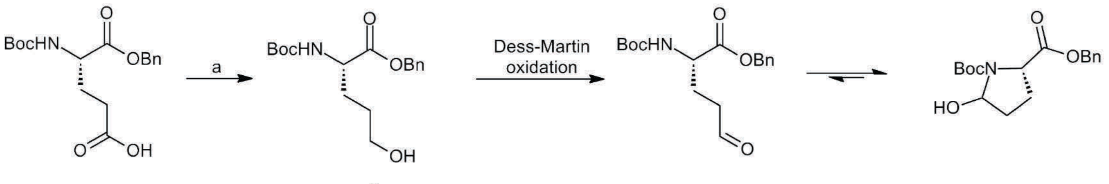

2

Figure 48: First steps towards the synthesis of Ahp precursor I. Reagents and conditions: (a) i. EtOCOCl, Et_3N, THF, -15 °C, 1 h; ii. $NaBH_4$, THF/H_2O (1:1), -15 °C, 1 h, then rt, 6 h (84%).

As a consequence, the synthesis plan was reconsidered and a bis-Boc-protection of the amine residue was pursued (Fig. 49). To this end, Boc glutamic acid benzyl ester was first converted to the methyl ester **3**. The second Boc group was introduced using Appela's protocol which yielded the di-Boc-protected methyl ester **4**.[112] The following mild DIBAL-H reduction of the methyl ester led to the respective aldehyde **5** in however only 27% yield as an overreduction to the alcohol could not be prevented in the tested reaction conditions. Nevertheless, in order to test the feasibility of the overall synthesis strategy, the synthesis was continued and the aldehyde **5** was converted smoothly to the α,β-unsaturated *tert*-butyl carboxylic ester **6** with a Wittig reaction. After this successful installation of the masked glutamic aldehyde equivalent, a change of the benzyl ester protecting group to an allyl ester protection was envisaged. This however, required a removal of the benzyl group without affecting the double bond of the α,β-unsaturated system. A selective hydrogenation protocol described by Shah *et. al.* that uses palladium(II) acetate as a catalyst and triethylsilane as an *in situ* source of hydrogen enabled the selective cleavage of the benzyl group in the presence of the double bond, affording the free carboxylic acid **7** in 62% yield.[113] The reaction however turned out to be more delicate than first expected. It turned out that the yields of this reaction depended on the batch size. Especially large reaction batches led to unsatisfying yields. Nonetheless, the carboxylic acid **7** was converted to the respective allyl ester using the well-established protocol by Kunz *et. al.* (*i. e.* allylation of the cesium salt of the carboxylic acid with allyl bromide).[114] The simultaneous removal of the *tert*-butyl ester and the Boc protection using trifluoroacetic acid then set the stage for the introduction of the Fmoc protection at the *N*-terminus to finally yield the desired Ahp precursor I (**1**). The reaction of the free amine **9** with Fmoc-Cl at a basic pH in a dioxane-water mixture however provided the desired product **1** only in 49% yield and turned out to be rather irreproducible if larger reaction batch sizes were used.[115]

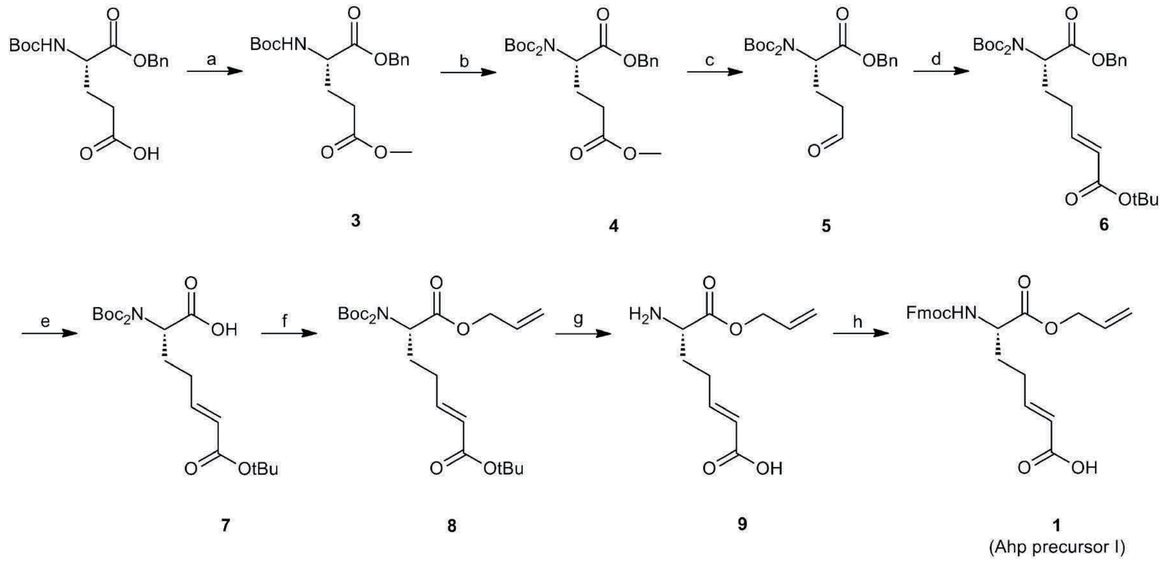

Figure 49: Alternative pathway to the generation of the Ahp precursor I (**1**). Reagents and conditions: (a) methyl iodide, K_2CO_3, acetone, reflux, 4 h (quant.); (b) Boc_2O, DMAP, CH_3CN, rt, 20 h (98%); (c) DIBAL-H, toluene, -78 °C, 5 h (27%); (d) i. $Ph_3P^+CH_2COO(CH_3)_3Cl$, 2 M NaOH/toluene (1:1); ii. **5**, ylide, CH_2Cl_2, rt, o/n (84%); (e) $Pd(OAc)_2$, Et_3SiH, Et_3N, CH_2Cl_2, rt, o/n (62%); (f) i. Cs_2CO_3, MeOH; ii. allylbromide, DMF, rt, o/n (76%); (g) TFA/CH_2Cl_2 (1:1), rt, 4 h; (h) FmocCl, $NaHCO_3$ (sat. solution), pH>8, dioxane/H_2O (1:1), 40 °C, rt, o/n (max. 49%).[115]

This discouraging result, along with the only moderate yields for the reduction of the methyl ester to the aldehyde, called for yet another reconsideration of the synthetic strategy. Consequently, the initial synthesis strategy was picked up again: In contrast to the first attempt, the aldehyde should however be generated at a later stage of the synthesis. Consequently, the alcohol **2** was converted to the silyl ether intermediate **10** before the second Boc group was introduced in order to obtain the fully protected amino acid **11** in an excellent yield. The next step in the synthesis was the exchange of the protection at the carboxylic acid functionality. Next, the benzyl ester was removed by hydrogenation. The reaction conditions for this hydrogenation reaction required some adjustment as the standard conditions using ethanol or methanol as the solvent resulted in a significant cleavage of the silyl ether protection. This circumstance was overcome by using ethyl acetate as the solvent for the hydrogenation reaction as described by Hirota and coworkers.[98] Using this procedure, the free acid **12** was obtained on a large scale in quantitative yields. The conversion of the free acid **12** to the allyl ester-protected intermediate **13** then proceeded smoothly using the previously established reaction conditions, providing the fully protected intermediate **13** in 95% yield. The cleavage of the silyl ether protecting group required some investigations again. The standard conditions using TBAF resulted instead of the formation of the desired alcohol in the formation of an undesired lactone species. A method using phosphomolybdic acid that was immobilized on silica gel was however able to cleave the silyl ether selectively. [116] Unfortunately, during chromatographic purification, one of the two Boc protecting groups was cleaved as well. Finally, a very mild Cu^{II}-mediated reaction provided the desired alcohol **14** in a high yield without any by-products.[117] The aldehyde **15** was then obtained by Dess-Martin oxidation and the subsequent Wittig reaction provided again the α,β-unsaturated, fully protected species **8**. After the simultaneous removal of the Boc groups and the *tert*-butyl ester, the conversion of **9** to the Ahp precursor I (**1**) was reinvestigated (Fig. 50). For the introduction of the Fmoc group, different reaction conditions were explored: Fmoc-Cl and Fmoc-OSu were compared alongside with different inorganic ($NaHCO_3$) and organic bases (Et_3N, DIEA), different solvent mixtures were also investigated such as a dioxane-water mixture or pure organic solvent. Unfortunately none of the conditions explored could provide the desired Fmoc-protected species.

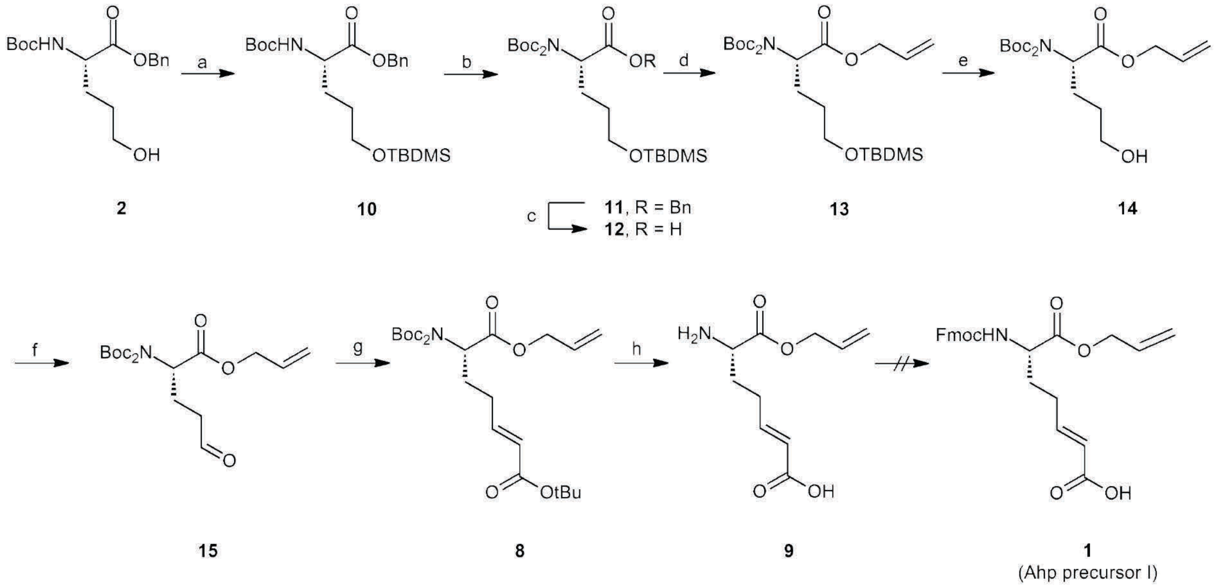

Figure 50: A new attempt to the synthesis of Ahp precursor I (**1**). Reagents and conditions: (a) TBDMSCl, imidazole, CH_2Cl_2, 0 °C to rt, o/n (95%); (b) Boc_2O, DMAP, CH_3CN, rt, 24 h (81%, b.r.s.m.); (c) 10% Pd/C, H_2, EtOAc, rt, 2.5 h (99%); (d) i. Cs_2CO_3, MeOH; ii. allylbromide, DMF, rt, o/n (95%); (e) $CuCl_2 * 2H_2O$, acetone/H_2O (95:5), reflux, 1 h (92%); (f) Dess-Martin periodinane, CH_2Cl_2, rt, 1 h (84%); (g) i. $Ph_3P^+CH_2COO(CH_3)_3Cl$, 2 M NaOH/toluene (1:1); ii. **15**, ylide, CH_2Cl_2, rt, o/n (94%); (h) TFA/CH_2Cl_2 (1:1), rt, 4 h.[115,118]

As an alternative, several methods to cleave the Boc groups selectively and leave the *tert*-butyl ester protection intact were then investigated. Depending on the reagents that were used, the cleavage of a single Boc group could be observed but also a complete decomposition of the material, most likely due to a Michael addition to the α,β-unsaturated system. The attempts to introduce a TMSE group as an alternative protection did not succeed; neither did the attempted exchange of the amine for an azide group.

An even more discouraging result was then obtained when the little amount of Ahp precursor I that had been obtained by the former reaction strategy was coupled to the solid phase: the synthesis of a model peptide could not be carried out successfully as the cleavage of the Fmoc group already resulted in the formation of unwanted side products, rendering the precursor not suitable for a use in solid-phase synthesis. The source of the undesired side reactions as well as the difficulties in the installation of any protecting group at the *N*-terminus is most likely the α,β-unsaturated system that is prone to nucleophilic attack, for example by the intramolecular amine group.

These findings consequently required a reconsideration of the design of the Ahp precursor structure. Hence, it was necessary to omit the conjugated double bond and investigate a strategy for the incorporation of an isolated double bond as the masked glutamic aldehyde equivalent alongside with a group that would allow the attachment to the solid phase. Owing to the difficulties experienced previously for the introduction of the Fmoc protecting group, an alternative strategy was to maintain the bis-Boc protection and explore alternative resins that would be stable under the acidic conditions required for the removal of the Boc groups as well as under the basic conditions required for the removal of Fmoc protecting groups.

In a first study towards such a system, a precursor with a terminal vinyl iodide which could be coupled to a borylated resin in a Suzuki reaction was investigated. This approach required in addition an exchange of the permanent allyl ester protection to a protecting group that is stable under the cross-coupling conditions as well as under the conditions required for the removal of the Boc and the Fmoc protection. These features are provided by the 2-(pyridyl)ethyl ester (Pet) protecting group that was introduced by Kunz and Kessler and can be removed after alkylation with mild base.[119,120] The application of this protecting group in solid-phase peptide synthesis has been demonstrated by Taylor *et. al.*.[121]

Furthermore, the new synthetic route envisaged the ring opening of a hemiaminal derived from pyroglutamic acid by a Wittig reaction, thereby completely avoiding the formation of a highly reactive intermediate aldehyde. Hence, the synthesis started from pyroglutamic acid which could readily be esterified with 2-(pyridyl)ethyl alcohol and protected with a Boc group at the amide position. The DIBAL-H reduction of the 2-pyrrolidone then yielded the hemiaminal that could be ring-opened by a Wittig reaction with Ph_3PCH_2I (Fig. 51).

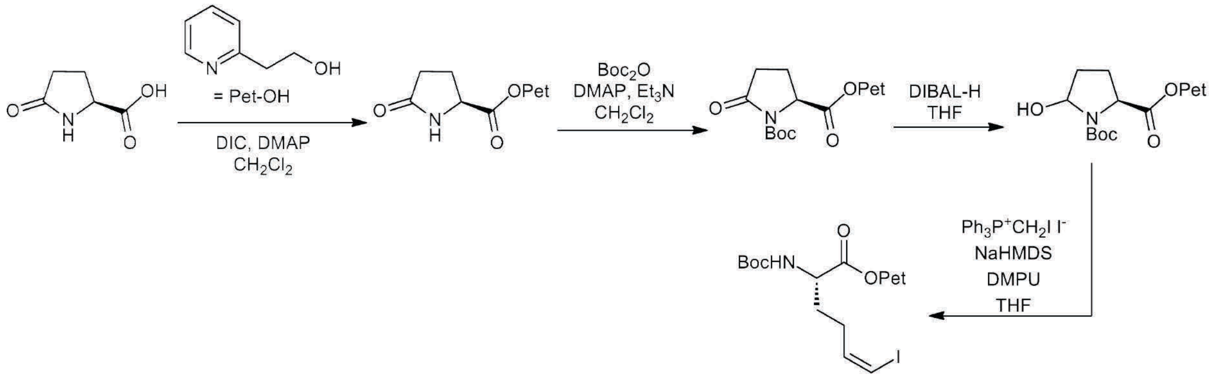
= Pet-OH
DIC, DMAP
CH2Cl2
OPet
Boc2O
DMAP, Et3N
CH2Cl2
Boc
DIBAL-H
THF
HO
Ph3P+CH2I I-
NaHMDS
DMPU
THF
BocHN
I

Figure 51: An alternative Ahp precursor suitable for the coupling to a borylated resin.

With this alternative precursor in hand, a Suzuki coupling to two different borylated resins was investigated (Fig.52).

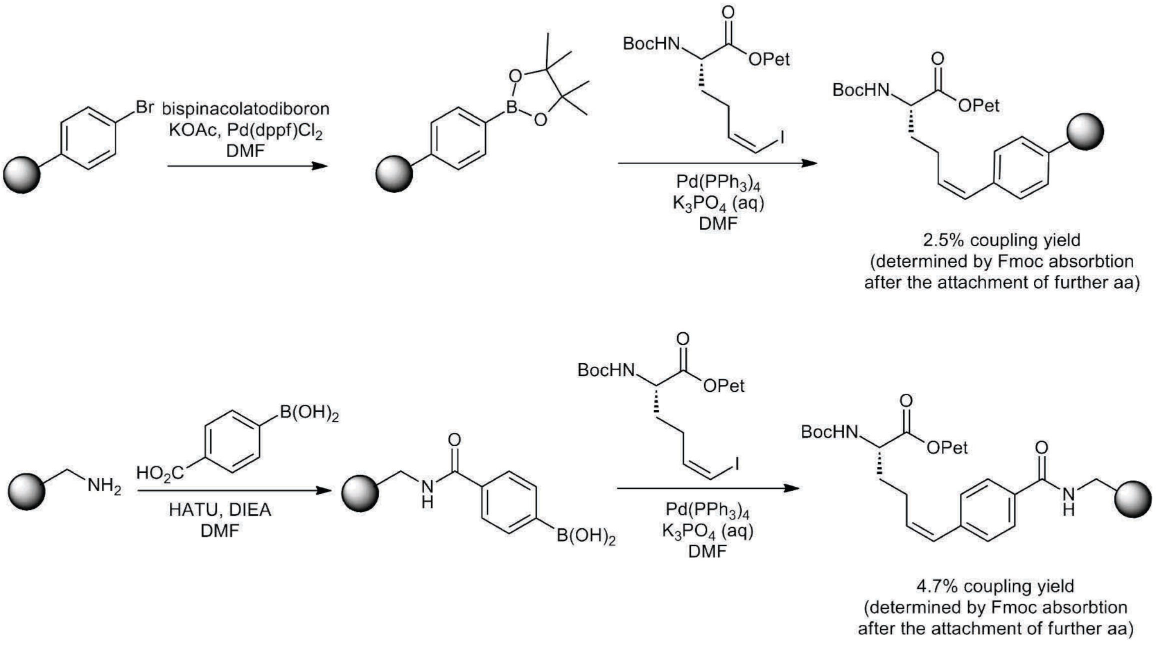
Br
bispinacolatodiboron
KOAc, Pd(dppf)Cl2
DMF
BocHN
OPet
I
Pd(PPh3)4
K3PO4 (aq)
DMF
2.5% coupling yield
(determined by Fmoc absorbtion
after the attachment of further aa)
NH2
HO2C
B(OH)2
HATU, DIEA
DMF
4.7% coupling yield
(determined by Fmoc absorbtion
after the attachment of further aa)

Figure 52: Attempted attachment of the vinyl iodide precursor to borylated resins.

The first resin was a boronic ester-modified resin that was generated by the reaction of 4-bromopolystyrene with bispinacolatodiboron. The reaction with the alternative Ahp precursor was monitored by Fmoc determination after the attachment of the second amino acid. For this combination of resin and precursor, only very low coupling yields were achieved, with a maximal loading of 2.5%.[122] As an alternative, a boronic acid-modified resin was also investigated; however, again only very low coupling yields could be achieved (4.7%) (Fig. 52).[123,124] Due to these disappointing results, the Suzuki-cross-coupling approach was not pursued further.

The final solution towards the synthesis of a suitable Ahp precursor II resulted from a reinvestigation of the second synthesis approach of Ahp precursor I. The idea was to use an alternative Wittig reagent that could provide on the one hand the free acid required for the attachment to a suitable resin and could on the other hand introduce an isolated (and no longer a conjugated) double bond, if aldehyde **15** was used. To set this into practice, a Wittig reagent derived from butyric acid was used and Ahp precursor II (**16**) could readily be synthesized from the aldehyde **15** (Fig. 53). For the Wittig reaction, different bases (NaHMDS, KHMDS, LHMDS), an addition of DMPU and different reaction conditions (-78 °C to rt) were explored. The best results were obtained with LHMDS without any additive and a slow warming of the reaction mixture from 0 °C to ambient temperature. The chromatographic purification of the free acid product required some effort to find an optimal solvent mixture and an adequate flow rate to ensure a pure product.[115,118]

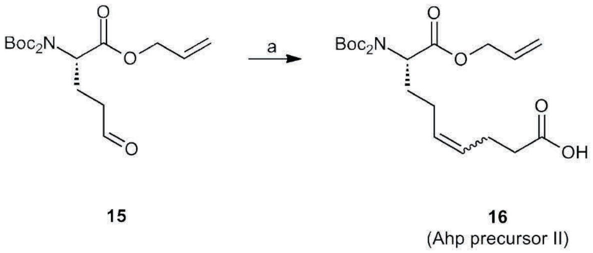

Figure 53: The final modification yielding Ahp precursor II (**16**). Reagents and conditions: a) i. $Ph_3P^+(CH_2)_3CO_2H$ Br^-, LHMDS,THF, 0 °C, 55 min; ii. **15**, THF, 0 °C to rt, o/n (64%).[115,118]

3.1.1.2 Development of a solid-phase strategy with Ahp precursor II

With the Ahp precursor II (**16**) in hands, a solid-phase synthesis strategy using this building block could finally be investigated. To this end, a synthesis of the natural product symplocamide A was envisaged. This natural product was isolated in 2007 and elucidated as a potent chymotrypsin inhibitor.[24] Furthermore, at the beginning of this dissertation no synthesis of symplocamide A had been reported.

Initially, first model studies on a symplocamide derivative in which the 3-bromo-4-methyl N-methyl tyrosine was replaced by an *N*-methyl phenylalanine moiety were performed. To this end, the Ahp precursor was coupled to amino-methylated polystyrene resin and the peptide sequence was assembled solely with standard conditions (HOBt/HBTU peptide coupling; DIC/DMAP esterification; PyBrOP coupling to mPhe) to test for general problems in the synthesis route. The conditions for the oxidative cleavage from the solid phase were adapted from the protocol provided by Meldal and coworkers, using OsO_4 and $NaIO_4$ in a one-pot reaction and adding DABCO to suppress the formation of hydroxymethyl ketones (Fig.54).[108]

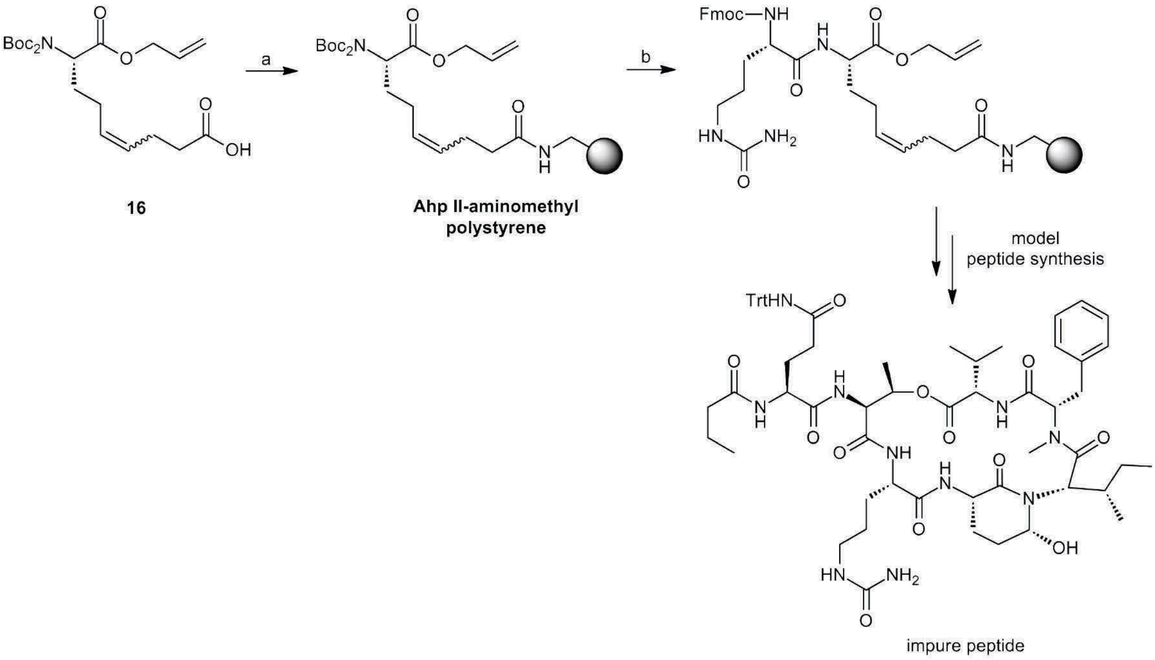

Figure 54: Synthesis of a first model peptide on amino-methylated polystyrene. Reagents and conditions: (a) i. amino-methylpolystyrene (0.9 mmol/g), **16** (1.2 eq.), HOBt, DIC, CH_2Cl_2/DMF (9:1), rt, 24 h; ii. CH_2Cl_2/DIEA/Ac_2O (3:1:1), 3h; (b) i. TFA/CH_2Cl_2 (1:1) 1 h; ii. Et_3N/CH_2Cl_2 (1:9), 2x 10 min; iii. Fmoc-Cit-OH, HOBt, HBTU, DIEA, DMF, 2 h (55%, by Fmoc determination, 2 steps).[115]

The peptide was cleaved from the resin and the crude peptide was purified by HPLC. A putatively pure peptide fraction was obtained by HPLC purification. The subsequent analysis of this fraction by LC-MS revealed however that the fraction still contained a large quantity of impurities.[115]

The extent of impurities found after resin cleavage gave rise to the suspicion that the polystyrene core of the resin used in the synthesis was not stable under the cleavage conditions. This hypothesis was reinforced by a simple test reaction in which the amino-methylated polystyrene was acylated with acetic anhydride and base. The resin was then subjected to the reaction conditions for the oxidative cleavage. A LC-MS analysis of the cleaved material showed clearly the same impurities that had been observed after the cleavage of the model peptide, proving that the polystyrene core is indeed instable under the cleavage conditions.

To overcome this obstacle, two alternative resins (NovaPEG amino resin and aminoPEGA resin, both from Novabiochem) that consist of a polyethylene-glycol core instead of a polystyrene core were investigated under the same conditions as the amino-methylated resin. For both resins, no impurities were observed after the cleavage. For practical reasons, NovaPEG amino resin was therefore chosen as the solid support in subsequent syntheses.

In a first study the model peptide that had previously been synthesized on the amino-methylated polystyrene was re-synthesized on the NovaPEG amino resin. Consequently, reaction conditions adapted to the different handling of the polyethylene-glycol-based resin had to be developed. For example, this resin shows a swelling behavior that is significantly different from the behavior of customary polystyrene-based resins and is especially difficult to dry to a constant weight. Therefore, tedious washings with anhydrous solvents and prolonged drying under high vacuum were performed prior to reactions that required a dry resin (for example an Fmoc determination). Furthermore, the coupling time for a regular peptide coupling was extended to four hours or sometimes even overnight to achieve complete conversions.

The coupling of the Ahp precursor to the NovaPEG amino resin was achieved with DIC/HOBt activation, followed by a capping step to block the remaining free amines. The removal of the Boc groups from the Ahp precursor was achieved by using a mixture of 50% TFA in dichloromethane. This was followed by a neutralization step with 10% triethylamine in dichloromethane. For the regular peptide couplings HOBt/HBTU activation was applied after the deprotection of the *N*-terminus. For the removal of the Fmoc protection a mixture of 20% piperidine in DMF was used.

After the coupling of the P_1 amino acid citrulline, the resin was dried thoroughly to enable the determination of the initial loading by an Fmoc determination. A full loading of the resin was not intended to prevent side-reactions during the *on-resin* macrolactamization reaction. Instead, a lower loading to ensure *pseudo*-dilution conditions similar to the conditions used for cyclization reactions in solution was envisaged. This was achieved by using 2.4 equivalents of the Ahp precursor **16** in the loading reaction which resulted in an initial loading of efficiency of 30% (0.20 mmol/g resin).

Next, a threonine building block was incorporated that did not feature a protecting group on the side chain hydroxyl function. The secondary alcohol of the threonine side chain is much less reactive than a primary amine in coupling reactions and therefore no laborious protection/deprotection sequence prior to the esterification on this moiety is therefore required. In the next steps, Fmoc-Gln(Trt)-OH was coupled, followed by butyric acid.

The subsequent esterification needed different activating reagents and a higher excess of reagents than a standard peptide coupling. To this end, the conditions for the esterification of the threonine side chain with valine were optimized. The best protocol consisted of four repetitive short-time (2 hours) couplings, using 10 equivalents of Fmoc-Val-OH and the coupling reagent (DIC) but only 1 equivalent of coupling additive (DMAP) in a mixture of dichloromethane and dimethylformamide. This procedure provided excellent coupling yields that were superior compared to the yields obtained for example by a single 24 hour coupling as determined by resin loading determination after the esterification (Fig. 55).

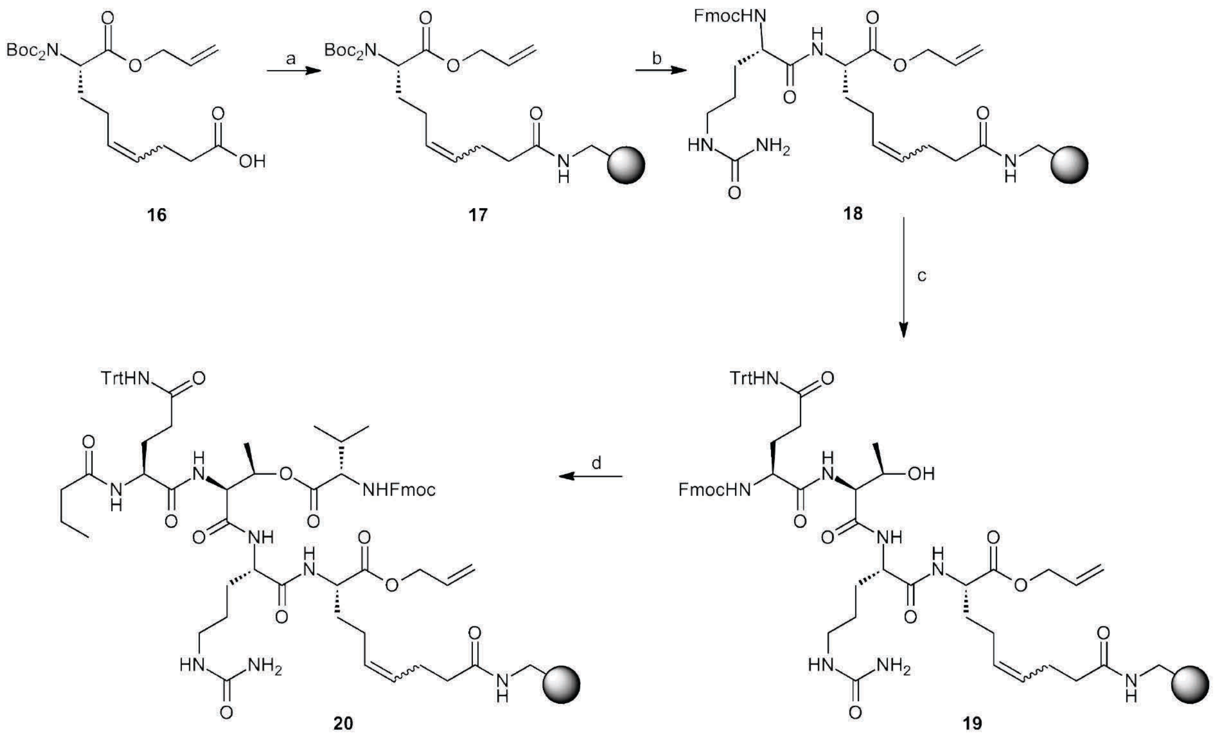

Figure 55: First steps in the synthesis of a symplocamide A model peptide on amino NovaPEG resin. Reagents and conditions: (a) i. amino NovaPEG resin (0.66 mmol/g), **16** (2.4 eq.), HOBt, DIC, CH_2Cl_2/DMF (9:1), 24 h; ii. CH_2Cl_2/DIEA/Ac_2O (3:1:1), 3 h (b) i. TFA/CH_2Cl_2 (1:1), 1 h; ii. Et_3N/CH_2Cl_2 (1:9), 2x 10 min; iii. Fmoc-Cit-OH, HOBt, HBTU, DIEA, DMF, 5 h (30%, by Fmoc determination, 2 steps); (c) i. piperidine/DMF (1:4), 2x 15 min; ii. Fmoc-Thr-OH, HOBT, HBTU, DIEA, DMF, 2 h; iii. piperidine/DMF (1:4), 2x 15 min; iv. Fmoc-Gln(Trt)-OH, HOBT, HBTU, DIEA, DMF, 2 h (88% by Fmoc determination, 2 couplings); (d) i. piperidine/DMF (1:4), 2x 15 min; ii. butyric acid, HOBT, HBTU, DIEA, DMF, 2 h; iii. Fmoc-Val-OH, DIC, DMAP, CH_2Cl_2/DMF (9:1), 4 x 2 h (79% by Fmoc determination, 2 couplings).[115]

Next, Fmoc-*N*-methyl phenylalanine was coupled, followed by cleavage of the Fmoc group. The coupling of Fmoc-Ile-OH to the *N*-methylated phenylalanine required harsher coupling conditions and was achieved by using PyBrOP as the coupling reagent and prolonging the reaction time to 24 hours. PyBrOP is the coupling reagent of choice for the difficult coupling to sterically hindered and less reactive amino acids such as *N*-methylated amino acids. After the attachment of the final amino acid isoleucine, the Fmoc protection on this amino acid as well as the allyl protection on the Ahp precursor needed to be removed to set the stage for the cyclization reaction. The Fmoc group was cleaved using the standard protocol, the regular washing protocol was supplemented by a tedious washing protocol and thorough drying in order to prepare the resin for the removal of the allyl protection. The removal of the allyl group was carried out using the protocol established by Vaz, using $Pd(PPh_3)_4$ as catalyst and morpholine as the scavenger and conducting the reaction in degassed solvent.[105] In order to remove residual catalyst, a tedious washing protocol was again required after the cleavage reaction.

For the *on-resin* macrolactamization, the conditions established during the first synthesis on the amino-methylated polystyrene resin were employed. Consequently, PyBOP as the coupling reagent along with the additive HOBt and the base DIEA were used and the reaction time was extended to 24 hours to ensure a complete conversion. As a further optimization, first HOBt and DIEA were added as a solution in DMF to the resin for the pre-activation of the free acid, followed by addition of PyBOP dissolved in DMF; the resulting suspension was then shaken for 24 hours. After the customary washing of the resin, a Kaiser test was carried out to check for full conversion, revealing a complete reaction after 24 hours. In addition, no intermolecular coupling products could be observed by LC-MS analysis after the cleavage from the resin, indicating the applicability of the found reaction conditions (Fig. 56).

In the first attempt to synthesize a symplocamide A model peptide, cleavage of the crude peptide from the resin was achieved by using the reaction conditions reported by the Meldal group.[108] In this procedure, a precipitation of sodium periodate and DABCO from the water-THF mixture was, however, observed. To prevent the precipitation as well as to account for the different swelling properties of the PEG-based resin, the cleavage conditions were adjusted. Sodium periodate and DABCO were dissolved individually in water, using ultrasonication to promote dissolution of the reagents. The reagent solutions were then added to the dry resin, which was subsequently allowed to swell in this mixture for 10 minutes. After this time, THF was added to obtain a 1:1 solvent mixture and the resin was shaken for 2 minutes. After this time, a solution of osmium tetroxide in *t*-BuOH was carefully added and the resin was shaken for 20 hours. For work-up, the highly toxic osmium tetroxide was quenched with sodium metabisulfite. The extraction of the resulting aqueous solution with organic solvents turned out to be rather tedious and best results were obtained with ethyl acetate.

In order to investigate the efficiency of the cleavage protocol, the cleavage of the crude peptide from the resin was carried out twice. The resulting crude mixtures were analyzed separately to investigate the impact of a double cleavage procedure on the yield of the solid-phase synthesis. As the second cleavage contained only traces of the desired peptide, only a single cleavage reaction was used in later Ahp cyclodepsipeptide syntheses. After the cleavage from the resin, the crude peptide with the trityl protecting group on the glutamine side chain was purified by HPLC, yielding the desired Ahp cyclodepsipeptide in 1.2% overall yield (based on **18**).[115]

Next, a cleavage of the trityl protecting of the glutamine side chain was attempted. To this end, a solution containing 95% trifluoroacetic acid and 2.5% water and TIS, respectively, was used. However, when the Ahp cyclodepsipeptide **24** was submitted to these conditions, a rapid and almost complete decomposition of the peptide was observed, owing most probably to the strong acidic conditions (Fig. 56).[115] This finding indicates that Ahp cyclodepsipeptides are not stable to strongly acidic conditions, calling for an adjustment of the synthetic route (*via* the use of alternative building blocks with differently cleavable protecting groups).

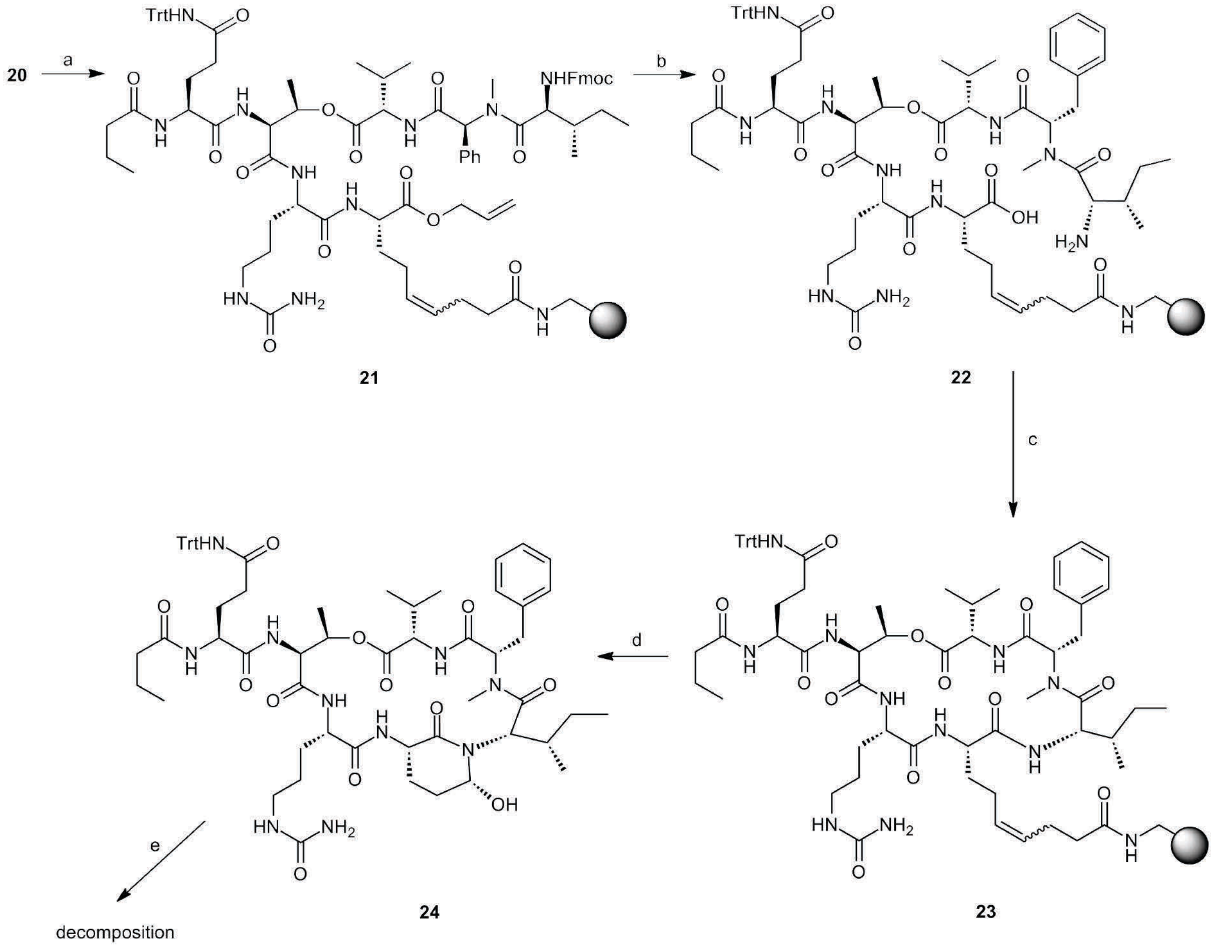

Figure 56: Synthesis of a symplocamide A model peptide on amino NovaPEG resin (continued). Reagents and conditions: (a) i. piperidine/DMF (1:4), 2x 15 min; ii. Fmoc-*N*MePhe-OH, HOBT, HBTU, DIEA, DMF, 2 h; iii. piperidine/DMF (1:4), 2x 15 min; iv. Fmoc-Ile-OH, PyBrOP, DIEA, DMF, 24 h (60%, by Fmoc determination, 2 couplings); (b) i. piperidine/DMF (1:4), 2x 15 min; ii. $Pd(PPh_3)_4$, morpholine, CH_2Cl_2, 30 min; (c). PyBOP, HOBt, DIEA, DMF, 24 h; (d) i. $NaIO_4$, OsO_4 (0.1 M in *t*-BuOH), DABCO, H_2O/THF (1:1), 20 h; ii. HPLC purification (1.2 % overall yield); (e) TFA/TIS/H_2O (95:2.5:2.5).[115]

Thus, in later syntheses of Ahp cyclodepsipeptides, protecting groups requiring strong acid for their removal should be avoided or cleaved before the formation of the Ahp moiety. Fortunately, the overall strategy for the synthesis of the Ahp cyclodepsipeptides however proved to be feasible.

3.1.2 Solid-phase total synthesis of symplocamide A

Consequently, to achieve a total synthesis of symplocamide A, an introduction of the glutamine moiety was by coupling of Boc-Gln-OH was envisaged, thereby leaving the side chain unprotected and rendering a later deprotection obsolete. An unprotected glutamine side chain is however always prone to form pyroglutamates under weak acidic conditions. The cleavage of the Boc group is however performed under strong acidic conditions. As the neutralization is carried out directly after the cleavage, the formation of pyroglutamates seemed rather unlikely in this case. In contrast, the possibility to use Boc-protected amino acid building blocks as an alternative to Fmoc-protected species also offered the opportunity to a simplified solution phase synthesis of amino acid building blocks. For example, the required unnatural tyrosine derivative 3-bromo-4-methyl-*N*-methyl tyrosine was synthesized as a Boc-protected derivative (Fig. 57). This building block was synthesized in a straightforward manner from (*L*)-tyrosine using a literature procedure for the first steps of the synthesis. To this end, a bromination of the aromatic moiety was performed, followed by introduction of the Boc group. Then, the ester as well as phenol moiety were methylated, followed by *N*-methylation with sodium hydride and methyl iodide in DMF. A fine-tuning of the conditions of the *N*-methylation was required to prevent a racemization of the amino acid building block; consequently, no racemization was detected when the reaction time was limited to one hour. Finally, the methyl ester was saponified, leading to the building block **29** for solid phase synthesis.[118,125]

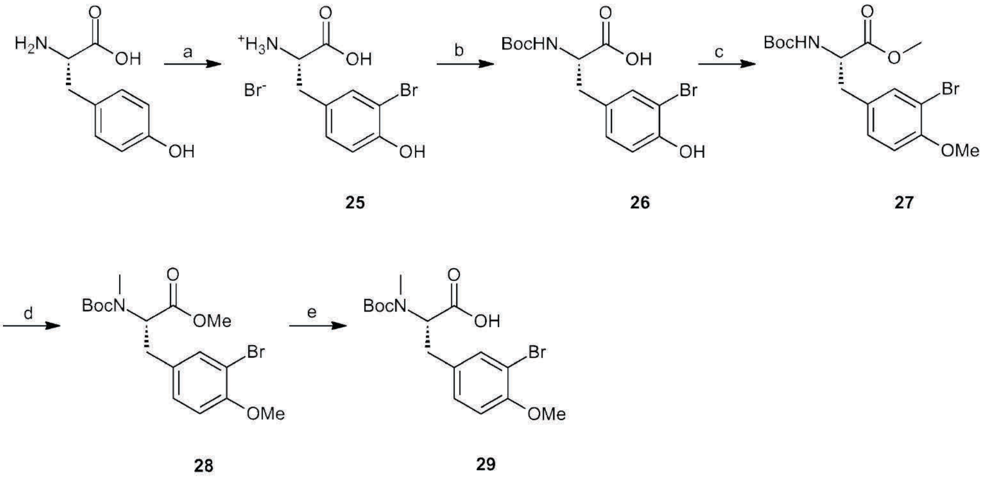

Figure 57: Synthesis of the *N*-methylated (3-Br,4-OMe) tyrosine building block for the symplocamide A synthesis. Reagents and conditions: (a) HBr in HOAc (33%), Br_2, HOAc, rt, 27 h (96%); (b) Boc_2O, 2 M NaOH, pH 9, *t*-BuOH/H_2O (9:1), rt, 1 h (93%); (c) i. **29**, Cs_2CO_3 (aq.), MeOH/H_2O (11:1); ii. Cs salt of **29**, CH_3I, DMF, rt, 18 h (70%)[125]; (d) NaH, CH_3I, DMF, rt, 1 h; (90%); (e) LiOH, THF/MeOH/H_2O (1.67:1:0.67), rt, 5 h (78%)[118].

With this tyrosine building block **29** in hands, the synthesis of symplocamide A was initiated. The loading of the resin with the Ahp precursor was adjusted slightly for this synthesis by using the coupling reagents HBTU/HOBt activation instead of the previously applied DIC/HOBt activation, leading to an enhanced coupling yield of 36%. In the other reaction steps, the reaction conditions of the model peptide synthesis were employed. Importantly, the reactions as well as their yields proved to be fully reproducible and were verified by intermediate loading determinations. The natural product symplocamide A could finally be obtained after the oxidative cleavage from the resin and a subsequent HPLC purification of the crude peptide in an overall yield of 3% (based on **31**) (Fig. 58). [115,118]

The spectroscopic data (NMR analysis, mass spectra, optical rotation) of the synthetic symplocamide A derivative thereby corresponded well to the data published for the isolated natural product symplocamide A[24], proving a successful synthesis of this natural product.

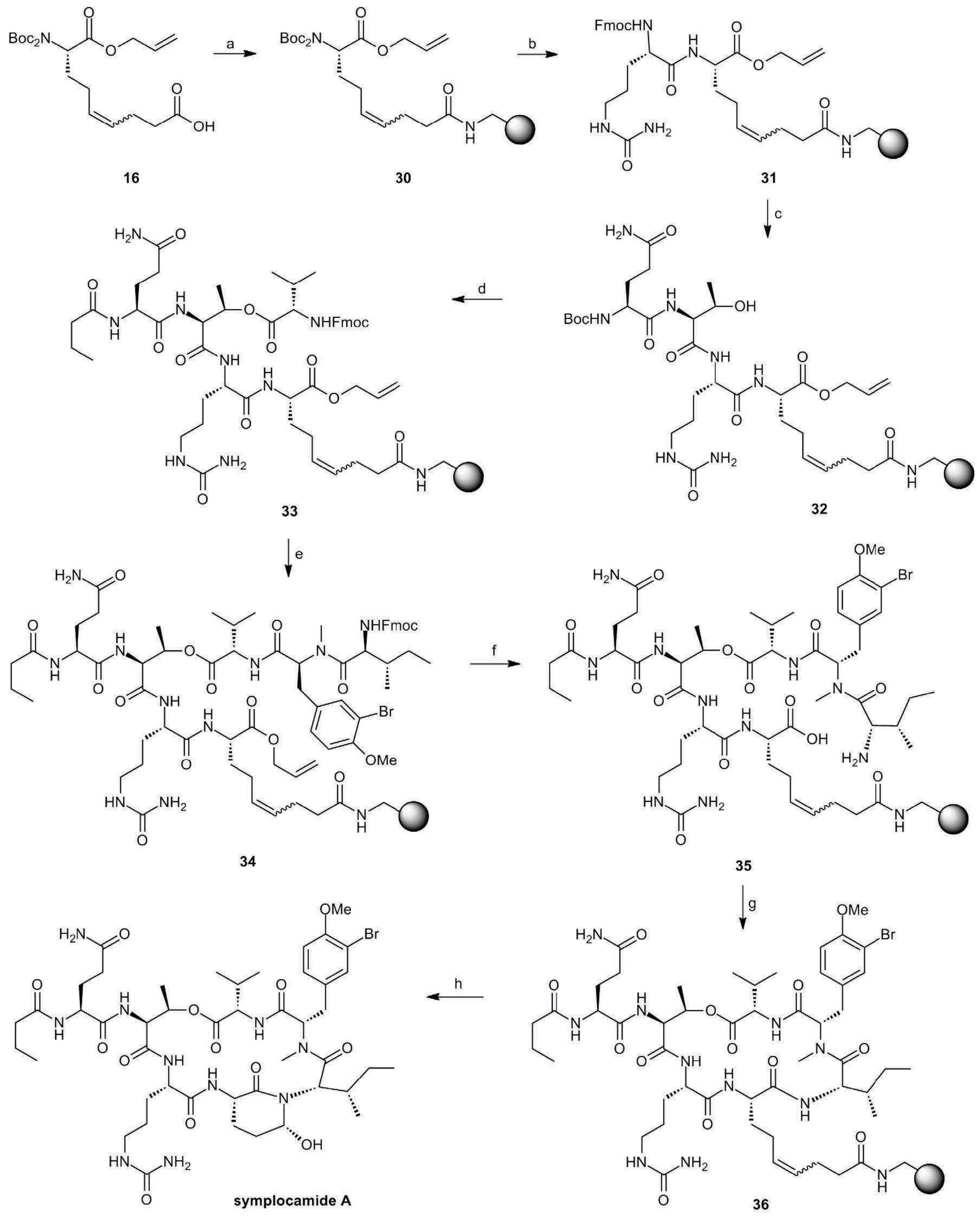

Figure 58: Solid-phase synthesis of symplocamide A. Reagents and conditions: (a) i. amino NovaPEG resin (0.66 mmol/g), **16** (2.5 eq.), HOBt, HBTU, DIEA, CH_2Cl_2/DMF (9:1), 24 h; ii. CH_2Cl_2/DIEA/Ac_2O (3:1:1), 2x 2h; (b) i. TFA/CH_2Cl_2 (1:1), 1 h; ii. Et_3N/CH_2Cl_2 (1:9), 2x 10 min; iii. Fmoc-Cit-OH, HOBt, HBTU, DIEA, DMF, 4 h (36%, by Fmoc determination, 2 steps); (c) i. piperidine/DMF (1:4), 2x 15 min; ii. Fmoc-Thr-OH, HOBT, HBTU, DIEA, DMF, 5 h; iii. piperidine/DMF (1:4), 2x 15 min; iv. Boc-Gln-OH, HOBT, HBTU, DIEA, DMF, 4 h; (d) i. TFA/CH_2Cl_2 (1:1), 1 h; ii. Et_3N/CH_2Cl_2 (1:9), 2x 10 min; iii. butyric acid, HOBT, HBTU, DIEA, DMF, 4 h; iv. Fmoc-Val-OH, DIC, DMAP, CH_2Cl_2/DMF (9:1), 4x2 h (92% by Fmoc determination, 4 couplings); (e) i. piperidine/DMF (1:4), 2x 15 min; ii. Boc-mTyr(3-Br, 4-OMe)-OH, HOBT, HBTU, DIEA, DMF, 4.5 h; iii. TFA/CH_2Cl_2 (1:1), 1 h; iv. Et_3N/CH_2Cl_2 (1:9), 2x 10 min; v. Fmoc-Ile-OH, PyBrOP, DIEA, DMF, 24 h (73%, by Fmoc determination , 2 couplings); (f) i. piperidine/DMF (1:4), 2x 15 min; ii. $Pd(PPh_3)_4$, morpholine, CH_2Cl_2, 30 min; (g) PyBOP, HOBt, DIEA, DMF, 24 h; (h) i. $NaIO_4$, OsO_4 (0.1 M in *t*-BuOH), DABCO, H_2O/THF (1:1), 20 h; ii. HPLC purification (3% overall yield). [115,118]

3.1.3 Biological evaluation of symplocamide A

After the successful synthesis of symplocamide A, its biological properties were investigated. To this end, its reported chymotrypsin-inhibitory properties were verified. The inhibition assay was performed using a previously established assay.[126-128] In these measurements, the synthetic symplocamide A displayed a K_i value of 0.32 ± 0.09 µM which is in good accordance with the literature report (lit.[24]), IC_{50} = 0.38 ± 0.08 µM). Due to this potent inhibition, an attempt to co-crystallize symplocamide A with its target protease chymotrypsin was undertaken by the Groll group (TU München). Yet, all investigated conditions unfortunately failed to deliver a suitable crystal for x-ray structure determinations. Furthermore, the cross-reactivity of symplocamide A was tested in a trypsin-inhibition assay; no inhibition of trypsin was detected.

In the original publication of the symplocamide A isolation and structure elucidation, it was suggested that symplocamide A could act also as a proteasome inhibitor.[24] To test this hypothesis, two different proteasome inhibition assays, the first being a fluorescence-based enzyme assay and the second being an activity-based profiling assay, were performed with symplocamide A. In both assays no inhibition of the proteasome or one of its subunits was observed. This result is however not surprising if one is aware of the fact that despite its deceptive nomenclature, the chymotryptic subunit of the proteasome is structurally highly different from the serine protease chymotrypsin and that an inhibitor of this protease is *not* automatically prone to inhibit this subunit. In addition, Gerwick *et. al.* also reported a significant *in vitro* cytotoxicity of symplocamide A in two cancer cell lines (NCI H-460 nonsmall lung cancer cells, IC_{50} = 40 nM; neuro-2A mouse neuroblastoma cells, IC_{50} = 29 nM[24]). The attempt to reproduce this activity, however, failed, probably due to an alternative assay system.

3.2 Development and biological investigation of natural product-derived canonical-conformation protease inhibitors

The Ahp cyclodepsipeptides have been recognized as members of the class of canonical-conformation serine protease inhibitors.[18] Originally, the canonical conformation was recognized as the inhibitory motif of several proteinaceous inhibitors and at least 18 non-homologous families of serine protease inhibitors are known to adopt the canonical conformation.[17,18] For the plant-derived Bowman-Birk type inhibitors, extensive studies regarding the sequential preferences and a minimal sequence that is required to adopt the canonical conformation have been carried out.[18,20,22] During their studies on the structure and bioactivities of peptidic inhibitors derived from Bowman-Birk type inhibitors, Leatherbarrow *et. al.* became aware of the similarity of the conformation adopted by Ahp cyclodepsipeptides upon binding to a protease and the canonical conformation adopted by the BBI-derived inhibitors. Indeed, a detailed comparison of the binding conformations of the different inhibitors revealed that the Ahp cyclodepsipeptides along with other macrocyclic inhibitors of bacterial origin also adopt the canonical conformation, thereby representing a remarkable example of a convergent evolution.[18,129] The Ahp unit is therefore proposed as crucial for the bioactivity as it stabilizes the canonical conformation by participation in the hydrogen bonding and enhances the selectivity of the inhibitor by occupation of the S_1’ subsite. Furthermore, the Ahp unit also occupies the region of the catalytic pocket in which the water molecule required for the hydrolysis of a peptidic substrate is commonly located. As a result, this water molecule is excluded from the enzyme, resulting in an increased hydrolytic stability of the inhibitor.[18,29] Consequently, Ahp cyclodepsipeptides represent lead structures for the design of small molecule analogs of the canonical-conformation serine protease inhibitors with the Ahp residue as central element to pre-arrange the cyclodepsipeptide into the canonical conformation. Despite the developed synthesis to Ahp cyclodepsipeptides, the installation of the Ahp residue into the cyclodepsipeptide structure is a laborious step. It would therefore be of interest to investigate if the Ahp residue is essential for achieving a canonical conformation or if synthetically easier accessible mimics can be designed.

Consequently, the next step in this dissertation was to investigate if structurally simplified cyclodepsipeptides in which a natural amino acid replaces the Ahp unit under retention of the biological activity can be developed. After an adequate replacement for the Ahp unit had been found, structure-activity analogs of the Ahp-mimicked peptides were synthesized to gain an in-depth insight into the mode of action and the structural determinants of these small molecule analogs of canonical-conformation inhibitors.

3.2.1 Development of a solid-phase strategy towards simplified analogs of Ahp cyclodepsipeptides

The new approach to simplified analogs of the Ahp cyclodepsipeptides required an alternative strategy for the solid phase assembly of the cyclodepsipeptides. In contrast to the solid-phase strategy for the synthesis of the Ahp cyclodepsipeptides, the synthesized cyclodepsipeptides were not cyclized on the resin but in solution. Therefore, a more straight-forward solid-phase synthesis was possible (Fig. 59). Cyclization of the linear peptides was carried out prior to the cleavage of the remaining protecting groups. Since the resulting cyclodepsipeptides were expected to display a higher stability towards acidic conditions than the Ahp cyclodepsipeptides, the use of protecting groups that are cleaved by strong acidic conditions (*e. g*. a trityl amide protection for glutamine) was considered to be possible during the envisioned synthesis.

2-chlorotrityl chloride resin was chosen as the solid support for this synthesis because it provides a reliable basis for the customary synthesis of peptides on solid phase. Regular Fmoc-based peptide chemistry can be carried out with this resin that is also compatible with palladium-mediated cleavage of allyl groups. Moreover, this resin allows to cleave peptides with weak acids from the solid support (leaving a free *C*-terminus) while the “standard” side chain protecting groups are maintained.[130]

As the anchoring point to the solid phase, the P_1 amino acid of the cyclodepsipeptide was chosen, enabling a combinatorial approach to different structure-activity analogs from one resin loaded with the selectivity-determining P_1 amino acid. After the attachment of the P_1 amino acid, the P_2 threonine residue was coupled to the resin, in analogy to the Ahp cyclodepsipeptide synthesis, without a protection of the side chain. After the coupling of the future P_3 and P_4 residues, the esterification was carried out under the conditions developed during the synthesis of the Ahp cyclodepsipeptides.[115,118] For the incorporation of the commercially not available *N*-methylated amino acids, the building block synthesis of the *N*-methylated amino acids had to be adjusted to the different solid support. In the synthesis of Ahp cyclodepsipeptides on solid support, a Boc protecting group was used for these building blocks. This protecting group is however not compatible with the acid labile 2-chlorotrityl chloride resin. The building block synthesis was therefore adapted to the new resin and instead of a Boc-protection, *N*-methyl amino acid derivatives with an Alloc-protection on the amino group were generated from the existing Boc protected derivatives. The Alloc group was removed during solid phase synthesis with the protocol developed by Vaz that was also used in the previous syntheses.[105] After the coupling of the *N*-methylated amino acid (or for structure-activity relationship studies an alternative amino acid on this position), a PyBrOP-mediated coupling was again performed to couple the next amino acid on the secondary amine. The final step of the solid-phase synthesis was then the coupling of the amino acid candidate for the replacement of the Ahp residue (P_1' position). After the cleavage from the resin, the linear peptide was then cyclized in solution and the remaining protecting groups were cleaved. Finally, the resulting cyclodepsipeptide was purified by HPLC providing pure material for the further biological evaluation. (Fig.59, Fig. 60)

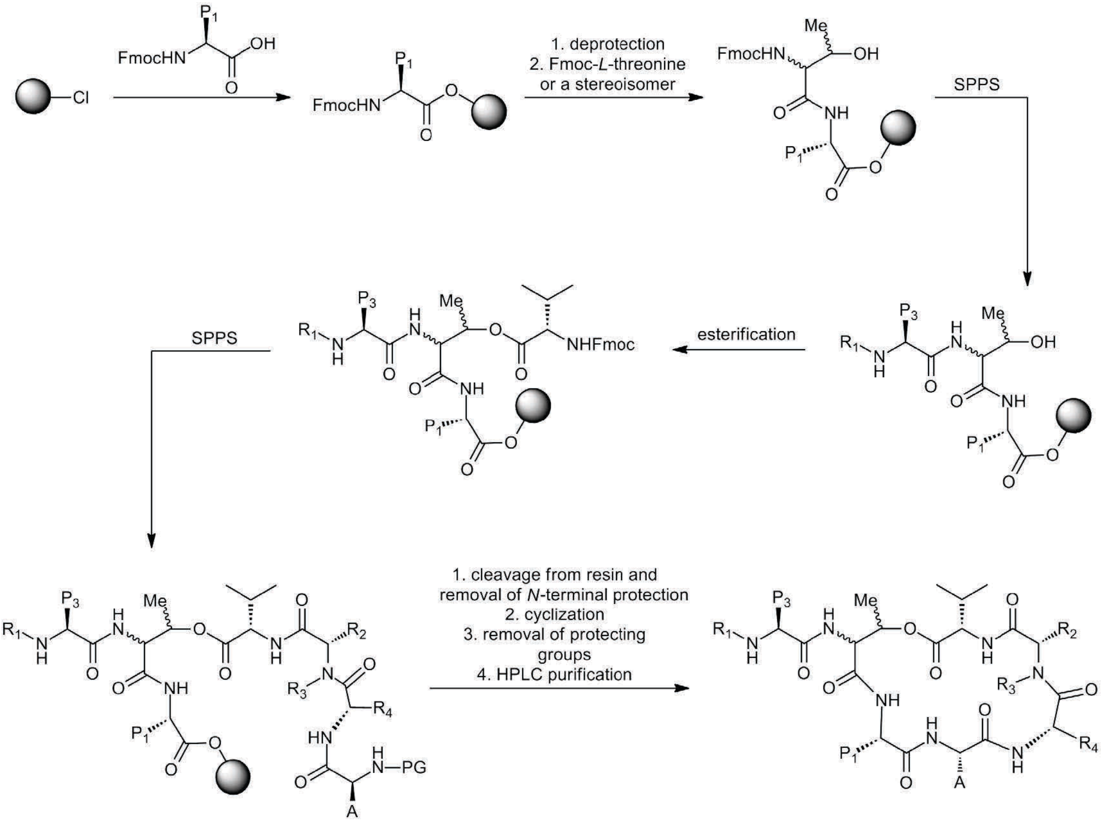
P1
FmocHN
OH
O
Cl
1. deprotection
2. Fmoc-*L*-threonine
or a stereoisomer
Me
OH
NH
SPPS
esterification
P3
R1
NHFmoc
1. cleavage from resin and
removal of *N*-terminal protection
2. cyclization
3. removal of protecting
groups
4. HPLC purification
R2
R3
R4
HN
N—PG
A

Figure 59: Synthetic strategy towards the solid-phase synthesis of Ahp cyclodepsipeptide-derived canonical-conformation analogs. P_1, P_3: amino acids occupying the S_1 or the S_3 subsite, respectively; R_1: P_4 amino acid (plus optional group); R_2, R_3: residues of the *N*-methylated analog or a substitution; R_4: side chain of P_2' amino acid; A: side chain of the amino acid replacing the Ahp moiety.

3.2.2 Synthesis of SAR analogs of Ahp-mimicked cyclodepsipeptides

This strategy allowed the synthesis of various simplified Ahp cyclodepsipeptide analogs (Fig. 60). For some cyclodepsipeptides, certain modifications of the synthesis route were necessary: For example, if serine was used as the Ahp replacement, for some analogs Boc-Ser(Bzl)-OH was used as the building block during synthesis. The Boc group could be cleaved without removing the benzyl ether protection on the serine side chain prior to the cyclization. This was important as the benzyl ether protection needed to remain intact during the cyclization reaction in order to prevent side reactions during the macrolactamization. Cleavage of the benzyl protecting group, however, turned out to require rather harsh reaction conditions (resulting in the need of a high amount of palladium on active charcoal (up to 40% wt) and 10% of acetic acid and overnight reaction times to achieve a full cleavage of the benzyl ether). These reaction conditions, however, proved to be incompatible with some modified *N*-methyl tyrosine derivatives (for example with a 3-bromo modification). Consequently, in these syntheses, Fmoc-Ser(Trt)-OH was used as the serine building block. For the cyclization of the linear depsipeptide, the following reaction conditions were used: As reagents, the combination of reagents established by Albericio *et. al.* during the synthesis of kahalalide F (*i. e.* PyBOP, DIEA) were used.[131] However, the procedure (low temperature, high dilution) was adapted from Shioiri's didemnin synthesis.[132] These reaction conditions led to a full conversion of the linear peptide to the macrocycle without detectable side products (for example from an intermolecular coupling).

Using these synthetic methodologies, a series of analogs of Ahp cyclodepsipeptides for the investigation of structure-activity relationships and evaluation of the structural determinants of the canonical conformation were synthesized (summarized in Figure 60 and Table 3).

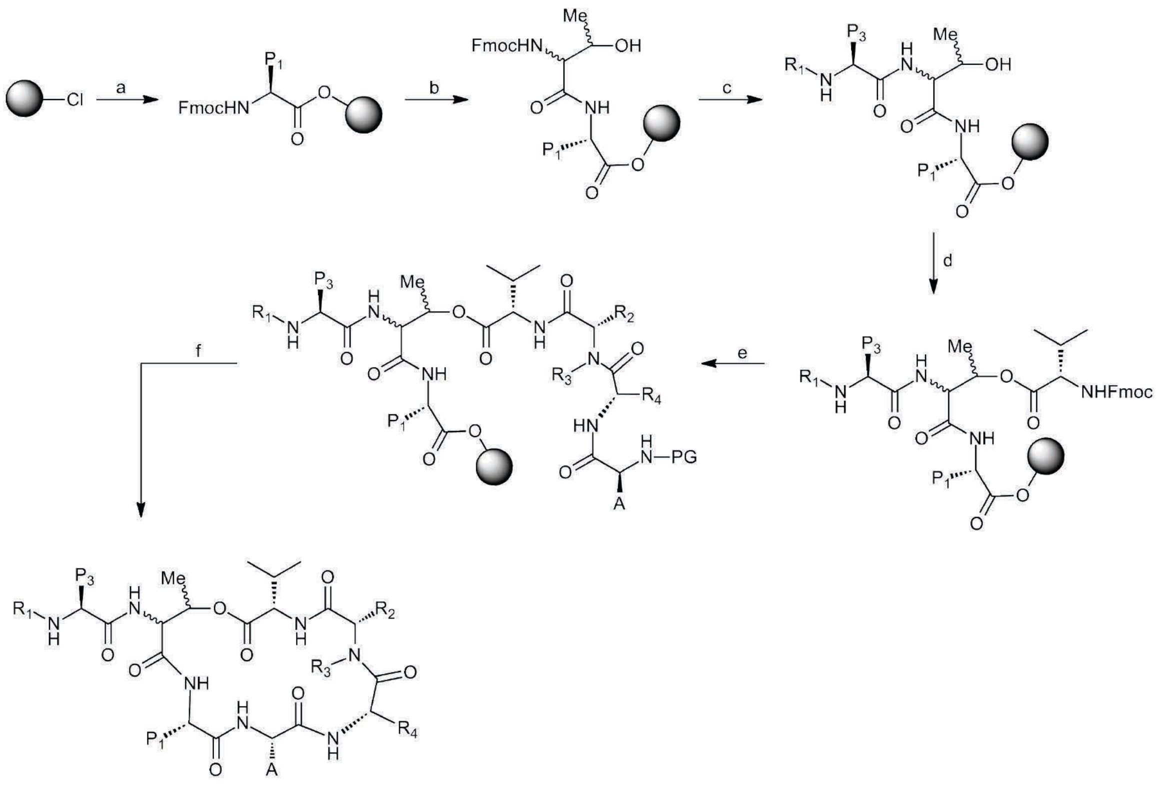

residues summarized in Table 3

Figure 60: Solid-phase synthesis of small molecule analogs of canonical-conformation β-(or γ-) hydroxy amino acid protease inhibitors derived from Ahp cyclodepsipeptides. Reagents and conditions (NOTE: for the individual reaction times *t*, refer to the experimental section): (a) i. P_1 amino acid, DIEA, CH_2Cl_2, on; ii. CH_2Cl_2/MeOH/DIEA (17:2:1), 3x 5 min; (b) i. piperidine/DMF (1:4), 2x 15 min; ii. threonine building block, HOBt, HBTU, DIEA, DMF, *t*; (c) i. piperidine/DMF (1:4), 2x 15 min; ii. P_3 amino acid; HOBt, HBTU, DIEA, DMF, *t*; iii. piperidine/DMF (1:4), 2x 15 min; iv. P_4 amino acid; HOBt, HBTU, DIEA, DMF, *t*; (optional: v. piperidine/DMF (1:4), 2x 15 min; vi. butyric acid, HOBt, HBTU, DIEA, DMF, *t*); (d) Fmoc-Val-OH, DIC, DMAP, CH_2Cl_2/DMF (9:1), 4 x 2 h; (e) i. piperidine/DMF (1:4), 2x 15 min; ii. *N*-methylated amino acid or analog; HOBt, HBTU, DIEA, DMF, *t*; iii. for Alloc protected derivatives: $Pd(PPh_3)_4$, morpholine, CH_2Cl_2, 30 min; for Fmoc-protected derivatives: piperidine/DMF (1:4), 2x 15 min; iv. P_2' amino acid, for secondary amines: PyBrOP, DIEA, 24 h; for primary amines: HOBt, HBTU, DIEA, DMF, *t*; v. piperidine/DMF (1:4), 2x 15 min; vi. amino acid replacing Ahp, HOBt, HBTU, DIEA, DMF, *t*; (f) depending on *N*-terminal protection: for Boc-protected species: i. AcOH/TFE/CH_2Cl_2 (1:1:3), 2 h; ii. HCl in dioxane (4 M) or TFA/TIS/CH_2Cl_2 (95:2.5:2.5); for Fmoc-protected species: i. piperidine/DMF (1:4); ii. AcOH/TFE/CH_2Cl_2 (1:1:3), 2 h; then for all species: iii. PyBOP, DIEA, 10 °C, 1 mM dilution, 2 d; iv. removal of remaining protecting groups (refer to experimental section); v. HPLC purification (overall yields: 1.0% to 12.3%, refer to experimental section).

Table 3: analogs of Ahp cyclodepsipeptides synthesized for the investigation of structure-activity-relationships.

compound	P_1	P_2 threonine	P_3	R^1	R^2	R^3	R^4	A
SAR-1	Cit	*L*	Gln	But	3-Br,4-OMeTyr	Me	Ile	Ser
SAR-2	Cit	*L*	Gln	But	3-Br,4-OMeTyr	Me	Ile	Hse
SAR-3	Cit	*L*	Gln	But	3-Br,4-OMeTyr	Me	Ile	Thr
SAR-4	Cit	*L*	Gln	But	4-OMeTyr	Me	Ile	Ser
SAR-5	Cit	*L*	Gln	But	Phe	Me	Ile	Ser
SAR-6	Cit	*L*	Gln	But	Phe	H	Ile	Ser
SAR-7	Cit	*L*	Gln	But	Pro	-	Ile	Ser
SAR-8	Cit	*D-allo*	Gln	But	Phe	Me	Ile	Ser
SAR-9	Cit	*L-allo*	Gln	But	Phe	Me	Ile	Ser
SAR-10	Leu	*L*	Thr	Ala-But	3-ClTyr	Me	Thr	Ser
SAR-11	Leu	*L*	Thr	Ala-But	3-ClTyr	Me	Thr	Thr
SAR-12	Leu	*L*	Thr	Ala-But	3-ClTyr	Me	Thr	Val

3.2.3 Biological evaluation of the SAR analogs and elucidation of critical parameters for the canonical conformation

After having synthesized a series of structure-activity analogs, a biological evaluation of the small molecule analogs was performed i) to identify adequate replacements for the Ahp unit and ii) to identify structural elements that have an influence on the molecule's ability to adopt the canonical conformation.

To this end, first analogs of symplocamide A (see section 3.1.2) were investigated.[115,118]

The first three analogs were designed to test for suitable substitutions of the Ahp moiety. To this end, the focus was set on commercially available amino acids bearing a hydroxylated side chain (as the Ahp residue also features a hydroxyl group in the β-position). Consequently, three different symplocamide A analogs with serine, homoserine and threonine (**SAR-1**, **SAR-2** and **SAR-3**, respectively) (Fig. 61) as replacement for the Ahp moiety were investigated.

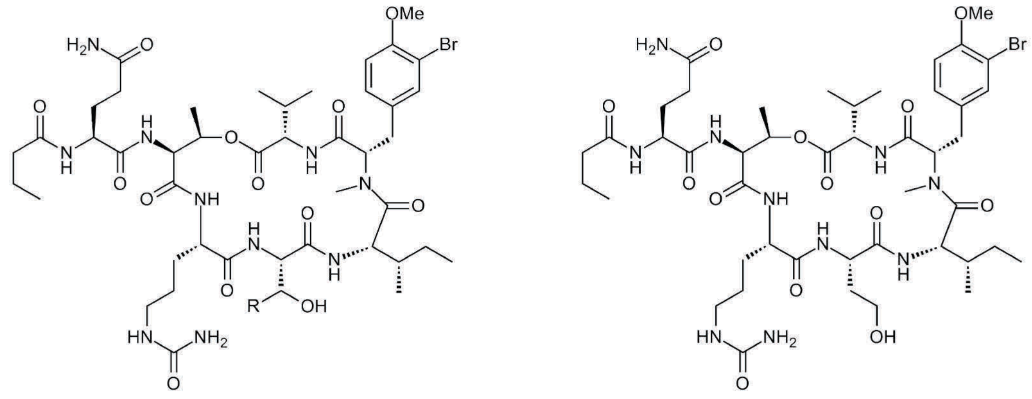

R = H, (Ser): **SAR-1**
R = CH_3, (Thr): **SAR-3**

SAR-2

Figure 61: A first set of SAR analogs for the evaluation of a suitable Ahp replacement.

The replacement of the Ahp moiety with homoserine and threonine did not provide active compounds; the replacement of the Ahp unit with serine, however, provided a peptide that displayed a K_i of 3.8 µM in a chymotrypsin inhibition assay[126-128], indicating serine as a proper mimic of the Ahp moiety.

With a proper Ahp mimic in hands, the structural determinants of the potent inhibition of the Ahp-mimicked cyclodepsipeptides were investigated. To this end, a first focus was set on the unusual 3-bromo-4-methyl *N*-methyl tyrosine residue that is located in the P_3' position of the inhibitor. In their studies of the BBI-derived peptides Leatherbarrow *et. al.* were able to identify the P_3' residue as the element that enforces the canonical conformation by forming a *cis* amide bond and thereby mimicking a β-turn element. In these BBI peptides, the P_3' residue is a conserved proline residue.[23] However, not only proline is known to enforce *cis* amide bonds, also *N*-methylated amino acids induce such *cis*-configured bonds.

The first modification of the 3-bromo-4-methoxy *N*-methyl tyrosine residue was the replacement by a 4-methyl *N*-methyl tyrosine (**SAR-4**) moiety which had only a weak influence on the inhibitory potency of the inhibitor (resulting in a K_i of 4.8 µM). This indicates that the bromine modification of the aromatic residue has only a subtle influence on the overall inhibitory potency. In contrast to this, the replacement of the methoxy group by incorporation of *N*-methylated phenylalanine (**SAR-5**) resulted in a drastic loss of activity (K_i = 56.1 µM), emphasizing the importance of the methoxy substitution on the aromatic system (Fig. 62). Interestingly, also our structure-activity relationships demonstrate that a *N*-methylated phenylalanine moiety on P_3' is much less active than for example a 4-methoxy tyrosine residue. However, several Ahp cyclodepsipeptides that display chymotrypsin inhibitory activity feature an *N*-methylated phenylalanine residue are still among the most potent inhibitors.[24] This pinpoints that other amino acid residues in the sequence have a more important influence on bioactivity.

For the present analogs, however, the influence of a methoxy substitution on the aromatic amino acid on the inhibitory potency cannot be denied.

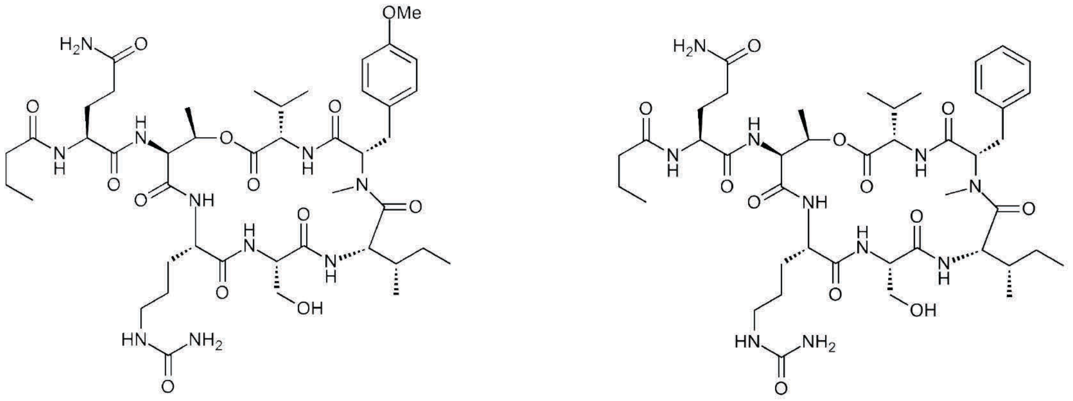

SAR-4 **SAR-5**

Figure 62: SAR analogs for the investigation of influence of the aromatic substitution.

Next, the influence of the *N*-methyl modification on bioactivity was tested. The presence of an element forcing a peptide bond into a *cis* conformation in the P_3' position has been evaluated as a crucial element for the bioactivity of canonical inhibitors because the canonical conformation strictly requires a *cis* amide bond in this position. [23,133] To inspect the effect of the presence or absence of a *cis* conformation in the P_3' position for the present small molecule analogs of Ahp cyclodepsipeptides, two different analogs were investigated. First, and in total accordance with the results of Leatherbarrow *et. al.*, the replacement of the *N*-methylated amino acid by a regular phenylalanine (**SAR-6**) was tested. This substitution resulted in a complete loss of bioactivity, thereby indicating the absence of the *cis* amide bond and simultaneously implicating its imperative presence in order to attain the canonical conformation. Furthermore, a replacement of the *N*-methylated amino acid with a proline (**SAR-7**) that is also able to enforce a *cis* amide bond resulted in a retention of the biological activity as **SAR-7** displayed a K_i of 16.1 µM (Fig. 63).

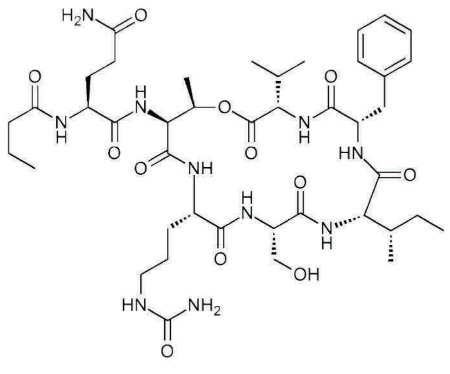

SAR-6

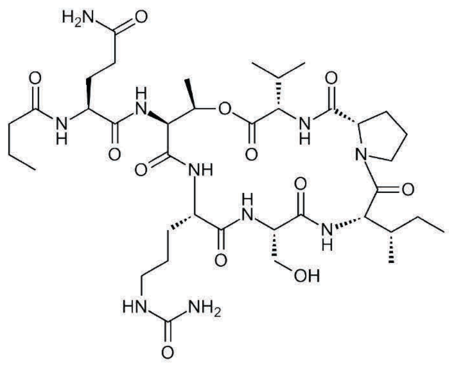

SAR-7

Figure 63: SAR analogs for the investigation of the effect of a *cis* amide bond on the inhibitory potency.

These results underline that also the Ahp-mimicked peptides act as small molecule analogs of canonical conformation inhibitors. Moreover, when comparing the inhibitory potencies of the proline Ahp-mimic **SAR-7** (K_i = 16.1 µM) and the two closely related *N*-methylated mimics **SAR-1** (K_i = 3.8 µM) and **SAR-4** (K_i = 4.8 µM) that incorporate a substituted aromatic side chain a clear trend towards substituted *N*-methylated aromatic amino acids for this compound class can be observed. Interestingly, a similar trend is seen with the natural Ahp cyclodepsipeptides:[24] none of the 51 Ahp cyclodepsipeptides that have recently been summarized due to their potent S1 serine protease inhibition incorporate a proline in the P_3’ position. Instead, in all cases a *N*-methylated aromatic amino acid is conserved in this position. This is quite remarkable as these unnatural *N*-methylated amino acids must be synthesized by the organism producing the respective Ahp cyclodepsipeptides. The conserved presence of these amino acids therefore indicates their significance for bioactivity.

Thus, the identification of a suitable Ahp-mimic not only enabled the investigation of the crucial determinants for inhibition; these substances also indicate the substantial elements in Ahp cyclodepsipeptides for adopting the canonical conformation, *i. e.* the *cis* amide bond at the P_3’ amino acid.

Next, the influence of the stereochemistry of the threonine moiety that forms the depsipeptide bond and its effect on the inhibitory potency of the compounds was verified. The replacement of the natural (*L*)-threonine moiety in the *N*-methyl phenylalanine derivative with either (*D*)-*allo*-threonine (**SAR-8**) or (*L*)-*allo*-threonine (**SAR-9**) provided inactive compounds again (Fig. 64). While incorporation of a (*D*)-*allo* threonine residue could change the overall conformation of the macrocyclic ring system, the result with the (*L*)-*allo*-threonine moiety is less clear.

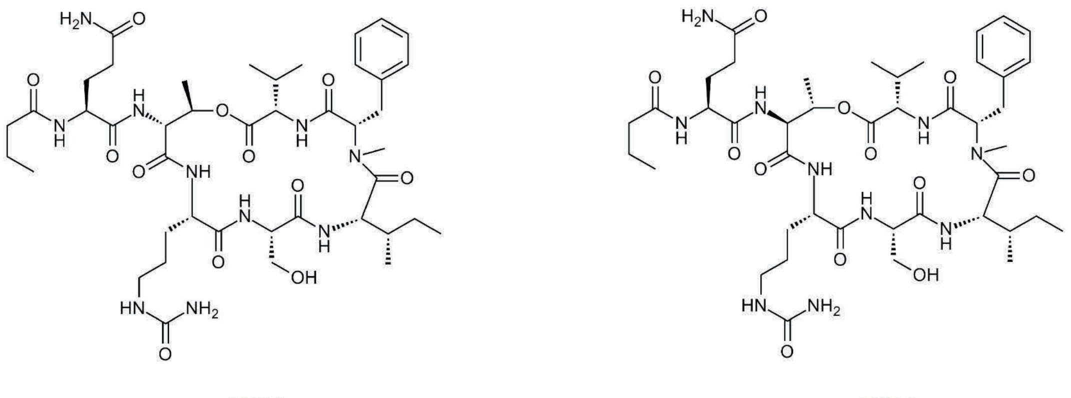

SAR-8 **SAR-9**

Figure 64: SAR analogs to study the effect of the threonine stereochemistry on the inhibitory potency.

However, this result supports a hypothesis discussed by Leatherbarrow *et. al.* for the BBI-derived inhibitors: in these peptides, a threonine residue in the P_2 position is able to form a hydrogen bond to the P_1' serine moiety and thereby directs the aliphatic part of the threonine side chain towards a close contact with the imidazole part of the enzyme's catalytic histidine. This contact is thought to interfere with a movement of the histidine that becomes necessary during the catalysis cycle and is proposed contribute to the inhibition of the protease.[18]

This scenario should in principle also be possible for the Ahp cyclodepsipeptides as well as the generated Ahp-mimics because the orientation of the aliphatic part of the threonine side chain is restricted due to the ester bond of the side chain's hydroxyl group. Hence, a different stereochemistry on the β-position of threonine would most probably result in a different orientation of the aliphatic part of the side chain, thereby preventing the contact to the histidine of the catalytic triad of the S1 serine protease and thus not impairing the mobility required for the cleavage of a substrate.

It has to be noted, however, that the requirement of a flexible histidine residue has been a matter of highly controversial debate within the scientific community. Several groups have contributed to this debate, basing their argumentation either on structural data obtained from x-ray analysis of protein crystals or on data generated by *in silico* molecular dynamics experiments. For all models of serine protease catalysis, the general acid-base catalysis by the histidine residue is a commonly accepted concept. In the first step of the reaction, the histidine acts as a general base by deprotonating the active site serine, thereby enabling the attack of the substrate and the formation of the first tetrahedral intermediate. In a later step of the cleavage reaction, histidine then acts as a general acid by donating a hydrogen to the amino leaving group. Afterwards, the histidine residue contributes to the deprotonation of the catalytic water molecule and finally donates a proton to the deprotonated serine in order to restore the enzyme to its active and free state. Some crucial questions concerning the progression of the reaction are however still unanswered. One of them is the reorganization of the reactive site after the formation of the first tetrahedral intermediate. This reorganization seems to be necessary because the histidine is positioned ideally to deprotonate the catalytic serine. However, this arrangement also catalyzes the back reaction of the first tetrahedral complex to the reactand complex, if the histidine moiety does not change its position, resulting in a lowered reaction rate. In a high resolution crystallographic study of acyl-enzyme structures, Radisky and coworkers were able to observe a slight out-of-plane swiveling of the imidazole and a simultaneous movement of the serine moiety that results in a shift of the imidazole from its ideal deprotonation position into closer proximity of the amine leaving group and the catalytic water. A complete ring-flip is ruled out, the subtle changes described seems to suffice to drive forward the reaction.[134] In accordance with this report, Fodor *et. al.* describe the movement of the histidine as a subtle 12° change of a torsion angle and emphasize the economic nature of this movement that enables the imidazole to adapt to two different nucleophilic attackers that are 2 Å apart in the crystal structure.[135] In quantum mechanics and molecular mechanics calculations of the deacetylation step of serine proteases, Richards *et. al.* furthermore observed that during the progression of the reaction, the binding site rearranges to release the modified substrate. This has led to the overall conclusion that the ring mobility of the histidine side chain ensures a direction of the reaction towards the formation of the product because the mobility enables a concerted rearrangement of the catalytic site.[136,137]

Concludingly, these different data support the hypothesis of subtle movements of the histidine residue during the catalysis cycle, a complete ring-flip of the histidine has however been ruled out.[134-138] The results obtained here for the Ahp-mimics with an altered threonine stereochemistry may serve as a humble contribution to the general debate. The loss of activity for these analogs indicates at least that an alteration in the prominent position of the inhibitor that is thought to interact with the histidine does indeed influence the activity of the targeted protease. It can however not be ruled out that the unnatural threonine stereochemistry may however also induce an altered overall conformation of the macrocycles.

With the previous encouraging results in hand, it was next evaluated if these results can also be transferred to a different member of the Ahp cyclodepsipeptides natural product class. If this were possible, the concept of Ahp mimicry could be considered as a global concept, thereby encouraging a further investigation of this type of small molecule serine protease inhibitors. The natural product chosen for this further investigation was the elastase inhibitor scyptolin A that displays a K_i of 0.16 μM against elastase and is one of two Ahp cyclodepsipeptide for which a crystal structure in complex with a target protease exists. Scyptolin A has been used in extensive enzyme inhibition and structural studies.[27,28]

To identify first an Ahp mimic for scyptolin A, two different analogs incorporating serine (**SAR-10**) or threonine (**SAR-11**) as a replacement for the Ahp moiety were synthesized. Both compounds fortunately showed a potent bioactivity, with the threonine analog **SAR-11** (K_i = 5.0 μM) being even more potent than the serine analog **SAR-10** (K_i = 19.1 μM) (Fig. 65).

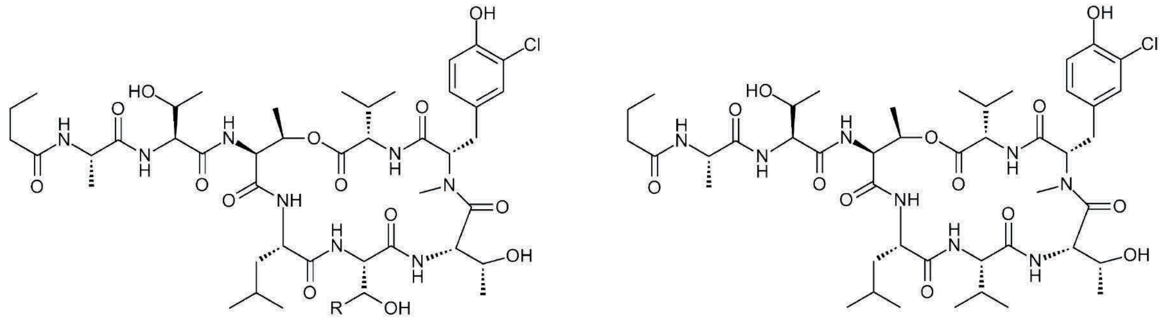

R = H, (Ser): **SAR-10**
R = CH$_3$, (Thr): **SAR-11**

SAR-12

Figure 65: SAR analogs for the investigation of a possible Ahp mimicry in scyptolin A.

The enhanced bioactivity of **SAR-11** with the threonine moiety over the serine derivative **SAR-10** is difficult to explain. A closer look however reveals two major different factors between the symplocamide A and the scyptolin A mimics. In symplocamide A, the P_1 residue is citrulline while the P_2' residue is isoleucine. In the scyptolin A analogs, P1 is leucine and P_2' is threonine. Thus, the P_1' residue serine or threonine can form different additional interactions between the P_1 and P_2' moieties that might have an influence on the overall efficiency to adopt the canonical conformation or the binding to the target protease.

The enhanced activity of **SAR-11** compared to its serine analog **SAR-**10 could be explained with the higher sterical demand of the threonine methyl group that consequently locks the threonine in a state of decreased rotational freedom. As a result, the molecule does not lose as much more degrees of freedom (*i. e.* entropy) upon binding; hence, the binding of the inhibitor might be favored.

In order to demonstrate the general requirement of a hydroxyl group in the side chain of the amino acid replacing the Ahp unit, a third scyptolin A analog that incorporated a valine (**SAR-12**) instead of threonine was tested. This compound was again inactive in the enzyme inhibitory assay, demonstrating the critical role of a hydroxyl group in the side chain of the Ahp replacement.

As an overview of the results of the structure-activity relationship studies the small molecule inhibitors evaluated in terms of their ability to adopt the canonical conformation and in terms of crucial elements for a potent inhibition are summarized in Table 4.

Table 4: Summarized modifications of the mimics of Ahp cyclodepsipeptides and the resulting bioactivities.

compound (mimic of)	Ahp replacement	further substitutions	K_i
SAR-1 (sym A)	Ser	-	3.8 µM
SAR-2 (sym A)	Hse	-	inactive
SAR-3 (sym A)	Thr	-	inactive
SAR-4 (sym A)	Ser	3-Br,4-OMe-mTyr→4-OMe-mTyr	4.8 µM
SAR-5 (sym A)	Ser	3-Br,4-OMe-mTyr→mPhe	56.1 µM
SAR-6 (sym A)	Ser	3-Br,4-OMe-mTyr→mPhe	inactive
SAR-7 (sym A)	Ser	3-Br,4-OMe-mTyr→Pro	16.1 µM
SAR-8 (sym A)	Ser	3-Br,4-OMe-mTyr→mPhe *L*-Thr→*D-allo*-Thr	inactive
SAR-9 (sym A)	Ser	3-Br,4-OMe-mTyr→mPhe *L*-Thr→*L-allo*-Thr	inactive
SAR-10 (scyp A)	Ser	-	19.1 µM
SAR-11 (scyp A)	Thr	-	5.0 µM
SAR-12 (scyp A)	Val	-	inactive

Overall, the present studies indicate that cyclodepsipeptides with an Ahp-mimicked moiety can also adopt a canonical conformation and thereby serve as potent S1 serine protease inhibitors. Despite their slightly reduced biological activities, their synthetically more facile access turns these mimics into highly interesting small molecules for performing protease research.

3.3 Synthesis and biological investigation of symplostatin 4

3.3.1 Development of a synthetic strategy for a convergent synthesis of symplostatin 4 and derivatives

In a second project during this dissertation, chemical biology investigations of the natural product symplostatin 4[103,104] were performed. To this end, a total synthesis of the natural product as well as derivatives thereof was required. The derivatives of symplostatin 4 were designed to incorporate functionalities that enable an activity-based approach for the investigation of biological activities and target identification. In addition, structure-activity relationship studies were envisaged to investigate the influence of the methyl-methoxypyrrolinone modification on the biological activity of symplostatin 4. To this end, an analog lacking the methyl-methoxypyrrolinone moiety was designed and derivatives for an activity-based approach were planned as well.

To enable an activity-based approach during the chemical biology studies, different tags were planned to be attached to symplostatin 4 and its analog lacking the methyl-methoxy pyrrolinone. First, alkyne-modified derivatives were synthesized. Moreover, rhodamine and biotin tags were attached to these derivatives by a 1,3-dipolar Huisgen cycloaddition (click reaction) of the corresponding alkyne-modified derivatives.

A rhodamine tag (or other fluorescent tags) allows a direct in-gel identification of labeled proteins by a read-out on a fluorescence scanner, whereas a biotin tag enables the identification of labeled enzymes by Western blotting. In addition, a biotin tag can be used to purify labeled enzymes with avidin- or streptavidin-based methods. A combination of the two tags is also possible by generating a so-called trifunctional probe[64] that incorporates a rhodamine and a biotin. These trifunctional probes provide the advantage of a direct visualization by fluorescence read-out combined with the possibility of an isolation and purification of labeled enzymes with just one probe. The downside of all tagged probes is however that, depending on the tag, the probes become quite bulky and their reaction in an assay may no longer resemble the behavior of the core molecule they were derived from. The attachment of a bulky tag can on the one hand prevent the binding to a target enzyme because the probe is sterically hindered. On the other hand it has also been observed that *e. g.* a rhodamine tag enhances the uptake of a probe in *in vivo* assays. A way to overcome the unwanted side effects of a tag attached to an activity-based probe is the use of probes that are modified to perform a click reaction after the labeling experiment.[139,140] The structures of such probes resemble much more to the original molecules and therefore potentially display a more similar labeling pattern.

In order to provide the highest flexibility in the future profiling experiments, symplostatin 4 and its analog lacking the methoxy-methylpyrrolinone were therefore synthesized as alkyne-modified, rhodamine-tagged, biotinylated and trifunctional versions (Fig. 66).

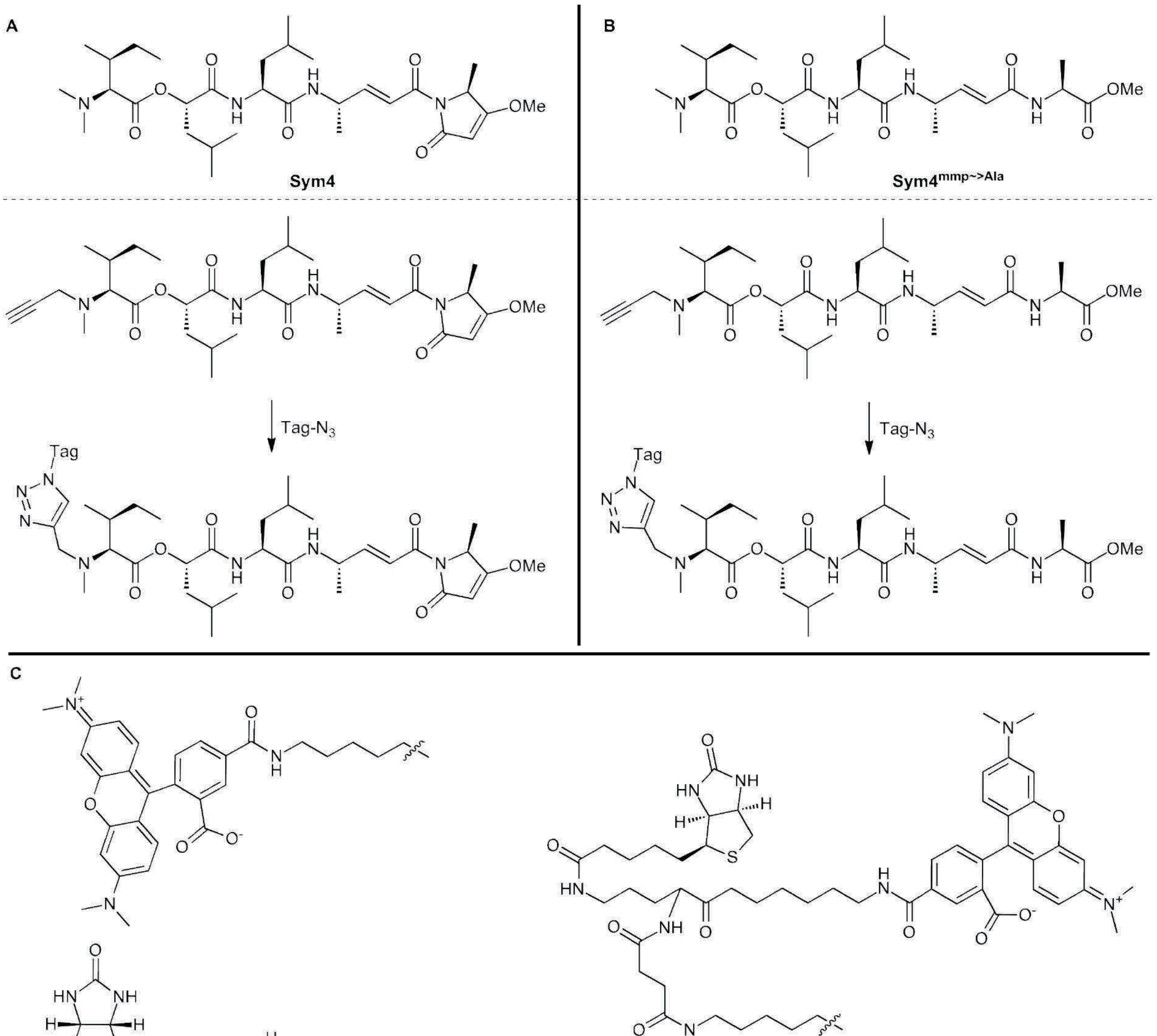

Figure 66: Symplostatin 4 and derivatives for the investigation by an activity-based approach. **A**: symplostatin 4 (**Sym4**, top) and its derivatives; **B**: symplostatin 4 analog lacking the methyl-methoxypyrrolinone (**Sym4**$^{\mathrm{mmp}\rightarrow\mathrm{Ala}}$, top) and its derivatives; **C**: tags attached to the alkyne-modified **Sym4** and **Sym4**$^{\mathrm{mmp}\rightarrow\mathrm{Ala}}$ derivatives by click reaction: rhodamine, rhodamine-biotin (trifunctional probe) and biotin (clockwise).

In order to gain a quick access to all envisioned derivatives, a convergent solution-phase synthesis starting from the crucial 4-(*S*)-amino-(*E*) pentenoic acid was planned initially. As only two of the building blocks (*i. e.* Boc-leucine and (*S*)-Hydroxyisocaproic acid) were commercially available, the other building blocks had to be generated for the synthesis. It was planned to synthesize the 4-(*S*)-amino-(*E*) pentenoic acid building block from Boc-alanine by Wittig methodology. The building blocks required for the *C*-terminal modification should both be accessible from (*L*)-alanine. In analogy to the synthesis of symplocamide A, (*S*)-Hydroxyisocaproic acid would be coupled without a protection of the hydroxyl group due to its lower reactivity. The isoleucine building block bearing either the di-methylated amine or the methylated and alkyne-modified amine was planned to be synthesized starting from isoleucine (Fig. 67).

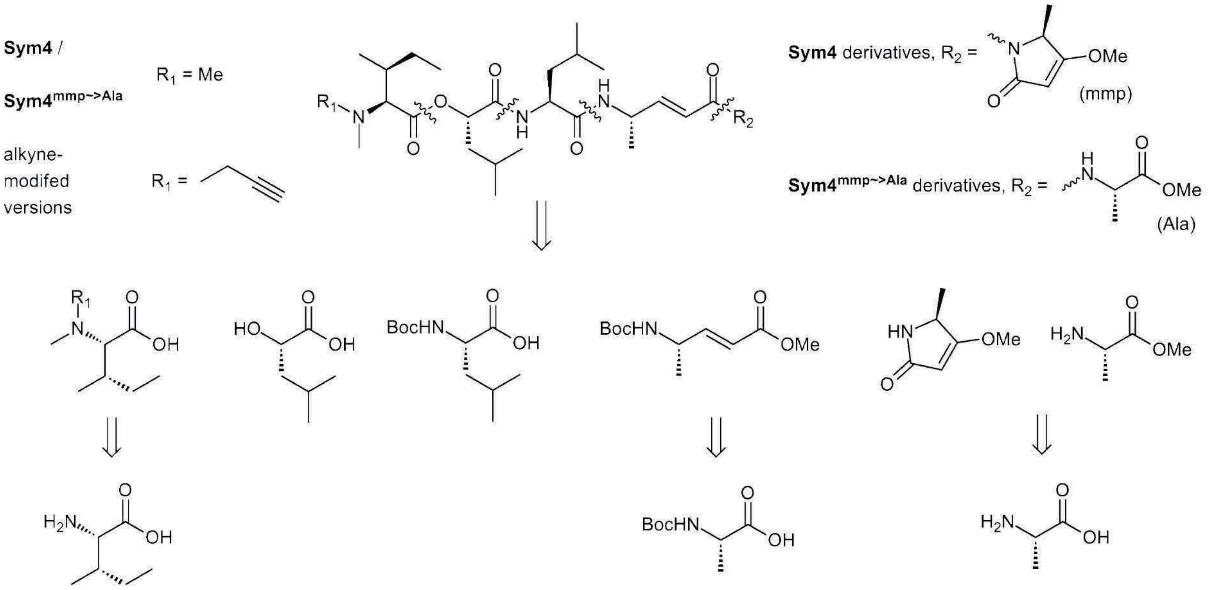

Figure 67: Initial synthetic strategy for the synthesis of symplostatin 4 and derivatives based on sequential couplings.

A first drawback of this strategy, however, was the observed difficult coupling of the methyl-methoxypyrrolinone building block to the 4-(*S*)-amino-(*E*)-pentenoic acid. The synthesis of the precursor methyl pyrrolidine-2,4-dione proceeded smoothly using a protocol by Tønder *et. al.* which involved the coupling of Boc alanine with Meldrum's acid followed by a rearrangement of the highly reactive intermediate to form the pyrrolidine-2,4-dione. The published introduction of an ethyl or a methyl group in order to obtain the methyl-ethoxypyrrolinone or the methyl-methoxypyrrolinone, respectively, with KHMDS as the base and EtOTs or MeOTs however could not reproduced successfully.[141] Nevertheless, this circumstance could be overcome by using Mitsunobu conditions, as reported by Poncet *et. al.* (Fig.68).[142]

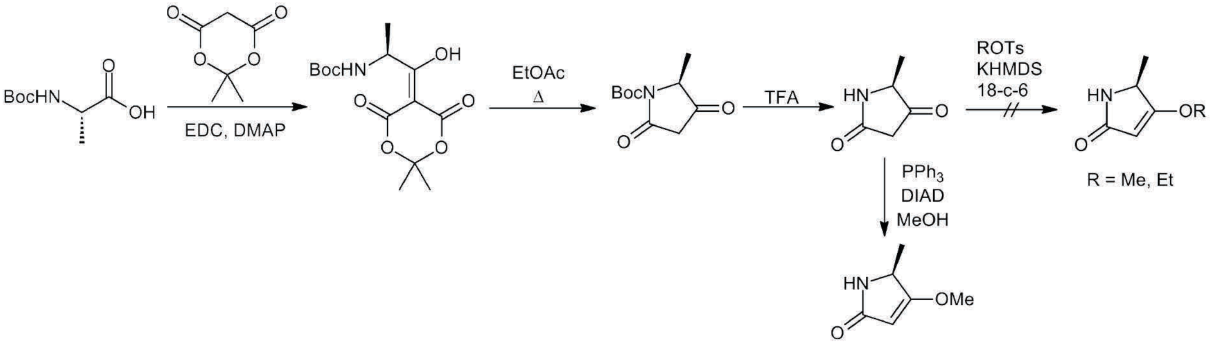
BocHN
OH
EDC, DMAP
BocHN
OH
EtOAc
Δ
BocN
TFA
HN
ROTs
KHMDS
18-c-6
HN
OR
R = Me, Et
PPh3
DIAD
MeOH
HN
OMe

Figure 68: Synthesis of the methyl-methoxypyrrolinone building block.[141,142]

With the methyl-methoxypyrrolinone derivative in hands, the coupling to a second amino acid residue was first explored in a model reaction with alanine. Despite the use of a strong base (LHMDS) to deprotonate the secondary amine and a strong coupling reagent (PyBrOP), the coupling could not be achieved successfully. The difficult coupling could however be overcome by the strategy introduced by Poncet *et. al.* in their synthesis of dolastatin 15. Instead of synthesizing the benzyl-methoxypyrrolinone (as an element of dolastatin 15) moiety individually, they generated the pyrrolinone residue after coupling to the precursor amino acid phenylalanine, followed by a rearrangement of a highly reactive intermediate obtained after the coupling of Meldrum's acid to the phenylalanine.[142]

This methodology also seemed to suit to the synthesis of symplostatin 4 and its derivatives. Consequently, coupling of alanine methyl ester to the 4-(*S*)-amino-(*E*)-pentenoic acid building block the **Sym4** as well as the **Sym4**$^{\mathbf{mmp \rightarrow Ala}}$ derivatives would allow its synthesis from a dipeptide building block (Fig. 69).

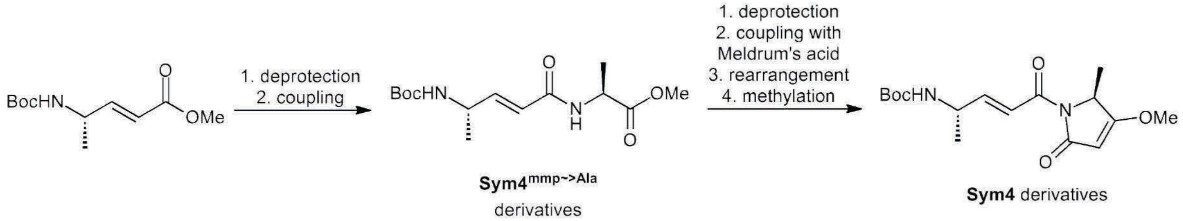
BocHN
OMe
1. deprotection
2. coupling
BocHN
OMe
N
H
Sym4mmp->Ala
derivatives
1. deprotection
2. coupling with
Meldrum's acid
3. rearrangement
4. methylation
BocHN
N
OMe
Sym4 derivatives

Figure 69: New approach to the 4-(*S*)-amino-(*E*)-pentenoic acid modified with alanine methyl ester or the methyl-methoxypyrrolinone.

The synthesis of the isoleucine building block that features a di-methylation on its amino group however turned out to be more difficult than originally anticipated. While the protection of isoleucine as an allyl ester or a methyl ester proceeded as expected, the di-methylation of the amine was complicated due to the high volatility of the resulting di-methylated product. Several methods for the introduction of the two methyl groups by reductive amination were examined: a method using paraformaldehyde and formic acid in water[143] or just paraformaldehyde and formic acid[144], a combination of paraformaldehyde, sodium borohydride and sulfuric acid[145] and a combination of paraformaldehyde and sodium cyanoborohydride.[146] Despite great efforts, the desired di-methylated isoleucine building block could not be isolated in satisfying yields.

This result, together with the already reconsidered approach to the synthesis of the 4-(*S*)-amino-pentenoic acid modified either with alanine methyl ester or the methyl-methoxypyrrolinone residue, called for the reconsideration of the sequential coupling strategy. Consequently, a new synthetic strategy consisting of the generation of an isoleucine-isocaproic acid depsipeptide which was subsequently modified *N*-terminally in order to obtain the di-methylated as well as the methylated and alkyne-modified variant was envisaged. The resulting depsipeptide fragments were then planned to be coupled to the different tripeptide fragments obtained from the *C*-terminal and *N*-terminal modification of 4-(*S*)-amino-pentenoic acid (Fig.70).

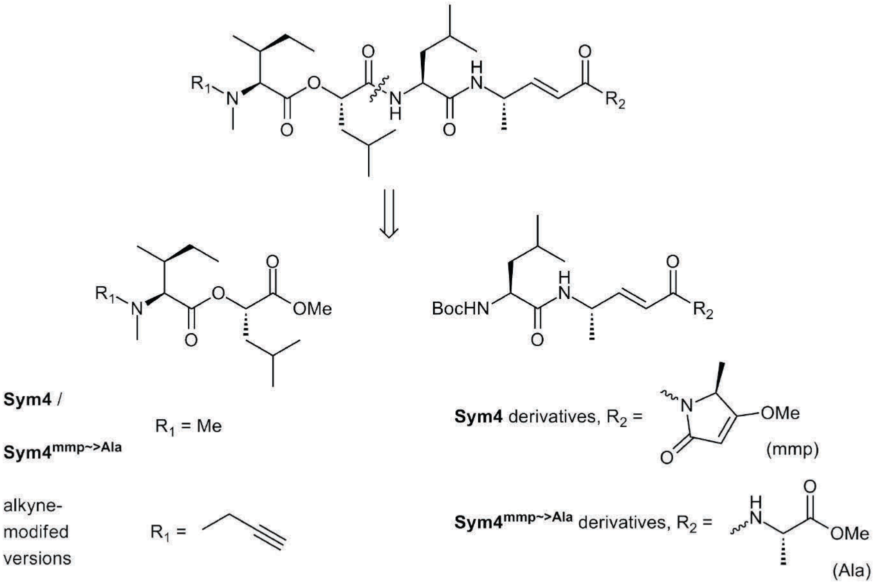

Figure 70: New fragment-based approach towards the synthesis of symplostatin 4 and derivatives.

3.3.2 Synthesis of symplostatin 4 and derivatives for the biological evaluation and target identification

This alternative synthetic strategy required the synthesis of building blocks such as the 4-(*S*)-amino-(*E*)-pentenoic acid moiety. This compound was readily synthesized from Boc-Ala-OH by adapting a protocol introduced by Pollini and coworkers.[147] In the first step, Boc-Ala-OH was converted to the Weinreb amide by reaction with DCC and *N,O*-dimethyl hydroxylamine. After a short work-up protocol, the resulting Weinreb amide was directly transformed to the aldehyde by reduction with $LiAlH_4$. The aldehyde was then transformed directly to the α,β-unsaturated methyl ester **37** by a Wittig reaction with methyl-2-(triphenylphosphoranylidene)acetate. The desired 4-(*S*)-amino-(*E*)-pentenoic acid building block **37** was obtained after chromatographic work-up in a yield of 59% starting from Boc-alanine. In the next step, this building block was deprotected and coupled with alanine methyl ester hydrochloride to obtain the dipeptide intermediate **38.**

38 was then converted to the tripeptides required for the synthesis of the **Sym4** derivatives as well as for the **Sym4**$^{\mathbf{mmp\rightarrow Ala}}$ derivatives. To obtain the tripeptide for the **Sym4** derivatives (*i. e.* the tripeptide with the methyl-methoxypyrrolinone residue), the dipeptide **38** was deprotected *C*-terminally using lithium hydroxide. The resulting free acid was then coupled with Meldrum's acid to obtain a highly reactive enol intermediate that rearranges to form the pyrrolidine-2,4-dione upon refluxing in acetonitrile. The methylation was carried out under Mitsunobu conditions using DEAD, methanol and triphenylphosphine providing the methyl-methoxypyrrolinone-modified dipeptide **39** in 90% yield from the protected dipeptide **38**.[142] The tripeptide **40** was accessed by sequential Boc deprotection and coupling with Boc leucine using HOBt/HBTU activation and acetonitrile as the solvent.[148] The tripeptide **40** was obtained in 85% yield.

In order to access the **Sym4**$^{\mathbf{mmp\rightarrow Ala}}$ derivatives, the dipeptide **38** was coupled with Boc leucine in the next step. So, first the Boc group was removed using trifluoroacetic acid in dichloromethane and the free amine intermediate was then coupled with Boc leucine. The tripeptide **41** was obtained in 99% yield using the same coupling conditions as for the synthesis of the tripeptide **40** (Fig. 71).

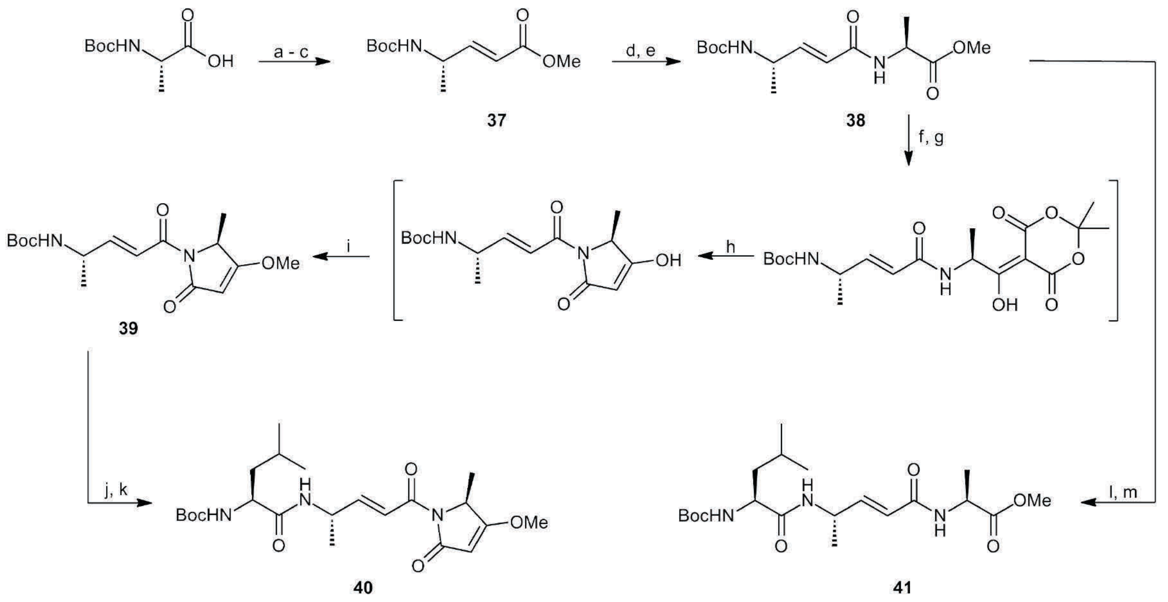

Figure 71: Synthesis of the *C*-terminal tripeptides **40** and **41**. Reagents and conditions: (a) *N,O*-dimethylhydroxylamine hydrochloride, Et_3N, DCC, CH_2Cl_2, rt, 1 h; (b) $LiAlH_4$, Et_2O, 0 °C, 20 min; (c) $Ph_3P=CHCOOMe$, CH_2Cl_2, rt, o/n (59%, 3 steps); (d) LiOH, THF/MeOH/H_2O (1.67:1:0.67), rt, 5 h; (e) H-Ala-OMe, HOBt, HBTU, DIEA, CH_3CN, 0 °C to rt, o/n (46%, 2 steps); (f) LiOH, THF/MeOH/H_2O (1.67:1:0.67), rt, 5 h; (g) 2,2-dimethyl-1,3-dioxane-4,6-dione, DMAP, EDC*HCl, CH_2Cl_2, -10 °C to rt, o/n; (h) CH_3CN, reflux, 1 h; (i) Ph_3P, MeOH, DEAD, THF, rt, o/n (90%, 4 steps); (j) TFA/CH_2Cl_2 (1:1), rt, 3 h; (k) Boc-Leu-OH, HOBt, HBTU, DIEA, CH_3CN, 0 °C to rt, o/n (85%, 2 steps); (l) TFA/CH_2Cl_2 (1:1), rt, 2 h; (m) Boc-Leu-OH, HOBt, HBTU, DIEA, CH_3CN, 0 °C to rt, o/n (99%, 2 steps).

With the two *C*-terminal tripeptides in hands, the two different *N*-terminal depsipeptides were next synthesized. The synthesis for both depsipeptides started from (*S*)-2-hydroxy-isocaproic acid which was first converted to its methyl ester using thionylchloride and methanol. The resulting methyl ester was directly submitted to the esterification reaction without a further purification because of its high volatility. The esterification with *N*-methylated Boc isoleucine was carried out using DCC as the coupling reagent and DMAP as the additive to enhance the reaction rate and the depsipeptide **42** was obtained in a yield of 55% from (*S*)-2-hydroxy-isocaproic acid. The moderate yield can be explained with the high volatility of the (*S*)-2-hydroxy-isocaproic acid methyl ester: during the removal of residual thionyl chloride *via* distillation under reduced pressure, a partial evaporation of the product also occurred.

To obtain the two different depsipeptide building blocks, the depsipeptide **42** either needed to be modified with a methyl group (yielding depsipeptide **43**) or with a propargyl group (yielding depsipeptide **44**). The deprotection of **42** was again carried out using trifluoroacetic acid in dichloromethane. The di-methylated depsipeptide **43** was then obtained by reacting the free secondary amine intermediate with methyl iodide in dimethylformamide using DIEA as the base; the desired compound **43** was obtained in a yield of 38%. In the case of the methyl and alkyne-modified depsipeptide **44,** the free secondary amide was reacted with propargyl bromide in acetonitrile using DIEA as the base. The reaction was warmed to 80 °C and required an overnight reaction, providing the desired methyl- and alkyne-modified depsipeptide **44** in 63% yield (Fig. 72).

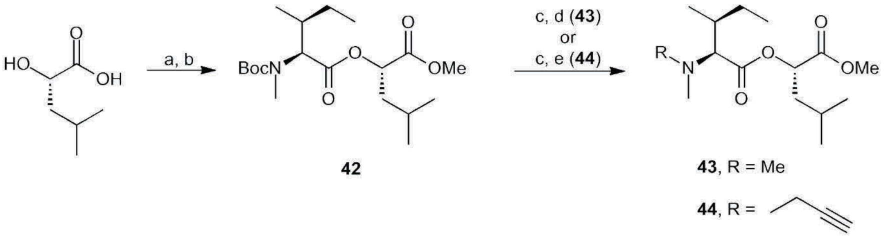

Figure 72: Synthesis of the two depsipeptide fragments **43** and **44**. Reagents and conditions:
(a) $SOCl_2$ (2 M in CH_2Cl_2), MeOH, 0 °C to rt, o/n; (b) Boc-*N*MeIle-OH, DMAP, DCC, CH_2Cl_2, 0 °C to rt, o/n (55%, 2 steps); (c) TFA/CH_2Cl_2, rt, 2 h; (d) CH_3I, DIEA, DMF, rt, 2 h (38%, 2 steps); (e) propargyl bromide (80% wt in toluene), DIEA, CH_3CN, 80 °C, o/n (63%, 2 steps).

With all four fragments in hands, the final assembly of the basic symplostatin 4 derivatives was initiated. To this end, the *C*-terminal depsipeptides were deprotected in order to obtain the free acid intermediates whereas the *N*-terminal Boc protecting group of the tripeptides needed to be cleaved. According to the original synthesis plan, the different fragments were then coupled using HOBt/HBTU activation in order to obtain the four different symplostatin 4 derivatives (Fig. 73). After the reaction work-up, all derivatives with the exception of **Sym4**$^{\text{mmp}\rightarrow\text{Ala}}$ were first purified by silica gel chromatography. The crude **Sym4**$^{\text{mmp}\rightarrow\text{Ala}}$ and smaller fractions of the three other pre-purified compounds were also purified by HPLC in order to obtain highly pure material for the biological investigations.

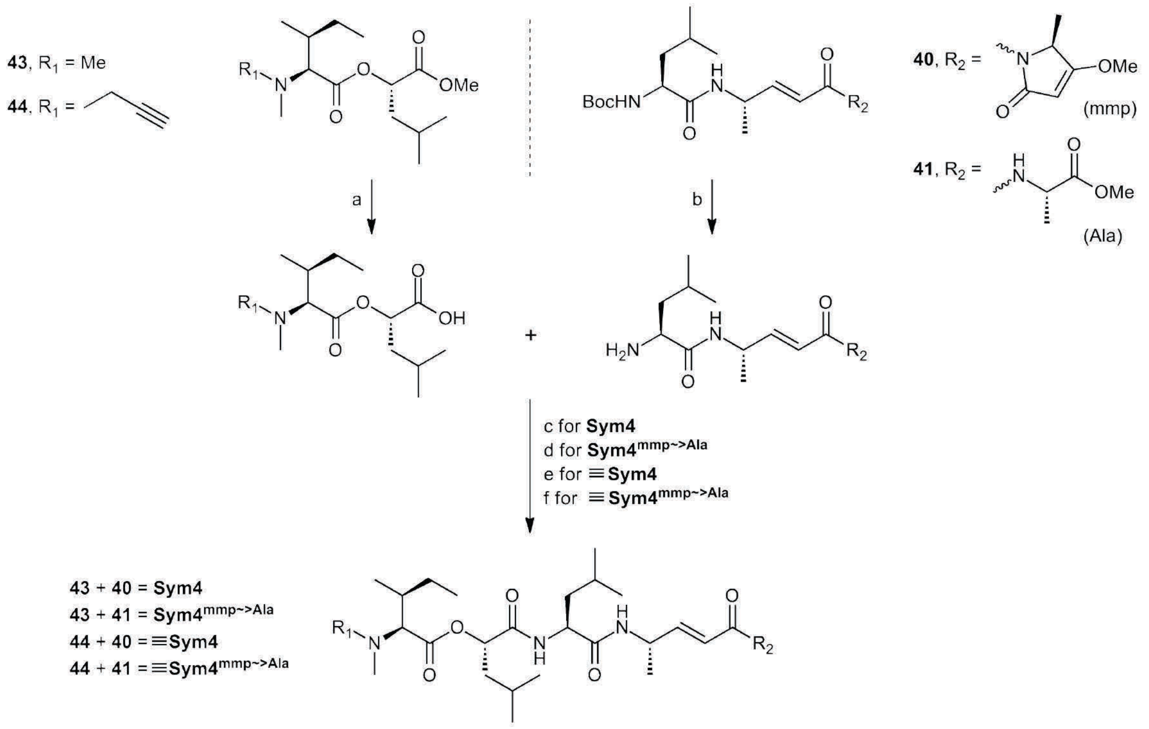

Figure 73: Synthesis of the symplostatin 4 derivatives. Reagents and conditions: (a) LiOH, THF/MeOH/H_2O (1.67:1:0.67), rt, 5 h; (b) TFA/CH_2Cl_2 (1:1), rt, 2 h; (c) HOBt, HBTU, DIEA, CH_3CN, 0 °C to rt, 5 h (91% (from **43**) after silica gel chromatography, 51% after additional HPLC, 3 steps); (d) HOBt, HBTU, DIEA, CH_3CN, 0 °C to rt, o/n (39% (from **43**) after HPLC, 3 steps); (e) HOBt, HBTU, DIEA, CH_3CN, 0 °C to rt, o/n (82% (from **44**) after silica gel chromatography, 64% after additional HPLC, 3 steps); (f) HOBt, HBTU, DIEA, CH_3CN, 0 °C to rt, 5 h (73% (from **44**) after silica gel chromatography, 53% after additional HPLC, 3 steps).

With the two alkyne-modified derivatives **≡Sym4** and **≡Sym4**$^{\text{mmp→Ala}}$ available, the additional derivatives modified with tags for the utilization in an activity-based approach were synthesized. The conditions for the click reaction were adapted from the conditions developed by Cravatt and coworkers for *in vivo* labeling.[139] However, the *in vitro* reactions carried out required an optimization of reaction conditions; in particular the amount of $CuSO_4$ was increased greatly in order to achieve a good conversion of the starting material. The corresponding reactions were monitored by LC-MS and stopped upon sufficient product formation. The purification of the different products turned out to be rather tedious and required customized conditions: The rhodamine-modified derivatives **Rh-Sym4** and **Rh-Sym4**$^{\text{mmp→Ala}}$ were purified by AluOx chromatography; in the case of **Rh-Sym4** a second chromatography was necessary to obtain pure material. For the purification of the trifunctional probes **Tri-Sym4** and **Tri-Sym4**$^{\text{mmp→Ala}}$ and the biotinylated probes **biotin-Sym4** and **biotin-Sym4**$^{\text{mmp→Ala}}$ C_{18} silica gel (reversed phase silica gel) was tested as an alternative stationary phase. In analogy to C_{18} HPLC purification an increasing gradient of acetonitrile in water was used and allowed their purification in a satisfying manner (Fig. 74).

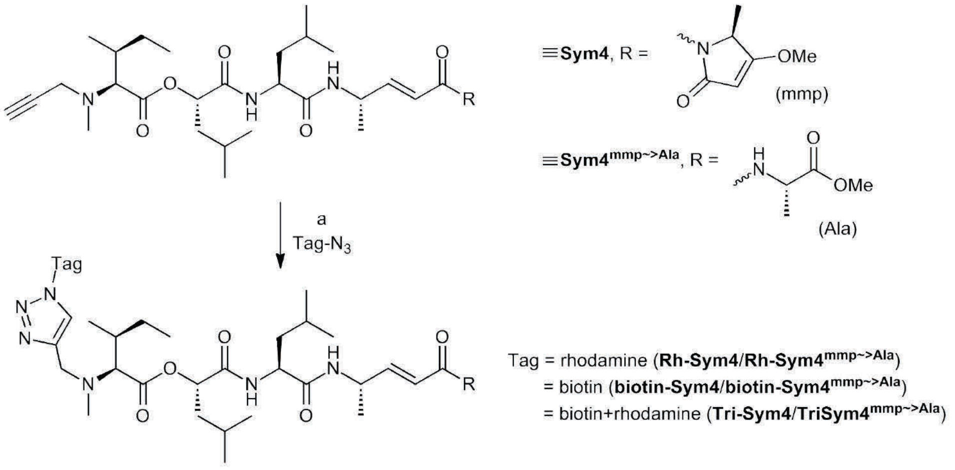
≡Sym4, R =
OMe
(mmp)
≡Sym4mmp~>Ala, R =
OMe
(Ala)
a
Tag-N3
Tag
R
Tag = rhodamine (Rh-Sym4/Rh-Sym4mmp~>Ala)
= biotin (biotin-Sym4/biotin-Sym4mmp~>Ala)
= biotin+rhodamine (Tri-Sym4/TriSym4mmp~>Ala)

Figure 74: Synthesis of the different probes for the chemical biology investigations. Reagents and conditions: (b) Tag-N_3, $CuSO_4$ (aq. solution), TBTA (100 mM in DMSO), TCEP (100 mM in H_2O), H_2O, rt, reaction monitoring by LC-MS, chromatographic work-up.

3.3.3 Biological investigation of symplostatin 4 in the model plant *Arabidopsis thaliana*

3.3.3.1 First experiments using symplostatin 4 probes in *Arabidopsis thaliana*

During a placement in the plant chemetics group of Dr. Renier van der Hoorn (MPI Cologne), the labeling of the *A. thaliana* proteome by symplostatin 4 and its derivatives was investigated by the means of ABPP.

To establish a reliable and most of all reproducible labeling procedure, the conditions of the labeling reaction with the different probes needed to be evaluated prior to the actual experiments. In a first set of labeling experiments, the optimal pH for the labeling of *A. thaliana* leaf extracts with the rhodamine-labeled probes **Rh-Sym4** and **Rh-Sym4$^{\text{mmp}\rightarrow\text{Ala}}$** was investigated. To this end, the leaf extracts were labeled at a constant probe concentration of 5 μM at different pH values (pH 3.0 to 9.0; 0.5 steps). From these experiments, pH 8 was determined as the optimal pH for the labeling with the symplostatin 4 probes.

A second set of experiments was aimed at the investigation of the concentration required for a well-detectable labeling. The experiment was carried out at pH 6 using different concentrations of the two probe molecules (0.2 to 10 μM; 0.2 steps to 1 μM, 2.0 steps to 10 μM). Here, a difference between the two probe molecules became apparent: **Rh-Sym4** showed a good labeling at 5 µM, while for **Rh-Sym4$^{\mathbf{mmp \rightarrow Ala}}$** the highest concentration of 10 µM was required to obtain a good labeling pattern.

These preliminary experiments established the conditions for the future labeling experiments. Moreover, they were also revealed that a labeling of leaf extracts with the probes gives a quite indistinct labeling pattern, *i. e.* too many enzymes are labeled by the probes. Owing to this finding, the *in vivo* labeling of *A. thaliana* with the probes was investigated in order to potentially obtain a better labeling pattern. In these experiments, all 6 differently-tagged probes (**Rh-Sym4**, **Rh-Sym4$^{\mathbf{mmp \rightarrow Ala}}$**, **biotin-Sym4**, **biotin-Sym4$^{\mathbf{mmp \rightarrow Ala}}$**, **Tri-Sym4** and **Tri-Sym4$^{\mathbf{mmp \rightarrow Ala}}$**) were investigated. Indeed, the labeling of *A. thaliana* cells did provide a clearer labeling pattern, thereby encouraging further *in vivo* experiments.

Additionally, two different set-ups of leaf infiltration experiments were carried out to investigate the *in vivo* labeling of the *A*. *thaliana* leaves: In the first set-up, the leaves were infiltrated *via* their petioles. For each experiment, three leaves were carefully set into the well of a 24-well plate filled with a solution containing the respective probe. In this set-up, different mutants of *A*. *thaliana* were investigated, besides the regularly used Col-0 (wild-type), the rd21, rA and aalp mutants were investigated. The incubation was carried out under the exclusion of light to prevent a decomposing of the fluorescent labels. Before the leaf extract was generated, the petioles were removed to ensure that only the *in vivo* labeling was determined and not an *ex vivo* labeling caused by a contamination of the extract.

In the second set-up, the leaves were infiltrated with the different probes *via* the stomata on the reverse side of the leaf. Besides the Col-0 type, 4 different mutants (628oe, rd21, aalp and rA) were investigated. To achieve the infiltration, the probe solution was carefully applied by pressing a syringe (without a cannula) to the reverse side of a detached leaf and pressing down the plunger; a successful infiltration is thereby visualized by the slight darkening of the leaves resulting from the uptake of the liquid into the vascular system. After the incubation, the detached leaves were incubated under the exclusion of light on damp blotting paper in a Petri dish. After the incubation the infiltrated leaves were treated in order to obtain the leaf extract that was then analyzed.

Unfortunately, none of the infiltration experiments provided a distinct labeling, although a repetition of the experiments would be highly desirable.

3.3.3.2 Identifying the target of symplostatin 4 in *Arabidopsis thaliana*

With the preliminary results from the *in vivo* labeling experiments in hands, the next step in the investigation of symplostatin 4 and its derivatives was the identification of the targets labeled by **Sym4** and the structure-activity analog **Sym4**$^{\mathbf{mmp \rightarrow Ala}}$. To achieve this, Dr. Farnusch Kaschani from the van der Hoorn group used the click derivatives **≡Sym4** and **≡Sym4**$^{\mathbf{mmp \rightarrow Ala}}$ in an *in vivo* labeling experiment with *A. thaliana* cells. The subsequent click experiment to tag the labeled enzymes with biotin and rhodamine was carried out with the Tri-azide reporter, following an established protocol.[149] After the click reaction the labeled enzymes were purified by avidin agarose beads (*via* the biotin tag). The enriched proteins were then separated by an SDS-PAGE and the bands were detected using a fluorescence scanner. The identification of the individual bands was carried out by nanoLC-MS/MS analysis after an in-gel digestion of the individual bands (Fig. 75).

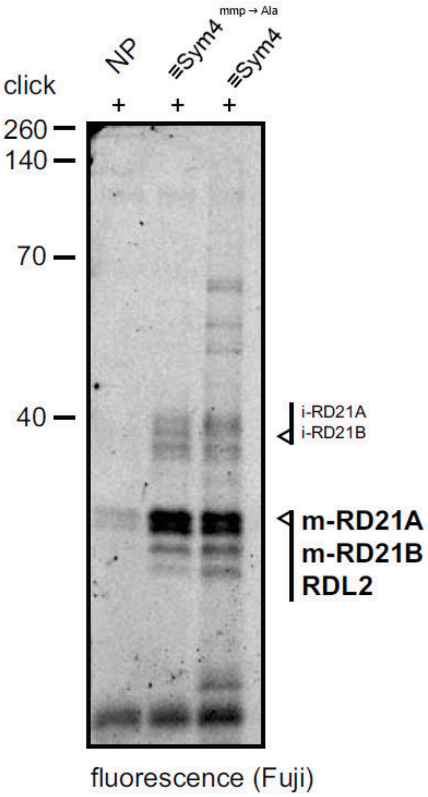

Figure 75: Fluorescence scan of the SDS-PAGE-resolved enzymes labeled by **≡Sym4** and **≡Sym4**$^{\mathbf{mmp \rightarrow Ala}}$. For the target-ID, the individual bands were cut out, digested (trypsin) and the fragments detected by nanoLC-MS/MS (work by F. Kaschani).

The major target of **Sym4** and **Sym4**$^{\mathbf{mmp\rightarrow Ala}}$ turned out to be the papain-like cysteine proteases RD21A and the homologous RD21B which are assigned to play a role in the plant immunity.[150] To a smaller extent, the protease RDL2 was also labeled by **Sym4** and **Sym4**$^{\mathbf{mmp\rightarrow Ala}}$. Moreover, these target identification experiments in the model plant *A. thaliana* showed no difference between the original natural product **Sym4** and its analog **Sym4**$^{\mathbf{mmp\rightarrow Ala}}$ with the putatively important methyl-methoxypyrrolinone unit as both molecules labeled RD21 A and RD21B with the same intensity.

3.3.4 Investigating the antimalarial activity of symplostatin 4 and target identification in *Plasmodium falciparum*

After having investigated the labeling of the proteome of the model plant *A. thaliana* and having achieved the identification of the molecular target of symplostatin 4 in this model system, the molecular basis of the antimalarial activity of symplostatin 4[103] (*i. e.* the activity reported for the chemically identical gallinamide A[104]) was investigated. To this end, a collaboration with the group of Prof. Dr. Matthew Bogyo (Department of Pathology, Stanford University, CA) was initiated, aiming to study the effects of **Sym4** and **Sym4**$^{\mathbf{mmp\rightarrow Ala}}$ on the malaria-causing parasite *Plasmodium falciparum*. From the structure of symplostatin 4 as well as from the preliminary studies of the labeling in *A. thaliana* which identified the cysteine protease RD21 as the target of **Sym4**, the hypothesis of parasital falcipains as the molecular target of **Sym4** arose.

In order to test this hypothesis, Dr. Edgar Deu Sandoval from the Bogyo group carried out several cell-based and activity-based assays. In a first cell-based assay the effect of **Sym4** and **Sym4**$^{\mathbf{mmp\rightarrow Ala}}$ on malaria parasites in the erythrocytic cycle was investigated. To this end, a synchronized cell culture of *P. falciparum* D10 at ring stage was treated with different concentrations of **Sym4** and **Sym4**$^{\mathbf{mmp\rightarrow Ala}}$. The effect of the inhibitors was then visualized 24 h after the treatment by Giemsa-stained thin blood smears. The cells treated with 0.1 µM **Sym4** already showed a distinct swollen food vacuole phenotype which is observed characteristically when the proteases involved in the early stage of hemoglobin digestion are inhibited or differently disturbed (*e. g.* by a genetic knock-out) and is caused by the accumulation of undigested hemoglobin.[50,53,151]

In contrast to this, the same effect was observed for **Sym4**$^{\mathbf{mmp\rightarrow Ala}}$ at a 100-fold higher concentration, indicating a significant difference between the two analogs. This difference might stem from a decreased uptake of the probe to the food vacuole or it may be caused by a less specific binding to the target caused by the absence of the mmp unit.

At high concentrations, however, both compounds seem to have a toxic effect on the parasite (Fig. 76). Importantly, at no tested concentration a lysis of the red blood cells was observed.

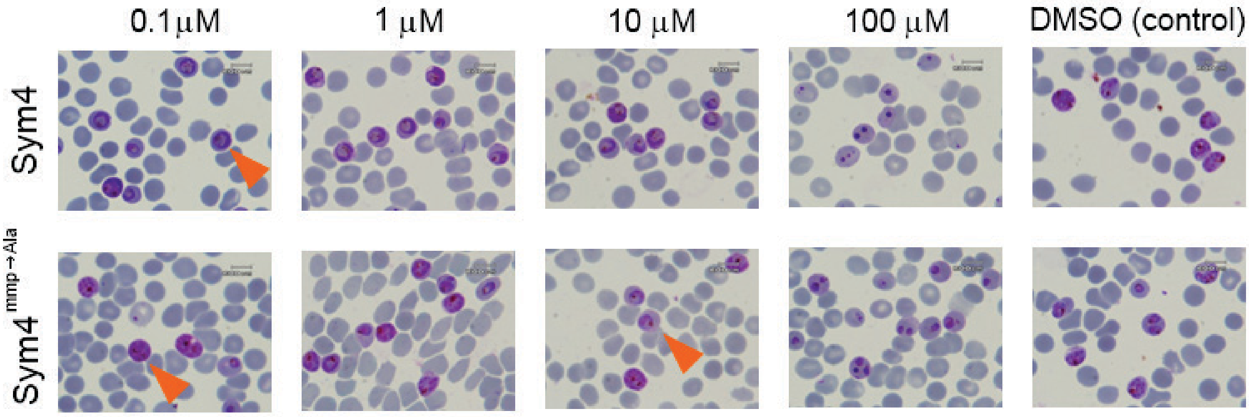

Figure 76: Effect of **Sym4** and **Sym4**$^{\mathbf{mmp\rightarrow Ala}}$ on *P. falciparum* D10 cells treated at ring stage with different concentrations of the probe. Significant phenotypes are indicated by arrows (work by E. Deu).

These first results were already very encouraging and in addition, a clear difference between the two symplostatin 4 analogs was observed. Encouraged by these findings, the focus was then set on the investigation of the effect of symplostatin 4 on the replication of the parasite. Hence, a cell culture at 2% parasitemia was treated with different concentrations of the inhibitors for 75 h and after this time, the parasitemia was determined by flow cytometry.[152] Again, a clear difference between **Sym4** and its analog **Sym4**$^{\mathbf{mmp\rightarrow Ala}}$ became apparent. The **Sym4**-treated cell culture displayed a potently inhibited parasite replication; the EC_{50} of **Sym4** was in the low micromolar range (EC_{50} = 0.7 ± 0.2 μM). **Sym4**$^{\mathbf{mmp\rightarrow Ala}}$ on the other hand only displayed an EC_{50} of 27 ± 7 μM, thereby confirming the results of the previous phenotype assay (Fig. 77).

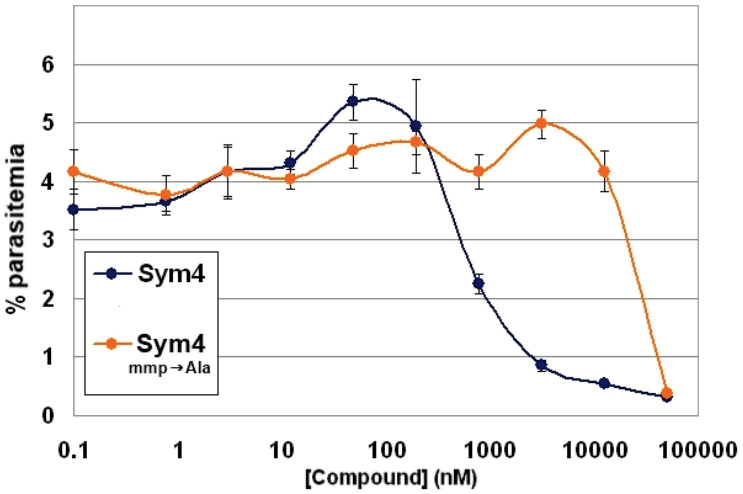

Figure 77: Investigation of the effects of **Sym4** and **Sym4**$^{\mathbf{mmp \rightarrow Ala}}$ on parasite replication (work by E. Deu).

With the results from the cell-based assays in hands that already indicated that one or more of the parasite's food vacuole cysteine proteases *i. e.* falcipain 2, falcipain 2′ and falcipain 3 (FP-2, FP-2′, FP-3)[50] may indeed be the target of **Sym4**, a focus was set on verifying this hypothesis by activity-based profiling experiments. In a first labeling experiment, **Rh-Sym4** and **Rh-Sym4**$^{\mathbf{mmp \rightarrow Ala}}$ were tested for their labeling of intact parasites (Fig. 78). Hence, purified schizonts were treated with the two different probes at a concentration of 10 µM. For **Rh-Sym4**, two strong bands in the 28 kDa region appeared, while for **Rh-Sym4**$^{\mathbf{mmp \rightarrow Ala}}$ only a very weak labeling in this region was detected. To investigate whether this labeling was caused by the respective probe or if it was just an artifact caused by the rhodamine tag, the experiment was also carried out in a competitive manner. To this end, the purified schizonts were pre-incubated with 10 µM of the non-tagged version and the click version of the respective rhodamine probe. Indeed, the bands in the 28 kDa region were sensitive to the pre-incubation with **Sym4** and **≡Sym4**, proving that the labeling was actually caused by the probe. Additionally, this experiment pinpointed to a clear difference between **Sym4** and **Sym4**$^{\mathbf{mmp \rightarrow Ala}}$ that had already become apparent in the previous experiments. This impairment of bioactivity caused by the exchange of the mmp unit for the alanine methyl ester moiety can be explained either with a reduced uptake of the probe by the parasite or more likely, by a much less efficient binding of the compound to its targets.

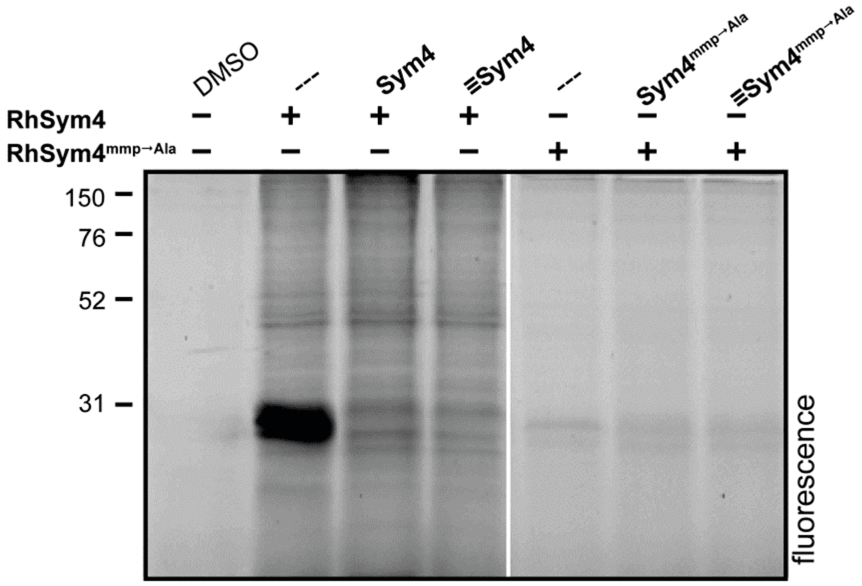

Figure 78: Labeling of intact parasites with **Rh-Sym4** and **Rh-Sym4**$^{\mathbf{mmp\rightarrow Ala}}$. Purified schizonts were labeled with 10 µM of the rhodamine-labeled probes for 1 h. For the competition experiments, the schizonts were pre-incubated with the non-fluorescent probes **Sym4** and **≡Sym4** or **Sym4**$^{\mathbf{mmp\rightarrow Ala}}$ and **≡Sym4**$^{\mathbf{mmp\rightarrow Ala}}$ (10 µM), then the labeling with **Rh-Sym4** or **Rh-Sym4**$^{\mathbf{mmp\rightarrow Ala}}$ was carried out for 1 h, the samples were boiled in loading buffer and the proteins were resolved by SDS-PAGE. The proteins were visualized by in-gel detection of fluorescence on a Typhoon scanner. (work of E. Deu)

Since the labeling in the 28 kDa region was a strong indicator for the inhibition of FP-2, FP-2$'$ and FP-3 (referred to as FP-2/3) that are known to migrate in the 28 kDa region and are important factors for the development at the erythrocytic stages, a competitive ABPP experiment with Cy5-labeled DCG-04 and the probes **Sym4** and **Sym4**$^{\mathbf{mmp\rightarrow Ala}}$ was carried out to test if **Sym4** and **Sym4**$^{\mathbf{mmp\rightarrow Ala}}$ indeed target FP-2/3. While FP-2/3 are responsible for the digestion of hemoglobin and are expressed at later developmental stages, FP-1 is expressed during the phase of host invasion and is thought to play a crucial role in host cell invasion.[153,154]

For the commonly used Cy5-DCG-04, the labeling pattern in *P. falciparum* is known and the targets have been identified. Thus, a competitive ABPP experiment can be used to identify if a small molecule probe is an inhibitor of the labeled enzymes.[153,154]

The competitive ABPP experiment was carried out with *P. falciparum* D10 lysates that were pre-incubated with different concentrations of **Sym4** or **Sym4**$^{\mathbf{mmp\rightarrow Ala}}$ for 30 min, then 1 µM of Cy5-DCG-04 was added and the labeling was stopped after 1 h by the addition of gel loading buffer. The labeled proteins were then resolved by SDS-PAGE and the fluorescence was detected by scanning the gel on a typhoon scanner.

For **Sym4**, the experiment revealed a low nanomolar (1.5 nM) inhibition of FP-2/3 as indicated by the disappearance of the DCG-04 bands, in addition, FP-1 was also inhibited but only at significantly higher concentrations (1.6 µM). The aminopeptidase DPAP-1 was not inhibited. In contrast to **Sym4**, the inhibition of FP-2/3 by **Sym4**$^{\mathbf{mmp \rightarrow Ala}}$ was much weaker; a reduced DCG-04 signal was detected starting from a concentration of 25 µM and an inhibition of FP-1 or DPAP-1 was not detected at all (Fig. 79).

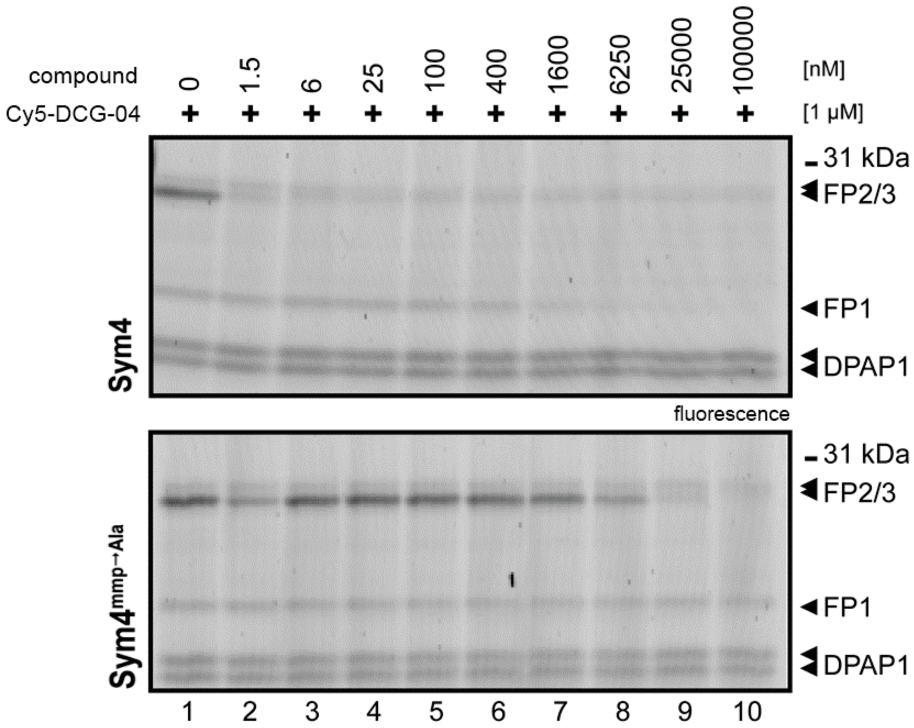
compound
Cy5-DCG-04
0
1.5
6
25
100
400
1600
6250
25000
100000
[nM]
+ + + + + + + + + +
[1 µM]
31 kDa
FP2/3
FP1
DPAP1
Sym4
fluorescence
31 kDa
FP2/3
FP1
DPAP1
Sym4mmp→Ala
1 2 3 4 5 6 7 8 9 10

Figure 79: Competitive ABPP experiments with Cy5-DCG-04 and **Sym4** or **Sym4**$^{\mathbf{mmp \rightarrow Ala}}$. **Sym4** potently inhibits FP-2/3 at a low nanomolar concentration (1.5 nM). (work of E. Deu)

The competitive APBB experiments were carried out in the same manner with the click probes **≡Sym4** and **≡Sym4**$^{\mathbf{mmp \rightarrow Ala}}$ that exhibited a similar labeling pattern as the unmodified probes, thereby indicating that in contrast to the *C*-terminal replacement of mmp by alanine methyl ester, the modification of the *N*-terminus did not influence the labeling behavior of the respective probe (Fig. 80).

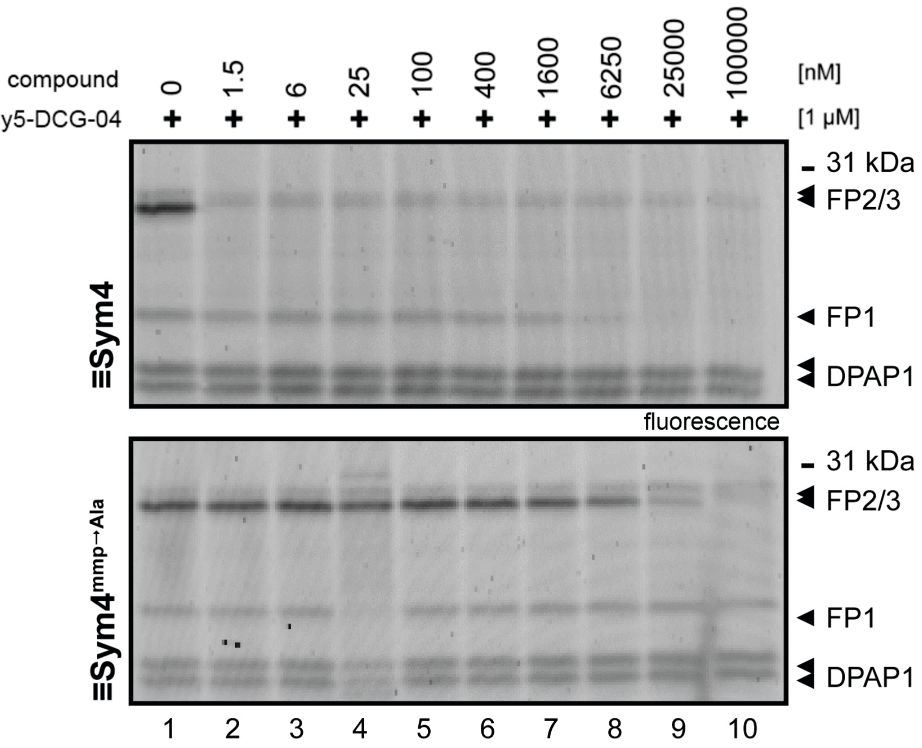

Figure 80: Competitive ABPP experiments with Cy5-DCG-04 and **≡Sym4** or **≡Sym4**$^{mmp\rightarrow Ala}$. **≡Sym4** also potently inhibits FP-2/3 at low nanomolar concentrations, similar to **Sym4**. It inhibits FP-1 above concentration of 25 µM. The derivative **≡Sym4**$^{mmp\rightarrow Ala}$ is a poor FP-2/3 inhibitor with no detectable inhibition of FP-1. (work of E. Deu)

Since **Sym4** turned out to be a highly potent inhibitor of FP-2/3, the parameters of inhibition were further investigated. Firstly, the kinetics of the inhibition as well as the mode of inhibition of FP-2 and FP-3 were investigated by determining the inhibition of substrate turnover for recombinant FP-2 and FP-3. This experiment revealed that **Sym4** is an irreversible inhibitor of FP-2 and FP-3 and that **Sym4** is approximately 10-fold more potent against FP-2 (k_i = 58600 ± 1400 $M^{-1}s^{-1}$) than against FP-3 (k_i = 7030 ± 250 $M^{-1}s^{-1}$). In summary, these assays performed for **Sym4** revealed that **Sym4** is one of the most potent FP-2/3 inhibitors reported to date[155].

In a further evaluation of the inhibition parameters of **Sym4**, the inhibition of the parasite's papain-like cysteine proteases by **Sym4** was also determined in intact parasites. To this end, a parasite culture of *P. falciparum* was treated with different concentrations of **Sym4** for 1 h then the RBCs were lysed with saponin, and the residual activity of the PLCPs in the parasite pellets was measured using Cy5-DCG-04 (Fig. 81). This assay revealed that **Sym4** is a sub-micromolar inhibitor of all falcipains in the intact parasites, preferentially inhibiting FP-2 (IC_{50} = 8.5 ± 1.3 nM) over FP-3 (IC_{50} = 22 ± 8 nM) or FP-1(IC_{50} = 140 ± 23 nM).

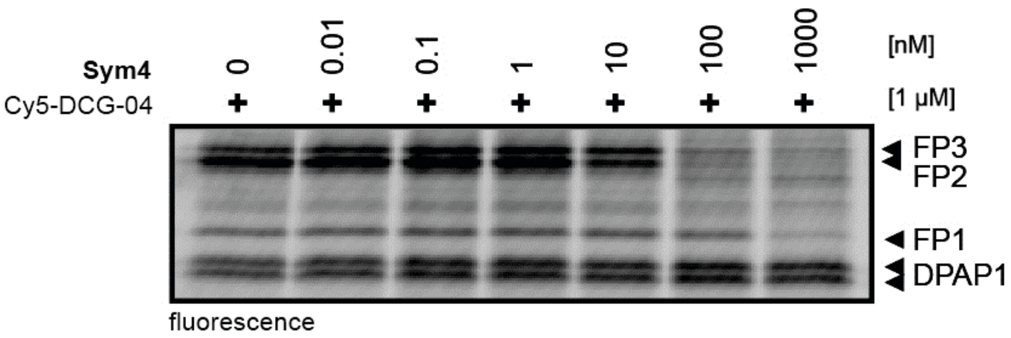

Figure 81: Inhibition of PLCPs by **Sym4** in intact parasite cells. (work of E. Deu)

In summary, the overall antimalarial activity of **Sym4** most likely results from a combined inhibition of FP-2 and FP-3 (and also to a certain extent of FP-1). It has to be noted that a lower concentration of **Sym4** is required to cause a food vacuole defect (0.1 µM) than to actually kill the parasites (EC_{50} = 0.7 µM) indicating that the inhibition of FP-2 is sufficient to effect a disturbance of the hemoglobin digestion in the food vacuole, yet it is not sufficient to kill the parasite. [52] The antimalarial activity of **Sym4** that results in a killing of the parasite is therefore most likely due to an inhibition of FP-3. The hemoglobinase activity of the falcipains has been suggested to be redundant, *i. e.* if FP-2 is inhibited, FP-3 is able to overtake its role in a rescue mechanism. FP-3 is, however, crucial for the survival of the parasite at a later developmental stage.[50] An evidence for this finding is provided by the fact that in knock-out experiments (that were also presented in the introduction of this work), a FP-2 knock-out indeed displays the prominent food vacuole defect but is yet viable, while an FP-3 knock-out could not be generated.[52]

Moreover, the present studies indicate that derivatives of symplostatin 4 that feature the mmp group represent promising new lead structures for the design of antimalarial agents. In fact, the findings from this study indicate that an incorporation of this group into rationally-designed small molecule inhibitors could significantly contribute to an enhancement of their biological activity.

4 Summary and Conclusions

During this PhD project two different natural product protease inhibitors and analogs derived from these natural products were studied. Natural products are regarded as privileged structures that have emerged from evolution to exert a biological effect. Consequently, natural products are regarded as pre-validated compounds owing to their natural origin and they represent valuable lead structures in drug discovery.[1,3] Accordingly, the investigation of their chemical synthesis as well as the molecular basis of their biological activity are interesting scientific questions addressed in the field of chemical biology.

4.1 Development of a general solid-phase synthesis for Ahp cyclodepsipeptides and synthesis of symplocamide A

The class of Ahp cyclodepsipeptides is known for its specific and, most intriguingly, non-covalent inhibition of S1 serine proteases and has been suggested as a target class in the investigation of serine protease inhibitors as drug targets.[25]

At the beginning of this PhD project, only two tedious and highly specialized solution-phase syntheses of Ahp cyclodepsipeptides were published.[100-102]

Consequently, the first goal of this thesis was the development of a more flexible synthesis approach to Ahp cyclodepsipeptides. This was accomplished by the development of a solid-phase synthesis strategy for Ahp cyclodepsipeptides. These syntheses were based on a general Ahp precursor that enabled the anchoring to the solid phase as well as the installation of the critical Ahp residue in the cyclodepsipeptide structure (Fig. 82).

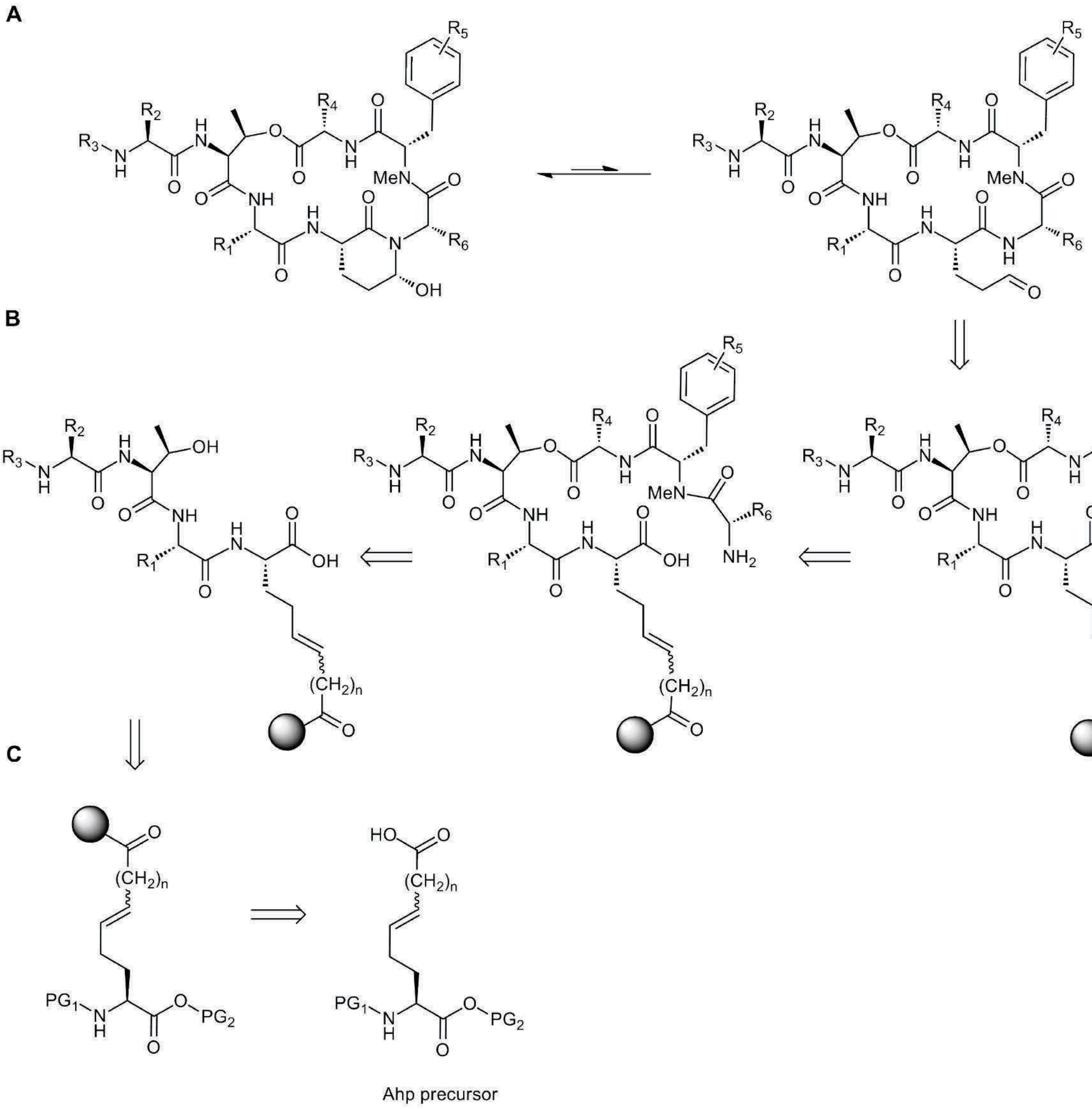

Figure 82: Retrosynthetic analysis of Ahp cyclodepsipeptides. **A**: The Ahp hemiaminal is formed spontaneously from an aldehyde precursor, if the cyclodepsipeptide framework is present. **B**: The aldehyde can be obtained by the oxidative cleavage of a masked glutamic aldehyde. The cyclization can be carried out as an *on-resin* macrolactamization; the esterification of the threonine side chain is a crucial step in the depsipeptide synthesis. **C**: The solid-phase synthesis starts from a suitable Ahp precursor that is coupled to the solid support *via* the carboxylic acid functionality incorporated its side chain.

The development of a suitable Ahp precursor was a more demanding task than first anticipated. In fact, the final precursor structure was the result of tedious investigations and frequent reconsiderations. This precursor allowed the generation of a glutamic aldehyde on solid support *via* a dihydroxylation-glycol cleavage protocol based on the previous works of the Meldal group.[106-108] In fact, this cleavage procedure was used in this PhD thesis for the first time to generate an aldehyde upon cleavage from the solid phase and therefore extends the repertoire of solid-phase cleavage methods. The solid-phase cleavage, however, required the use of an alternative resin based on a polyethylene glycol core in place of the commonly used polystyrene resins because polystyrene resins turned out to be incompatible to the employed reaction conditions.

Finally, the Ahp cyclodepsipeptide symplocamide A was generated successfully with the newly developed synthetic strategy (Fig. 83)[115,118] The analytic data collected for synthetic symplocamide A corresponded well to the data published for the compound isolated from natural sources.[24]

In addition to the spectral data, the biological activity of the synthetic symplocamide A was also validated. In a chymotrypsin inhibition assay the synthetic material proved to be as potent as the isolated compound, displaying a K_i of 0.32 ± 0.09 μM which is in good accordance with the literature report (lit.[24], IC_{50} = 0.38 ± 0.08 μM). The reported cytotoxicity against two cancer cell lines as well as a suggested putative proteasome inhibition, however, could not be confirmed for the synthetic material in the assays used here.

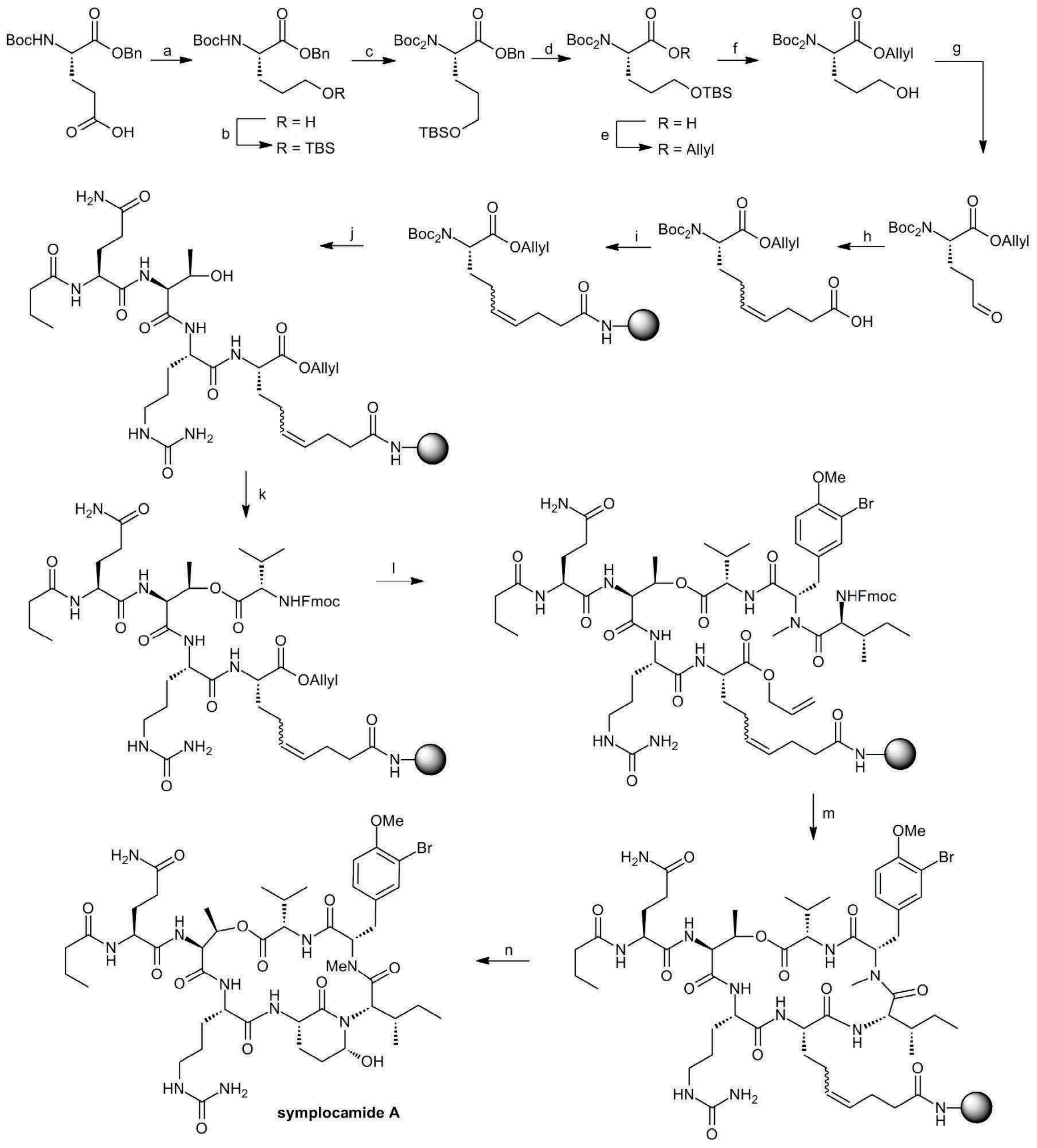

Figure 83: Total synthesis of symplocamide A.[115,118] Reagents and conditions: (a) i. EtOCOCl, Et_3N, THF, -15 °C, 1 h, ii. $NaBH_4$, THF/H_2O (1:1), -15 °C, 1 h, then rt, 6 h (84%); (b) TBDMSCl, imidazole, CH_2Cl_2, 0 °C to rt, o/n (95%); (c) Boc_2O, DMAP, CH_3CN, rt, 24 h (81%, b.r.s.m.); (d) 10% Pd/C, H_2, EtOAc, rt, 2.5 h (99%); (e) i. Cs_2CO_3, MeOH; ii. allylbromide, DMF, rt, o/n (95%); (f) $CuCl_2*2H_2O$, acetone/H_2O (95:5), reflux, 1 h (92%); (g) Dess-Martin periodinane, CH_2Cl_2, rt, 1 h (84%); (h) i. $Ph_3P^+(CH_2)_3CO_2H\ Br^-$, LHMDS,THF, 0 °C, 55 min; ii. **15**, THF, 0 °C to rt, o/n (64%). (i) i. amino NovaPEG resin, HOBt, HBTU, DIEA, CH_2Cl_2-DMF; ii. CH_2Cl_2/DIEA/Ac_2O (3:1:1); iii. CH_2Cl_2/DIEA/Ac_2O (3:1:1), 3h; (j) i. TFA/CH_2Cl_2 (1:1); ii. Et_3N/CH_2Cl_2 (1:9); iii. Fmoc-Cit-OH, HOBt, HBTU, DIEA, DMF, 5h (30%, by Fmoc determination, 2 steps); iv. piperidine/DMF (1:4); v. Fmoc-Thr-OH, HOBt, HBTU, DIEA, DMF, 2h; vi. piperidine/DMF (1:4); vii. Fmoc-Gln(Trt)-OH, HOBt, HBTU, DIEA, DMF, 2h (88% by Fmoc determination, 2 couplings); viii. piperidine/DMF (1:4); ix. butyric acid, HOBt, HBTU, DIEA, DMF, 2h; (k) Fmoc-Val-OH, DCC, DMAP, CH_2Cl_2/DMF (9:1); 79% by Fmoc determination, 2 couplings); (l) i. piperidine/DMF (1:4); ii. Fmoc-*N*MePhe-OH, HOBt, HBTU, DIEA, DMF, 2h; iii. piperidine/DMF (1:4); iv. Fmoc-Ile-OH, PyBrOP, DIEA, DMF, 24h (60%, by Fmoc determination, 2 couplings); (m) i. piperidine, DMF; ii. $Pd(PPh_3)_4$, morpholine, CH_2Cl_2; iii. PyBOP, HOBt, DIEA, DMF; (n) OsO_4, $NaIO_4$, DABCO, *t*-BuOH, THF/H_2O (3% overall yield).

4.2 Synthesis and biological evaluation of small molecule analogs of proteinaceous serine protease inhibitors adopting the canonical conformation

Since the Ahp cyclodepsipeptides had only recently been recognized as inhibitors that adopt the canonical conformation and thereby belong to the larger class of small molecule analogs of canonical-conformation proteinaceous serine protease inhibitors[18], the question arose if the Ahp residue is truly essential to form a canonical conformation. Indeed, it became apparent during this project that the synthesis of tailor-made Ahp cyclodepsipeptides is doable but nevertheless laborious. Consequently, synthetically easier accessible Ahp-mimics were sought.

To gain a quick and flexible access to the desired Ahp analogs, a new solid-phase synthesis was developed adapting some methodology from the previous synthesis of symplocamide A and using the specificity-determining P_1 amino acid as the anchoring point to the solid phase. Such an approach should enable access to a multitude of inhibitors for one protease by a combinatorial approach (Fig. 84).

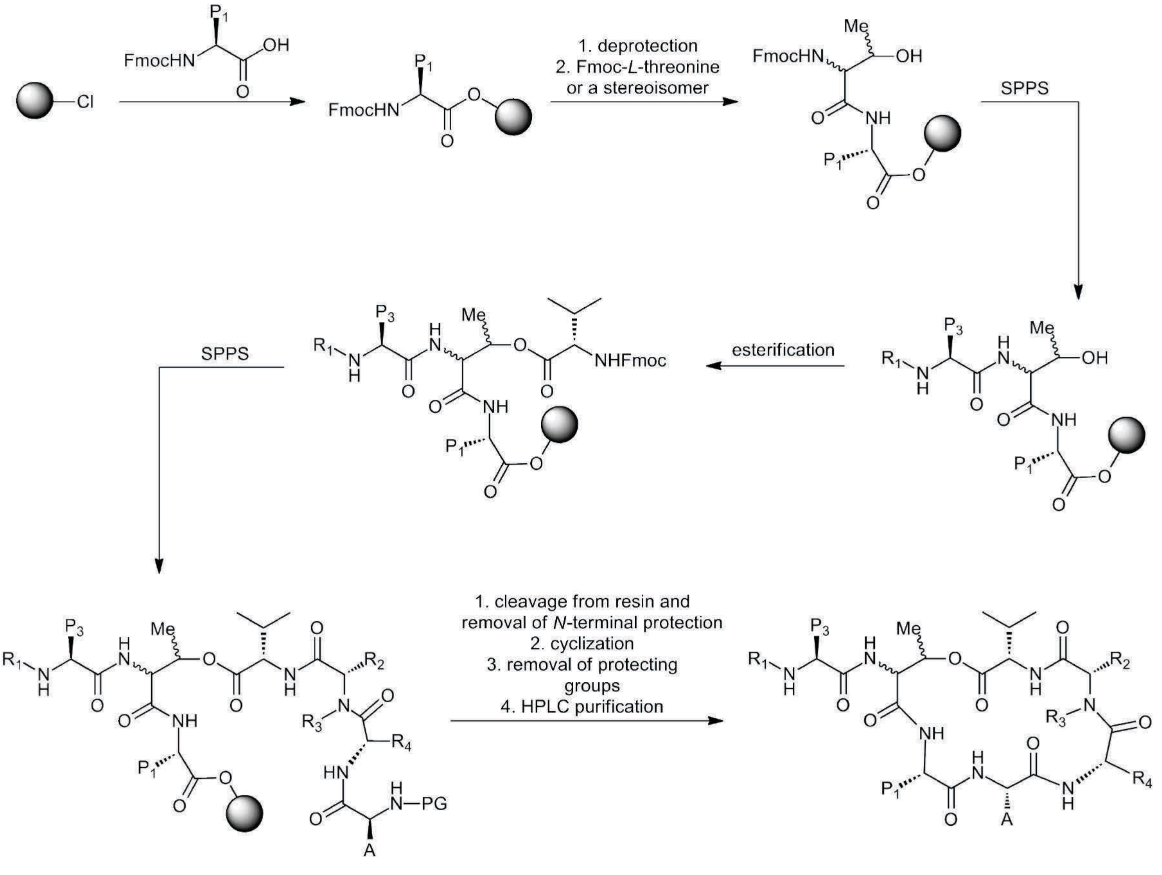
FmocHN
P1
OH
O
Cl
1. deprotection
2. Fmoc-L-threonine
or a stereoisomer
Me
SPPS
esterification
R1
P3
NHFmoc
R2
R3
R4
A
N—PG
1. cleavage from resin and
removal of N-terminal protection
2. cyclization
3. removal of protecting
groups
4. HPLC purification

Figure 84: General synthetic strategy for the synthesis of structure-activity analogs of Ahp cyclodepsipeptides, the residues are summarized in Table 5.

A first set of symplocamide A analogs then proved that the Ahp unit could indeed be replaced by the - also hydroxylated - amino acid serine. On the other hand the hydroxylated amino acids threonine and homoserine did not provide active compounds.

The possibility of replacing the Ahp unit by serine then paved the way for the investigation of the elements that are required for the macrocycle to adopt the canonical conformation and thereby act as a non-covalent inhibitor of serine proteases. The different structure-activity analogs that were investigated are summarized in Table 5:

Table 5: Structure-activity analogs investigated to determine the crucial elements for the adoption of the canonical conformation.

compound (mimic of)	Ahp replacement	further substitutions	K_i
SAR-1 (Sym A)	Ser	-	3.8 µM
SAR-2 (Sym A)	Hse	-	inactive
SAR-3 (Sym A)	Thr	-	inactive
SAR-4 (Sym A)	Ser	3-Br,4-OMe-mTyr→4-OMe-mTyr	4.8 µM
SAR-5 (Sym A)	Ser	3-Br,4-OMe-mTyr→mPhe	56.1 µM
SAR-6 (Sym A)	Ser	3-Br,4-OMe-mTyr→mPhe	inactive
SAR-7 (Sym A)	Ser	3-Br,4-OMe-mTyr→Pro	16.1 µM
SAR-8 (Sym A)	Ser	3-Br,4-OMe-mTyr→mPhe *L*-Thr→*D-allo*-Thr	inactive
SAR-9 (Sym A)	Ser	3-Br,4-OMe-mTyr→mPhe *L*-Thr→*L-allo*-Thr	inactive
SAR-10 (Scyp A)	Ser	-	19.1 µM
SAR-11 (Scyp A)	Thr	-	5.0 µM
SAR-12 (Scyp A)	Val	-	inactive

As already expected from the works of Leatherbarrow *et. al.*[23] the most crucial element for the adoption of the canonical conformation is an amino acid that supports the formation of a *cis* amide bond in the P_3' position. In the Ahp cyclodepsipeptides this residue is a conserved *N*-methylated aromatic amino acid[24], in the case of the BBI-derived inhibitors investigated by Leatherbarrow and coworkers, a proline is conserved.[23] For the present Ahp-mimicked cyclodepsipeptides, modified tyrosines in this position were superior to a proline residue or an even less active analog with a *N*-methyl phenylalanine residue. The possibility to substitute the conserved *N*-methylated amino acid with a proline clearly demonstrates that these analogs of Ahp depsipeptides are truly canonical-conformation inhibitors that require the reinforcement of the *cis* amide bond in the P_3' position.

Another structure element that was investigated and that has been suggested to play a role in the inhibition of serine proteases, is the threonine residue forming the depsipeptide linkage with the P_4' valine moiety. For the BBI inhibitors investigated by Leatherbarrow *et. al.* a threonine in the P_2 position is able to form a hydrogen bond to the P_1' serine and thereby directs the aliphatic part of the threonine side chain towards a close contact with the imidazole part of the enzyme's catalytic histidine. This contact is thought to interfere with a movement of the histidine that becomes necessary during the catalysis cycle and is proposed contribute to the inhibition of the protease.[18] Such a direction of the aliphatic part of the threonine side chain could indeed also be possible for Ahp cyclodepsipeptides and their structurally simplified analogs since the side chain is fixed by the ester bond and the direction of the methyl group is determined by the stereochemistry of the amino acid. Indeed, when the natural (*L*)-threonine residue was replaced by (*D*)-*allo*- or (*L*)-*allo*-threonine the resulting analogs were inactive against chymotrypsin. It has to be noted, however, that the requirement of a flexible histidine is discussed controversially in the scientific community. The results obtained here may yet be a humble contribution to this debate, hinting that indeed a blocking of the histidine's movement may interfere with the processing of the substrate and thereby contribute to the inhibitory mode-of-action. On the other hand, the loss of activity may also result from an overall altered conformation of the macrocycle.

To finally prove that the concept of substituting the Ahp moiety in an Ahp cyclodepsipeptide with another amino acid is a global concept that affect other proteases than chymotrypsin, a different protease needed to be addressed. To achieve this, three different analogs of the natural product scyptolin A[27,28] were synthesized and tested for their inhibition of the target protease elastase. Fortunately, two of the three analogs were active against elastase, the expected serine analog and, surprisingly, also the analog with threonine as a replacement of the Ahp moiety.

The third analog incorporating a valine as a replacement for the Ahp moiety was inactive against elastase, pinpointing the requirement of a hydroxyl group in the side chain of the

Ahp replacement. In the Ahp residue, the hydroxyl group plays a crucial role forming one of the two intramolecular hydrogen bonds with the peptidic backbone, thereby reinforcing the rigid structure of the molecule that contributes to the inhibitory potency. The present data indicate that also serine- and threonine analogs can form such hydrogen bonds, thereby stabilizing the canonical conformation.

In summary, a general and flexible approach to the solid-phase combinatorial synthesis of Ahp cyclodepsipeptides was developed during this PhD work. The strategy was proven by the synthesis of the natural product symplocamide A which then served as starting point for the synthesis of more easily accessible analogs for structure-activity relationship studies. In these analogs the Ahp moiety was replaced by amino acids that are commercially available. For the synthesis of these analogs, a global, combinatorial solid-phase synthesis strategy was developed and several SAR analogs were synthesized.

As a result of the structure-activity-relationship studies serine and threonine could be determined as adequate replacements of the Ahp moiety. Furthermore, the crucial determinants that are required to adopt the canonical conformation could be studied as well as the mode-of-inhibition using the newly developed Ahp-mimics.

For future investigations, it would also be highly desirable to obtain a co-crystal structure or a NMR structure of one of the Ahp-mimicked analogs with their target protease in order to confirm the findings that so far are based only on enzyme inhibition assays. So far, all attempts to obtain a co-crystal structure with chymotrypsin or elastase were, however, not successful.

Another aspect that would be worthwhile to investigate in future studies is the structural basis of the different inhibitory activities of threonine- and serine-mimics of scyptolin A. The substitution of the Ahp moiety in these compounds with threonine resulted in a more potent species than the respective serine analog. A possible explanation for this unexpected finding could be a hindered rotation (and thus pre-organization) of the threonine side chain. Inhibitor binding would therefore result in less entropy loss (in comparison to the respective serine analog), thereby the binding may be favored energetically. A possible explanation for the absence of this effect in the symplocamide A analogs could be that here the threonine side chain hydroxyl group may form a hydrogen bond with the side chain of citrulline; this arrangement however would prevent the formation of the intramolecular hydrogen bond that reinforces the conformation of the macrocycle. To prove this hypothesis, future investigations are however required and could involve on the one hand the synthesis of further analogs incorporating different P_1 residues or Ahp substitutions with more bulky side chain modifications. Finally, structural studies of the Ahp-mimics as well as the elucidation of the molecular binding mode via NMR or x-ray should provide the structural information required to prove the hypothesis.

Overall, the newly developed small molecule analogs of proteinaceous serine protease inhibitors may serve as tools in chemical biology to investigate serine proteases, their mode of action and their inhibition; furthermore, they could also serve as leads for the development of potent, selective and most importantly non-covalent drugs directed against serine proteases.

4.3 Development of a convergent synthesis of symplostatin 4 and derivatives for the target identification and biological evaluation

The second project that was carried out during this PhD thesis involved the investigation of the natural product symplostatin 4[103] that is also known by the name gallinamide A.[104] The interest in this natural product came from its molecular structure that consists of a prominent Michael acceptor system that has been recognized as a warhead for cysteine proteases and the rare *C*-terminal methoxy-methylpyrrolinone (mmp) residue as well as the interesting biological activities reported the compound. Consequently, symplostatin 4 seemed to be a natural product that could be a useful tool in chemical biology investigations, for example after conversion into an activity-based probe. Furthermore, the role of the mmp unit could be investigated by replacing this moiety with another amino acid.

To gain a quick access to symplostatin 4 (**Sym4**), an analog lacking the mmp moiety (**Sym4**$^{\mathbf{mmp \rightarrow Ala}}$) and also derivatives of these substances that would function as probes in ABPP, a highly convergent, fragment-based synthesis was developed (Fig. 85). To enable a flexible conversion of **Sym4** and **Sym4**$^{\mathbf{mmp \rightarrow Ala}}$ into suitable probes for ABPP, alkyne-modified versions of the two molecules were generated (**≡Sym4** and **≡Sym4**$^{\mathbf{mmp \rightarrow Ala}}$). They were then converted either into activity-based probes by reaction with azide-modified tags by a 1,3-dipolar Huisgen cycloaddition (click reaction) or used directly in a labeling and modified by a click reaction after the labeling. For the highest possible flexibility, rhodamine-, biotin- and trifunctional versions of both molecules were also generated (Fig. 86).

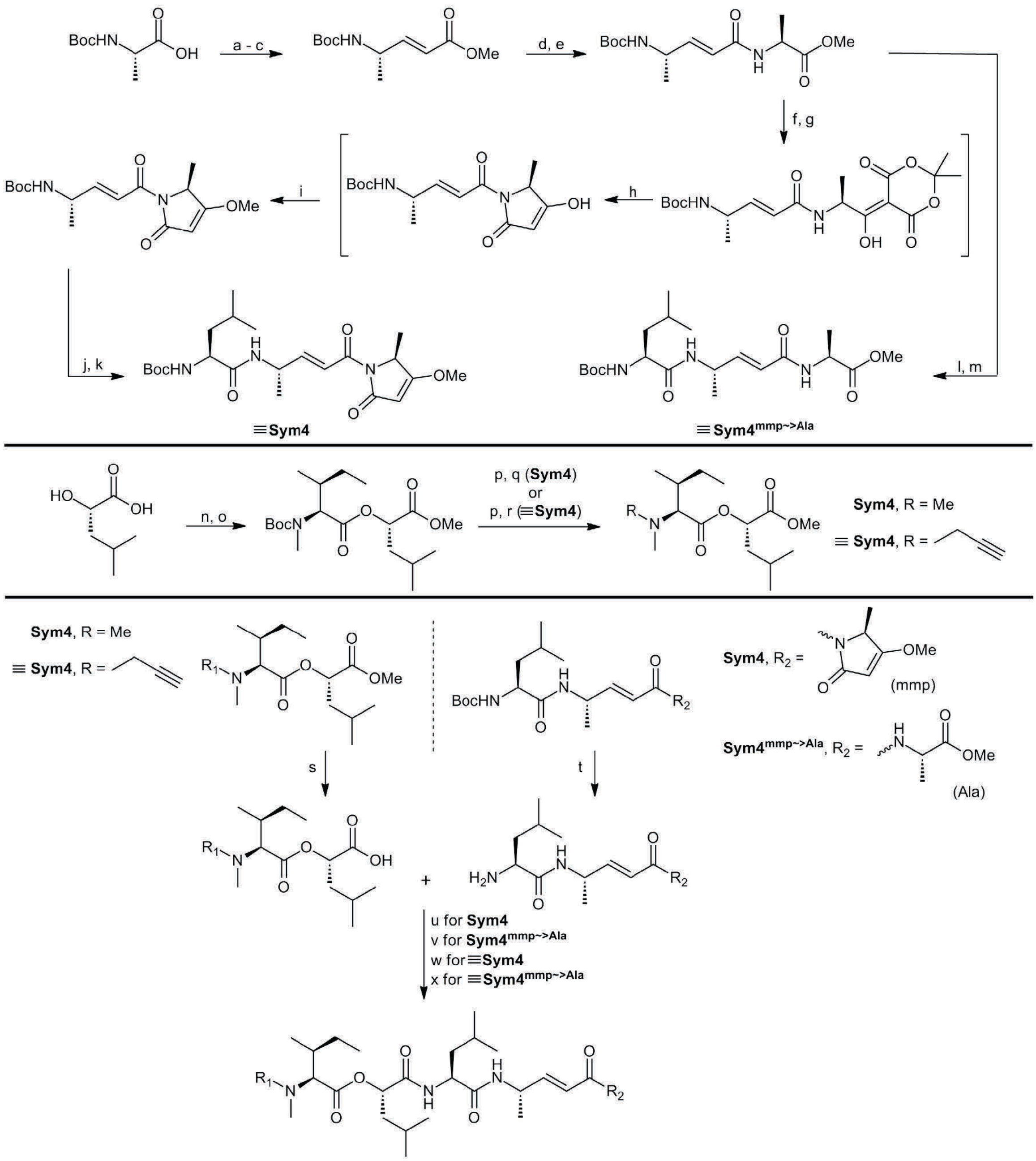
a - c
d, e
f, g
h
i
j, k
l, m
≡Sym4
≡Sym4mmp~>Ala
n, o
p, q (Sym4)
or
p, r (≡Sym4)
Sym4, R = Me
≡ Sym4, R =
Sym4, R = Me
≡ Sym4, R =
Sym4, R2 =
(mmp)
Sym4mmp~>Ala, R2 =
(Ala)
s
t
u for Sym4
v for Sym4mmp~>Ala
w for ≡Sym4
x for ≡Sym4mmp~>Ala

Figure 85: Convergent synthesis of symplostatin 4 and analogs. Reagents and conditions: (a) *N,O*-dimethylhydroxylamine hydrochloride, Et_3N, DCC, CH_2Cl_2, rt, 1 h; (b) $LiAlH_4$, Et_2O, 0 °C, 20 min; (c) $Ph_3P{=}CHCOOMe$, CH_2Cl_2, rt, o/n (59%, 3 steps); (d) LiOH, THF/MeOH/H_2O (1.67:1:0.67), rt, 5 h; (e) H-Ala-OMe, HOBt, HBTU, DIEA, CH_3CN, 0 °C to rt, o/n (46%, 2 steps); (f) LiOH, THF/MeOH/H_2O (1.67:1:0.67), rt, 5 h; (g) 2,2-dimethyl-1,3-dioxane-4,6-dione, DMAP, EDC*HCl, CH_2Cl_2, -10 °C to rt, o/n; (h) EtOAc, reflux, 1 h; (i) Ph_3P, MeOH, DEAD, THF, rt, o/n (90%, 4 steps); (j) TFA/CH_2Cl_2 (1:1), rt, 3 h; (k) Boc-Leu-OH, HOBt, HBTU, DIEA, CH_3CN, 0 °C to rt, o/n (85%, 2 steps); (l) TFA/CH_2Cl_2 (1:1), rt, 2 h; (m) Boc-Leu-OH, HOBt, HBTU, DIEA, CH_3CN, 0 °C to rt, o/n (99%, 2 steps); (n) $SOCl_2$ (2 M in CH_2Cl_2), MeOH, 0 °C to rt, o/n; (o) Boc-*N*MeIle-OH, DMAP, DCC, CH_2Cl_2, 0 °C to rt, o/n (55%, 2 steps); (p) TFA/CH_2Cl_2, rt, 2 h; (q) CH_3I, DIEA, DMF, rt, 2 h (38%, 2 steps); (r) propargyl bromide (80% wt in toluene), DIEA, CH_3CN, 80 °C, o/n (63%, 2 steps); (s) LiOH, THF/MeOH/H_2O (1.67:1:0.67), rt, 5 h; (t) TFA/CH_2Cl_2 (1:1), rt, 2 h; (u) HOBt, HBTU, DIEA, CH_3CN, 0 °C to rt, 5 h (91% after silica gel chromatography, 51% after additional HPLC, 3 steps); (v) HOBt, HBTU, DIEA, CH_3CN, 0 °C to rt, o/n (39% after HPLC, 3 steps); (w) HOBt, HBTU, DIEA, CH_3CN, 0 °C to rt, o/n (82% after silica gel chromatography, 64% after additional HPLC, 3 steps); (x) HOBt, HBTU, DIEA, CH_3CN, 0 °C to rt, 5 h (73% after silica gel chromatography, 53% after additional HPLC, 3 steps).

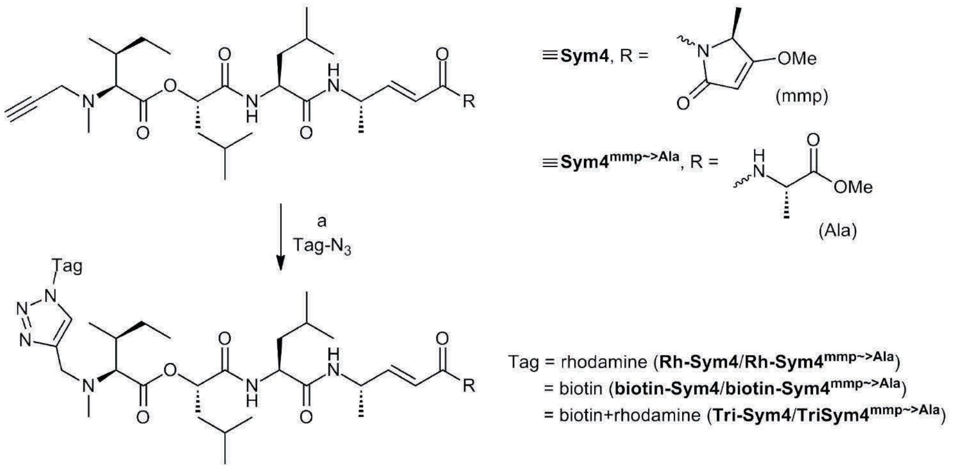
≡Sym4, R =
OMe
(mmp)
≡Sym4mmp~>Ala, R =
OMe
(Ala)
a
Tag-N3
Tag = rhodamine (Rh-Sym4/Rh-Sym4mmp~>Ala)
= biotin (biotin-Sym4/biotin-Sym4mmp~>Ala)
= biotin+rhodamine (Tri-Sym4/TriSym4mmp~>Ala)

Figure 86: Synthesis of the differently modified probes for ABPP. Reagents and conditions: (b) Tag-N_3, $CuSO_4$ (aq. solution), TBTA (100 mM in DMSO), TCEP (100 mM in H_2O), H_2O, rt, reaction monitoring by LC-MS, chromatographic work-up.

During a placement in the group of Dr. Renier van der Hoorn (MPI for Plant Breeding research, Cologne), symplostatin 4 and its derivatives were investigated for their labeling of the *Arabidopsis thaliana* proteome. In preliminary labeling experiments the optimal conditions for the *in vivo* labeling were established; additionally, some *in vivo* infiltration experiments were carried out, yet without remarkable results.

The target identification for **Sym4** and **Sym4**$^{\mathbf{mmp \rightarrow Ala}}$ was then carried out by Dr. Farnusch Kaschani, who was able to identify the papain-like cysteine proteases RD21A and RD21B as the major targets of **Sym4** and **Sym4**$^{\mathbf{mmp \rightarrow Ala}}$ in *A. thaliana* by *in vivo* labeling of *A. thaliana* cells. RD21 has been assigned a role in the plant immune system.[150] Of note, a difference in the labeling pattern of **Sym4** and **Sym4**$^{\mathbf{mmp \rightarrow Ala}}$ was not observed in these experiments (Fig. 87).

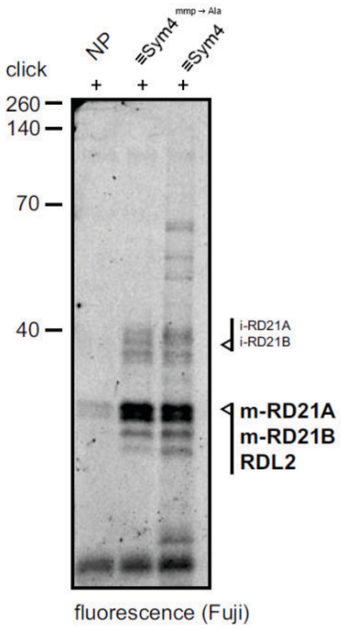

Figure 87: Fluorescence scan of the SDS-PAGE-resolved enzymes labeled *in vivo* by **≡Sym4** and **≡Sym4**$^{\mathbf{mmp\rightarrow Ala}}$. The labeling was carried out *in vivo*, followed by an *in vitro* click reaction with Tri-N_3 and affinity purification of the labeled enzymes on agarose gel. After the resolution of the labeled enzymes, the individual protein bands were excised from the gel, digested with trypsin and analyzed by nanoLC-MS/MS. (work by F. Kaschani)

Having successfully identified papain-like cysteine proteases as the targets of symplostatin 4 in plant cells, the investigation of the antimalarial effect of symplostatin 4[104] was initiated under the hypothesis that the antimalarial activity might stem from an inhibition of the parasital falcipains. This project was carried out in collaboration with the group of Prof. Dr. Matthew Bogyo (Department of Pathology, Stanford University, CA); all experiments were carried out by Dr. Edgar Deu Sandoval.

In a first, cell-based assay the effect of **Sym4** and **Sym4**$^{\mathbf{mmp\rightarrow Ala}}$ on malaria parasites in the erythrocytic cycle became apparent: cells treated with 0.1 μM **Sym4** showed a distinct swollen food vacuole phenotype which is related to a disturbance of the proteases involved in the early stage hemoglobin digestion.[50,53,151] In contrast to this, the cells had to be treated with a 100-fold higher concentration of **Sym4**$^{\mathbf{mmp\rightarrow Ala}}$ to observe the same effect, indicating a clear difference between the two analogs that might stem from either a decreased uptake of **Sym4**$^{\mathbf{mmp\rightarrow Ala}}$ or a less specific binding to the target enzyme(s) (Fig. 88, **A**). Importantly, at no applied concentration, a lysis of the red blood cells could be observed.

After having studied the direct phenotypic effect of symplostatin 4 on the living parasite, the overall effect on parasite replication was investigated. This allows to evaluate if the effect observed at an early stage of the parasite life cycle has an influence on the total development and replication (*i. e.* the progression of the disease). Hence, cell cultures at 2% parasitemia were treated with different concentrations of the inhibitors for 75 h and after this time, the parasitemia was determined by flow cytometry (Fig. 88, **B**).[152] Again, a clear difference between **Sym4** and its analog **Sym4**$^{\mathbf{mmp\rightarrow Ala}}$ became apparent, thereby confirming the results of the previous phenotype assay.

Since the results from the cell-based assays already indicated strongly that one or more of the parasite's food vacuole cysteine proteases, *i. e.* falcipain 2, falcipain 2′ and falcipain 3 (FP-2, FP-2′, FP-3)[50] as the targets of **Sym4**, a focus was set on verifying this hypothesis by activity-based profiling experiments. Firstly, **Rh-Sym4** and **Rh-Sym4**$^{\mathbf{mmp\rightarrow Ala}}$ were tested for their labeling of intact parasites. Indeed, two strong bands in the 28 kDa region appeared for **Rh-Sym4**, while for **Rh-Sym4**$^{\mathbf{mmp\rightarrow Ala}}$ only a very weak labeling in this region could be detected. The bands were sensitive to a pre-incubation with **Sym4** and **≡Sym4**, indicating that the labeling is not an artifact caused by the rhodamine tag (Fig. 88, **C**). This labeling in the 28 kDa region was already a strong indicator for the inhibition of FP-2, FP-2′ and FP-3 (referred to as FP-2/3) that are known to migrate in the 28 kDa region.[153,154] A competitive ABPP experiment with Cy5-labeled DCG-04 and the probes **Sym4** and **Sym4**$^{\mathbf{mmp\rightarrow Ala}}$ was therefore carried out to test if **Sym4** and **Sym4**$^{\mathbf{mmp\rightarrow Ala}}$ indeed labeled FP-2/3.

Sym4 was revealed to be a nanomolar inhibitor (1.5 nM) of FP-2/3; in addition, FP-1 was also inhibited at higher concentrations (1.6 μM). The aminopeptidase DPAP-1 was not inhibited (Fig. 88, **D**). **Sym4**$^{\mathbf{mmp\rightarrow Ala}}$ on the other hand inhibited FP-2/3 only weakly (25 μM); an inhibition of FP-1 or DPAP-1 could not be detected at all.

For the potent FP-2/3 inhibitor **Sym4** the parameters of inhibition were then further investigated. A substrate turnover experiment with recombinant FP-2 and FP-3 revealed that **Sym4** is an irreversible inhibitor of FP-2 and FP-3 and that it is approximately 10-fold more potent against FP-2 than it is against FP-3. In summary, the assays revealed **Sym4** as one of the most potent FP-2/3 inhibitors reported to date.[155] The determination of the IC$_{50}$ values for the different PLCPs revealed that **Sym4** preferentially inhibits FP-2 over FP-3 and FP-1. Indeed, all falcipains are inhibited in the sub-micromolar range (Fig. 88, **E**). A summary of all biological activities of **Sym4** and **Sym4**$^{\mathbf{mmp\rightarrow Ala}}$ is presented in Table 6.

Table 6: Summarized antimalarial activities of **Sym4** and **Sym4$^{mmp\rightarrow Ala}$**.

	Sym4	**Sym4$^{mmp\rightarrow Ala}$**
food vacuole defect observed at	0.1 µM	10 µM
EC_{50} (from replication assay)	0.7 ± 0.2 µM	27 ± 7 µM
labeling of FP-2/3 in intact parasites at 10 µM	strong	weak
FP-2/3 inhibition starting from (comp. assay)	1.5 nM	25 µM
FP-1 inhibition starting from (comp. assay)	1.6 µM	not observed
k_i(FP-2) / $M^{-1}s^{-1}$	58600 ± 1400	not determined
k_i(FP-2) / $M^{-1}s^{-1}$	7030 ± 250	not determined
IC_{50}(FP-2)	8.5 ± 1.3 nM	not determined
IC_{50}(FP-3)	22 ± 8 nM	not determined
IC_{50}(FP-1)	140 ± 23 nM	not determined

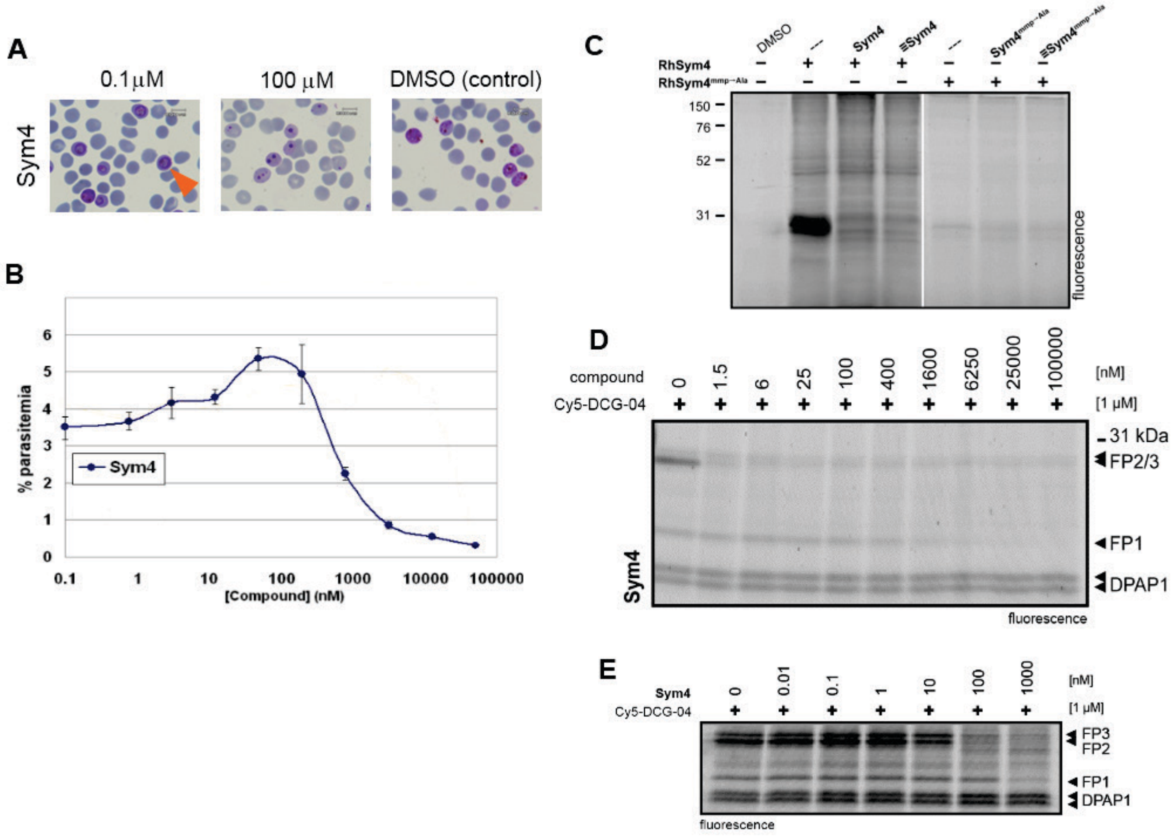

Figure 88: Summarized results of the investigation of the antimalarial activity of **Sym4**. **A**: food vacuole phenotype caused by **Sym4** treatment of *P. falciparum* D10 at ring stage; **B**: effect of **Sym4** treatment on replication of *P. falciparum*; **C-E**: ABPP experiments with **Sym4** and ABPP analogs: labeling of intact parasite cells (**C**), competitive ABPP with Cy5-DCG-04 (**D**), competitive ABPP with Cy5-DCG-04 in order to determine IC_{50} values (**E**). (work by E. Sandoval)

In summary, the overall antimalarial activity of **Sym4** most likely results from a combined inhibition of FP-2 and FP-3 (and to a lesser extent FP-1). The food vacuole defect observed at an early stage of the parasital development is most likely caused by the inhibition of FP-2; the decreased replication (*i. e.* killing of the parasite) is in contrast most likely caused by the inhibition of FP-3 that has been demonstrated to be the determining factor for parasite survival.[52]

In conclusion, the natural product symplostatin 4 has been studied in two different organisms. The targets of symplostatin 4 in *A. thaliana* have been identified to be the PLCPs RD21A and RD21B. For the labeling in the model plant, no difference in the labeling pattern between **Sym4** and its analog lacking the putatively important mmp unit was observed.

The antimalarial activity of symplostatin 4 was studied extensively, revealing **Sym4** to be a highly potent inhibitor of the plasmodial falcipains. Here, a significant difference between **Sym4** and **Sym4**$^{\mathbf{mmp \rightarrow Ala}}$ was observed. **Sym4** may in the future serve as a lead structure for the development of new antimalarial drugs inhibiting the parasite's falcipains; the different ABPP probes may furthermore be used for labeling experiments and investigation of different proteomes.

5 Zusammenfassung und Ausblick

Im Rahmen dieser Dissertation wurden zwei unterschiedliche Naturstoffe, die als Proteaseinhibitoren wirken, sowie Analoga, die von diesen Naturstoffen abgeleitet wurden untersucht. Naturstoffe können aufgrund ihrer häufig vorhandenen Bioaktivität als privilegierte Strukturen betrachtet werden, die sich im Zuge der Evolution entwickelt haben. Deswegen können Naturstoffe als vor-validierte Substanzen angesehen werden, die bei der Suche nach neuen Wirkstoffen als wertvolle Leitstrukturen dienen können.[1,3] Die Untersuchung von Synthesewegen zur chemischen Darstellung von Naturstoffen als auch die Aufklärung der molekularen Basis ihrer Bioaktivität stellen somit interessante Fragestellungen dar, die im Themengebiet der Chemischen Biologie behandelt werden.

5.1 Entwicklung einer allgemeinen Festphasen-Synthese von Ahp-Cyclodepsipeptiden und Synthese von Symplocamide A

Die Naturstoffklasse der Ahp-Cyclodepsipeptide ist für ihre spezifische und bemerkenswerte nicht-kovalente Inhibierung der S1 Serinproteasen bekannt; dementsprechend wurden sie auch als wichtige Leitstruktur für die Entwicklung von Serinprotease-Inhibitoren z. B. zur Anwendung in der Wirkstoffforschung erkannt.[25]

Zu Beginn dieser Dissertation waren lediglich zwei aufwändige und spezialisierte Lösungssynthesen von Ahp-Cyclodepsipeptiden bekannt[100-102], so dass die erste Aufgabe die Entwicklung eines flexibleren Synthesewegs für Ahp-Cyclodepsipeptide war. So sollte ein Zugang zu maßgeschneiderten Ahp-Cyclodepsipeptiden erhalten werden, um z. B. den Inhibitionsmodus besser im Detail studieren zu können. Verwirklicht wurde dieser Ansatz durch die Entwicklung einer Festphasensynthese-Strategie für die Ahp-Cyclodepsipeptide. Um diese Strategie zu verwirklichen, wurde dabei eine Ahp-„Vorstufe“ entwickelt, welche sowohl als Anker in der Festphasensynthese diente als auch zum geeigneten Zeitpunkt in einen Glutaminsäurealdehyd (als Vorstufe der Ahp-Gruppe) umgewandelt werden konnte. Erst die Entwicklung dieses Bausteins machte eine flexible Festphasensynthese von Ahp-Cyclodepsipeptiden möglich (Abb. 89).

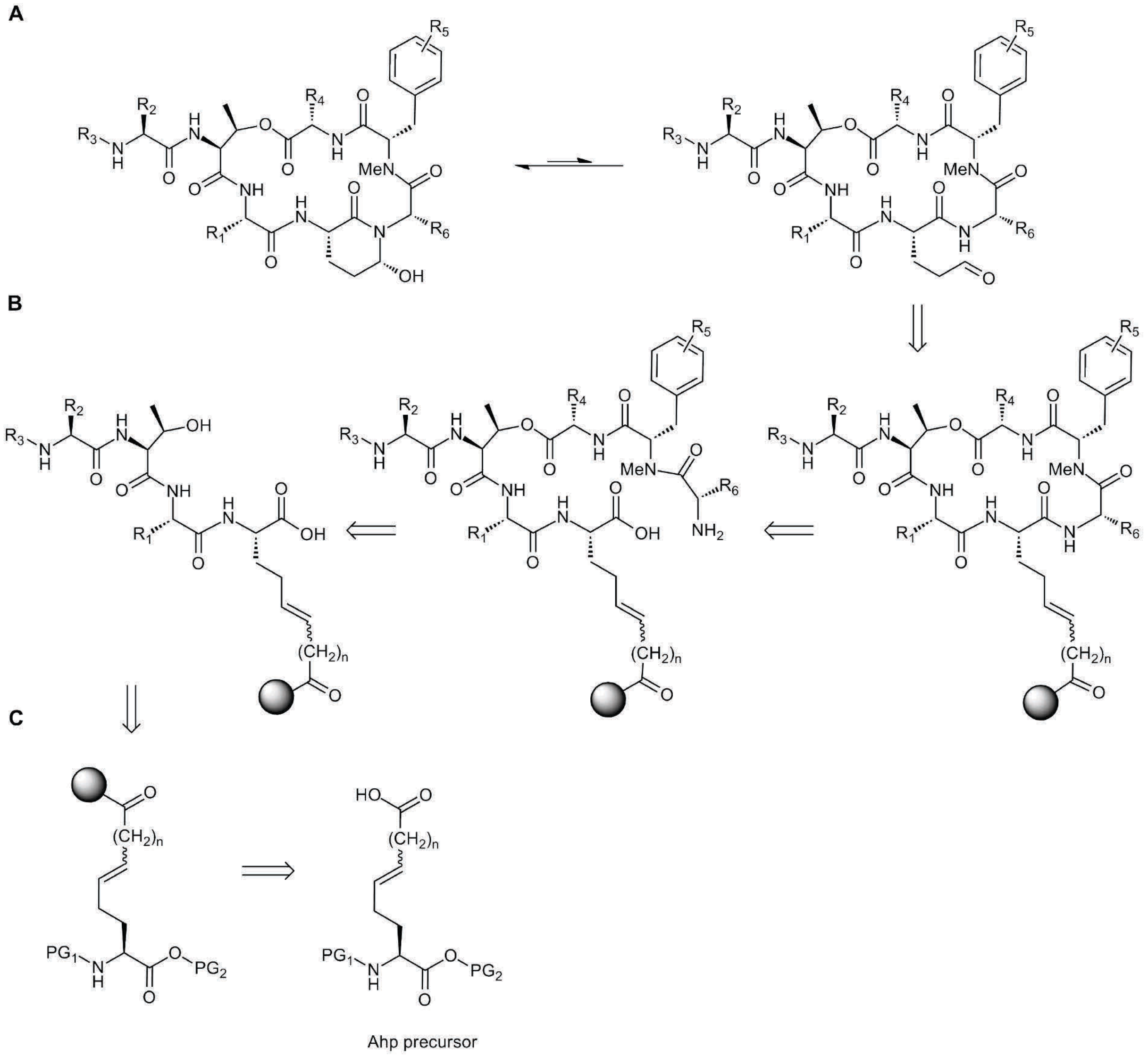

Abbildung 89: Retrosynthese der Ahp-Cyclodepsipeptide. **A**: Die Ahp-Hemiaminalstruktur bildet sich bei Ahp-Cyclodepsipeptiden spontan aus einer Aldehyd-Vorstufe. **B**: Der Aldehyd wird durch die oxidative Abspaltung eines maskierten Glutaminsäurealdehyds erzeugt. Die Cyclisierung erfolgt an der festen Phase als Macrolaktamisierung; die Veresterung der Threoninseitenkette ist einer der grundlegenden Schritte der Depsipeptidsynthese. **C**: Die Festphasensynthese geht von einer geeigneten Ahp-Vorstufe aus, die über eine Säurefunktion am Harz verankert ist.

Die Entwicklung einer geeigneten Ahp-Vorstufe stellte sich als eine anspruchsvollere Aufgabe dar, als der erste Anschein vermuten ließ. Die letztendlich verwendete Ahp-Vorstufe wurde erst nach einer langen Entwicklungsarbeit erhalten und stellt das Resultat mühevoller Studien und häufiger Änderungen in der Syntheseplanung dar.

Das Herzstück der Synthesestrategie ist die, im Rahmen der Ahp-Vorstufe, hier neu-entwickelte Abspaltungsmethode, bei welcher ein Glutaminsäurealdehyd über einen Dihydroxylierungs- und anschließenden Glykolspaltungsprozess erzeugt wird. Das Protokoll basiert dabei auf den vorhergehenden Arbeiten von Meldal *et. al.*,[106-108] als

Abspaltungmethode zur Generierung eines Aldehyds bei der Abspaltung wurde diese Reaktionssequenz hier jedoch zum ersten Mal eingesetzt und stellt somit eine Ergänzung zum Repertoire der Abspaltmethoden von der festen Phase dar. Um diese neuartige Abspaltmethode jedoch verwenden zu können, musste das für die Festphasen-Synthese verwendete Harz angepasst werden. Statt eines gebräuchlichen Polystyrol-Harzes, das sich unter den Abspaltbedingungen als nicht stabil erwiesen hatte, wurde bei dieser Methode ein Polyethylenglycol-Harz verwendet.

Mithilfe der neuentwickelten Methodik konnte schließlich der Naturstoff Symplocamide A erfolgreich an der festen Phase synthetisiert werden (Abb. 90). Die analytischen Daten, die dabei für das synthetische Symplocamide A aufgenommen wurden, stimmten dabei sehr gut mit den Daten für den Naturstoff publizierten Werten überein.[24]

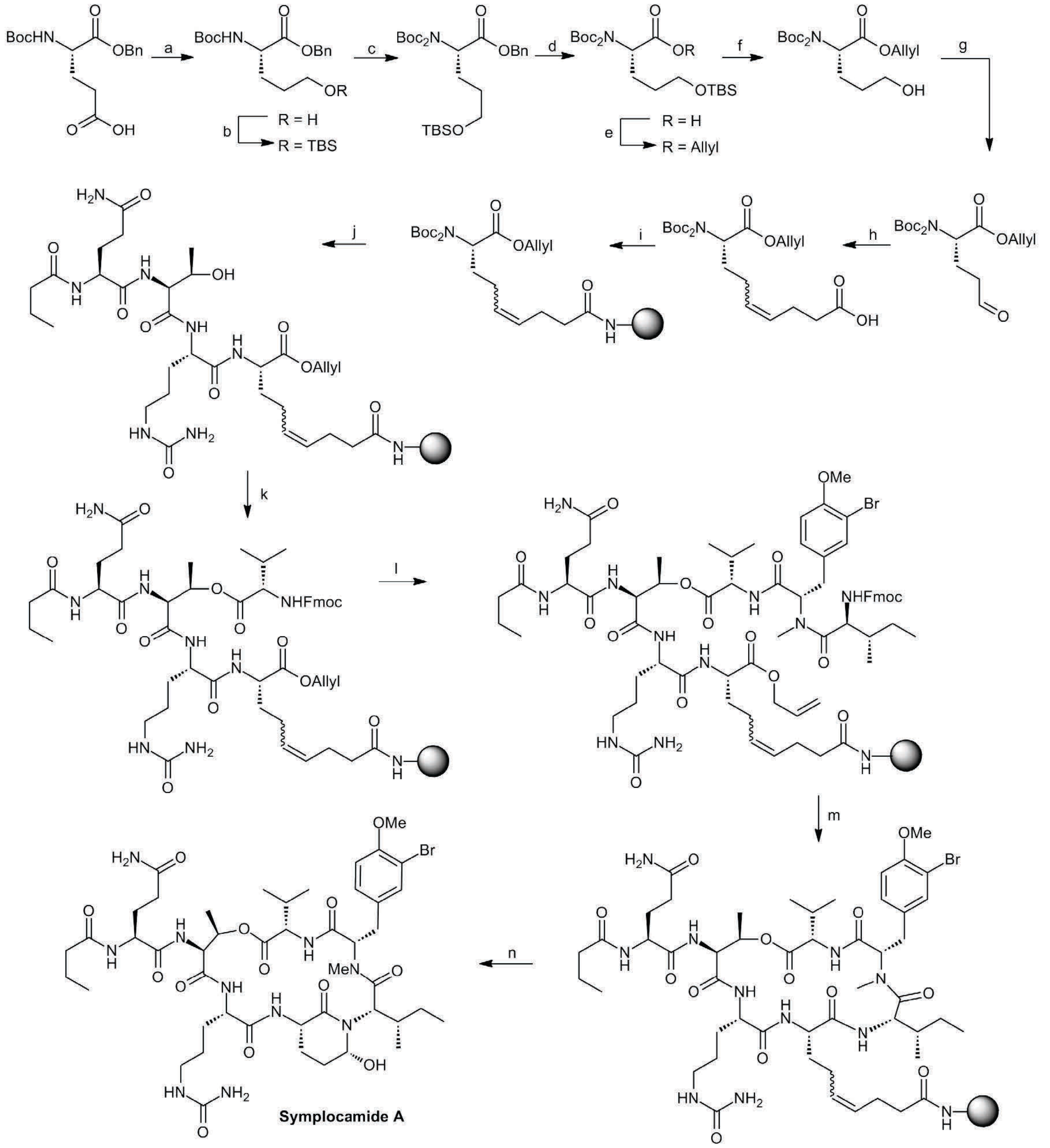

Abbildung 90: Totalsynthese von Symplocamide A.[115,118] Reagenzien und Reaktionsbedingungen: (a) i. EtOCOCl, Et_3N, THF, -15 °C, 1 h, ii. $NaBH_4$, THF/H_2O (1:1), -15 °C, 1 h, dann RT, 6 h (84%); (b) TBDMSCl, Imidazol, CH_2Cl_2, 0 °C-RT, ü/N (95%); (c) Boc_2O, DMAP, CH_3CN, RT, 24 h (81%, b.r.s.m.); (d) 10% Pd/C, H_2, EtOAc, RT, 2.5 h (99%); (e) i. Cs_2CO_3, MeOH; ii. Allylbromid, DMF, RT, ü/N (95%); (f) $CuCl_2*2H_2O$, Aceton/H_2O (95:5), Rückfluss, 1 h (92%); (g) Dess-Martin-Periodinan, CH_2Cl_2, RT, 1 h (84%); (h) i. $Ph_3P^+(CH_2)_3CO_2H\ Br^-$, LHMDS,THF, 0 °C, 55 min; ii. **15**, THF, 0 °C-RT, ü/N (64%). (i) i. Amino NovaPEG resin, HOBt, HBTU, DIEA, CH_2Cl_2/DMF (9:1); ii. CH_2Cl_2/DIEA/Ac_2O (3:1:1); iii. CH_2Cl_2/DIEA/Ac_2O (3:1:1), 3h; (j) i. TFA/CH_2Cl_2 (1:1); ii. Et_3N/CH_2Cl_2 (1:9); iii. Fmoc-Cit-OH, HOBt, HBTU, DIEA, DMF, 5h (30%, laut Fmoc-Bestimmung, 2 Stufen); iv. Piperidin/DMF (1:4); v. Fmoc-Thr-OH, HOBt, HBTU, DIEA, DMF, 2h; vi. Piperidin/DMF (1:4); vii. Fmoc-Gln(Trt)-OH, HOBt, HBTU, DIEA, DMF, 2h (88% laut Fmoc-Bestimmung, 2 Kupplungen); viii. Piperidin/DMF (1:4); ix. Buttersäure, HOBt, HBTU, DIEA, DMF, 2h; (k) Fmoc-Val-OH, DCC, DMAP, CH_2Cl_2/DMF (9:1); 79% laut Fmoc-Bestimmung, 2 Kupplungen); (l) i. Piperidin/DMF (1:4); ii. Fmoc-*N*MePhe-OH, HOBt, HBTU, DIEA, DMF, 2h; iii. Piperidin/DMF (1:4); iv. Fmoc-Ile-OH, PyBrOP, DIEA, DMF, 24h (60%, laut Fmoc-Bestimmung, 2 Kupplungen); (m) i. Piperidin/DMF (1:4); ii. $Pd(PPh_3)_4$, Morpholin, CH_2Cl_2; iii. PyBOP, HOBt, DIEA, DMF; (n) OsO_4, $NaIO_4$, DABCO, *t*-BuOH, THF/H_2O (3% Gesamtausbeute).

Neben den spektroskopischen Daten wurde auch die biologische Aktivität des synthetischen Symplocamide A validiert. In einem Inhibitionassay mit Chymotrypsin stellte sich die synthetische Substanz (K_i = 0.32 ± 0.09 μM) als ebenso potent wie der Naturstoff heraus (lit.[24], IC_{50} = 0.38 ± 0.08 μM). Die in der Originalpublikation festgestellte Zytotoxizität gegenüber zwei Krebszelllinien, sowie eine mögliche Inhibierung des Proteasoms durch Symplocamide A konnten jedoch in den, im Rahmen der Dissertation, verwendeten Testsystemen nicht festgestellt werden.

5.2 Synthese und biologische Evaluierung von „Small-molecule"-Analoga proteinogener Serinproteaseinhibitoren mit kanonischer Konformation

Trotz der bekannten Serinproteasehemmeigenschaften der Ahp-Cyclodepsipeptide wurde erst unlängst erkannt, dass auch diese Substanzen als Inhibitoren mit einer kanonischen Konformation wirken.[18] Sie werden somit zur Klasse der „Small-molecule"-Analoga proteinogener Serinproteaseinhibitoren gezählt. Dabei ist die kritische Rolle der Ahp-Einheit in der Stabilisierung der kanonischen Konformation bereits ausführlich untersucht worden. Dies führte zur Frage, ob diese Einheit jedoch durch eine andere Funktionalität unter Beibehaltung der Bioaktivität ersetzt werden kann. Dies ist insbesondere daher von Interesse, da im Verlauf der Dissertation klar wurde, dass mit der neu entwickelten Synthesestrategie zwar die Synthese maßgeschneiderter Ahp-Cyclodepsipeptide möglich ist, diese jedoch immer mehrstufige Synthesen einzelner Bausteine und eine sorgsame Festphasensynthese benötigen. Deshalb wurde nach einer Möglichkeit gesucht, die Ahp-Einheit durch eine besser zugängliche, d. h. im besten Fall kommerziell erhältliche, Aminosäuren zu ersetzen. Im Anschluss an eine erfolgreiche Substitution der Ahp-Einheit sollten dann die kritischen Elemente für die Einnahme der kanonischen Konformation in diesen Ahp-Analoga untersucht werden.

Für eine möglichst schnelle und flexible Synthese der geplanten Ahp-Analoga wurde eine neue Festphasensynthese entwickelt, die einen Teil der Methodik der vorangegangenen Synthese von Symplocamide A aufgreift. Als Anker an die feste Phase wurde die P_1-Aminosäure gewählt, da diese die Spezifität eines Inhibitors bestimmt und in einem kombinatorischen Ansatz viele Varianten eines Inhibitors zugänglich sind (Abb. 91).

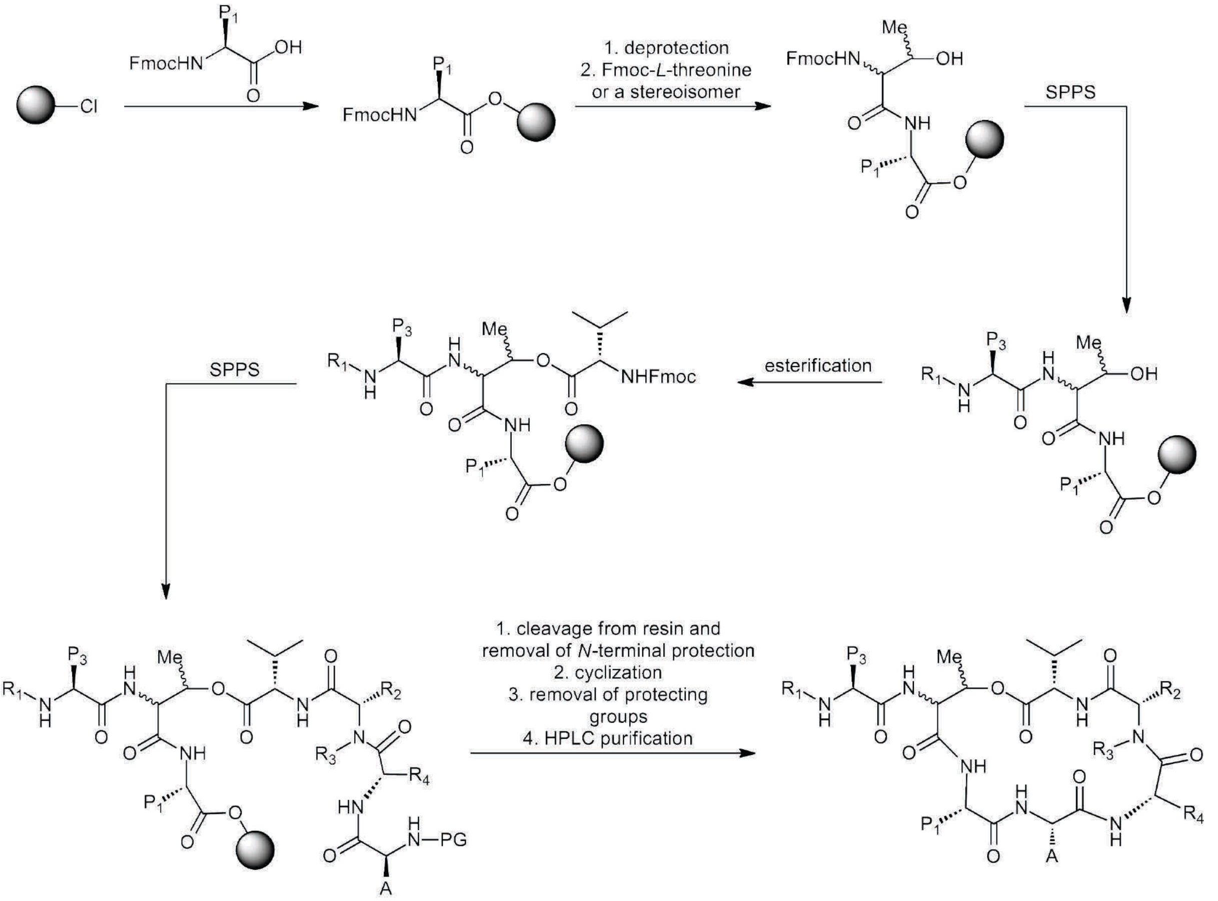
1. deprotection
2. Fmoc-*L*-threonine
or a stereoisomer
SPPS
esterification
SPPS
1. cleavage from resin and
removal of *N*-terminal protection
2. cyclization
3. removal of protecting
groups
4. HPLC purification

Abbildung 91: Allgemeine Festphasen-Synthese zur Herstellung von Struktur-Wirkungsanaloga von Ahp-Cyclodepsipeptiden. Die Reste R und P sind in Tabelle 7 zusammengefasst.

Mit einem ersten Satz von Symplocamide A-Analoga konnte dann zunächst der Beweis erbracht werden, dass die Ahp-Einheit durch die - ebenfalls hydroxylierte - Aminosäure Serin ersetzt werden kann. Zwei weitere Analoga, die die Aminosäuren Threonin und Homoserin enthielten, waren hingegen inaktiv im Inhibitionsassay.

Die Substitution der Ahp-Einheit durch Serin ermöglichte dann die Untersuchung der Elemente, die zur Einnahme einer kanonischen Konformation essentiell sind. Die verschiedenen Analoga, mit denen diese Struktur-Wirkungsbeziehungen untersucht wurden sind in Tabelle 7 zusammengefasst.

Tabelle 7: Struktur-Wirkungsanaloga zur Auffindung der essentiellen Strukturelemente in der kanonischen Konformation.

Substanz (abgeleitet von)	Ahp-Substitution	weitere Substitutionen	K_i
SAR-1 (Sym A)	Ser	-	3.8 µM
SAR-2 (Sym A)	Hse	-	inaktiv
SAR-3 (Sym A)	Thr	-	inaktiv
SAR-4 (Sym A)	Ser	3-Br,4-OMe-mTyr→4-OMe-mTyr	4.8 µM
SAR-5 (Sym A)	Ser	3-Br,4-OMe-mTyr→mPhe	56.1 µM
SAR-6 (Sym A)	Ser	3-Br,4-OMe-mTyr→mPhe	inaktiv
SAR-7 (Sym A)	Ser	3-Br,4-OMe-mTyr→Pro	16.1 µM
SAR-8 (Sym A)	Ser	3-Br,4-OMe-mTyr→mPhe *L*-Thr→*D*-*allo*-Thr	inaktiv
SAR-9 (Sym A)	Ser	3-Br,4-OMe-mTyr→mPhe *L*-Thr→*L*-*allo*-Thr	inaktiv
SAR-10 (Scyp A)	Ser	-	19.1 µM
SAR-11 (Scyp A)	Thr	-	5.0 µM
SAR-12 (Scyp A)	Val	-	inaktiv

Wie bereits aufgrund der umfangreichen Arbeiten von Leatherbarrow *et. al.*[3] vermutet worden war, spielt insbesondere die Aminosäure in der P_3‘-Position, welche eine *cis*-Amidbindung eingehen muss, eine wichtige Rolle für die Einnahme der kanonischen Konformation. Bei Ahp-Cyclodepsipeptiden ist an dieser Stelle eine konservierte *N*-methylierte aromatische Aminosäure zu finden[24], im Falle der von Leatherbarrow untersuchen Bowman-Birk-artigen Inhibitoren findet sich hier ein konserviertes Prolin.[23]

Für die hier untersuchen Ahp-Analoga wurde eine deutliche Präferenz für methylierte Tyrosine gegenüber einem Prolin und einem, in seiner Aktivität drastisch herabgesetzten, *N*-Methylphenylalaninderivat festgestellt. Die Substitutionsfähigkeit der konservierten *N*-methylierten Aminosäure durch ein Prolin verifiziert dabei, dass es sich bei den hier hergestellten Analoga von Ahp-Cyclodepsipeptiden tatsächlich um Inhibitoren mit kanonischer Konformation handelt, da diese Konformation durch eine *cis*-Amidbindung in der P_3‘-Position erzwungen wird.

Ein weiteres Strukturelement, dem eine Rolle bei der Inhibition von Serinproteasen zugeschrieben wird, ist der Threoninrest in P_2-Position, mit dessen Seitenkette die Depsipeptidbindung zum P_4‘-Valin hergestellt wird. In den von Leatherbarrow untersuchen BBI-Inhibitoren bildet ein Threonin in der P_2-Position eine Wasserstoffbrücke mit dem Serin in der P_1’-Position aus, wodurch der aliphatische Teil der Threoninseitenkette so dirigiert wird, dass er in einem engen Kontakt mit dem Imidazolrest des Histidins der katalytischen Triade steht. Dieser Kontakt steht im Verdacht, eine Bewegung des Imidazolrestes, die im Zuge des Katalysezyklus notwendig wird, zu blockieren und damit zur Inhibition beizutragen.[18]

Eine ähnliche Dirigierung des aliphatischen Teils der Threoninseitenkette wäre auch für die Ahp-Cyclodepsipeptide denkbar, da die Seitenkette durch die Esterbindung fixiert ist und die Orientierung der Methylgruppe durch die Stereochemie der Aminosäure festgelegt wird.

Tatsächlich waren die im Hinblick auf diese Hypothese hergestellten Analoga, in denen das natürliche (*L*)-Threonin durch (*D*)-*allo*- oder (*L*)-*allo*-Threonin ersetzt wurde, im anschließenden Enzymassay inaktiv. Es muss jedoch beachtet werden, dass die Notwendigkeit einer Bewegung des Histidins während der Katalyse immer noch höchst kontrovers diskutiert wird. Die hier gewonnenen Erkenntnisse stellen nichtsdestotrotz einen bescheidenen Beitrag zu dieser Debatte dar und geben zumindest einen Hinweis darauf, dass eine Blockierung des Histidins einen Einfluss auf die Prozessierung eines Substrats haben könnte und somit zur Inhibition beiträgt. Andererseits könnte der Verlust der Aktivität auch das Resultat einer veränderten Gesamtkonformation des Makrozyklus sein.

Um abschließend zu zeigen, dass der Ersatz der Ahp-Einheit in einem Ahp-Cyclodepsipeptid nicht nur bei den bisher studierten Chymotrypsin-Inhibitoren funktioniert, sondern ein globaleres Konzept darstellt, sollte eine weitere Protease mit der entwickelten Methodik adressiert werden. Um dies zu bewerkstelligen, wurden drei Ahp-Analoga des Naturstoffs Scyptolin A[27,28] hergestellt und im Hinblick auf die Inhibition der Zielprotease Elastase getestet. Erfreulicherweise waren zwei der drei synthetisierten Analoga in dem Enzymassay aktiv. Neben dem erwarteten Serin-Analogon war überaschenderweise auch ein Analogon aktiv, in dem Threonin als Ahp-Ersatz verwendet wurde. In der Tat zeigte dieses Derivat sogar eine stärkere Aktivität als das Serin-Analogon. Im dritten Analogon war die Ahp-Einheit durch Valin ersetzt worden; diese Substanz war jedoch inaktiv, wodurch die Notwendigkeit einer Hydroxylfunktion in der Seitenkette der P_1'-Aminosäure unterstrichen wurde. Der

Hydroxylgruppe in Ahp wird eine wichtige Rolle bei der Inhibierung zugeschrieben, da sie eine der zwei intramolekularen Wasserstoffbrücken mit dem Peptidrückgrat bildet. Diese sind zur Festigung der rigiden macrocyclischen Struktur erforderlich. Die vorliegenden Daten deuten darauf hin, dass auch bei den Ahp-Mimetika ein ähnliches System vorliegt.

Zusammenfassend wurde im Rahmen dieser Dissertation ein allgemeiner und flexibler Ansatz zur Festphasensynthese von Ahp-Cyclodepsipeptiden entwickelt. Als Beweis für die Anwendbarkeit dieser neuen Strategie wurde der Naturstoff Symplocamide A synthetisiert. Symplocamide A diente dann als Ausgangspunkt für die Synthese besser zugänglicher Analoga für die Untersuchung von Struktur-Wirkungsbeziehungen. In diesen Analoga wurde die Ahp-Einheit durch kommerziell erhältliche Aminosäuren ersetzt; die Synthese erfolgte über einen allgemeinen, kombinatorischen Festphasenansatz.

Die hydroxylierten Aminosäuren Serin und Threonin wurden zunächst als mögliche Substitutionen für die Ahp-Einheit bestimmt. Desweiteren wurden die kritischen Elemente identifiziert, die zur Einnahme der kanonischen Konformation notwendig sind und ein Einblick in den Mechanismus der Inhibition gewonnen.

Im Rahmen weitergehender Untersuchungen der Ahp-Analoga wären zusätzliche Daten sowohl zur Struktur der Mimetika als auch zum Bindungsmodus mit der Protease höchst wünschenswert. Diese könnten z. B. durch eine Komplex-Kristallstruktur eines Analogons mit seiner Zielprotease oder alternativ über eine Strukturanalyse mittels NMR-Spektroskopie erhalten werden. Diese Daten würden dazu beitragen, die ausschließlich auf Studien der Enzyminhibierung basierenden Ergebnisse auf eine breitere Grundlage zu stellen. Alle Versuche solche strukturellen Daten zu erhalten (z. B. durch Ko-Kristallisation mit Chymotrypsin oder Elastase und anschließender Röntgenstrukturanalyse) blieben bisher jedoch leider erfolglos.

Ein weiterer Aspekt, der Gegenstand weiterreichender Untersuchungen sein könnte, ist die Aufklärung der molekularen Basis der unterschiedlichen Bioaktivität Threonin und Serin-substituierter Derivate von Scyptolin A. In der Tat war bei diesen Ahp-Mimetika das Threonin-Ahp-Mimetikum aktiver als die entsprechende Serin-Variante. Eine mögliche Erklärung hierfür könnte eine eingeschränkte Rotation der Seitenkette sein (und somit Präorganisation des Inhibitors), die einen geringeren Entropieverlust bei der Bindung an das Protein bewirkt. Interessanterweise wurde bei Symplocamide A dieser Effekt jedoch nicht beobachtet, was daran liegen könnte, dass in diesem Fall die Möglichkeit einer

Wasserstoffbrückenbindung zwischen der Hydroxylgruppe in der Threoninseitenkette mit der P_1-Aminosäure Citrullin besteht, so dass die, für die Inhibition notwendige, Wasserstoffbrücke mit dem Peptidrückgrat nicht ausgebildet werden kann. Zur Unterstützung dieser Hypothese sind jedoch weitergehende Studien notwendig. Diese könnten z. B. mit weiteren Analoga, die unterschiedliche P_1-Reste oder Ahp-Substitutionen mit sterisch anspruchsvolleren Seitenketten enthalten, durchgeführt werden; andererseits könnte auch eine NMR-Struktur der Inhibitoren in Lösung und eine Aufklärung des Bindungsmodus z. B. über eine Kristallstruktur für die bereits vorliegenden Analoga die erforderlichen strukturellen Informationen liefern.

Insgesamt können die hier entwickelten „Small-molecule“-Analoga proteinogener Serinproteaseinhibitoren sicher einen Beitrag zur weitergehenden Untersuchung von Proteasen, ihrem Wirkmechanismus und ihrer Inhibition mit Methoden der Chemischen Biologie leisten. Desweiteren wäre auch ein Einsatz dieser Analoga als Leitstrukturen zum Auffinden potenter, selektiver und am wichtigsten nicht-kovalenter Wirkstoffe zur Hemmung von Proteasen denkbar.

5.3 Entwicklung einer konvergenten Synthese für Symplostatin 4 und Derivaten für die Target-Identifizierung und biologische Evaluierung

Im Rahmen eines zweiten Projekts wurde der Naturstoff Symplostatin 4 (**Sym4**)[103] untersucht. Symplostatin 4 wurde aus einem marinen Organismus isoliert und ist identisch mit dem Naturstoff Gallinamid A, der potente anti-Malaria-Eigenschaften zeigt.[104] Symplostatin 4 enthält dabei zwei interessante Strukturelemente, die es zu einem wertvollen Werkzeug für biologische Untersuchung machen können: Zum einen enthält Symplostatin 4 ein Michael-Akzeptorsystem, dass empfänglich für einen nukleophilen Angriff beispielsweise durch Cysteinproteasen ist, zum anderen ist es *C*-terminal mit einer ungewöhnlichen und seltenen Methoxy-Methylpyrrolinon-Gruppe (mmp) modifiziert. Neben der biologischen Aktivität von **Sym4** sollte auch die Rolle der mmp-Einheit mit Hilfe eines Analogons, in dem die mmp-Einheit ersetzt wurde, untersucht werden.

Um einen schnellen Zugang zu Symplostatin 4 (**Sym4**), einem Analogon ohne die mmp-Einheit (**Sym4**$^{\mathbf{mmp \rightarrow Ala}}$) und Derivaten dieser Verbindungen, die als ABPP-Sonden fungieren können, zu erhalten, wurde eine hochkonvergente, auf einer Fragmentkondensation basierende Synthese entwickelt. (Abb. 92). Um eine flexible Umwandlung von **Sym4** und **Sym4**$^{\mathbf{mmp \rightarrow Ala}}$ zu Sonden für das ABPP zu ermöglichen, wurden zusätzlich Alkin-modifizierte Varianten der beiden Moleküle generiert (**≡Sym4 u**nd **≡Sym4**$^{\mathbf{mmp \rightarrow Ala}}$), die entweder im Rahmen einer 1,3-dipolaren Huisgen-Cycloaddition (Click-Reaktion) mit einer Reportereinheit modifiziert werden können oder direkt für ein Labeling eingesetzt und im Anschluss an dieses, im Rahmen einer Click-Reaktion, modifiziert werden können. Um die größtmögliche Flexibilität zu erreichen, wurden auf diesem Wege sowohl Rhodamin-, Biotin- als auch trifunktionale Versionen beider Moleküle hergestellt (Abb. 93).

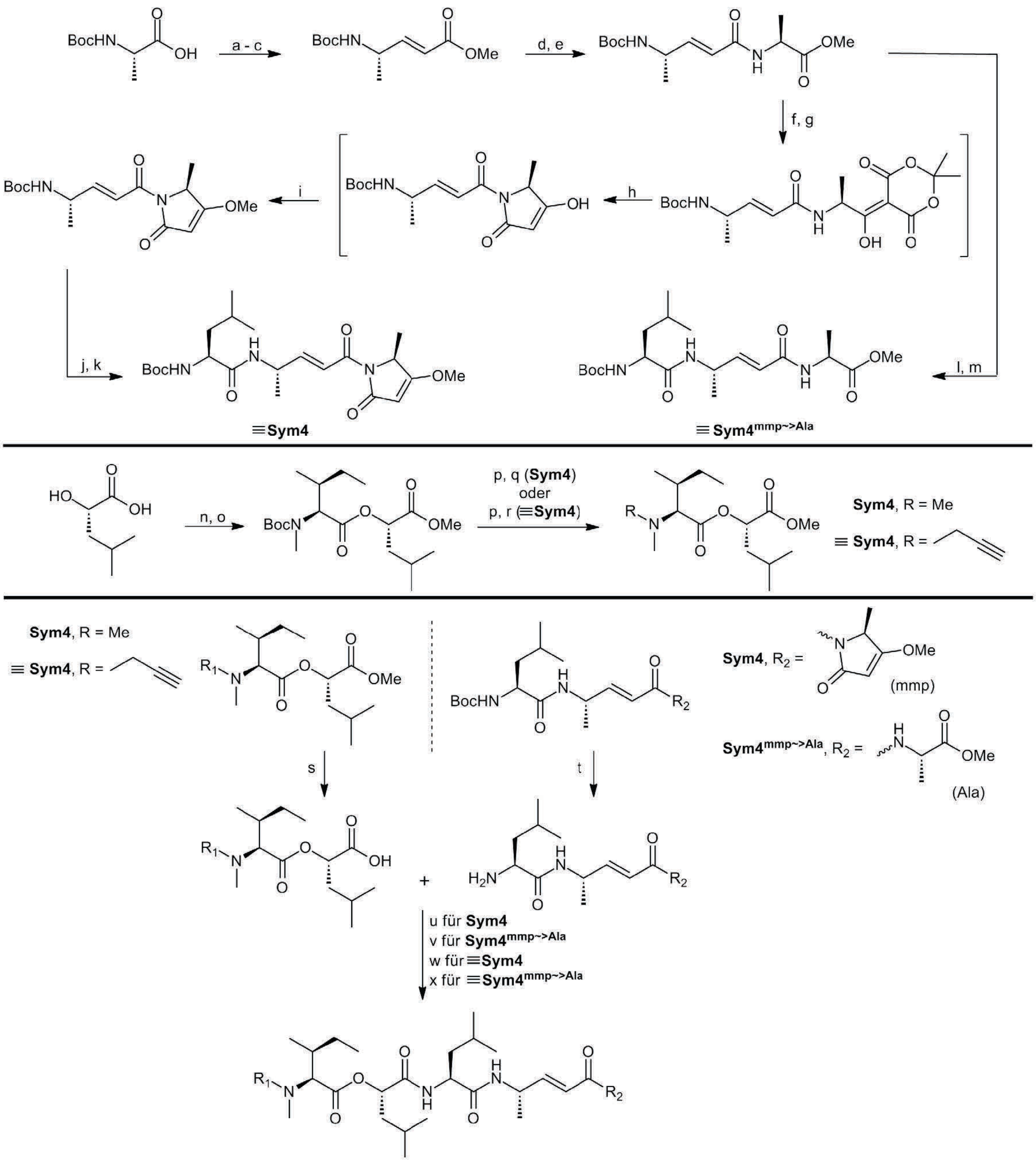
a - c
d, e
f, g
h
i
j, k
l, m
≡Sym4
≡Sym4mmp~>Ala
n, o
p, q (Sym4)
oder
p, r (≡Sym4)
Sym4, R = Me
≡ Sym4, R =
Sym4, R = Me
≡ Sym4, R =
Sym4, R2 =
(mmp)
Sym4mmp~>Ala, R2 =
(Ala)
s
t
u für Sym4
v für Sym4mmp~>Ala
w für ≡Sym4
x für ≡Sym4mmp~>Ala

Abbildung 92: Konvergente Synthese von Symplostatin 4 und Analoga. Reagenzien und Reaktionsbedingungen: (a) *N,O*-Dimethylhydroxylamin-Hydrochlorid, Et_3N, DCC, CH_2Cl_2, RT, 1 h; (b) $LiAlH_4$, Et_2O, 0 °C, 20 min; (c) $Ph_3P=CHCOOMe$, CH_2Cl_2, RT, ü/N (59%, 3 Stufen); (d) LiOH, THF/MeOH/H_2O (1.67:1:0.67), RT, 5 h; (e) H-Ala-OMe, HOBt, HBTU, DIEA, CH_3CN, 0 °C-RT, ü/N (46%, 2 Stufen); (f) LiOH, THF/MeOH/H_2O (1.67:1:0.67), RT, 5 h; (g) 2,2-Dimethyl-1,3-dioxan-4,6-dion, DMAP, EDC*HCl, CH_2Cl_2, -10 °C-RT, ü/N; (h) EtOAc, Rückfluss, 1 h; (i) Ph_3P, MeOH, DEAD, THF, RT, ü/N (90%, 4 Stufen); (j) TFA/CH_2Cl_2 (1:1), RT, 3 h; (k) Boc-Leu-OH, HOBt, HBTU, DIEA, CH_3CN, 0 °C-RT, ü/N (85%, 2 Stufen); (l) TFA/CH_2Cl_2 (1:1), RT, 2 h; (m) Boc-Leu-OH, HOBt, HBTU, DIEA, CH_3CN, 0 °C-RT, ü/N (99%, 2 Stufen); (n) $SOCl_2$ (2 M in CH_2Cl_2), MeOH, 0 °C-RT, ü/N; (o) Boc-*N*MeIle-OH, DMAP, DCC, CH_2Cl_2, 0 °C-RT, ü/N (55%, 2 Stufen); (p) TFA/CH_2Cl_2, RT, 2 h; (q) CH_3I, DIEA, DMF, RT, 2 h (38%, 2 Stufen); (r) Propargylbromid (80 Gew% in Toluol), DIEA, CH_3CN, 80 °C, ü/N (63%, 2 Stufen); (s) LiOH, THF/MeOH/H_2O (1.67:1:0.67), RT, 5 h; (t) TFA/CH_2Cl_2 (1:1), RT, 2 h; (u) HOBt, HBTU, DIEA, CH_3CN, 0 °C-RT, 5 h (91% nach Kieselgelchromatographie, 51% nach zusätzlicher HPLC, 3 Stufen); (v) HOBt, HBTU, DIEA, CH_3CN, 0 °C-RT, ü/N (39% nach HPLC, 3 Stufen); (w) HOBt, HBTU, DIEA, CH_3CN, 0 °C-RT, ü/N (82% nach Kieselgelchromatographie, 64% nach zusätzlicher HPLC, 3 Stufen); (x) HOBt, HBTU, DIEA, CH_3CN, 0 °C-RT, 5 h (73% nach Kieselgelchromatographie, 53% nach zusätzlicher HPLC, 3 Stufen).

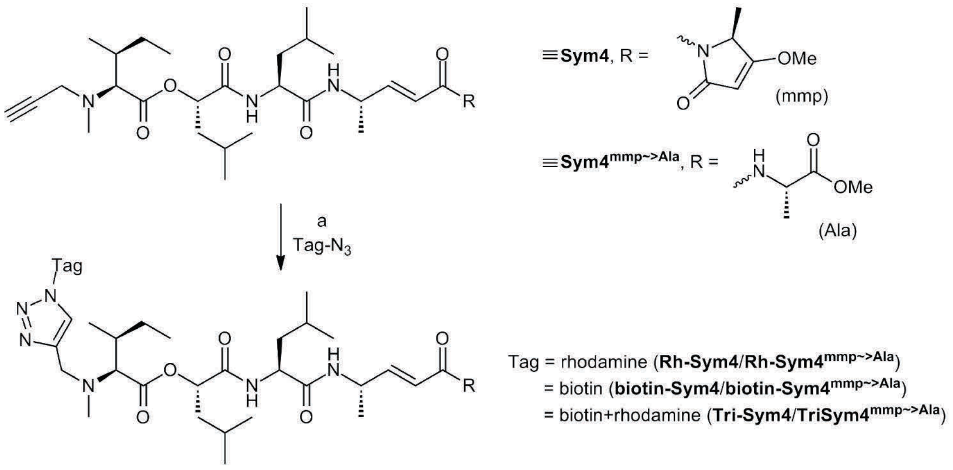
≡Sym4, R =
OMe
(mmp)
≡Sym4mmp~>Ala, R =
OMe
(Ala)
a
Tag-N3
Tag
R
Tag = rhodamine (Rh-Sym4/Rh-Sym4mmp~>Ala)
= biotin (biotin-Sym4/biotin-Sym4mmp~>Ala)
= biotin+rhodamine (Tri-Sym4/TriSym4mmp~>Ala)

Abbildung 93: Synthese der unterschiedlich-modifizierten Sondenmoleküle für ABPP-Experimente. Reagenzien und Reaktionsbedingungen: (b) Tag-N_3, $CuSO_4$ (wässr. Lösung), TBTA (100 mM in DMSO), TCEP (100 mM in H_2O), H_2O, RT, Reaktionskontrolle mittels LC-MS, chromatographische Aufreinigung.

Während eines Aufenthalts in der Gruppe von Dr. Renier van der Hoorn (MPI für Pflanzenzüchtungsforschung, Köln) wurden Symplostatin 4 und seine Derivate im Hinblick auf das Labeling des Proteoms der Modellpflanze *Arabidopsis thaliana* untersucht. Hierzu wurden zunächst die Reaktionsbedingungen für ein optimales *in vivo*-Labeling ermittelt. Anschließend durchgeführte Infiltrationsexperimente konnten jedoch keine weiterreichenden Ergebnisse liefern.

Die Targetidentifizierung für **Sym4** und **Sym4**$^{\mathbf{mmp \rightarrow Ala}}$ wurde dann von Dr. Farnusch Kaschani durchgeführt, der die Papain-artigen Cysteinproteasen (*papain-like cysteine proteases-PLCPs*) RD21A und RD21B als Zielenzyme von **Sym4** und **Sym4**$^{\mathbf{mmp \rightarrow Ala}}$ identifizieren konnte (Abb. 94). RD21 wird eine Beteiligung an der Immunantwort von Pflanzen zugeschrieben.[150] Bemerkenswerterweise konnte hier kein Unterschied zwischen **Sym4** und seinem Derivat ohne die mmp-Einheit festgestellt werden.

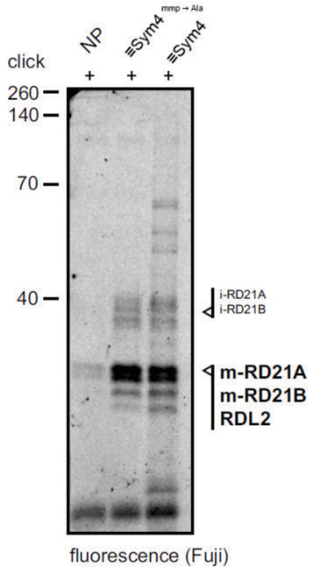

Abbildung 94: Fluoreszenz-Scan der durch SDS-PAGE aufgetrennten Enzyme, die *in vivo* von **≡Sym4** und **≡Sym4**$^{\mathbf{mmp\rightarrow Ala}}$ markiert wurden. Das Labeling wurde *in vivo* ausgeführt, anschließend wurde *in vitro* eine Click-Reaktion mit Tri-N$_3$ durchführt und die markierten Enzyme wurden mittels Affintätschromatographie aufgereinigt. Nach der Auftrennung der Enzyme mittels SDS-PAGE wurden die Enzymbanden ausgeschnitten und ein Gelverdau mit Trypsin durchgeführt. Die Identifikation der markierten Enzyme erfolgte mittels nanoLC-MS/MS. (F. Kaschani)

Nach der erfolgreichen Identifizierung der molekularen Targets von Symplostatin 4 in Pflanzenzellen sollte auch der anti-Malaria-Effekt von Symplostatin 4, der für die chemisch identische Substanz Gallinamid A publiziert worden war,[104] untersucht werden. Diese Untersuchungen erfolgten in Zusammenarbeit mit der Gruppe von Prof. Dr. Matthew Bogyo (Department of Pathology, Stanford University, CA), sämtliche Experimente wurden dabei von Dr. Edgar Deu Sandoval durchgeführt.

Im Rahmen eines ersten Zell-basierten Assays wurde zunächst der Effekt einer Behandlung von Malariaparasiten im erythrozytischen Zyklus mit **Sym4** und **Sym4**$^{\mathbf{mmp\rightarrow Ala}}$ untersucht. Für **Sym 4** zeigte sich dabei schon ab einer Konzentration von 0.1 µM der bekannte Defekt der Nahrungsvakuole. Ein solcher Effekt wird z. B. durch eine gestörte Aktivität der Proteasen, die im frühen erythrozytischen Zyklus für den Hemoglobinverdau zuständig sind, hervorgerufen.[50,53,151] Interessanterweise benötigte **Sym4**$^{\mathbf{mmp\rightarrow Ala}}$ eine 100-fach höhere Inhibitorkonzentration zum Hervorrufen eines vergleichbaren Effektes. Der hier klar zu beobachtende Unterschied zwischen den beiden Analoga kann dabei entweder mit einer verminderten Resorption von **Sym4**$^{\mathbf{mmp\rightarrow Ala}}$ oder einer schlechteren Bindung an die Zielprotease(n) erklärt werden (Abb. 95, **A**). Eine wichtige Nebenbeobachtung im Rahmen dieses Experiments war, dass bei keiner der verwendeten Konzentrationen eine Lyse der roten Blutkörperchen auftrat.

Im Anschluss an diese phänotypsiche Untersuchung wurde der Einfluss einer Symplostatin 4-Behandlung auf die Replikation einer *P. falciparum*-Zellkultur untersucht, dies ist mit dem Fortschreiten der Malariainfektion im Wirt zu vergleichen. Um die Replikation unter Symplostatin 4-Einfluss zu studieren, wurden Zellkulturen mit 2% Parasitenbefall mit verschiedenen Konzentrationen von **Sym4** und dem Analogon **Sym4**$^{\mathbf{mmp\rightarrow Ala}}$ behandelt und der Parasitenbefall nach 75 Stunden mittels Durchflusszytometrie bestimmt (Abb. 95, **B**).[152] Auch hier zeigte sich erneut ein klarer Unterschied in der Potenz der beiden Symplostatin 4-Varianten, der den Trend des Phänotypen-Assays bestätigt.

Die Ergebnisse der Zellassays hatten somit bereits einen indirekten Hinweis darauf gegeben, dass die parasitären Cysteinproteasen der Nahrungsvakuole, also Falcipain 2, Falcipain 2‘ sowie Falcipain 3 (FP-2, FP-2’, FP-3)[50] die Zielproteasen von **Sym4** sein könnten. Dies sollte im Rahmen von ABPP-Experimenten verifiziert werden.

Dazu wurde zunächst ein Labeling intakter Parasiten mit **Rh-Sym4** und **Rh-Sym4**$^{\mathbf{mmp\rightarrow Ala}}$ durchgeführt. Dabei wurden für **Rh-Sym4** zwei starke Banden im Bereich von 28 kDa beobachtet, bei **Rh-Sym4**$^{\mathbf{mmp\rightarrow Ala}}$ trat jedoch im gleichen Bereich lediglich ein schwaches Signal auf. Die Banden für **Rh-Sym4** waren empfindlich gegenüber einer Präinkubation mit den Reporter-freien Versionen **Sym4** und **≡Sym4**. Dies deutete darauf hin, dass das Labeling tatsächlich durch die Funktionalität der Sonde und nicht durch die Rhodamineinheit verursacht wird (Abb. 95, **C**).

Das im 28 kDa-Bereich beobachtete Labeling war bereits ein starkes Indiz dafür, dass tatsächlich FP-2, FP-2’ und FP-3 (bezeichnet als FP-2/3), die bekanntermaßen in diesem Bereich migrieren,[153,154] von **Sym 4** inhibiert werden. Im Rahmen eines kompetitiven ABPP-Experiments mit der Sonde Cy5-DCG-04 wurde diese Hypothese anschließend verifiziert. Hierzu wurde **Sym4** als ein nanomolarer Inhibitor (1.5 nM) von FP-2/3 identifiziert, zusätzlich wurde bei höheren Konzentrationen (1.6 µM) auch FP-1 inhibiert. Die Aminopeptidase DPAP-1 hingegen wurde nicht gehemmt (Abb. 95, **D**). **Sym4**$^{\mathbf{mmp\rightarrow Ala}}$ erwies sich lediglich als schwacher FP-2/3-Inhibitor (25 µM); weder FP-1 noch DPAP-1 wurden von **Sym4**$^{\mathbf{mmp\rightarrow Ala}}$ inhibiert.

Für den hochpotenten FP-2/3-Inhibitor **Sym4** wurden dann zusätzlich weitere Parameter der Inhibition bestimmt. Ein Experiment mit rekombinantem FP-2 und FP-3, in dem die

Substratumwandlung studiert wurde, zeigte erstens, dass **Sym4** ein irreversibler Inhibitor von FP-2 und FP-3 ist und zweitens, dass FP-2 mit einer 10-fach größeren Potenz als FP-3 inhibiert wird. Somit ist **Sym4** einer der derzeit potentesten FP-2/3-Inhibitoren.[155] Die Bestimmung der IC_{50}-Werte für die unterschiedlichen PLCPs zeigte zudem, dass **Sym4** FP-2 mit der höchsten Präferenz inhibiert, gefolgt von FP-3 und FP-1; dabei wurde für alle Zielproteasen eine sub-mikromolare Hemmung gemessen (Abb. 95, **E**). Die Ergebnisse der biologischen Untersuchungen sind in Tabelle 8 zusammengefasst.

Tabelle 8: Zusammenfassung der Anti-Malaria-Aktivitäten von **Sym4** und **Sym4**$^{\mathrm{mmp}\rightarrow\mathrm{Ala}}$.

	Sym4	**Sym4**$^{\mathrm{mmp}\rightarrow\mathrm{Ala}}$
Nahrungsvakuolendefekt beobachtet ab	0.1 µM	10 µM
EC_{50} (aus Replikationsassay)	0.7 ± 0.2 µM	27 ± 7 µM
Labeling von FP-2/3 in intakten Parasiten bei 10 µM	stark	schwach
FP-2/3 Inhibition ab (kompet. Assay)	1.5 nM	25 µM
FP-1 Inhibition ab (kompet. Assay)	1.6 µM	nicht beobachtet
k_i(FP-2) / $M^{-1}s^{-1}$	58600 ± 1400	nicht bestimmt
k_i(FP-2) / $M^{-1}s^{-1}$	7030 ± 250	nicht bestimmt
IC_{50}(FP-2)	8.5 ± 1.3 nM	nicht bestimmt
IC_{50}(FP-3)	22 ± 8 nM	nicht bestimmt
IC_{50}(FP-1)	140 ± 23 nM	nicht bestimmt

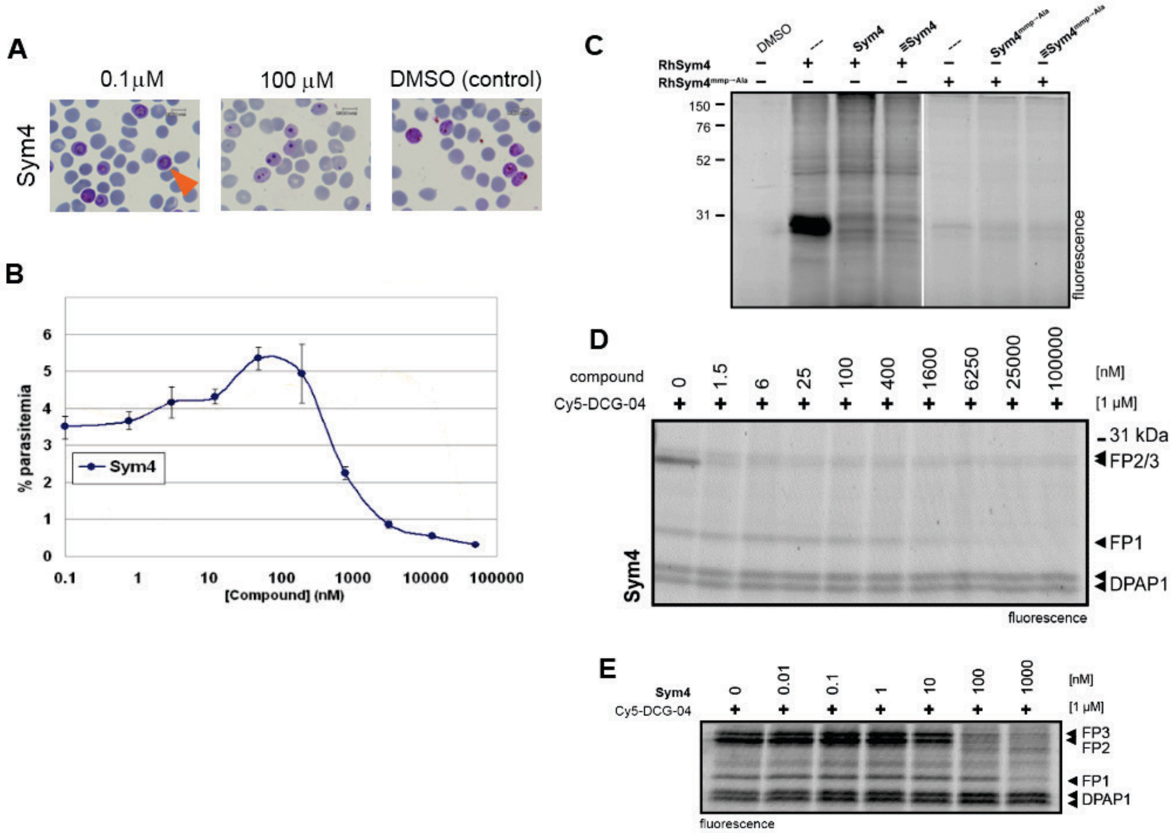

Abbildung 95: Zusammenfassung der anti-Malaria-Untersuchungen für **Sym4**. **A**: Nahrungsvakuolendefekt nach der Behandlung von *P. falciparum* D10 im Ringstadium mit **Sym4**; **B**: Effekt einer **Sym4**-Behandlung auf die Replikation von *P. falciparum*; **C-E**: ABPP-Experimente mit **Sym4** und ABPP-Analoga: Labeling intakter Parasiten (**C**), kompetitives ABPP mit Cy5-DCG-04 (**D**), kompetitives ABPP mit Cy5-DCG-04 zur Bestimmung der IC_{50}-Werte (**E**). (E. Sandoval)

Zusammenfassend ist festzustellen, dass die anti-Malaria-Aktivität von **Sym4** höchstwahrscheinlich aus einer kombinierten Inhibition von FP-2 und FP-3 (und in geringerem Maße auch FP-1) resultiert. Der Defekt der Nahrungsvakuole, der bereits in einer frühen Entwicklungsstufe des Parasiten beobachtet wird, hat seine Ursache dabei wahrscheinlich in der Inhibition von FP-2. Die verminderte Replikation (d. h. die Abtötung des Parasiten) wird am wahrscheinlichsten durch eine Inhibition von FP-3 verursacht. FP-3 wird die wichtigste Rolle im Hinblick auf das Überleben und die Weiterentwicklung des Parasiten zugeschrieben.[52]

Insgesamt wurde der Naturstoff Symplostatin 4 in zwei sehr unterschiedlichen Organismen studiert. Als Zielproteasen in *A. thaliana* konnten die PLCPs RD21A und RD21B identifiziert werden. Im Rahmen der Labeling-Experimente in der Modellpflanze konnte kein Unterschied zwischen **Sym4** und **Sym4**$^{\text{mmp}\rightarrow\text{Ala}}$ festgestellt werden.

Die anti-Malaria-Aktivität von Symplostatin 4 wurde eingehend studiert, dabei wurde **Sym4** als ein hochpotenter Inhibitor der parasitären Falcipaine identifiziert. Im Rahmen dieser Untersuchungen wurde ein klarer Unterschied in der Inhibitionspotenz zwischen **Sym4** und **Sym4**$^{\mathbf{mmp \rightarrow Ala}}$ beobachtet.

In Zukunft könnte **Sym 4** als Leitstruktur bei der Suche nach Wirkstoffen gegen Malaria eingesetzt werden und darüber hinaus auch für das Profiling weiterer Proteome verwendet werden.

6 Experimental

6.1 General methods and instruments

Reagents

Reagents were purchased from Acros, Senn Chemicals, Fluka, J.T. Baker, Merck, Novabiochem, Riedel de Haen, Iris, Roth or Sigma-Aldrich and were used without further purification. Anhydrous solvents in the highest available quality were purchased from the same suppliers.

Thin layer chromatography (TLC)

TLC was carried out on Merck aluminum pre-coated silica gel plates (20 × 20 cm, $60F_{254}$) using ultraviolet light irradiation at 254 nm or the following developing reagents. Eluents and R_f values are given in the respective experiment. Reversed-phase TLC was carried out on Merck aluminum pre-coated silica gel plates (60 RP-18 $F_{254}S$) using ultraviolet light irradiation at 254 nm or the following developing reagents.

Reagent A: 20 g of phosphomolybdic acid hydrate in 80 mL ethanol

Reagent B: 1.5 g $KMnO_4$, 10 g K_2CO_3 and 1.25 mL of 10% aq. NaOH in 200 mL water.

Silica gel flash liquid chromatography

Column chromatography purifications were performed with silica gel from Acros (particle size 35-70 µm). Reversed-phase chromatography was performed with LiChroprep RP-18 (40-63µm) from Merck.

Reversed-phase liquid chromatography - electrospray ionization mass spectrometry (LC-MS)

LC-MS analyses were performed on an HPLC system from Agilent (1200 series) with an Eclipse XDB-C18, 5 µm column from Agilent (peak detection at 210 nm) and a Thermo Finnigan LCQ Advantage Max ESI-Spectrometer. A linear gradient of solvent B (0.1% formic acid in acetonitrile) in solvent A (0.1% formic acid in water) was used at 1 mL/min flow rate.

Gradient C_{18}: 0 min / 10% B → 1 min / 10% B → 10 / 100% B → 12 min / 100% B → 15 min / 10% B.

Alternatively, a system consisting of an Agilent (1100 series) HPLC from Hewlett-Packard (peak detection at 210 nm) equipped with a CC 250/4 Nucleosil 120-5 C4 column from

Macherey-Nagel, connected to a Thermo Finnigan LCQ Advantage Max ESI-Spectrometer was used. A linear gradient of solvent B (0.1% formic acid in acetonitrile) in solvent A (0.1% formic acid in water) was employed at 1mL/min flow rate.

Gradient C_4: 0 min / 10% B → 1 min / 10% B → 10 min / 100% B → 12 min / 100% B → 15 min / 10% B.

Preparative reversed-phase high performance liquid chromatography (prep HPLC)

Purification of the compounds was performed on a Varian HPLC system (Pro Star 215) with a VP 250/21 Nucleosil C18PPN-column from Macherey-Nagel and detection at 210 nm. Alternatively, a C4 column from Macherey-Nagel was used. Linear gradients of solvent B (0.1% TFA in acetonitrile) in solvent A (0.1% TFA in water) were applied at a 25 mL/min flow rate.

Nuclear magnetic resonance spectroscopy (NMR)

Nuclear magnetic resonance (NMR) spectra were recorded on a Varian Mercury 400 system (400 MHz for ^{1}H- and 100 MHz for ^{13}C-NMR), a Bruker Avance DRX 500 system (500 MHz for ^{1}H- and 126 MHz for ^{13}C-NMR), a Varian Unity Inova 600 system (600 MHz for ^{1}H- and 151 MHz for ^{13}C-NMR) or a Bruker Avance II 700 MHz system (700 MHz for ^{1}H and 176 MHz for ^{13}C-NMR). ^{1}H NMR spectra are reported in the following manner: chemical shifts (δ) in ppm calculated with reference to the residual signals of undeuterated solvent, multiplicity (s, singlet; d, doublet; t, triplet; dd, doublet of doublet; dt, doublet of triplet; m, multiplet; b, broad signal), coupling constants (*J*) in Hertz (Hz), and number of protons (H).

High resolution mass spectrometry (HRMS)

HRMS measurements were performed on a TRACE GC Ultra DFS (GC/EI) instrument from Thermo Scientific. Alternatively, an Accela/LTQ Orbitrap (LC/ESI) system from Thermo Scientific was used.

Optical rotation

Optical rotations were measured with a Polartronic HH8 polarimeter from Schmidt + Haensch. Concentrations *c* are given in g/100 mL, the solvent used is given with the respective data.

6.2 Solution synthesis of the Ahp precursors I and II

(*S*)-Benzyl-2-(*tert*-butoxycarbonylamino)-5-hydroxypentanoate (2)

Boc-(*S*)-glutamic acid benzyl ester (5.00 g, 14.8 mmol) was dissolved in anhydrous THF (60 mL) under an argon atmosphere and cooled to -15 °C in an ice-acetone cooling bath. Upon the successive addition of triethylamine (6.2 mL, 44.5 mmol, 3 eq.) and ethyl chloroformate (4.2 mL, 44.5 mmol, 3 eq.) a white precipitate formed. After the addition the reaction mixture was maintained at -15 °C for 1 h. Subsequently, sodium borohydride (2.24 g, 59.3 mmol, 4 eq.) dissolved in water (60 mL) was carefully added to the reaction mixture at -15 °C resulting in the dissolution of the precipitate. After stirring at -15 °C for 1 further hour, the reaction mixture was allowed to warm to RT. A TLC check after 5 h indicated the complete consumption of the starting material.

The reaction mixture was quenched with 1 M aq. $KHSO_4$ solution (100 mL) and the aqueous phase was extracted with ethyl acetate (3x 100 mL). The combined organic extracts were washed with brine (150 mL), dried over Na_2SO_4 and evaporated to dryness. The crude material was purified by flash column chromatography (50% ethyl acetate in cyclohexane), affording (*S*)-benzyl-2-(*tert*-butoxycarbonylamino)-5-hydroxypentanoate (**2**).

Yield: 4.03 g (12.5 mmol, 84%) as a pale yellow oil.

TLC (50% ethyl acetate in cyclohexane): $R_f = 0.36$.

$[\alpha]_D^{20}$ -2.3 (*c* 0.98 in $CHCl_3$); (lit.[101],.$[\alpha]_D$ -3.9 (*c* 1.0 in $CHCl_3$)).

^1H NMR (400 MHz, $CDCl_3$): δ 7.32-7.34 (m, 5 H), 5.10-5.19 (m, 2H), 4.29-4.34 (m, 1H), 3.58 (t, *J* = 6.20 Hz, 2H), 1.93-2.00 (m, 1H), 1.84-1.91 (m, 1H), 1.66-1.76 (m, 1H), 1.53-1.60 (m, 2H), 1.41 (s, 9H).

^{13}C NMR (100 MHz, $CDCl_3$): δ 172.6, 141.0, 135.3, 128.5, 128.4, 128.2, 79.8, 65.0, 61.8, 53.2, 29.2, 28.2, 25.4.

LC-MS: t_R = 8.90 min (C_{18}), *m/z* = 346($M^+ + Na^+$, 30%), 224(M^+ - Boc, 100).

HRMS (EI)*: m/z* calcd for $C_{17}H_{25}O_5N^+$ $[M + H]^+$ 324.1805, found 324.1810.

(*S*)-1-Benzyl-5-methyl-2-(*tert*-butoxycarbonylamino)pentanedioate (3)

Boc-(*S*)-Glu-OBn (5.00 g, 14.8 mmol) was dissolved in acetone and potassium carbonate (18.4 g, 133.4 mmol, 9 eq.) and methyl iodide (2.8 mL, 44.5 mmol, 3 eq.) were added at RT. Subsequently, the reaction mixture was heated to reflux. After 4 h a TLC reaction control indicated a complete conversion of the starting material. The reaction mixture was cooled to RT and quenched by addition of saturated aq. NH_4Cl solution (120 mL). The aqueous phase was extracted with ethyl acetate (5x 150 mL) and the unified organic phases were dried over Na_2SO_4.

After evaporation to dryness the crude product was purified by flash column chromatography (17% ethyl acetate in cyclohexane) affording pure (*S*)-1-benzyl-5-methyl-2-(*tert*-butoxycarbonylamino)pentanedioate (**3**).

Yield: 5.20 g mg (14.8 mmol, quant.) as a yellow oil.
TLC (17% ethyl acetate in cyclohexane): R_f = 0.25.
^{1}H NMR (400 MHz, $CDCl_3$): δ 7.32-7.38 (m, 5H), 5.17 (d, *J* = 2.4 Hz, 2H), 4.33-4-43 (m, 1H), 3.66 (s, 3H), 2.31-2.45 (m, 2H), 2.15-2.23 (m, 1H), 1.91-2.01 (m, 1H), 1.42 (s, 9H).
^{13}C NMR (100 MHz, $CDCl_3$): δ 173.1, 172.0, 155.3, 135.2, 128.6, 128.4, 128.2, 80.0, 67.2, 53.0, 51.7, 30.0, 28.2, 27.7.
LC-MS: t_R = 10.00 min (C_{18}), *m/z* = 252(M^+ - Boc, 100%), 352.18 calcd for $C_{18}H_{26}NO_6^+$.

(*S*)-1-Benzyl-5-methyl-2-(bis(*tert*-butoxycarbonylamino))pentanedioate (4)

(*S*)-1-Benzyl-5-methyl-2-(*tert*-butoxycarbonylamino)pentanedioate (**3**, 5.06 g, 14.4 mmol) was dissolved in acetonitrile (150 mL) and transferred to a dry flask under an argon atmosphere. 4-(dimethylamino)pyridine (1.76 g, 14.4 mmol, 1 eq.) dissolved in acetonitrile (20 mL) and liquidified Boc anhydride (16.5 mL, 72.0 mmol, 5 eq.) were added to the solution successively at RT. During the addition of Boc anhydride, the color of the reaction solution changed from clear to yellow and during the progression of the reaction to a deep red. After stirring at RT for 20 h a TLC reaction control indicated a complete reaction.

Water (150 mL) was added to the reaction solution and the aqueous phase was extracted with ethyl acetate (3x 250 mL); the sluggish phase separation was accelerated by the addition of small amounts of brine. The combined extracts were washed with 1 N HCl (300 mL) and brine (4x 250 mL) and dried over Na_2SO_4 and evaporated to dryness. The crude material was purified by flash column chromatography (17% ethyl acetate in cyclohexane to afford (*S*)-1-benzyl-5-methyl-2-(bis(*tert*-butoxycarbonylamino))pentanedioate (**4**).

Yield: 6.35 g mg (14.1 mmol, 98%) as a colorless oil.
TLC (17% ethyl acetate in cyclohexane): $R_f = 0.24$.
^{1}H NMR (400 MHz, $CDCl_3$): δ 7.31-7.34 (m, 5H), 5.15 (d, *J* = 1.2 Hz, 2H), 4.96-4.99 (m, 1H), 3.66 (s, 3H), 2.47-2.56 (m, 1H), 2.37-2.46 (m, 2H), 2.16-2.26 (m, 1H), 1.44 (s, 18H).
^{13}C NMR (100 MHz, $CDCl_3$): δ 173.1, 170.1, 152.0, 135.6, 128.4, 128.1, 128.0, 83.3, 66.8, 57.5, 51.6, 30.6, 27.9, 24.8.
LC-MS: t_R = 11.52 min (C_{18}), *m/z* = 474(M^+ + Na, 100%), 252(M^+ - 2Boc, 70), 452.23 calcd for $C_{23}H_{34}NO_8^+$.

(*S*)-1-Benzyl-2-(bis(*tert*-butoxycarbonylamino))-5-oxopenanoate (5)

(*S*)-1-Benzyl-5-methyl-2-(bis(*tert*-butoxycarbonylamino))pentanedioate (**4**, 3.70 g, 8.19 mmol) was dissolved in anhydrous toluene (82 mL, 0.1 M) under an argon atmosphere and the solution was cooled to -78 °C in a dry ice/acetone cooling bath. DIBAL-H (1 M in toluene, 20.5 mL, 20.5 mmol, 2.2 eq.) was added dropwise over a period of 2 h at -78 °C and the reaction solution was stirred at -78 °C for another 2 h. The reaction was quenched by slow addition of a potassium-sodium-tartrate solution (60 mL) under vigorous stirring at -78 °C. The quenched reaction mixture was allowed to warm to ambient temperature, the phases were separated and the aqueous phase was extracted with DCM (2x 60 mL). The combined organic extracts were dried over Na_2SO_4 and the solvent was evaporated to dryness. The crude material was purified by flash column chromatography (20% ethyl acetate in cyclohexane) affording (*S*)-1-benzyl-2-(bis(*tert*-butoxycarbonylamino))-5-oxopenanoate (**5**).

Yield: 918 mg (2.18 mmol, 27%) as a colorless oil.
TLC (20% ethyl acetate in cyclohexane): $R_f = 0.24$.
^{1}H NMR (400 MHz, $CDCl_3$): δ 9.77 (t, *J* = 0.8 Hz, 1H), 7.30-7-36 (m, 5H), 5.16 (d, *J* = 2.8 Hz, 2H), 4.90-4.93 (m, 1H), 2.58-2.64 (m, 1H), 2.47-2.56 (m, 2H), 2.15-2.23 (m, 1H), 1.45 (s, 18H).
^{13}C NMR (100 MHz, $CDCl_3$): δ 200.9, 170.1, 152.1, 145.3, 128.5, 128.2, 128.0, 83.4, 66.9, 57.5, 40.5, 28.0, 22.2.

LC-MS: t_R = 11.21 min (C_{18}), *m/z* = 444(M^+ + Na, 100%), 344(M^+ - Boc + Na, 25), 422.22 calcd for $C_{22}H_{32}NO_7^+$.

(*S,E*)-7-Benzyl-1-*tert*-butyl-6-(bis(*tert*-butoxycarbonylamino))-hept-2-enedioate (6)

preparation of the ylide

To prepare the ylide (2-*tert*-butoxy-2-oxoethyl)triphenylphosphonium chloride (2.50 g, 6.05 mmol) was dissolved in 2 M NaOH (100 mL) and toluene (100 mL) was added. The resulting the biphasic reaction mixture was stirred vigorously at RT for 1 h. The phases were separated and the aqueous phase was extracted with toluene (1x 100 mL). The combined organic extracts were dried over Na_2SO_4. Evaporation to dryness then yielded the ylide as a white solid.

Wittig reaction

(*S*)-1-Benzyl-2-(bis(*tert*-butoxycarbonylamino))-5-oxopenanoate (**5**, 866 mg, 2.05 mmol) was dissolved in DCM (100 mL) and the ylide (1.55 g, 4.11 mmol, 2 eq.), prepared as described above, was added to the solution. The reaction mixture was stirred at RT overnight; after this time a TLC reaction control indicated a complete reaction. The reaction was quenched by the addition of water (80 mL). The phases were separated and the aqueous phase was extracted with ethyl acetate (2x 80 mL). The combined organic extracts were dried over Na_2SO_4 and the solvent was evaporated. The crude product was dissolved in a minimal amount of MeOH, mixed with silica gel and evaporated to dryness. This residue was submitted to flash chromatography purification (12.5 % ethyl acetate in cyclohexane) to afford (*S,E*)-7-benzyl-1-*tert*-butyl-6-(bis(*tert*-butoxycarbonylamino))-hept-2-enedioate (**6**).

Yield: 900 mg (1.73 mmol, 84%) as a pale yellow oil.
TLC (12.5% ethyl acetate in cyclohexane): R_f = 0.30.
^{1}H NMR (400 MHz, $CDCl_3$): δ 7.31-7.35 (m, 5H), 6.79-6.86 (m, 1H), 5.76 (d, *J* = 15.6 Hz, 1H), 5.15 (d, *J* = 3.6 Hz, 2H), 4.87-4.91 (m, 1H) 2.22-2.36 (m, 3H) 2.05-2.11 (m, 1H) 1.47 (s, 9H), 1.45 (s, 18H).
^{13}C NMR (100 MHz, $CDCl_3$): δ 170.3, 167.8, 152.1, 146.2, 135.6, 128.5, 128.2, 128.0, 123.8, 83.2, 80.1, 66.9, 57.7, 28.8, 28.1, 27.9.
LC-MS: t_R = 12.77 min (C_{18}), *m/z* = 542(M^+ + Na, 100%), 442(M^+ - Boc + Na, 50), 520.29 calcd for $C_{28}H_{42}NO_8^+$.

(*S,E*)-7-(*tert*-Butoxy)-2-(bis-(*tert*-butoxycarbonylamino))-7-oxohept-5-enoic acid (7)

Triethylsilane (354 µL, 2.23 mmol, 1.4 eq.), triethylamine (100 µL, 0.72 mmol, 0.45 eq.) and palladium(II) acetate (18 mg, 0.08 mmol, 0.05 eq.) were dissolved in anhydrous DCM (15 mL) in a dry flask under an argon atmosphere and stirred for 15 min. (*S,E*)-7-Benzyl-1-*tert*-butyl-6-(bis(*tert*-butoxycarbonylamino))-hept-2-enedioate (**6**, 828 mg, 1.59 mmol) dissolved in anhydrous DCM (15 mL) and kept under an argon atmosphere was added dropwise to the reaction at RT. The resulting mixture was stirred overnight at ambient temperature. A TLC reaction control indicated a complete consumption of the starting material. The reaction mixture was quenched by the addition of sat. aq. NH_4Cl (25 mL) and the aqueous phase was extracted with diethyl ether (2x 25 mL). The combined organic extracts were washed with brine (50 mL) and dried over Na_2SO_4. After evaporation to dryness the crude product was purified by flash column chromatography (gradient: 20% to 50% ethyl acetate in cyclohexane) affording (*S,E*)-7-(*tert*-butoxy)-2-(bis-(*tert*-butoxycarbonylamino))-7-oxohept-5-enoic acid (**7**).

Yield: 423 mg (0.98 mmol, 62%) as a colorless oil.
TLC (50% ethyl acetate in cyclohexane): $R_f = 0.24$.
^{1}H NMR (400 MHz, $CDCl_3$): δ 6.79-6.87 (m, 1H), 5.77 (d, *J* = 15.6 Hz, 1H), 4.91-4.94 (m, 1H), 2.22-2.29 (m, 3H), 2.05-2.10 (m, 1H), 1.50 (s, 18H), 1.47 (s, 9H).
^{13}C NMR (100 MHz, $CDCl_3$): δ 175.8, 165.8, 151.9, 146.1, 123.8, 83.5, 80.2, 57.4, 29.0, 287, 28.1, 28.0.
LC-MS: t_R = 11.00 min (C_{18}), *m/z* = 452(M^+ + Na, 100%), 174(M^+ - 2Boc - *t*Bu, 100), 430.24 calcd for $C_{21}H_{26}NO_8^+$.

(*S,E*)-7-Allyl 1-*tert*-butyl-6-(bis(*tert*-butoxycarbonylamino))hept-2-enedioate (8)

Synthesis from 7: (*S,E*)-7-(*tert*-Butoxy)-2-(bis-(*tert*-butoxycarbonylamino))-7-oxohept-5-enoic acid (**7**, 373 mg, 0.87 mmol) and cesium carbonate (283 mg, 0.87 mmol, 1 eq.) were dissolved in anhydrous MeOH (15 mL) and the mixture was evaporated to dryness. The resulting solid was then co-evaporated four times with toluene (15 mL) to obtain the cesium salt of **7** as a white solid. This cesium salt was suspended in DMF (20 mL) and allyl bromide (1.5 mL, 17.4 mmol, 20 eq.) was added at RT. The reaction mixture was stirred overnight at RT, the solvent was removed and the resulting yellowish solid was co-evaporated twice with toluene (20 mL) to remove residual DMF. The crude product was purified by flash column chromatography (12.5% ethyl acetate in cyclohexane), yielding (*S,E*)-7-allyl 1-*tert*-butyl-6-(bis(*tert*-butoxycarbonylamino))hept-2-enedioate (**8**).

Yield: 310 mg (0.66 mmol, 76%) as a colorless oil.

Synthesis from 15: (*S*)-Allyl-2-(bis(*tert*-butoxycarbonylamino))-5-oxopentanoate (**15**, 831 mg, 2.24 mmol) was dissolved in dichloromethane and the ylide of (2-*tert*-butoxy-2-oxoethyl)triphenylphosphonium chloride (prepared as described, 1.26 g, 3.36 mmol, 1.5 eq.) was added to the solution. The reaction mixture was stirred overnight at ambient temperature. Subsequently, the solvent was removed and the crude product was purified by flash column chromatography (12.5% ethyl acetate in cyclohexane), to afford (*S,E*)-7-allyl 1-*tert*-butyl-6-(bis(*tert*-butoxycarbonylamino))hept-2-enedioate (**8**).

Yield: 986 mg (2.10 mmol, 94%) as a colorless oil.
TLC (12.5% ethyl acetate in cyclohexane): $R_f = 0.23$.
^{1}H NMR (400 MHz, $CDCl_3$): δ 6.80-6.87 (m, 1H), 5.84-5.94 (m, 1H), 5.76 (d, *J* = 15.6 Hz, 1H), 5.31 (dd, *J* = 1.6 Hz, 17.2 Hz, 1H), 5.21 (dd, *J*= 1.2 Hz, 9.2 Hz, 1H), 4.85-4.87 (m, 1H), 4.60-4.62 (m, 2H), 2.21-2.32 (m, 3H), 2.04-2.10 (m, 1H), 1.49 (s, 18H), 1.47 (s, 9H).
^{13}C NMR (100 MHz, $CDCl_3$): δ 170.2, 165.8, 152.1, 146.2, 131.7, 123.8, 118.1, 83.3, 80.1, 65.7, 57.7, 28.7, 28.3, 28.1, 28.0.
LC-MS: t_R = 12.47 min (C_{18}), *m/z* = 491(M^+ + Na, 50%), 214(M^+ - 2Boc - *t*Bu, 100), 470.27 calcd for $C_{24}H_{40}NO_8^+$.

(*S,E*)-7-(Allyloxy)-6-amino-7-oxohept-2-enoic acid (9)

(*S,E*)-7-Allyl 1-*tert*-butyl-6-(bis(*tert*-butoxycarbonylamino))hept-2-enedioate (**8**, 43 mg, 0.09 mmol) was dissolved in anhydrous DCM (1 mL) and trifluoroacetic acid (1 mL) was added to the solution at ambient temperature. A TLC reaction control after 4 h indicated a complete reaction. The solvent was removed and the resulting oil was co-evaporated twice with toluene (2 mL) to remove residual trifluoroacetic acid. The crude material was used directly in the next reaction without a further purification.

(*S,E*)-6-(((9*H*-Fluoren-9-yl)methoxy)carbonylamino)-7-(allyloxy)-7-oxohept-2-enoic acid (1)

(*S,E*)-7-(Allyloxy)-6-amino-7-oxohept-2-enoic acid (**9**, 19 mg, 0.09 mmol) was dissolved in water (0.5 mL) and heated to 40 °C. To this solution, FmocCl (26 mg, 0.1 mmol, 1.1 eq.) dissolved in dioxane (1 mL) was added dropwise and the speed of the addition was adjusted to maintain a clear reaction solution. Saturated aq. $NaHCO_3$ (0.5 mL) was added and the pH was determined 10 min after the addition, indicating a pH > 8. The resulting reaction mixture was stirred overnight at 40 °C. After cooling to RT, water (1 mL) was added to the reaction solution and the mixture was extracted with ethyl acetate (2 x 5 mL). Some ethyl acetate was added and the aqueous phase was adjusted to pH 1 by addition of 0.2 M HCl. The combined organic extracts were washed with 1 N HCl (2x 100 mL) and brine (100 mL) and dried over Na_2SO_4. After the evaporation of the solvent the crude product was purified by flash column chromatography (50 % ethyl acetate in cyclohexane) to yield (*S,E*)-6-(((9*H*-fluoren-9-yl)methoxy)carbonylamino)-7-(allyloxy)-7-oxohept-2-enoic acid (**1**).

Yield: 19 mg (0.04 mmol, 49%) as a white solid.
TLC (50% ethyl acetate in cyclohexane): $R_f = 0.11$.
^{1}H NMR (400 MHz, $CDCl_3$): δ 7.75-7.77 (m, 2H), 7.59-7.61 (m, 2H), 7.38-7.42 (m, 2H), 7.30-7.33 (m, 2H), 7.00-7.06 (m, 1H), 5.84-5.96 (m, 2H), 5.37-5.39 (m, 1H), 5.25-5.32 (m, 1H), 4.63-4.70 (m, 2H), 4.39-4.48 (m, 3H), 4.20-4.23 (m, 1H), 2.22-2.35 (m, 2H), 2.05-2.10 (m, 1H), 1.79-1.88 (m, 1H) .
^{13}C NMR (100 MHz, $CDCl_3$): δ171.6, 170.8, 155.8, 149.6, 143.6, 141.3, 131.2, 127.7, 127.1, 125.0, 121.6, 120.0, 199.4, 67.0, 66.3, 53.4, 47.2, 31.0, 28.0.
LC-MS: t_R = 9.82 min (C_{18}), *m/z* = 436(M^+, 100%), 214(M^+ - Fmoc, 35), 436.18 calcd for $C_{25}H_{25}NO_6^+$.

(*S*)-Benzyl-2-(*tert*-butoxycarbonylamino)-5-(*tert*-butyldimethylsilyloxy)pentanoate (10)

(*S*)-Benzyl-2-(*tert*-butoxycarbonylamino)-5-hydroxypentanoate (**2**, 3.92 g, 12.1 mmol) was dissolved in DCM (80 mL) and cooled to 0 °C. Imidazole (2.00 g, 30.3 mmol, 1.2 eq.) and *tert*-butyldimethylsilyl chloride (2.19 g, 14.5 mmol , 2.5 eq.) were added to the solution successively. The reaction mixture was maintained at 0 °C for 1 h and then allowed to warm to RT overnight. Water was added to the reaction mixture, the phases were separated and the aqueous phase was extracted with ethyl acetate (3x 80 mL). The combined organic extracts were washed with 1 M aq. $KHSO_4$ solution (150 mL) and saturated aq. $NaHCO_3$ solution (150 mL), dried over Na_2SO_4 and evaporated to dryness. The crude product was purified by flash column chromatography (10% ethyl acetate in cyclohexane) to afford (*S*)-benzyl-2-(*tert*-butoxycarbonylamino)-5-(*tert*-butyldimethyl-silyloxy)pentanoate (**10**).

Yield: 5.05 g (11.5 mmol, 95%) as a yellow oil.
TLC (10% ethyl acetate in cyclohexane): $R_f = 0.35$.
$[\alpha]_D^{20}$ -5.8 (*c* 1.13 in $CHCl_3$).
^{1}H NMR (400 MHz, $CDCl_3$): δ 7.32-7.35 (m, 5H), 5.13-5.19 (m, 2H), 4.31-4,36 (m, 1H), 3.58-3.61 (t, *J* = 6.05, 2H), 1.94-1.95 (m, 1H), 1.76-1.85 (m, 1H), 1.51-1.56 (m, 2H), 1.43 (s, 9H), 0.88 (s, 9H), 0.03 (s, 6H).
^{13}C NMR (100 MHz, $CDCl_3$): δ 172.6, 155.4, 135.5, 128.5, 128.3, 128,1, 79.6, 66.8, 62.2, 53.3, 29.0, 28.3, 25.9, 18.3, -5.4 .
LC-MS: t_R = 13.31 min (C_{18}), *m/z* = 460($M^+ + Na^+$, 40%), 338(M^+ - Boc, 100) 438.27 calcd for $C_{23}H_{40}NO_5Si^+$.
HRMS (EI)*: m/z* calcd for $C_{23}H_{40}O_5NSi^+$ $[M + H]^+$ 438.2670, found 438.2670.

(*S*)-Benzyl-2-(bis(tert-butoxycarbonyl)amino)-5-(*tert*-butyldimethylsilyloxy)-pentanoate (11)

(*S*)-Benzyl-2-(*tert*-butoxycarbonylamino)-5-(*tert*-butyldimethylsilyloxy)pentanoate (**10**, 4.94 g, 11.3 mmol) was dissolved in acetonitrile (80 mL). After the addition of 4-(dimethylamino)pyridine (2.07 g, 16.9 mmol, 1.5 eq.) at RT, the mixture was stirred for 10 min. Subsequently, liquidified Boc anhydride (13.0 mL, 56.5 mmol, 5 eq.) was added and the reaction mixture was stirred for 24 h at RT, thereby turning from a pale yellow color to bright red. The reaction was quenched by the addition of water (80 mL) and the aqueous phase was extracted with ethyl acetate (3x 80 mL); the sluggish phase separation was accelerated by the addition of brine in small portions. The combined organic extracts were washed with 1 M aq. HCl (150 mL) and brine (4x 150 mL), the solvent was removed. The crude mixture of product and unreacted starting material was purified by flash column chromatography (5% ethyl acetate in cyclohexane). First, (*S*)-benzyl-2-(bis(tert-butoxycarbonyl)amino)-5-(*tert*-butyldimethylsilyloxy)pentanoate (**11**) eluted from the column, followed by the starting material **10**.

Yield: 3.88 g (7.2 mmol, 64%, 81% b.r.s.m.) as a colorless oil.

TLC (5% ethyl acetate in cyclohexane): $R_f = 0.26$.

$[\alpha]_D^{20}$ -20.2 (*c* 1.26 in $CHCl_3$).

^{1}H NMR (400 MHz, $CDCl_3$): δ 7.31-7.33 (m, 5H), 5.11-5.18 (m, 2H), 4.88-4.92 (m, 1H), 3.61-3.65 (dt, *J* = 6.40, 1.38 Hz, 2H), 2.12-2.14 (m, 1H), 1.91-2.01 (m, 1H), 1.54-1.61 (m, 2H), 1.44 (s, 18H), 0.88 (s, 9H), 0.03 (s, 6H) .

^{13}C NMR (100 MHz, $CDCl_3$): δ 170.7, 152.2, 135.7, 128.4, 128.0, 127.9, 82.9, 66.7, 62.6, 58.1, 29.6, 27.9, 26.0, 25.9, 18.3, -5.3.

LC-MS: t_R = 11.29 min (C_4), *m/z* = 1097($2M^+ + Na^+$, 100%), 438(M^+ - Boc, 35) 538.77 calcd for $C_{28}H_{48}NO_7Si^+$.

HRMS (EI)*: m/z* calcd for $C_{56}H_{94}O_{14}N_2NaSi_2^+$ $[2M + Na]^+$ 1097.6136, found 1097.6141.

(*S*)-2-(bis(*tert*-Butoxycarbonyl)amino)-5-(*tert*-butyldimethylsilyloxy)pentanoic acid (12)

(*S*)-Benzyl-2-(bis(*tert*-butoxycarbonyl)amino)-5-(*tert*-butyldimethylsilyloxy)pentanoate (**11**, 5.85 g, 10.9 mmol) was dissolved in ethyl acetate (80 mL) and transferred to a 2-neck round bottom flask equipped with a rubber septum and a stop-cock under an argon atmosphere. Palladium on activated charcoal (10%, 2.93 g, 5 %wt) was added in small portions at RT through a funnel that was flushed with ethyl acetate (70 mL in total) after each portion. The flask was equipped with a hydrogenation balloon and carefully flushed with hydrogen by opening the stop-cock from time to time. The hydrogenation was carried out for 2.5 h at RT, and the reaction mixture was filtered through a pad of Celite®, which was rinsed thoroughly with ethyl acetate (4x 100 mL). Evaporation to dryness afforded pure (*S*)-2-(bis(*tert*-butoxycarbonyl)amino)-5-(*tert*-butyldimethylsilyloxy)-pentanoic acid (**12**).

Yield: 4.84 g (10.8 mmol, 99%) as a white solid.

$[\alpha]_D^{20}$ -19.8 (*c* 0.91 in $CHCl_3$).

^{1}H NMR (400 MHz, $CDCl_3$): δ 4.91-4.95 (m, 1H), 3.62-3.65 (dt, *J* = 6.30, 1.74 Hz, 2H), 2.11-2.20 (m, 1H), 1.91-2.00 (m, 1H), 1.54-1.59 (m, 2H), 1.50 (s, 18H), 0.89 (s, 9H), 0.04 (s, 6H).

^{13}C NMR (100 MHz, $CDCl_3$): δ 177.1, 152.0, 83.2, 62.5, 57.8, 29.5, 27.9, 26.1, 25.9, 18.3, -5.3.

LC-MS: t_R = 11.31 min (C_{18}), *m/z* = 917($2M^+ + Na^+$, 100%), 347(M^+ - Boc, 20) 448.65 calcd for $C_{21}H_{42}NO_7Si^+$.

HRMS (EI)*: m/z* calcd for $C_{42}H_{82}O_{14}N_2NaSi_2^+$ $[2M + Na]^+$ 917.5197, found 917.5191.

(*S*)-Allyl-2-(bis(*tert*-butoxycarbonyl)amino)-5-(*tert*-butyldimethylsilyloxy)-pentanoate (13)

(*S*)-2-(bis(*tert*-Butoxycarbonyl)amino)-5-(*tert*-butyldimethylsilyloxy)pentanoic acid (**12**, 4.61 g, 10.3 mmol) and cesium carbonate (3.36 g, 10.3 mmol, 1 eq.) were dissolved in anhydrous MeOH (40 mL). The solvent was evaporated and the resulting solid was co-evaporated twice with toluene (40 mL) to obtain the cesium salt of **12** as a white solid. This cesium salt was suspended in DMF (80 mL) and allyl bromide (17.4 mL, 206 mmol, 20 eq.) was added slowly at RT. The reaction mixture was stirred at RT overnight, the solvent was evaporated and the residue was co-evaporated twice with toluene (40 mL) to remove residual DMF. The crude material was purified by flash column chromatography (10% ethyl acetate in cyclohexane) to yield (*S*)-allyl-2-(bis(*tert*-butoxycarbonyl)amino)-5-(*tert*-butyldimethylsilyloxy)pentanoate (**13**).

Yield: 4.75 g (9.7 mmol, 95%) as a pale yellow oil.
TLC (5% ethyl acetate in cyclohexane): $R_f = 0.13$.
$[\alpha]_D^{20}$ -20.1 (*c* 1.21 in $CHCl_3$).
^{1}H NMR (400 MHz, $CDCl_3$): δ 5.81-5.93 (m, 1H), 5.28-5.32 (dd, *J* = 17.20, 1.55 Hz, 1H), 5.18-5.21 (dd, *J* = 10.50, 1.45 Hz, 1H), 4.86-4.88 (m, 1H), 4.58-4.60 (m, 2H), 3.60-3.64 (dt, *J* = 6.40, 1.80 Hz, 2H), 2.12-2.21 (m, 1H), 1.89-1.96 (m, 1H), 1.54-1.60 (m, 2H), 1.48 (s, 9H), 0.87 (s, 9H), 0.03 (s, 6H).
^{13}C NMR (100 MHz, $CDCl_3$): δ 170.5, 152.1, 131.9, 117.9, 82.9, 65.5, 62.6, 58.1, 29.6, 27.9, 26.2, 25.9, 18.3, -5.3.
LC-MS: t_R = 14.37 min, *m/z* = 510($M^+ + Na^+$, 100%), 410(M^+ - Boc + Na^+, 80) 487.70 *z* calcd for $C_{24}H_{45}NO_7Si^+$.
HRMS (EI)*: m/z* calcd for $C_{24}H_{45}O_7NNaSi^+$ $[M + Na]^+$ 510.2858, found 510.2860.

(*S*)-Allyl-2-(bis(*tert*-butoxycarbonyl)amino)-5-hydroxypentanoate (14)

(*S*)-Allyl-2-(bis(*tert*-butoxycarbonyl)amino)-5-(*tert*-butyldimethylsilyloxy)pentanoate (**13**, 4.63 g, 9.5 mmol) was dissolved in a solution of 5% water in acetone (100 mL) at RT. Copper(II) chloride dihydrate (81 mg, 0.5 mmol, 0.05 eq.) was added and the green-bluish reaction solution was heated to reflux; the color of the solution faded to a lighter green upon heating. A TLC check after 1 h indicated a complete conversion of the starting material. The solvent was evaporated to dryness and the crude product was purified by flash column chromatography (33% ethyl acetate in cyclohexane) to afford (*S*)-allyl-2-(bis(*tert*-butoxycarbonyl)amino)-5-hydroxypentanoate (**14**).

Yield: 3.27 g (8.7 mmol, 92%) as a colorless oil.
TLC (33% ethyl acetate in cyclohexane): R_f = 0.26.
$[\alpha]_D^{20}$ -30.2 (*c* 1.01 in $CHCl_3$).
^{1}H NMR (400 MHz, $CDCl_3$): δ 5.82-5.91 (m, 1H), 5.26-5.31 (dd, *J* = 17.20, 1.50 Hz, 1H), 5.17-5.20 (dd, *J* = 10.50, 1.40 Hz, 1H), 4.85-4.89 (m, 1H), 4.57-4.59 (m, 2H), 3.62-3.65 (t, *J* = 6.40, 2H), 2.17-2.26 (m, 1H), 1.87-1.97 (m, 1H), 1.57-1.64 (m, 2H), 1.46 (s, 18H).
^{13}C NMR (100 MHz, $CDCl_3$): δ 170.5, 152.1, 131.7, 118.0, 83.1, 65.6, 62.1, 57.9, 29.3, 27.9, 26.1.
LC-MS: t_R = 9.90 min (C_{18}), *m/z* = 396(M^+ + Na^+, 100%), 295(M^+ - Boc + Na^+, 80), 173(M^+ - 2Boc, 70) 374.45 calcd for $C_{18}H_{32}NO_7^+$.
HRMS (EI)*: m/z* calcd for $C_{18}H_{31}O_7NNa^+$ $[M + Na]^+$ 396.1990, found 396.1993.

(*S*)-Allyl-2-(bis(*tert*-butoxycarbonyl)amino)-5-oxopentanoate (15)

(*S*)-Allyl-2-(bis(*tert*-butoxycarbonyl)amino)-5-hydroxypentanoate (**14**, 1.60 g, 4.3 mmol) was dissolved in anhydrous DCM under an argon atmosphere. Dess-Martin´s periodinane (1.91 g, 4.5 mmol, 1.05 eq.) was added in one portion at RT resulting in a slight warming of the reaction mixture. The reaction mixture was stirred at RT for 1.5 h, whereon a TLC check indicated the complete conversion of the starting material. The reaction mixture was quenched by addition of saturated aq. K_2CO_3 solution (60 mL), the phases were separated and the aqueous layer was extracted with ethyl acetate (3x 60 mL). The combined organic extracts were washed with brine (150 mL), dried over Na_2SO_4 and the solvent was evaporated.

The crude product was purified by flash column chromatography (17% ethyl acetate in cyclohexane) yielding (*S*)-allyl-2-(bis(*tert*-butoxycarbonyl)amino)-5-oxopentanoate (**15**) which was directly used in the next step.

Yield: 1.34 g (3.6 mmol, 84%) as a colorless oil.
TLC (17% ethyl acetate in cyclohexane): R_f = 0.23.
$[\alpha]_D^{20}$ -26.2 (*c* 1.26 in $CHCl_3$).
^{1}H NMR (400 MHz, $CDCl_3$): δ 9.75 (s, 1H), 5.83-5.92 (m, 1H), 5.27-5.32 (dd, J = 17.20, 1.50 Hz, 1H), 5.18-5.21 (dd, J = 10.50, 1.40 Hz, 1H), 4.86-4.90 (m, 1H), 4.58-4.60 (m, 2H), 2.48-2.59 (m, 3H), 2.13-2.20 (m, 1H), 1.47 (s, 18H).
^{13}C NMR (100 MHz, $CDCl_3$): δ 200.8, 169.9, 152.0, 131.7, 118.2, 83.4, 65.7, 57.4, 40.4, 27.9, 22.3.
LC-MS: t_R = 11.11 min (C_{18}), *m/z* = 394($M^+ + Na^+$, 80%), 294(M^+ - Boc + Na^+, 90) 372.20 calcd for $C_{18}H_{30}NO_7^+$.
HRMS (EI)*: m/z* calcd for $C_{18}H_{30}O_7N^+$ $[M + H]^+$ 372.2017, found 372.2018.

(*S*)-9-(Allyloxy)-8-(bis(*tert*-butoxycarbonyl)amino)-9-oxonon-4-enoic acid (16)

3-(Carboxypropyl)triphenylphosphonium bromide (1.92 g, 4.5 mmol, 1.5 eq.) was suspended in anhydrous THF (20 mL) under an argon atmosphere. A 1 M lithium bis(trimethylsilyl)amide solution in THF (9.7 mL, 9.7 mmol, 3.25 eq.) was added within 40 min to the suspension at RT. The resulting dark red solution was stirred for additional 15 min at RT. The solution was then cooled to 0 °C and (*S*)-allyl-2-(bis(*tert*-butoxycarbonyl)-amino)-5-oxopentanoate (**15**, 1.11 g, 3.0 mmol) dissolved in THF (20 mL) was added over 40 min. The reaction mixture was allowed to warm to room temperature. A TLC check after 4 h indicated a completed reaction.

Subsequently, 2 M HCl was added to the reaction mixture until an acidic pH was obtained. The aqueous phase was extracted with ethyl acetate (3x 40mL) and the combined extracts were dried over Na_2SO_4. After evaporation of the solvent the crude mixture was purified by flash column chromatography (50% ethyl acetate in cyclohexane) affording (*S*)-9-(Allyloxy)-8-(bis(*tert*-butoxycarbonyl)amino)-9-oxonon-4-enoic acid (**16**) in a 9:1 ratio (*Z*/*E*).

Yield: 824 mg (1.9 mmol, 64%) as a yellow oil.

TLC (50% ethyl acetate in cyclohexane): R_f = 0.35.

^{1}H NMR (500 MHz, $CDCl_3$): δ) 5.83-5.91 (m, 1H), 5.43-5.44 (t, *J* = 5.20 Hz 1H), 5.37-5.42 (dt, *J* = 11.10 Hz, 5.90 Hz, 1H), 5.27-5.31 (d, *J* = 16.20 Hz, 1H), 5.17-5.19 (d, *J* = 10.50 Hz, 1H), 4.83-4.86 (m, 1H), 4.57-4.58 (d, *J* = 5.35 Hz, 2H), 2.28-2.40 (m, 4H), 2.11-2.19 (m, 2H), 2.02-2.06 (m, 1H), 1.89-1.95 (m, 1H), 1.47 (s, 18H).

^{13}C NMR (126 MHz, $CDCl_3$): δ 178.9, 170.5, 152.1, 131.8, 130.3, 130.0, 128.9, 128.4, 117.9, 83.0, 65.6, 57.8, 33.9, 29.7, 29.5, 29.1, 27.9.

LC-MS: t_R = 10.73 min (C_{18}), *m/z* = 486(M^+ + 2Na^+, 45%), 464(M^+ + Na^+, 45), 242(M^+ - 2Boc, 100) 442.24 calcd for $C_{22}H_{36}NO_8^+$.

HRMS (EI)*: m/z* calcd for $C_{22}H_{36}O_8N^+$ $[M + H]^+$ 442.2435, found 442.2436.

6.3 Synthesis of the *N,O*-dimethyl-3-bromotyrosine building block 29

(*S*)-Methyl-3-(3-bromo-4-methoxyphenyl)-2-(*tert*-butoxycarbonyl(methyl)amino)-propanoate (28)

The starting material (*S*)-methyl-3-(3-bromo-4-methoxyphenyl)-2-(*tert*-butoxycarbonylamino)propanoate (**27**) was prepared in 3 steps following a literature procedure.[125] For methylation of the amine, sodium hydride (60% suspension in mineral oil, 187 mg, 4.7 mmol, 1.2 eq.) was suspended in DMF (5 mL) and the suspension was stirred at ambient temperature. Methyl iodide (927 µL, 15.6 mmol, 4 eq.) and (*S*)-methyl-3-(3-bromo-4-methoxyphenyl)-2-(*tert*-butoxy-carbonylamino)propanoate (**27**, 1.51 mg, 3.9 mmol) were dissolved in DMF (5 mL) and added to the sodium hydride suspension. The resulting clear reaction solution was stirred for 1 h at RT and the reaction was quenched by the slow addition of saturated aq. NH_4Cl solution (10 mL). The aqueous phase was extracted with ether (3x 20 mL) and the combined organic extracts were washed with brine (2x 20 mL) and dried over Na_2SO_4. After evaporation to dryness the crude product was purified by flash column chromatography (33% ethyl acetate in cyclohexane) to afford (*S*)-methyl-3-(3-bromo-4-methoxyphenyl)-2-(*tert*-butoxycarbonyl(methyl)amino)-propanoate (**28**).

Yield: 1.41 g (3.5 mmol, 90%) as a colorless oil.
TLC (33% ethyl acetate in cyclohexane): $R_f = 0.54$.
$[\alpha]_D^{20}$ – 57.1 (*c* 0.93 in $CHCl_3$).
^{1}H NMR (500 MHz, $CDCl_3$): δ 7.35 (s, 1H) 7.01-7.10 (m, 1H), 6.78-6.80 (d, *J* = 8.4 Hz, 1H), 4.80 (m, 0.5H), 4.50-4.51 (m, 0.5H) (Boc rotamers), 3.83 (s, 3H), 3.72 (s, 3H), 3.17-3.19 (m, 1H), 2.87-2.96 (m, 1H), 2.70 (s, 3H), 1.33-1.37 (d, *J* = 20.2 Hz, 9H).
^{13}C NMR (126 MHz, $CDCl_3$): δ (some peaks appear double due to Boc rotamers, for this case the second peak is given in parentheses) 171.5 (171.2), 155.7, 154.8 (154.6), 133.6 (133.5), 131.2 (131.0), 129.0 (128.0), 111.9, 111,5 (111.3), 80.3 (80.0), 61.2, 56.2, 52.1, 34.2 (33.7), 32.2 (32.0), 28.1.
LC-MS: t_R = 10.93 min (C_{18}), *m/z* = 302(M^+ - Boc, 100%).
HRMS (EI)*:* *m/z* calcd for $C_{17}H_{25}O_5NBr^+$ $[M + H]^+$ 402.0911, found 402.0910, *m/z* calcd for $C_{17}H_{25}O_5N^{18}Br^+$ $[M + H]^+$ 404.0890, found 404.0889.

(*S*)-3-(3-Bromo-4-methoxyphenyl)-2-(*tert*-butoxycarbonyl(methyl)amino)propanoic acid (29)

To a solution of (*S*)-methyl-3-(3-bromo-4-methoxyphenyl)-2-(*tert*-butoxycarbonyl-(methyl)-amino)-propanoate (**28**, 1.30 g, 3.2 mmol) in THF (10 mL) and MeOH (6 mL), a solution of lithium hydroxide (155 mg, 6.5 mmol, 2 eq.) in water (4 mL) was added at ambient temperature. The reaction mixture was stirred for 5 h at RT. 1 M HCl was added to the reaction mixture until a pH of ~4 was reached. The solution was diluted with brine (20 mL) and DCM (20 mL). The phases were separated and the aqueous phase was extracted with DCM (1x 20 mL). The combined extracts were dried over Na_2SO_4 and the solvent was evaporated to dryness. The crude product was purified by flash column chromatography (10% MeOH in chloroform) to afford (*S*)-3-(3-bromo-4-methoxyphenyl)-2-(*tert*-butoxycarbonyl(methyl)amino)propanoic acid (**29**).

Yield: 985 mg (2.5 mmol, 78%) as white solid.

TLC (10% MeOH in chloroform): R_f = 0.41.

$[\alpha]_D^{20}$ -44.3 (*c* 1.15 in $CHCl_3$).

^{1}H NMR (500 MHz, $CDCl_3$): δ 7.37-7.39 (d, *J* = 10.5 Hz, 1H), 7.04-7.13 (m, 1H), 6.81-6.83 (d, *J* = 8.4 Hz, 1H), 4.74-4.75 (m, 0.5H), 4.61-4.62 (m, 0.5H) (Boc rotamers), 3.86 (s, 3H), 3.21-3.24 (m, 1H), 2.91-3.05 (m, 1H), 2.69-2.76 (d, *J* = 32.2 Hz, 3H), 1.35-1.41 (d, *J* = 27.1 Hz, 9H).

^{13}C NMR (126 MHz, $CDCl_3$): δ (some peaks appear double due to Boc rotamers, for this case the second peak is given in parentheses) 176.0 (175.8), 156.2, 154.8 (154.7), 133.7 (133.5), 131.0 (130.8), 129.0 (128.9), 112.0, 111.7 (117.2), 80.8, 61.1 (60.4), 56.2, 34.0 (33.5), 33.1 (32.3), 28.2 (28.1).

LC-MS: t_R = 9.45 min (C_{18}), *m/z* = 288(M^+ - Boc, 90%).

HRMS (EI)*: m/z* calcd for $C_{16}H_{23}O_5NBr^+$ $[M + H]^+$ 388.0754, found 388.0756, *m/z* calcd for $C_{16}H_{23}O_5N^{18}Br^+$ $[M + H]^+$ 390.0734, found 390.0735.

6.4 Solid-phase syntheses

6.4.1 General methods of the solid-phase syntheses

***Method A:** Boc deprotection and neutralization*

The dry resin was transferred to a syringe reactor and swelled in an appropriate amount of DCM for 10 min. The solvent was removed and a freshly prepared solution of 50% trifluoroacetic acid in DCM was added. The resulting suspension was shaken for 5 min, the solution was removed, fresh TFA/DCM solution was added and the resulting suspension was shaken for 1 h. The resin was filtered off and washed with DCM (2x 1 min) and 2-propanol (2x 1 min).

For neutralization, a 10% solution of triethyl amine in DCM was added to the resin and the resulting suspension was shaken for 10 min. This procedure was repeated once more, then the resin was washed alternately with DCM and 2-propanol (3x 1 min) and finally with DMF (2x 1 min).

***Method B:** Fmoc deprotection*

A solution of 20% piperidine in DMF was added to the resin and the resulting suspension was shaken for 15 min. The solution was removed from the resin and the solid support was washed with DMF (5x 1 min). Fresh piperidine/DMF solution was added and the resulting suspension was shaken once more for 15 min. The solution was removed and the resin was washed alternately with MeOH and DCM (3x 1 min) and finally with DMF (5x 1 min).

***Method C:** Allyl ester/Alloc deprotection*

In addition to the regular washing protocol performed after amino acid couplings, an additional washing protocol was required to prepare the resin for cleavage of an allyl ester/Alloc. The resin was washed with MeOH (2x 1 min), alternatingly with MeOH and DCM (2x 1 min), DMF (5x 1 min), NMP (5x 1 min), DCM (2x 1 min) and finally with diethyl ether (2x 1 min). Subsequently, the resin was then dried under high vacuum (overnight for NovaPEG resin, 1 h for chlorotrityl resin).

For the cleavage of the allyl ester or the Alloc group, the dried resin was transferred into a pear shaped flask under an argon atmosphere and was degassed under high vacuum for

15 min using an ultrasonication bath. The resin was washed with degassed DCM (3x 2 min) and during this washing step argon was bubbled through the suspension. After each washing step, the solvent was removed carefully using a cannula. After the last washing step, degassed DCM was added, followed by a solution of degassed morpholine (24 eq.) in degassed DCM. Again, argon was bubbled through the suspension for 2 min. Finally, $Pd(PPh_3)_4$ (0.25 eq.) dissolved in degassed DCM was added to the suspension and argon was again bubbled through the resulting suspension for 2 min. The reaction flask was subsequently placed on an orbital shaker and shaken gently for 30 min.

The resin was removed carefully with a glass pipette and transferred to a syringe reactor to facilitate the washing steps. The resin was washed with DCM (3x 1 min), NMP (3x 1 min) and DCM (4x 1 min). This washing procedure was repeated once more. The washing procedure was then continued with DCM (3x 1 min), NMP (3x 1 min), a 0.02 M solution of Et_2NCS_2Na in NMP (3x 5 min), NMP (5x 1 min) and DMF (2x 1 min).

Method D: *Amino acid coupling*

The amino acid (4 eq.) was dissolved in an appropriate amount of DMF. Subsequently, HOBt (4 eq.), HBTU (3.5 eq.) and DIEA (3 eq.) were added to the amino acid solution and the resulting mixture was gently shaken for 1 min to pre-activate the amino acid. The solution was added to the resin, the resulting reaction suspension was shaken for an appropriate time (2 to 24 h, respective values are given in the experiment description). The reaction solution was discarded and the resin was washed with DMF (2x 1 min), alternatingly with MeOH and DCM (3x 1 min) and then again with DMF (5x 1 min).

***Method E*:** *Esterification of the threonine sidechain*

For the esterification of the threonine sidechain, Fmoc-Val-OH (10 eq.), DIC (10 eq.) and DMAP (1 eq.) were dissolved in a 10% solution of DMF in DCM and added directly to the resin. The coupling was performed for 2 h and repeated 3 times in total. Between the individual couplings, the resin was washed with DMF (2x 1 min), alternatingly with MeOH and DCM (3x 1 min) and with DMF (2x 1 min). After the final coupling, the resin was then washed with DMF (2x min), alternatingly with MeOH and DCM (3x 1 min) and with DMF (5x 1 min).

***Method F:** Fmoc determination*

A small aliquot of dry resin (~ 5 mg) was transferred into a 25 mL pear shaped flask and a freshly prepared 20% piperidine in DMF solution (5 mL) was added (in total 10 mL of the piperidine/DMF solution were prepared, either for dilution of the sample and as a reference blank for the UV measurement). The resulting suspension was shaken for 20 min. The resin was allowed to settle and the UV absorption of 1 mL of the cleavage solution or a dilution thereof (e.g 33%) was measured, using a Cary instrument type 100 Bio. The silica glass cuvettes had a thickness of 10 mm. The measurement was repeated at least 3 times.
According to the formula

$$c = \frac{A \cdot V}{\varepsilon \cdot d \cdot m \cdot F} \left[mmol / g \right]$$

in which *A* is the absorption at 300.7 nm, *V* the total volume (here: 5 [mL]), ε the extinction coefficient (here: 780 [ml/mmol ·mm]), *d* the thickness of the cuvette (here: 10 [mm]), *m* the mass of resin in [g] and *F* the dilution factor (1, 1/3, 1/6, …), the loading of the resin was determined from the measurement of the absorption.

***Method G:** Kaiser test*

A few beads were sampled into a small vial. 3 drops of a 5% solution of ninhydrine in ethanol, 2 drops of a 20% solution of phenole in ethanol and 3 drops of a 2% solution of aq. potassium cyanide (0.001 M) in pyridine were added and the resulting suspension was heated to 100 °C for 5 min. A blue solution and/or blue beads indicate the presence of primary amines.

***Method H:** Chloranil test*

A few beads were sampled into a small vial. 2 drops of a 2% solution of acetaldehyde in DMF and 2 drops of a 2% solution of chloranil in DMF were added to the resin. The resulting suspension was allowed to stand for at 5-10 min at RT. Blue- to green-stained beads indicate the presence of secondary amines.

Method I: *Cleavage from 2-chlorotrityl resin*

The dried resin was transferred to a fresh solid phase reactor and a solution of acetic acid/ trifluoroethanol/DCM (20%/20%/60%) was added. The mixture was shaken for 2 h at RT. After this time the solution containing the cleaved peptide was collected and the resin was washed once with the cleavage solution and with DCM (3x 2 min); these solutions were also collected. The solvent was removed and the remaining oil was co-evaporated twice with cyclohexane to remove residual acetic acid.

Method J: *full deprotection of cleaved peptides (removing Trt, Boc and t-Bu)*

The crude peptide was dissolved in trifluoroacetic acid/DCM/tri*iso*propylsilane (95%/2.5%2.5%) (~1 mL) and stirred for 2 h at RT. The reaction mixture was added to cold ether resulting in the precipitation of the crude peptide. The suspension was centrifuged and the pellet was washed once with cold ether. After centrifugation the remaining pellet was dried by evaporation of the ether at RT and normal pressure.

Method K: *Hydrogenation to remove the benzyl ether protection on the serine sidechain*

The crude peptide was dissolved in EtOH (1 mL/100 mg crude peptide) and acetic acid (0.1 mL/100 mg crude peptide) and transferred to a two-neck round bottom flask equipped with a stop-cock and a rubber septum under an argon atmosphere containing Pd/C catalyst (10 %, 0.4 mg catalyst/mg crude product). The flask was equipped with a hydrogenation balloon and flushed with hydrogen by opening the stop-cock from time to time. The hydrogenation was carried out overnight at RT and the reaction mixture was filtered through a short pad of Celite® which was washed intensively with MeOH. The solvent was removed and the residue was dissolved in the minimal amount of ethyl acetate (and optionally a few drops of MeOH to enhance solubility). This solution was added to cold ether, resulting in the precipitation of the crude peptide. The suspension was centrifuged and the pellet was washed once with cold ether and dried after centrifugation.

6.4.2 Solid-phase synthesis of the symplocamide A model Ahp cyclodepsipeptide 19

Coupling of (*S*)-9-(Allyloxy)-8-(bis(*tert*-butoxycarbonyl)amino)-9-oxonon-4-enoic acid (16) to NovaPEG amino resin

NovaPEG amino resin (0.66 mmol/g, 1.00 g, 0.66 mmol) was transferred to a glass solid-phase reactor under an argon atmosphere and swollen in a mixture of 10% anhydrous DMF in anhydrous DCM for 30 min under gentle shaking.

(*S*)-9-(Allyloxy)-8-(bis(*tert*-butoxycarbonyl)amino)-9-oxonon-4-enoic acid (**16**, 706 mg, 1.60 mmol, 2.4 eq.), HOBt (446 mg, 3.30 mmol, 5 eq.) and DIC (514 µL, 3.30 mmol, 5 eq.) were dissolved in a 10% mixture of anhydrous DMF in anhydrous DCM (10 mL) and stirred for 20 min. This pre-activated solution was added to the pre-swollen resin and shaken for 24 h at RT. The reaction solution was removed and the resin was washed with DMF (2x 1 min), MeOH (2x 1 min) and DCM (2x 1 min). To eliminate remaining amino groups on the resin, a capping reaction was carried out. To this end, the resin was shaken with a mixture of acetic anhydride/DIEA/DCM (1:1:3) for 3 h and washed with DMF (2x 1 min), alternately with MeOH and DCM (3x 1 min) and finally with DMF (2 x 1 min). A Kaiser test performed according to *method G* then indicated the complete capping of all unreacted amines.

The resin loaded with the Ahp precursor will be called NovaPEG-Ahp5COAll (**17**) in the following descriptions.

Coupling of Fmoc-Cit-OH to NovaPEG-Ahp5-COAll (17)

The resin **17** (0.66 mmol) was deprotected according to *method A*. The coupling of Fmoc-Cit-OH to the resin was performed using *method D*. The amounts of reagents used were:

Fmoc-Cit-OH: 1.05 g, 2.64 mmol
HOBt: 332 mg, 2.64 mmol
HBTU: 877 mg, 2.31 mmol
DIEA: 327 µL, 1.98 mmol.

The coupling was performed for 5 h. A Kaiser test performed according to *method G* indicated a complete coupling reaction.

After the regular washing, an additional washing step was carried out using alternately anhydrous MeOH and DCM (3x 1 min) and finally anhydrous ether (3x 1 min). The resulting resin **18** was dried under high vacuum overnight.

The Fmoc determination carried out with 6.4 mg of resin according to *method F* revealed a resin loading of 0.20 mmol/g (30%).

Sequential coupling of Fmoc-Thr-OH and Fmoc-Gln(Trt)-OH to NovaPEG-Ahp5-COAll-Cit4-Fmoc (18)

NovaPEG-Ahp5-COAll-Cit4-Fmoc (**18**, loading of 0.20 mmol/g, 1.12 g, 0.22 mmol) was deprotected according to *method B*. The coupling of Fmoc-Thr-OH*H_2O to the resin was performed using *method D*. The following amounts of reagents were used:

Fmoc-Thr-OH*H_2O: 322 mg, 0.90 mmol
HOBt: 121 mg, 0.90 mmol
HBTU: 298 mg, 0.78 mmol
DIEA: 111 µL, 0.67 mmol.

The coupling reaction was performed for 2 h. A Kaiser test performed according to *method G* indicated a complete coupling reaction.

NovaPEG-Ahp5-COAll-Cit4-Thr3-Fmoc (0.20 mmol) was deprotected according to *method B*. The coupling of Fmoc-Gln(Trt)-OH to the resin was performed using *method D*. The amounts of reagents were:

Fmoc-Gln(Trt)-OH: 547 mg, 0.90 mmol
HOBt: 121 mg, 0.90 mmol
HBTU: 298 mg, 0.78 mmol
DIEA: 111 µL, 0.67 mmol.

The coupling was performed for 2 h. A Kaiser test following *method G* indicated a complete coupling reaction.

After the regular washing, an additional washing step was carried out using alternately anhydrous MeOH and DCM (3x 1 min) and finally anhydrous ether (3x 1 min). The resulting resin **19** was dried under high vacuum overnight.

The Fmoc determination carried out with 5.1 mg of resin according to *method F* revealed a resin loading of 0.17 mmol/g (77%, 2 couplings).

Coupling of butyric acid to NovaPEG-Ahp5-COAll-Cit4-Thr3-Gln2(Trt)-Fmoc (19) and esterification of the threonine sidechain with Fmoc-Val-OH

NovaPEG-Ahp5-COAll-Cit4-Thr3-Gln2(Trt)-Fmoc (**19**, loading of 0.17 mmol/g, 1.14 g, 0.20 mmol) was deprotected according to *method B*. The coupling of butyric acid to the resin was performed using *method D*. The amounts of reagents were:

butyric acid: 73 µL, 0.80 mmol
HOBt: 108 mg, 0.80 mmol
HBTU: 265 mg, 0.70 mmol
DIEA: 99 µL, 0.60 mmol.

The coupling reaction was performed for 2 h and a Kaiser test performed according to *method G* indicated a complete coupling reaction after this time.

The esterification of the threonine sidechain was carried out following *method E*. The amounts of reagents used for this reaction were:

Fmoc-Val-OH: 679 mg, 2.00 mmol, 10 eq.
DIC: 312 µL, 2.00 mmol, 10 eq.
4-(dimethylamino)pyridine: 24 mg, 0.2 mmol, 1 eq.

After the washing protocol, the resin was washed additionally with anhydrous solvents: alternately MeOH and DCM (3x 1 min) and ether (3x 1 min). The resulting resin **20** was dried overnight under high vacuum.

An Fmoc determination performed according to *method F* with 4.9 mg of resin gave a loading of 0.15 mmol/g (79%, 2 couplings).

Sequential coupling of Fmoc-*N*MePhe-OH and Fmoc-Ile-OH to NovaPEG-Ahp5-COAll-Cit4-Thr3(O-CO-Val8-Fmoc)-Gln2(Trt)-But1 (20)

NovaPEG-Ahp5-COAll-Cit4-Thr3(O-CO-Val8-Fmoc)-Gln2(Trt)-But1 (**20**, loading of 0.15 mmol/g, 1.07 g, 0.16 mmol) was deprotected according to *method B*. The coupling of Fmoc-*N*MePhe-OH to the resin was performed using *method D*. The amounts of reagents were:

Fmoc-*N*MePhe-OH: 199 mg, 0.64 mmol
HOBt: 86 mg, 0.64 mmol
HBTU: 213 mg, 0.56 mmol
DIEA: 79 µL, 0.48 mmol.

The coupling was performed for 2 h. A Kaiser test performed according to *method G* indicated a complete coupling reaction.

NovaPEG-Ahp5-COAll-Cit4-Thr3(O-CO-Val8-mPhe7-Fmoc)-Gln2(Trt)-But1 was deprotected according to *method B*. For the coupling of Fmoc-Ile-OH to the *N*-methylated amino acid, PyBrOP was used as the coupling reagent. The following reagents were dissolved in DMF, pre-activated for 1 min and then added to the resin.

Fmoc-Ile-OH: 283 mg, 0.8 mmol, 5 eq.
PyBrOP: 366 mg, 0.78 mmol, 4.9 eq.
DIEA: 264 µL, 1.6 mmol, 10 eq.

The coupling was performed for 24 h. A chloranil test performed according to *method H* indicated a complete coupling.

After the regular washing, an additional washing protocol using anhydrous solvents was performed. The resin was washed alternately with MeOH and DCM (3x 1 min) and ether (3x 1 min) and the resulting resin **21** was dried under high vacuum overnight.

The following Fmoc determination with 4.9 mg of resin was carried out using *method F* revealed a loading of 0.088 mmol/g (60%, 2 couplings).

Deprotection of NovaPEG-Ahp5-COAll-Cit4-Thr3(O-CO-Val8-mPhe7-Ile6-Fmoc)-Gln2(Trt)-But1 (21)

The Fmoc deprotection of NovaPEG-Ahp5-COAll-Cit4-Thr3(O-CO-Val8-mPhe7-Ile6-Fmoc)-Gln2(Trt)-But1 (**21**, 0.088 mmol/g, 1.09 g, 0.096 mmol) was carried out using *method B*, the resin was then treated according to *method C* in order cleave the allyl ester protection.

This procedure afforded the NovaPEG-Ahp5-COOH-Cit4-Thr3(O-CO-Val8-mPhe7-Ile6-NH_2)-Gln2-But1 (**22**) intermediate.

On resin macrolactamization of NovaPEG-Ahp5-COOH-Cit4-Thr3(O-CO-Val8-mPhe7-Ile6-NH$_2$)-Gln2(Trt)-But1 (22)

HOBt (104 mg, 0.77 mmol, 8 eq.) and DIEA (190 µL, 1.15 mmol, 12 eq.) were dissolved in DMF and added to resin **22**. The resin was shaken for 1 min and a solution of PyBOP (171 mg, 0.38 mmol, 4 eq.) in DMF was added to the resin, which was shaken for 24 h.

The resin was washed with DMF (2x 1 min), alternatingly with MeOH and DCM (3x 1 min), DMF (5x 1 min), DCM (2x 1 min) and finally with ether (3x 1 min) and the resin was dried under high vacuum for 1 h. A Kaiser test according to *method G* indicated a complete reaction.

Oxidative cleavage from the resin to obtain Ahp peptide 24

Sodium periodate (205 mg, 0.96 mmol, 10 eq.) and DABCO (54 mg, 0.48 mmol, 5 eq.) were suspended in water (8 mL), sonificated briefly and added to resin **23** (0.096 mmol). The resin was allowed to stand in this mixture for 10 min, then THF (8 mL) was added and the resulting suspension was shaken for 2 min. Subsequently, a 0.1 M solution of osmium tetroxide in *tert*-butanol (59 µL, 0.005 mmol, 0.05 eq.) was added to the suspension, which was shaken for 20 h.

The cleavage solution was collected and quenched with an aq. saturated sodium metabisulfite solution. The resin was washed with a 1:1 (v/v) solution of THF/water (5x 20 mL) and the washing phases were added to the sodium metabisulfite solution. The phases in this solution were allowed to separate and the aqueous phase was extracted with ethyl acetate (5x 80 mL). The combined organic extracts were dried over Na_2SO_4 and the solvent was evaporated. The resulting crude mixture was re-dissolved in ethyl acetate (1 mL) followed by transfer of the whole reaction mixture to cold ether, thereby causing the crude product to precipitate as a white solid. The precipitate was centrifuged at 4 °C; the supernatant removed and fresh cold ether was added. The suspension was sonificated briefly and centrifuged again at 4 °C, the supernatant was removed and the precipitate was allowed to dry.

The crude product (58 mg) was purified by preparative HPLC using a preparative C_4 column and a linear gradient starting from 10% acetonitrile in H_2O to yield 3.1 mg (2.6 µmol, 1.2%) of Ahp cyclodepsipeptide **24** as a white solid.

^{1}H NMR (600 MHz, DMSO-d$_6$): δ 8.48 (d, *J* = 8.5 Hz, 1H), 8.27 (s, 1H), 8.04 (d, *J* = 7.8 Hz, 1H), 7.73 (d, *J* = 9.2 Hz, 1H), 7.65 (d, *J* = 9.4 Hz, 1H), 7.34 (d, *J* = 9.1 Hz, 1H), 7.24-7.28 (m, 5H), 7.16-7.20 (m, 15H), 6.09 (bs, 1H), 5.92 (bs, 2H), 5.15-5.17 (m, 1H), 4.93-4.92 (m, 1H), 4.66-4.67 (m, 1H), 4.44-4.45 (m, 1H), 4.43-4.44 (m, 1H), 4.39-4.41 (m, 1H), 4.32-4.33 (m, 1H), 4.24-4.23 (m, 1H), 3.76-3.75 (m, 1H), 3.51 (s, 3H), 3.10-3.06 (m, 2H), 3.02 (s, 1H), 2.92 (d, *J* = 5.6 Hz, 1H), 2.37-2.39 (m, 1H), 2.14-2.09 (m, 3H), 2.03-2.00 (m, 2H), 1.99-1.96 (m, 2H), 1.86-1.84 (m, 2H), 1.72-1.75 (m, 2H), 1.69-1.64 (m, 2H), 1.52-1.56 (m, 4H), 1.29 – 1.27 (m, 2H), 1.23 (s, 3H), 1.21-1.22 (m, 5H), 0.88-0.84 (m, 3H), 0.75 (d, *J* = 6.8 Hz, 3H), 0.61 (d, *J* = 3.1 Hz, 3H), -0.25 (d, *J* = 6.4 Hz, 1H);

LC-MS: t_R = 9.91 min, *m/z* = 1207(M^+ + Na^+,100%), 1185 (M^+ - H^+, 20) 1185.63 calcd for $C_{64}H_{85}N_{10}O_{12}^+$.

6.4.3 Solid-phase synthesis of symplocamide A

Coupling of (*S*)-9-(Allyloxy)-8-(bis(*tert*-butoxycarbonyl)amino)-9-oxonon-4-enoic acid (16) to NovaPEG amino resin

NovaPEG amino resin (0.66 mmol/g, 1.00 g, 0.66 mmol, 1 eq.) was transferred to a glass solid-phase reactor under an argon atmosphere and swelled in anhydrous DCM (20 mL) for 1 h. (*S*)-9-(Allyloxy)-8-(bis(*tert*-butoxycarbonyl)amino)-9-oxonon-4-enoic acid (**16**, 729 mg, 1.65 mmol, 2.5 eq.), HOBt (357 mg, 2.64 mmol, 4 eq.), HBTU (877 mg, 2.31 mmol, 3.5 eq.) and anhydrous DIEA (327 µL, 1.98 mmol, 3 eq.) were dissolved in a solution of 10% anhydrous DMF in anhydrous DCM (15 mL) under an argon atmosphere and pre-activated for 30 min at RT. The solvent was removed from the resin and re-suspended in a 10% DMF in DCM solution (15 mL) and shaken gently for 10 min. The pre-activated amino acid solution was added to the resin and the resulting suspension was shaken for 24 h.

The reaction solution was removed and the resin was washed with DMF (2x 1 min), MeOH (2x 1 min) and DCM (2x 1 min). A capping step was subsequently performed to block unreacted amines. To this end, a solution of DCM, DIEA and acetic anhydride (3:1:1, (v/v/v)) was added to the resin and the resulting suspension was shaken for 2 h. After removal of the solution, a fresh capping solution was added and the resin was again shaken for 2 h. The resin was washed with DMF (5x 1 min), alternately with MeOH and DCM (3x 1 min) and finally with DMF (2x 1 min). The subsequent Kaiser test performed according to *method G* indicated the complete capping of all unreacted amines. The resulting resin is named as NovaPEG-Ahp5COAll (**30**) in the following.

Coupling of Fmoc-Cit-OH to NovaPEG-Ahp5COAll (30)

The resin **30** (0.66 mmol) was deprotected following *method A*. The coupling of Fmoc-Cit-OH to the resin was performed according to *method D*. The amounts of reagents were:
Fmoc-Cit-OH: 1.05 g, 2.64 mmol
HOBt: 357 mg, 2.64 mmol
HBTU: 877 mg, 2.31 mmol
DIEA: 327 µL, 1.98 mmol.
The coupling reaction was performed for 4 h. After the regular washing, an additional washing procedure consisting of washing alternately with anhydrous MeOH and DCM (3x 1 min) and finally anhydrous ether (3x 1 min) was performed. The resin was then dried under high vacuum overnight.
A Kaiser test according to *method G* indicated a quantitative coupling.
The loading of the resulting NovaPEG-Ahp5COAll-Cit4-Fmoc resin (**31**) was measured as described in *method F* using 5.8 mg of resin and revealed a resin loading of 0.24 mmol/g (36% loading yield, 2 couplings).

Sequential coupling of Fmoc-Thr-OH and Boc-Gln-OH to NovaPEG-Ahp5COAll-Cit4-Fmoc (31)

NovaPEG-Ahp5COAll-Cit4-Fmoc (**31**, loading of 0.24 mmol/g, 1.12 g, 0.27 mmol) was deprotected according to *method B*. The coupling of Fmoc-Thr-OH to the resin was performed using *method D.* The amounts of reagents used for the coupling were:
Fmoc-Thr-OH*H_2O: 388 mg, 1.08 mmol
HOBt: 146 mg, 1.08 mmol
HBTU: 359 mg, 0.95 mmol
DIEA: 134 µL, 0.81 mmol.

The coupling was performed for 5 h. The Kaiser test performed following *method G* remained negative, thereby indicating a complete conversion of **31** to NovaPEG-Ahp5COAll-Cit4-Thr3-Fmoc.

NovaPEG-Ahp5COAll-Cit4-Thr3-Fmoc (0.27 mmol) was deprotected following to *method B*. The coupling of Boc-Gln-OH to the resin was carried out using *method D.* The amounts of reagent were:

Boc-Gln-OH: 266 mg, 1.08 mmol
HOBt: 146 mg, 1.08 mmol
HBTU: 359 mg, 0.95 mmol
DIEA: 134 µL, 0.81 mmol.

The coupling was performed for 4 h. The Kaiser test performed according to *method G* indicated a complete conversion to NovaPEG-Ahp5COAll-Cit4-Thr3-Gln2-Boc (**32**).

Coupling of butyric acid (But-OH) to NovaPEG-Ahp5COAll-Cit4-Thr3-Gln2-Boc (32) and esterification of the threonine sidechain with Fmoc-Val-OH

The deprotection of NovaPEG-Ahp5COAll-Cit4-Thr3-Gln2-Boc (**32**, 0.27 mmol) was performed according to *method A*. The coupling of butyric acid to the resin was achieved following *method D.* The amounts of reagents were:

But-OH: 99 µL, 1.08 mmol
HOBt: 146 mg, 1.08 mmol
HBTU: 359 mg, 0.95 mmol
DIEA: 134 µL, 0.81 mmol.

The coupling was performed for 4 h. The Kaiser test carried out according to *method G* indicated a complete conversion of **32** to NovaPEG-Ahp5COAll-Cit4-Thr3-Gln2-But1.

The esterification of the threonine sidechain with Fmoc-Val-OH was carried out according to *method E* using the following amounts of reagents:

Fmoc-Val-OH: 916 mg, 2.70 mmol, 10 eq.
4-(dimethylamino)pyridine: 33 mg, 0.27 mmol, 1 eq.
N,N'-di*iso*propylcarbodiimide: 421 µL, 2.70, 10 eq.

After the washing step an additional washing step consisting of washing alternately with anhydrous MeOH and DCM (3x 1 min) and anhydrous ether (3x 1 min) was performed. The resin was dried under high vacuum overnight.

The loading of NovaPEG-Ahp5COAll-Cit4-Thr3(O-CO-Val8-Fmoc)-Gln2-But1 (**33**) was measured as described in *method F* using 6.8 mg of resin, revealing a resin loading of 0.22 mmol/g (92%, 4 couplings).

Sequential coupling of *N*-Boc-*N*-Methyl-3-bromomethyltyrosine (Boc-mTyr(3-Br,4-OMe)-OH) (29) and Fmoc-Ile-OH to NovaPEG-Ahp5-COAll-Cit4-Thr3(O-CO-Val8-Fmoc)-Gln2-But1 (33)

NovaPEG-Ahp5COAll-Cit4-Thr3(O-CO-Val8-Fmoc)-Gln2-But1 (**33**, 0.22 mmol/g, 1.19 g, 0.26 mmol) was deprotected following *method B*. The coupling of Boc-mTyr(3-Br,4-OMe)-OH to the resin was carried out using *method D.* The amounts of reagents used for this reaction were:

Boc-mTyr(3-Br,4-OMe)-OH (**29**): 396 mg, 1.02 mmol
HOBt: 138 mg, 1.02 mmol
HBTU: 339 mg, 0.89 mmol
DIEA: 126 µL, 0.77 mmol.

The coupling was performed for 4.5 h. The Kaiser test performed following *method G* indicated a complete conversion to NovaPEG-Ahp5-COAll-Cit4-Thr3(O-CO-Val8-mTyr7(3-Br,4-OMe)-Boc)-Gln2-But1.

The deprotection of NovaPEG-Ahp5-COAll-Cit4-Thr3(O-CO-Val8-mTyr7(3-Br,4-OMe)-Boc)-Gln2-But1 (0.26 mmol) was performed according to *method A*. The coupling of Fmoc-Ile-OH to the resin was carried out using PyBrOP as the coupling reagent. The following reagents were dissolved in DMF, pre-activated for 1 min and then added to the resin.

Fmoc-Ile-OH: 451 mg, 1.28 mmol, 5 eq.
PyBrOP: 583 mg, 1.25 mmol, 4.9 eq.
DIEA: 421 µL, 2.55 mmol, 10 eq.

The coupling was performed for 24 h. After the coupling, the resin was washed with DMF (2x 1 min), alternately with MeOH and DCM (3x 1 min), DMF (5x 1 min), alternately with anhydrous MeOH and DCM (3x 1 min) and finally with anhydrous ether (3x 1 min). Subsequently, the resin was dried under high vacuum overnight. The chloranil test according to *method H* remained negative, indicating a complete conversion to NovaPEG-Ahp5-COAll-Cit4-Thr3(O-CO-Val8-mTyr7(3-Br,4-OMe)-Ile6-Fmoc)-Gln2-But1 (**34**)

The loading of NovaPEG-Ahp5-COAll-Cit4-Thr3(O-CO-Val8-mTyr7-(3-Br,4-OMe)-Ile6-Fmoc)-Gln2-But1 (**34**) was measured as described in *method F* using 5.0 mg of resin, revealing a loading of 0.16 mmol/g (73%, 2 couplings).

Full deprotection of NovaPEG-Ahp5-COAll-Cit4-Thr3(O-CO-Val8-mTyr7-(3-Br,4-OMe)-Ile6-Fmoc)-Gln2-But1 (34)

The final Fmoc deprotection of **34** (0.16 mmol/g, 1.27 g, 0.20 mmol) was performed according to *method B* and the resulting resin was then treated according to *method C* in order to cleave the allyl ester protection.

This procedure then afforded the NovaPEG-Ahp5-COOH-Cit4-Thr3(O-CO-Val8-mTyr7-(3-Br,4-OMe)-Ile6-NH_2)-Gln2-But1 (**35**) intermediate.

On resin macrolactamization of NovaPEG-Ahp5-COOH-Cit4-Thr3(O-CO-Val8-mTyr7-(3-Br, 4-OMe)-Ile6-NH_2)-Gln2-But1 (35)

To the fully deprotected intermediate resin **35** (0.20 mmol), a solution of HOBt (216 mg, 1.60 mmol, 8 eq.) and DIEA (397 µL, 2.40 mmol, 12 eq.) in DMF was added and the resulting suspension was shaken 1 min for pre-activation. A solution of PyBOP (357 mg, 0.80 mmol, 4 eq.) in DMF was added and the resulting reaction mixture was shaken for 24 h.

The resin was washed with DMF (2x 1 min), alternately with MeOH and DCM (3x 1 min), DMF (5x 1 min), DCM (2x 1 min) and finally with diethyl ether (2x 1 min). The resin was then dried under high vacuum for 1 h, resulting in resin **36**. A Kaiser test following *method G* indicated a complete reaction.

Oxidative cleavage of resin 36 to symplocamide A

Sodium periodate (428 mg, 2.00 mmol, 10 eq.) and DABCO (112 mg, 1.00 mmol, 5 eq.) were suspended in water (8 mL), sonificated briefly and added to resin **36** (0.20 mmol). The resin was allowed to swell in this mixture for 10 min, after which THF (8 mL) was added and the resulting suspension was shaken for 2 min. Subsequently, a 0.1 M solution of osmium tetroxide in *tert*-butanol (123 µL, 0.01 mmol, 0.05 eq.) was added to the suspension, which was shaken for further 20 h.

The cleavage solution was collected and quenched with an aq. saturated sodium metabisulfite solution (100 mL). The resin was washed with a 1:1 (v/v) solution of THF/water (5x 20 mL), the washing phases were added to the sodium metabisulfite solution. The phases in this solution were allowed to separate and the aqueous phase was extracted with ethyl acetate (5x 80 mL). The combined organic extracts were dried over Na_2SO_4 and the solvent was evaporated. The resulting crude mixture was re-dissolved in ethyl acetate (1 mL) and a few drops of trifluoroacetic acid were added, followed by transfer of the whole reaction mixture to cold ether, thereby causing the crude product to precipitate as a white solid. The precipitate was centrifuged at 4 °C; the supernatant removed and fresh cold ether was added. The suspension was sonificated briefly and centrifuged again at 4 °C, then the supernatant was removed and the precipitate was allowed to dry.

The crude product (65 mg) was purified by preparative HPLC (0 min / 10% B → 3 min / 10% B → 15 min / 32% B → 40 min / 45% B → 41 min / 100% B → 51 min / 100% B) to afford 8.4 mg (8 µmol, 3%) symplocamide A as a light yellow glass.
$[\alpha]_D^{20}$ -21.7 (*c* 0.06 in MeOH).
^{1}H NMR (600 MHz, DMSO-d_6): δ 8.49 (d, J = 8.65 Hz, 1H), 8.05 (d, J = 7.30 Hz, 1H), 7.82 (d, J = 8.95 Hz, 1H), 7.66 (d, J = 9.00 Hz, 1H), 7.34 (d, J = 9.25 Hz, 1H), 7.31 (bs, 1H), 7.20 (d, J = 7.15 Hz, 1H), 7.03 (d, J = 8.40 Hz, 1H), 6.74 (bs, 1H), 6.13 (bs, 1H), 5.97 (bs, 1H), 5.51 (m, 1H), 5.37 (bs, 2H), 5.06 (d, J = 11.80 Hz, 1H), 4.93 (bs, 1H), 4.65 (m, 1H), 4.48-4.49 (m, 1H), 4.44 (m, 1H), 4.37-4.39 (m, 2H), 4.25 (m, 1H), 3.77 (s, 1H), 3.22-3.24 (m, 1H), 2.94 (m, 1H), 2.77-2.80 (m, 1H), 2.74 (s, 3H), 2.57-2.61 (m, 1H), 2.16-2.17 (m, 2H), 2.12 (t, J = 6.75 Hz, 2H), 2.04-2.06 (m, 1H), 1.98-2.01 (m, 2H), 1.78-1.80 (m, 1H), 1.73-1.75 (m, 4H), 1.53 (m, 2H), 1.46 (m, 1H), 1.24 (m, 2H), 1.21 (d, J = 5.50 Hz, 2H), 1.10 (m, 2H), 0.87 (m, 6H), 0.76 (d, J = 6.20 Hz, 3H), 0.63 (m, 3H), -0.14 (d, J = 5.50 Hz, 3H).
^{13}C NMR (151 MHz, DMSO-d_6): δ 174.4, 174.0, 172.5, 172.4, 170.3, 169.8, 169.5, 169.3, 169.3, 158.1, 154.6, 129.8, 128.1, 126.5, 116.5, 111.2, 74.1, 72.05, 63.0, 60.6, 56.4, 54.9, 54.3, 52.5, 52.2, 49.0, 37.2, 36.6, 35.2, 33.1, 32.9, 31.7, 31.4, 30.3, 28.9, 28.8, 28.7, 26.7, 25.2, 22.2, 19.4, 18.8, 17.8, 17.8, 13.9, 13.7, 10.4.
LC-MS: t_R = 7.35 min, *m/z* = 1053($M^+ + H^+$,75%), 1035 ($M^+ - H_2O$, 100).
HRMS (ESI)*: m/z* calcd for $C_{46}H_{72}O_{13}N_{10}Br^+$ $[M + H]^+$ 1051.4458, found 1051.4463, *m/z* calcd for $C_{46}H_{72}O_{13}N_{10}{}^{81}Br^+$ $[M + H]^+$ 1053.4438, found 1053.4446.

6.4.4 Synthesis of structure-activity analogs of Ahp cyclodepsipeptides

6.4.4.1 Synthesis of SAR-1 and SAR-2: (1: Ahp→Ser, 2: Ahp→Hse)

Loading of Fmoc-Cit-OH onto 2-chlorotrityl resin

2-chlorotrityl resin (1.6 mmol/g, 1.20 g, 1.92 mmol) was transferred to a glass solid-phase reactor under an argon atmosphere. To the resin was added a solution of Fmoc-Cit-OH (917 mg, 2.30 mmol, 1.2 eq.) and DIEA (2.12 mL, 7.68 mmol, 4.0 eq.) in DCM (15 mL) and the resin was shaken gently at RT overnight. The resin was capped with a solution of DCM/MeOH/DIEA (85%/10%/5%) which was applied 3x 5 min. The resin was washed with DMF (2x 1 min), alternatingly with MeOH and DCM (3x 1 min), DMF (3x 1 min) and finally with DCM (3x 1 min). After drying under high vacuum, the loading of the resin was determined according to *method F* and the loading was determined to 0.62 mmol/g (39%). The resulting resin was used for the syntheses of **SAR-1**, **SAR-2**, **SAR-4**, **SAR-6**, **SAR-7**, **SAR-8** and **SAR-9**.

Coupling of Fmoc-Thr-OH, Fmoc-Gln(Trt)-OH and butyric acid

The dried resin (0.62 mmol/g, 520 mg, 0.32 mmol) was transferred into a solid-phase syringe reactor for the subsequent couplings.
The resin was deprotected prior to every coupling according to *method B*.
The amino acids were coupled using the protocol described in *method D*.
A Kaiser test following the protocol in *method G* was performed after each coupling.
The following amounts of reagents and coupling times were used for the respective couplings:
HOBt: 173 mg, 1.28 mmol
HBTU: 425 mg, 1.12 mmol
DIEA: 160 µL, 0.96 mmol.

Fmoc- Thr-OH*H_2O: 460 mg, 1.28 mmol
The coupling was performed for 2 h, the Kaiser test performed after the coupling remained negative, indicating a complete coupling.

Fmoc-Gln(Trt)-OH: 782 mg, 1.28 mmol

The coupling was performed for 2 h, after which the Kaiser test turned positive. The required double coupling was performed as an overnight reaction using the same amounts of reagents again. The Kaiser test performed after this coupling remained negative.

butyric acid: 117.5 µL, 1.28 mmol

The coupling was performed for 5 h, after which the Kaiser test remained negative, thereby indicating a complete coupling.

Esterification with Fmoc-Val-OH

The esterification of the threonine side chain was performed following *method E*, using the following amounts of reagents:

Fmoc-Val-OH: 1.09 g, 3.20 mmol
di*iso*propyl carbodiimide: 499 µL, 3.20 mmol
(4-dimethylamino)pyridine: 39 mg, 0.32 mmol.

Coupling of Alloc-(Br,OMe)-mTyr-OH, Fmoc-Ile-OH and Fmoc-Ser(Trt)-OH (SAR-1) or Fmoc-Hse(Trt)-OH (SAR-2)

The resin was deprotected prior to the coupling according to *method B*.

The coupling with Alloc-(Br,OMe)-mTyr-OH was carried out using the following amounts of reagents and following *method D*:

HOBt: 173 mg, 1.28 mmol
HBTU: 425 mg, 1.12 mmol
DIEA: 160 µL, 0.96 mmol.
Alloc-(Br,OMe)-mTyr-OH: 476 mg, 1.28 mmol.

The Kaiser test performed according to *method G* remained negative after a coupling time of 6 h. The washing and subsequent removal of the Alloc group was then carried out as described in *method C*. The following amounts of reagents were used for the deprotection reaction:

morpholine: 672 µL, 7.68 mmol
$Pd(PPh_3)_4$: 92 mg, 0.08 mmol.

The subsequent coupling with Fmoc-Ile-OH was carried out using the following amounts of reagents:
PyBrOP: 731 mg, 1.57 mmol, 4.9 eq.
DIEA: 529 µL, 3.2 mmol, 10 eq.
Fmoc-Ile-OH: 565 mg, 1.60 mmol, 5.0 eq.

The coupling was performed for 24 h, the resin was washed as described in *method D* after the coupling. Additionally, the resin was washed with DCM (3x 1 min) and ether (3x 1 min) and dried under high vacuum for 1 h.

The chloranil test carried out after 24 h of coupling remained negative, thereby indicating a complete reaction.

After drying, the resin was divided into three equal portions (0.62 mmol/g, 0.11 mmol each) and transferred to fresh solid-phase syringe reactors.

The coupling with Fmoc-Ser(Trt)-OH or Fmoc-Hse(Trt)-OH was performed as a double coupling as described in *method D* using the following amounts of reagents:
HOBt: 60 mg, 0.44 mmol
HBTU: 146 mg, 0.39 mmol
DIEA: 55 µL, 0.33 mmol

SAR-1: Fmoc-Ser(Trt)-OH: 251 mg, 0.44 mmol
SAR-2: Fmoc-Hse(Trt)-OH: 257 mg, 0.44 mmol

After a reaction time of 2x 2 h, a Kaiser test performed according to *method G* remained negative for both sequences.

After removal of the Fmoc group according to *method B* the resins were additionally washed with DCM (2x 1 min) and ether (3x 1 min) and dried under high vacuum for 1 h.

Cleavage from the solid phase

The peptides were cleaved from the resins according to *method I* and the ether precipitation yielded 200 mg of crude peptide for **SAR-1** and 100 mg for **SAR-2**.

Cyclization of the linear peptide and removal of the trityl protecting groups

The cyclization was carried out analogously for both peptides; the respective amounts of reagents are given in brackets.

The crude peptide (**SAR-1**: 200 mg, 200 µmol / **SAR-2**: 100 mg, 100 µmol) was dissolved in precooled DMF (190 mL / 90 mL) and cooled to 10 °C. DIEA (198 µL, 1200 µmol, / 99 µL, 600 µmol, 6.0 eq.) was added and the flasks containing the reaction solutions were placed on an orbital shaker and shaken gently. PyBOP (312 mg, 600 µmol / 156 mg, 300 µmol, 3.0 eq.) dissolved in pre-cooled DMF (10 mL) was added and the mixture was gently shaken at 10 °C for 2 d. After this time, the solvent was removed and the residue was co-evaporated twice with toluene. The remaining crude mixture was dissolved in a minimal amount of ethyl acetate (and optionally a few drops of MeOH to enhance solubility). This solution was added to cold ether, resulting in the precipitation of the crude peptide. The suspension was centrifuged and the pellet was washed once with cold ether, centrifuged and dried subsequently.

The trityl protecting groups were removed as described in *method J*.

The crude peptides were purified by preparative HPLC using a preparative C_{18} column and a linear gradient of acetonitrile in H_2O, starting from 10% acetonitrile.

After the purification the solvent was removed and the products were lyophilized.

SAR-1:

Yield: 4.60 mg (4.5 µmol, 4.1%) as a white powder.

^{1}H NMR (600 MHz, DMSO-d$_6$) δ 8.52 (d, *J* = 6.6 Hz, 1H), 8.48 (d, *J* = 7.6 Hz, 1H), 8.02 (d, *J* = 7.9 Hz, 1H), 7.99 (dd, *J* = 8.0, 3.4 Hz, 1H), 7.46 (d, *J* = 2.0 Hz, 1H), 7.30 (s, 1H), 7.15 (d, *J* = 8.3 Hz, 1H), 7.04-7.01 (m, 2H), 6.79 (bs, 2H), 5.93 (bs, 1H), 5.29-5.23 (m, 3H), 4.64-4.61 (m, 1H), 4.48-4.44 (m, 1H), 4.33-4.30 (m, 1H), 4.24-4.20 (m, 2H), 4.13-4.09 (m, 2H), 3.79 (s, 3H), 3.60 (dd, *J* = 10.5, 5.5 Hz, 1H), 3.53 (dd, *J* = 10.6, 6.8 Hz, 1H), 3.23 (dd, *J* = 14.1, 6.5 Hz, 1H), 3.03-3.00 (m, 3H), 2.73 (dd, *J* = 14.1, 7.9 Hz, 1H), 2.69 (s, 3H), 2.14-2.06 (m, 8H), 1.85-1.83 (m, 1H), 1.75-1.72 (m, 4H), 1.53-1.49 (m, 4H), 1.12 (d, *J* = 6.5 Hz, 3H), 0.88-0.83 (m, 3H), 0.82-0.79 (m, 6H), 0.70 (t, *J* = 7.4 Hz, 3H), 0.39 (d, *J* = 6.2 Hz, 3H).

LC-MS: t_R = 7.43 min (C_{18}), *m/z* = 1027.47($M^+ + H^+$, 100%), 1027.43 calcd for $C_{44}H_{70}BrN_{10}O_{13}^+$.

SAR-2:

Yield: 1.10 mg (1.1 µmol, 1.0%) as a white powder.

^{1}H NMR (600 MHz, DMSO-d$_6$) δ 8.66 (d, *J* = 8.5 Hz, 1H), 8.43 (d, *J* = 8.2 Hz, 1H), 8.39 (d, *J* = 8.8 Hz, 1H), 8.12 (d, *J* = 7.8 Hz, 1H), 7.61 (d, *J* = 2.0 Hz, 1H), 7.45 (d, *J* = 2.0 Hz, 1H), 7.18 (s, 1H), 7.09 (s, 1H), 7.01 (s, 1H), 6.83 (bs, 2H), 5.93 (bs, 1H), 5.42 (bs, 2H), 5.12-5.09 (m, 1H), 4.54-4.53 (m, 1H), 4.49-4.48 (m, 1H), 4.34-4.33 (m, 1H), 4.29-4.28 (m, 1H), 4.26-4.24 (m, 1H), 4.22-4.21 (m, 1H), 3.81 (s, 3H), 3.11-3.08 (m, 5H), 3.03 (s, 3H), 2.62-2.61 (m, 1H), 2.39 (dd, *J* = 3.7, 1.9 Hz, 1H), 2.12-2.06 (m, 10H), 1.74-1.72 (m, 1H), 1.52-1.46 (m, 8H), 0.95 (d, *J* = 7.0 Hz, 3H), 0.86-0.83 (m, 3H), 0.81-0.79 (m, 6H), 0.70-0.66 (m, 3H), 0.59-0.57 (m, 3H).

LC-MS: t_R = 6.23 min (C_{18}), *m/z* = 1041.33($M^+ + H^+$, 100%), 1041.44 calcd for $C_{45}H_{72}BrN_{10}O_{13}^+$.

6.4.4.2 Synthesis of SAR-3 (Ahp→Thr)

Loading of Fmoc-Cit-OH onto 2-chlorotrityl resin

2-chlorotrityl resin (1.6 mmol/g, 250 mg, 0.40 mmol) was transferred to a glass solid-phase reactor under an argon atmosphere. To the resin was added a solution of Fmoc-Cit-OH (182 mg, 0.48 mmol, 1.2 eq.) and DIEA (264 µL, 7.68 mmol, 4.0 eq.) in DCM (6 mL) and the resin was shaken gently at RT overnight. The resin was capped with a solution of DCM/MeOH/DIEA (85%/10%/5%) which was applied 3x for 5 min. The resin was washed with DMF (2x 1 min), alternatingly with MeOH and DCM (3x 1 min), DMF (3x 1 min) and finally with DCM (3x 1 min). After drying under high vacuum, the loading of the resin was determined according to *method* F, revealing a loading of 0.46 mmol/g (29 %).

Coupling of Fmoc-Thr-OH, Fmoc-Gln(Trt)-OH and butyric acid

The dried resin (0.36 mmol/g, 342 mg, 0.16 mmol) was transferred to a solid-phase syringe reactor for the subsequent couplings.

The resin was deprotected prior to every coupling according to *method B*.

The amino acids were coupled using the protocol described in *method D*.

A Kaiser test following the protocol in *method G* was performed after each coupling.

The following amounts of reagents and coupling times were used for the respective couplings:

HOBt: 87 mg, 0.64 mmol

HBTU: 213 mg, 0.56 mmol

DIEA: 79 µL, 0.48 mmol.

Fmoc-Thr-OH*H_2O: 87 mg, 0.64 mmol

The coupling was performed for 2 h, the Kaiser test performed after the coupling remained negative, indicating a complete coupling.

Fmoc-Gln(Trt)-OH: 391 mg, 0.64 mmol

The coupling was performed as an overnight reaction, after which the Kaiser test remained negative, indicating a complete coupling.

butyric acid: 59 µL, 0.64 mmol
The coupling was performed for 4 h, after which the Kaiser test remained negative for both reactions, indicating a complete coupling.

Esterification with Fmoc-Val-OH

The esterification of the threonine side chain was performed following *method E*, using the following amounts of reagents:
Fmoc-Val-OH: 543 mg, 1.60 mmol
di*iso*propyl carbodiimide: 249 µL, 1.60 mmol
(4-dimethylamino)pyridine: 20 mg, 0.16 mmol.

Coupling of Alloc-(Br,OMe)-mTyr-OH, Fmoc-Ile-OH and Fmoc-Thr(*t*Bu)-OH

The resin was deprotected prior to the coupling according to *method B*.
The coupling with Alloc-(Br,OMe)-mTyr-OH was carried out using the following amounts of reagents and following *method D*:
HATU: 266 mg, 0.8 mmol, 5 eq.
DIEA: 263 µL, 1.60 mmol, 10 eq.
Alloc-(Br,OMe)-mTyr-OH: 238 mg, 0.64 mmol, 4 eq.

The Kaiser test performed according to *method G* remained negative after a coupling time of 24 h. The washing and subsequent removal of the Alloc group was carried out as described in *method C*. The following amounts of reagents were used for the deprotection reaction:
morpholine: 336 µL, 3.84 mmol
$Pd(PPh_3)_4$: 46 mg, 0.04 mmol.

The subsequent coupling with Fmoc-Ile-OH was carried out using the following amounts of reagents:
PyBrOP: 365 mg, 0.78 mmol, 4.9 eq.
DIEA: 263 µL, 1.60 mmol, 10 eq.
Fmoc-Ile-OH: 283 mg, 0.80 mmol, 5.0 eq.

The coupling was performed for 24 h, the resin was washed as described in *method D* after the coupling. The chloranil test carried out according to *method H* after the 24 h coupling remained negative, thereby indicating a complete coupling.

The coupling with Fmoc-Thr(*t*Bu)-OH was performed for 6 h as described in *method D* using the following amounts of reagents:

HOBt: 87 mg, 0.64 mmol

HBTU: 213 mg, 0.56 mmol

DIEA: 79 µL, 0.48 mmol.

Fmoc-Thr(*t*Bu)-OH: 254 mg, 0.64 mmol

A Kaiser test performed according to *method G* remained negative for both sequences.

After removal of the Fmoc group according to *method B* the resin was washed additionally with DCM (2x 1 min) and ether (3x 1 min) and dried under high vacuum for 1 h.

Cleavage from the solid phase

The peptide was cleaved from the resin according to *method I*, the ether precipitation yielded 160 mg of the crude peptide.

Cyclization of the linear peptide and removal of the trityl protecting groups

The crude peptide (160 mg, 117 µmol) was dissolved in pre-cooled DMF (110 mL) and cooled to 10 °C. DIEA (116 µL, 702 µmol, 6.0 eq.) was added to the solution and the flask containing the reaction solution was placed on an orbital shaker and shaken gently. PyBOP (183 mg, 351 µmol, 3.0 eq.) dissolved in pre-cooled DMF (10 mL) was added and the reaction mixture was gently shaken at 10 °C for 2 d. The solvent was removed and the residue was co-evaporated twice with toluene. The remaining crude mixture was dissolved in the minimal amount of ethyl acetate (and optionally a few drops of MeOH to enhance solubility). This solution was added to cold ether, resulting in the precipitation of the crude peptide. The suspension was centrifuged and the pellet was washed once with cold ether, centrifuged and dried subsequently.

The trityl protecting groups were removed as described in *method J*.

The crude peptide was purified by preparative HPLC using a preparative C_{18} column and a linear gradient of acetonitrile in H_2O, starting from 10% acetonitrile. After the purification the solvent was removed and the product was lyophilized.

SAR-3:

Yield: 3.54 mg (3.4 µmol, 2.1%) as a white powder.

^{1}H NMR (500 MHz, DMSO-d_6) δ 8.57 (d, *J* = 6.3 Hz, 1H), 8.28 (d, *J* = 7.5 Hz, 1H), 8.02 (d, *J* = 3.4 Hz, 1H), 8.00 (d, *J* = 2.5 Hz, 1H), 7.47 (d, *J* = 2.0 Hz, 1H), 7.30 (s, 1H), 7.20 (s, 1H), 7.10 (s, 1H), 7.00 (d, *J* = 3.5 Hz, 1H), 6.80 (bs, 2H), 5.92 (bs, 1H), 5.20-5.16 (m, 1H), 5.11 (bs, 2H), 4.60-4.55 (m, 1H), 4.46-4.43 (m, 1H), 4.31-4.26 (m, 3H), 4.19 – 4.15 (m, 1H), 4.10-4.05 (m, 1H), 3.88 (d, *J* = 3.0 Hz, 1H), 3.79 (s, 3H), 2.94-2.91 (m, 3H), 2.77-2.72 (m, 2H), 2.68 (s, 3H), 2.12-2.06 (m, 9H), 1.54-1.48 (m, 8H), 1.12 (d, *J* = 6.5 Hz, 3H), 0.97-0.94 (m, 3H), 0.87-0.83 (m, *J* = 7.4 Hz, 6H), 0.78 (d, *J* = 6.8 Hz, 3H), 0.68 (t, *J* = 7.1 Hz, 3H), 0.56 (d, *J* = 5.7 Hz, 3H).

LC-MS: t_R = 7.63 min (C_{18}), *m/z* = 1041.40(M^+ + H^+, 100%), 1041.44 calcd for $C_{45}H_{72}BrN_{10}O_{13}^+$.

6.4.4.3 Synthesis of SAR-4 and SAR-7: (4: Ahp→Ser, Br,OMe-mTyr→OMe-mTyr, 7: Ahp→Ser, Br,OMe-mTyr→Pro)

Coupling of Fmoc-Thr-OH, Fmoc-Gln(Trt)-OH and butyric acid

The dried resin (0.62 mmol/g, 520 mg, 0.32 mmol) was transferred into a solid-phase syringe reactor for the subsequent couplings.

The resin was deprotected prior to every coupling according to *method B*.

The amino acids were coupled using the protocol described in *method D*.

A Kaiser test following the protocol in *method F* was performed after each coupling.

The following amounts of reagents and coupling times were used for the respective couplings:

HOBt: 173 mg, 1.28 mmol

HBTU: 425 mg, 1.12 mmol

DIEA: 160 µL, 0.96 mmol.

Fmoc- Thr-OH*H_2O: 460 mg, 1.28 mmol

The coupling was performed for 2 h, the Kaiser test performed after the coupling remained negative, indicating a complete coupling.

Fmoc-Gln(Trt)-OH: 782 mg, 1.28 mmol

The coupling was performed for 2 h, after which the Kaiser test remained negative, indicating a complete coupling.

butyric acid: 117.5 µL, 1.28 mmol

The coupling was performed as an overnight reaction, after which the Kaiser test remained negative, indicating a complete coupling.

Esterification with Fmoc-Val-OH

The esterification of the threonine side chain was performed according to *method E*, using the following amounts of reagents:

Fmoc-Val-OH: 1.09 g, 3.20 mmol

di*iso*propyl carbodiimide: 499 µL, 3.20 mmol

(4-dimethylamino)pyridine: 39 mg, 0.32 mmol.

After the regular washing protocol, the resin was additionally washed with DCM (3x 1 min) and ether (3x 1 min) and dried under high vacuum for 1 h. The dried resin was then divided into four equal portions and transferred into fresh solid-phase syringe reactors.

Sequential coupling of Alloc-(Br,OMe)-mTyr-OH (SAR-4) or Fmoc-Pro-OH (SAR-7), Fmoc-Ile-OH and Boc-Ser(OBzl)-OH

The resin (0.62 mmol/g, 0.08 mmol) was deprotected prior to every coupling according to *method B*.

The following two couplings were carried out using the given amounts of reagents according to *method D*:

HOBt: 43 mg, 0.32 mmol

HBTU: 106 mg, 0.28 mmol

DIEA: 40 µL, 0.24 mmol.

SAR-4: Alloc-(Br,OMe)-mTyr-OH: 119 mg, 0.32 mmol.

SAR-7: Fmoc-Pro-OH: 108 mg, 0.32 mmol.

For **SAR-4** the Kaiser test performed according to *method G* remained negative after a coupling time of 3 h. The washing and subsequent removal of the Alloc group was carried out as described in *method C*. The following amounts of reagents were used for the deprotection reaction:
morpholine: 168 µL, 1.92 mmol
$Pd(PPh_3)_4$: 23 mg, 0.02 mmol.

For **SAR-7** the Kaiser test following the protocol of *method G* was performed after 3 h coupling and indicated an incomplete coupling. A double coupling was performed for 2 h using the same amounts of reagents, which resulted in a negative Kaiser test. The removal of the Fmoc protection was carried out following the protocol described in *method B*.

The subsequent coupling with Fmoc-Ile-OH was carried out in the same manner for both sequences using the following amounts of reagents:
PyBrOP: 175 mg, 0.39 mmol, 4.9 eq.
DIEA: 132 µL, 0.8 mmol, 10 eq.
Fmoc-Ile-OH: 141 mg, 0.40 mmol, 5.0 eq.

The coupling was performed for 24 h, the resins were washed as described in *method D* after the coupling.

For **SAR-4**, the chloranil test carried out with the protocol of *method H* was positive, indicating an incomplete coupling. The required double coupling was performed using the same amounts of reagents again, the reaction time was 4 h, after which the chloranil test remained negative.

For **SAR-7** the chloranil test carried out after the 24 h coupling remained negative, thereby indicating a complete coupling.

The coupling with Boc-Ser(OBzl)-OH was performed as described in *method D* as an overnight reaction using the following amounts of reagents:
HOBt: 43 mg, 0.32 mmol
HBTU: 106 mg, 0.28 mmol
DIEA: 40 µL, 0.24 mmol
Boc-Ser(OBzl)-OH: 95 mg, 0.32 mmol.

The Kaiser test performed as described in *method G* remained negative for both sequences, thereby indicating a complete coupling. Additionally, after the regular washing protocol the resins were washed with DCM (2x 1 min) and ether (3x 1 min) and dried under high vacuum for 1 h.

Cleavage from the solid phase and deprotection

The peptides were cleaved from the resins according to *method I*. The Boc and trityl protecting groups were removed using the protocol described in *method J*; the ether precipitation yielded 60 mg of crude peptide for both sequences.

Cyclization of the linear peptide and removal of the benzyl ether protection

The crude peptides (60 mg, 60 µmol) were dissolved in pre-cooled DMF (50 mL) and the solutions were maintained at 10 °C. DIEA (59.5 µL, 360 µmol, 6.0 eq.) was added and the flasks containing the reaction solutions were placed on an orbital shaker and shaken gently. PyBOP (94 mg, 180 µmol, 3.0 eq.) dissolved in pre-cooled DMF (10 mL) was added and the mixtures was gently shaken at 10 °C for 2 d. The solvent was removed and the residue was co-evaporated twice with toluene. The remaining crude mixtures were dissolved in a minimal amount of ethyl acetate (and optionally a few drops of MeOH to enhance solubility). The resulting solutions were added to cold ether, resulting in the precipitation of the crude peptide. The suspension was centrifuged and the pellet was washed once with cold ether and dried subsequently, yielding 150 mg of crude product for each sequence.

The benzyl group was removed from the crude cyclized peptides with the hydrogenation performed following *method K*.

An LC-MS analysis carried out after the hydrogenation indicated that the hydrogenation for **SAR-4** had also resulted in the removal of the aromatic bromine besides the cleavage of the benzyl group.

The crude peptides were then purified by preparative HPLC using a preparative C_{18} column and a linear gradient of acetonitrile in H_2O, starting from 10% acetonitrile.

After the purification the solvent was removed and the products were lyophilized.

SAR-4:

Yield: 2.90 mg (3.1 µmol, 3.8%) as a white powder.

^{1}H NMR (600 MHz, DMSO-d$_6$) δ 8.56 (d, *J* = 6.6 Hz, 1H), 8.47 (d, *J* = 7.7 Hz, 1H), 8.01-7.99 (m, 2H), 7.29 (s, 1H), 7.17 (d, *J* = 5.9 Hz, 1H), 7.15-7.12 (m, 2H), 6.85-6.81 (m, 2H), 6.79 (bs, 2H), 5.92 (bs, 1H), 5.37 (bs, 2H), 5.26-5.23 (m, 1H), 4.64-4.61 (m, 1H), 4.48-4.43 (m, 1H), 4.33-4.29 (m, 2H), 4.23-4.20 (m, 2H), 4.12-4.10 (m, 1H), 3.69 (s, 3H), 3.60-3.58 (m, 1H), 3.29-3.27 (m, 1H), 3.25-3.23 (m, 1H), 2.95-2.91 (m, 4H), 2.69 (s, 3H), 2.15-2.05 (m, 8H), 1.85-1.81 (m, 1H), 1.53-1.48 (m, 4H), 1.27-1.23 (m, 4H), 1.10 (d, *J* = 6.5 Hz, 3H), 0.85 (t, *J* = 7.4 Hz, 3H), 0.82-0.79 (m, 6H), 0.72 (t, *J* = 7.4 Hz, 3H), 0.43 (d, *J* = 6.3 Hz, 3H).

LC-MS: t_R = 7.79 min (C_{18}), *m/z* = 947.53($M^+ + H^+$, 100%), 947.52 calcd for $C_{44}H_{71}N_{10}O_{13}^+$.

SAR-7:

Yield: 4.85 mg (5.7 µmol, 7.1%) as a white powder.

^{1}H NMR (600 MHz, DMSO-d$_6$) δ 8.48 (d, *J* = 8.4 Hz, 1H), 8.09-8.05 (m, 2H), 7.81 (d, *J* = 9.2 Hz, 1H), 7.30 (bs, 2H), 6.96 (d, *J* = 5.0 Hz, 1H), 6.78 (bs, 1H), 6.59 (d, *J* = 6.7 Hz, 1H), 5.97 (bs, 2H), 5.24-5.20 (m, 1H), 4.66-4.64 (m, 1H), 4.47-4.45 (m, 1H), 4.41-4.39 (m, 1H), 4.34-4.31 (m, 1H), 4.27-4.25 (m, 1H), 4.23-4.20 (m, 2H), 3.66-3.62 (m, 1H), 3.56-3.49 (m, 3H), 3.44-3.41 (m, 1H), 2.94 (t, *J* = 6.8 Hz, 2H), 2.26-2.22 (m, 1H), 2.19-2.14 (m, 1H), 2.13-2.08 (m, 4H), 2.01-1.96 (m, 1H), 1.94-1.91 (m, 1H), 1.89-1.84 (m, 2H), 1.80-1.75 (m, 2H), 1.73-1.68 (m, 2H), 1.54-1.49 (m, 2H), 1.47-1.43 (m, 2H), 1.37-1.32 (m, 2H), 1.13 (d, *J* = 6.3 Hz, 3H), 0.86 (t, *J* = 7.4 Hz, 3H), 0.84-0.81 (m, 3H), 0.81-0.78 (m, 9H).

LC-MS: t_R = 6.90 min (C_{18}), *m/z* = 853.47($M^+ + H^+$, 100%), 853.48 calcd for $C_{38}H_{65}N_{10}O_{12}^+$.

6.4.4.4 Synthesis of SAR-5 (simplified SymA analog, Ahp→Ser, Br,OMe-mTyr→mPhe)

Loading of Fmoc-Cit-OH onto 2-chlorotrityl resin

2-chlorotrityl resin (1.6 mmol/g, 500 mg, 0.80 mmol) was transferred to a glass solid-phase reactor under an argon atmosphere. To the resin was added a solution of Fmoc-Cit-OH (382 mg, 0.96 mmol, 1.2 eq.) and DIEA (529 µL, 3.2 mmol, 4.0 eq.) in DCM (6 mL). The resin was shaken gently at RT overnight and capped with a solution of DCM/MeOH/DIEA (85%/10%/5%) which was applied 3x for 5 min. After the capping step, the resin was washed with DMF (2x 1 min), alternatingly with MeOH and DCM (3x 1 min), DMF (3x 1 min) and finally with DCM (3x 1 min). After drying under high vacuum for 1 h, the loading of the resin was determined according to *method* F, revealing a loading of 0.33 mmol/g (20%).

Coupling of Fmoc-Thr-OH, Fmoc-Gln(Trt)-OH and butyric acid

The dried resin (0.33 mmol/g, 700 mg, 0.23 mmol) was transferred to a solid-phase syringe reactor for the subsequent couplings.

The resin was deprotected prior to every coupling according to *method B*.

The amino acids were coupled using the protocol described in *method D*.

A Kaiser test following the protocol in *method G* was performed after each coupling.

The following amounts of reagents and coupling times were used for the respective couplings:

HOBt: 125 mg, 0.92 mmol

HBTU: 307 mg, 0.81 mmol

DIEA: 115 µL, 0.69 mmol.

Fmoc-Thr-OH: 315 mg, 0.92 mmol

The coupling was performed for 2 h, after which the Kaiser test remained positive. A double coupling was performed for additional 2 h, using the same amounts of reagents. The Kaiser test performed after this second coupling was negative, indicating a complete coupling.

Fmoc-Gln(Trt)-OH: 564 mg, 0.92 mmol

The coupling was performed for 2 h, after which a Kaiser test remained positive. A double coupling was performed for additional 2 h, using the same amounts of reagents. The Kaiser test performed after this second coupling was negative, indicating a complete coupling.

butyric acid: 85 µL, 0.92 mmol

The coupling was performed for 4 h, after which the Kaiser test remained positive. A double coupling was performed overnight, using the same amounts of reagents. The Kaiser test performed after this second coupling was negative, indicating a complete coupling.

Esterification with Fmoc-Val-OH

The esterification of the threonine side chain was performed following *method E*, using the following amounts of reagents:
Fmoc-Val-OH: 781 mg, 2.30 mmol
di*iso*propyl carbodiimide: 358 µL, 2.30 mmol
(4-dimethylamino)pyridine: 28 mg, 0.23 mmol.

After the regular washing steps, the resin was washed additionally with DCM (3x 1 min) and ether (3x 1 min) and dried under high vacuum for 1 h.
An Fmoc determination performed according to *method F* revealed a loading of 0.33 mmol/g (quant.).

Coupling of Fmoc-NMePhe, Fmoc-Ile-OH and Boc-Ser(OBzl)-OH

The dried resin (0.33 mmol/g, 835 mg, 0.23 mmol) was transferred into a fresh solid phase syringe reactor for the subsequent couplings.
The resin was deprotected prior to every coupling according to *method B*.
Fmoc-*N*MePhe-OH (371 mg, 0.924 mmol) was coupled using *method D* and the same amounts of coupling reagents as in the prior couplings.
A Kaiser test following the protocol of *method F* was performed after an overnight coupling and indicated an incomplete coupling. The double coupling was performed for 4 h using the same amounts of reagents and this time the Kaiser test remained negative.
The coupling to the *N*-methylated amino acid required different coupling reagents. A solution of Fmoc-Ile-OH (406 mg, 1.15 mmol, 5.0 eq.), PyBrOP (525 mg, 1.13 mmol, 4.9 eq.) and DIEA (380 µL, 2.30 mmol, 10.0 eq.) in DMF was added to the resin, which was then shaken for 24 h. The washing steps were performed according to *method D*. A chloranil test performed following the protocol described in *method H* indicated a complete coupling.
The coupling with Boc-Ser(OBzl)-OH (273 mg, 0.924 mmol) was performed overnight following the protocol of *method D*. Additionally, after the regular washing protocol the resin was washed with DCM (2x 1 min) and ether (3x 1 min) and dried under high vacuum for 1 h.

Cleavage from the solid phase and deprotection

The peptide was cleaved from the resin according to *method I*. The Boc and trityl protecting groups were removed using the protocol described in *method J*, the ether precipitation yielded 300 mg of crude peptide.

Cyclization of the linear peptide and removal of the benzyl ether protection

The crude peptide (150 mg, 147 µmol) was dissolved in DMF (140 mL) and cooled to 2 °C. DIEA (144 µL, 876 µmol, 6.0 eq.) and PyBOP (228 mg, 441 µmol, 3.0 eq.) were added and the mixture was stirred at 2 °C for 2 d. After this time the solvent was removed and the residue was co-evaporated twice with toluene. The remaining crude mixture was dissolved in a minimal amount of ethyl acetate (and optionally a few drops of MeOH to enhance solubility). This solution was added to cold ether, resulting in the precipitation of the crude peptide. The suspension was centrifuged and the pellet was washed once with cold ether and dried subsequently.

The benzyl group was removed from 200 mg of crude cyclized peptide; the hydrogenation was performed following *method K*.

The crude peptide was purified by preparative HPLC using a preparative C_{18} column and a linear gradient of acetonitrile in H_2O, starting from 10% acetonitrile. After the purification the solvent was removed and the product was lyophilized.

SAR-5:

Yield: 9.19 mg (10 µmol, 4.4%) as white powder.

^{1}H NMR (600 MHz, DMSO-d_6) δ 8.55 (d, *J* = 6.8 Hz, 1H), 8.46 (d, *J* = 7.7 Hz, 1H), 7.99 (m, 3H), 7.63 (d, *J* = 8.6 Hz, 1H), 7.29-7.22 (m, 5H), 6.78 (bs, 1H), 5.94 (bs, 1H), 5.34 (t, *J* = 7.2 Hz, 1H), 5.26 (bs, 2H), 4.63 (m, 1H), 4.45 (m, 1H), 4.34-4.29 (m, 2H), 4.26-4.17 (m, 2H), 4.15-4.09 (m, 1H), 3.61 (dd, *J* = 10.6, 5.6 Hz, 1H), 3.54 (dd, *J* = 10.5, 6.7 Hz, 1H), 3.34 (dd, *J* = 14.0, 7.1 Hz, 1H), 3.04-2.99 (m, 1H), 2.93 (t, *J* = 6.7 Hz, 2H), 2.75 (dd, *J* = 14.3, 7.7 Hz, 1H), 2.71 (s, 3H), 2.17-2.05 (m, 8H), 1.76-1.72 (m, 1H), 1.54-1.44 (m, 8H), 1.10 (d, *J* = 6.5 Hz, 3H), 0.87-0.84 (m, 3H), 0.81-0.79 (m, 6H), 0.71 (t, *J* = 7.4 Hz, 3H), 0.36 (d, *J* = 6.2 Hz, 3H).

LC-MS: t_R = 7.74 min (C_{18}), *m/z* = 917.47($M^+ + H^+$, 100%), 917.51 calcd for $C_{43}H_{69}N_{10}O_{12}^+$.

6.4.4.5 Synthesis of SAR-6: (Ahp→Ser, Br,OMe-mTyr→Phe)

Coupling of Fmoc-Thr-OH, Fmoc-Gln(Trt)-OH and butyric acid

The dried resin (0.62 mmol/g, 260 mg, 0.16 mmol) was transferred into a solid-phase syringe reactor for the subsequent couplings.

The resin was deprotected prior to every coupling according to *method B*.

The amino acids were coupled using the protocol described in *method D*.

A Kaiser test following the protocol in *method G* was performed after each coupling.

The following amounts of reagents and coupling times were used for the respective couplings:

HOBt: 86 mg, 0.64 mmol

HBTU: 212 mg, 0.56 mmol

DIEA: 40 µL, 0.48 mmol.

Fmoc- Thr-OH*H_2O: 230 mg, 0.64 mmol

The coupling was performed for 2 h; the Kaiser test performed after the coupling remained negative, indicating a complete coupling.

Fmoc-Gln(Trt)-OH: 391 mg, 0.64 mmol

The coupling was performed for 2 h, after which the Kaiser test performed according to *method* G remained negative, thereby indicating a complete coupling.

butyric acid: 58.7 µL, 0.64 mmol

The coupling was performed as an overnight reaction, after which the Kaiser test remained negative, thereby indicating a complete coupling.

Esterification with Fmoc-Val-OH

The esterification of the threonine side chain was performed following *method E*, using the following amounts of reagents:

Fmoc-Val-OH: 543 mg, 1.60 mmol

di*iso*propyl carbodiimide: 250 µL, 1.60 mmol

(4-dimethylamino)pyridine: 20 mg, 1.60 mmol.

After the regular washing protocol, the resin was washed additionally with DCM (3x 1 min) and ether (3x 1 min) and dried under high vacuum for 1 h. The dried resin was then divided into two equal portions and transferred into fresh solid-phase syringe reactors.

Coupling of Fmoc-Phe-OH, Fmoc-Ile-OH and Boc-Ser(OBzl)-OH

The resin (0.62 mmol/g, 0.08 mmol) was deprotected prior to every coupling according to *method B*.

The following two couplings were carried out using the following amounts of reagents and according to *method D*:

HOBt: 43 mg, 0.32 mmol

HBTU: 106 mg, 0.28 mmol

DIEA: 40 µL, 0.24 mmol.

Fmoc-Phe-OH: 124 mg, 0.32 mmol

A Kaiser test following the protocol of *method G* was performed after a 2 h coupling time and indicated an incomplete coupling; the subsequent double coupling was performed overnight using the same amounts of reagents. The Kaiser test performed after this second coupling remained negative.

Fmoc-Ile-OH: 113 mg, 0.32 mmol.

The coupling was performed as an overnight reaction, the Kaiser test performed after the reaction was positive. The required double coupling required was performed using the same amounts of reagents, the reaction time was 4 h, after which the Kaiser test remained negative.

For the coupling with Boc-Ser(OBzl)-OH the amounts of reagents were adjusted regarding the previous incomplete couplings. The coupling was performed as described in *method D* for 5 h using the following amounts of reagents:

HOBt: 65 mg, 0.48 mmol, 6.0 eq.

HBTU: 159 mg, 0.42 mmol, 5.3 eq.

DIEA: 60 µL, 0.36 mmol, 4.5 eq.

Boc-Ser(OBzl)-OH: 142 mg, 0.48 mmol, 6.0 eq.

The Kaiser test performed as described in *method G* remained negative, thereby indicating a complete coupling. Additionally, after the regular washing protocol, the resin was furthermore washed with DCM (2x 1 min) and ether (3x 1 min) and dried under high vacuum for 1 h.

Cleavage from the solid phase and deprotection

The peptide was cleaved from the resin according to *method I*. The Boc and trityl protecting groups were removed using the protocol described in *method J*; the ether precipitation yielded 100 mg of crude peptide.

Cyclization of the linear peptide and removal of the benzyl ether protection

The crude peptide (100 mg, 98 µmol) was dissolved in pre-cooled DMF (90 mL) and cooled to 10 °C. DIEA (96 µL, 584 µmol, 6.0 eq.) was added and the flask containing the reaction solution was placed on an orbital shaker and shaken gently. PyBOP (152 mg, 292 µmol, 3.0 eq.) dissolved in pre-cooled DMF (10 mL) was added and the reaction mixture was gently shaken at 10 °C for 2 d. After this time the solvent was removed and the residue was co-evaporated twice with toluene. The remaining crude mixture was dissolved in a minimal amount of ethyl acetate (and optionally a few drops of MeOH to enhance solubility). This solution was added to cold ether, resulting in the precipitation of the crude peptide. The suspension was centrifuged and the pellet was washed once with cold ether and dried subsequently, yielding 220 mg of crude product.

The benzyl group was removed from the crude cyclized peptide and the hydrogenation was performed according to *method K*.

The crude peptide was purified by preparative HPLC using a preparative C_{18} column and a linear gradient of acetonitrile in H_2O, starting from 10% acetonitrile.

After the purification the solvent was removed and the product was lyophilized.

SAR-6:

Yield: 8.87 mg (9.8 µmol, 12.3%) as a white powder.

^{1}H NMR (600 MHz, DMSO-d_6) δ 8.39 (d, *J* = 6.0 Hz, 1H), 8.26 (s, 1H), 8.04 (d, *J* = 7.8 Hz, 1H), 7.85 (d, *J* = 8.0 Hz, 1H), 7.44 (d, *J* = 7.3 Hz, 1H), 7.36 (d, *J* = 9.0 Hz, 1H), 7.26-7.24 (m, 3H), 7.20-7.16 (m, 2H), 6.76 (bs, 2H), 5.96 (bs, 2H), 5.66 (d, *J* = 6.6 Hz, 1H), 5.11-5.09 (m, 1H), 4.67-4.65 (m, 1H), 4.52-4.49 (m, 1H), 4.45-4.42 (m, 1H), 4.31-4.27 (m, 2H), 4.11-4.08 (m, 1H), 3.97-3.93 (m, 1H), 3.69-3.64 (m, 2H), 3.26 (d, *J* = 3.8 Hz, 1H), 3.23 (d, *J* = 3.4 Hz, 1H), 2.96 (t, *J* = 6.7 Hz, 1H), 2.76-2.70 (m, 2H), 2.13-2.06 (m, 8H), 1.88-1.85 (m, 1H), 1.81-1.77 (m, 1H), 1.70-1.66 (m, 1H), 1.53-1.47 (m, 3H), 1.43-1.37 (m, 3H), 1.17 (d, *J* = 6.5 Hz, 3H), 0.96 (d, *J* = 6.6 Hz, 3H), 0.85-0.82 (m, 6H), 0.61 (t, *J* = 7.3 Hz, 3H), 0.53 (d, *J* = 6.9 Hz, 3H).

LC-MS: t_R = 7.47 min (C_{18}), *m/z* = 903.47($M^+ + H^+$, 100%), 903.49 calcd for $C_{42}H_{67}N_{10}O_{12}^+$.

6.4.4.6 Synthesis of SAR-8 and SAR-9 (8: Ahp→Ser, Br,OMe-mTyr→mPhe, *L*-Thr→*D-allo*-Thr; 9: Ahp→Ser, Br,OMe-mTyr→mPhe, *L*-Thr→*L-allo*-Thr)

Coupling of Fmoc-protected *D*- or *L-allo*-Thr-OH, Fmoc-Gln(Trt)-OH and butyric acid

Two portions of dried resin (0.62 mmol/g, 130 mg, 0.08 mmol) were transferred into individual solid-phase syringe reactors for the subsequent couplings.

The resins were deprotected prior to every coupling according to *method B*.

The amino acids were coupled using the protocol described in *method D*.

A Kaiser test following the protocol in *method G* was performed after each coupling.

The following amounts of reagents and coupling times were used for the respective couplings:

HOBt: 43 mg, 0.32 mmol
HBTU: 106 mg, 0.28 mmol
DIEA: 40 µL, 0.24 mmol.

SAR-8: Fmoc-*D*-allo-Thr-OH: 109 mg, 0.32 mmol
SAR-9: Fmoc-*L*-allo-Thr-OH: 109 mg, 0.32 mmol

The coupling was performed for 2 h, the Kaiser test performed after the coupling remained negative for both reactions, indicating a complete coupling.

The following couplings were performed for both peptide sequences in the same manner.

Fmoc-Gln(Trt)-OH: 195 mg, 0.32 mmol

The coupling was performed for 2 h, after which the Kaiser test remained negative for both reactions, indicating a complete coupling.

butyric acid: 29.4 µL, 0.32 mmol

The coupling was performed as an overnight reaction, after which the Kaiser test remained negative for both reactions, indicating a complete coupling.

Esterification with Fmoc-Val-OH

The esterification of the threonine side chain was performed following *method E*, using the following amounts of reagents for both sequences:

Fmoc-Val-OH: 272 mg, 0.80 mmol
di*iso*propyl carbodiimide: 125 µL, 0.80 mmol
(4-dimethylamino)pyridine: 10 mg, 0.08 mmol.

Coupling of Fmoc-NMePhe, Fmoc-Ile-OH and Boc-Ser(OBzl)-OH

The resins were deprotected prior to every coupling according to *method B*.

Fmoc-*N*MePhe-OH (128 mg, 0.32 mmol, 4.0 eq.) was coupled using *method D*.

A Kaiser test following the protocol in *method G* was performed after a 2 h coupling time and indicated an incomplete coupling. The required double coupling was performed overnight using the same amounts of reagents, resulting in a negative Kaiser test.

The coupling to the *N*-methylated amino acid was performed using PyBrOP activation. To the resins was added a solution of Fmoc-Ile-OH (141 mg, 0.40 mmol, 5.0 eq.), PyBrOP (183 mg, 0.39 mmol, 4.9 eq.) and DIEA (132 µL, 0.8 mmol, 10.0 eq.) in DMF and the resulting suspensions were shaken for 24 h. The washing steps were performed according to *method D*. A chloranil test performed following the protocol described in *method H* turned positive for both sequences. The coupling was repeated using the same amounts of reagents and a coupling time of 4 h after which the chloranil test remained negative.

For the coupling with Boc-Ser(OBzl)-OH the amounts of reagents were adjusted in light of the previous incomplete couplings. The coupling was performed as described in *method D* for 5 h using the following amounts of reagents:

HOBt: 65 mg, 0.48 mmol, 6.0 eq.

HBTU: 159 mg, 0.42 mmol, 5.3 eq.

DIEA: 60 µL, 0.36 mmol, 4.5 eq.

Boc-Ser(OBzl)-OH: 142 mg, 0.48 mmol, 6.0 eq.

The Kaiser test performed as described in *method G* remained negative for both sequences, thereby indicating a complete coupling. Additionally, after the regular washing protocol the resins were washed with DCM (2x 1 min) and ether (3x 1 min) and dried.

Cleavage from the solid phase and deprotection

The peptides were cleaved from the resins according to *method I*. The Boc and trityl protections were removed using the protocol described in *method J*; the ether precipitation yielded 100 mg of crude peptide for each sequence.

Cyclization of the linear peptide and removal of the benzyl ether protection

The crude peptides (100 mg, 98 µmol) were dissolved in pre-cooled DMF (90 mL) and cooled to 10 °C. DIEA (96 µL, 584 µmol, 6.0 eq.) was added and the flasks containing the reaction solutions were placed on an orbital shaker and shaken gently. PyBOP (152 mg, 292 µmol, 3.0 eq.) dissolved in pre-cooled DMF (10 mL) was added and the mixtures were shaken gently at 10 °C for 2 d. After this time the solvent was removed and the residues were co-evaporated twice with toluene. The remaining crude mixtures were dissolved in a minimal amount of ethyl acetate (and optionally a few drops of MeOH to enhance solubility). The solutions were added to cold ether, resulting in the precipitation of the crude peptides. The suspensions were centrifuged and the pellet was washed once with cold ether, centrifuged and dried subsequently, yielding 220 mg of crude product for each sequence.

The benzyl group was removed from the crude cyclized peptides; the corresponding hydrogenation was performed following *method K*.

The crude peptides were purified by preparative HPLC using a preparative C_{18} column and a linear gradient of acetonitrile in H_2O, starting from 10% acetonitrile.

After the purification the solvent was removed and the products were lyophilized.

SAR-8:

Yield: 2.70 mg (2.9 µmol, 3.7%) as a white powder.

^{1}H NMR (600 MHz, DMSO-d$_6$) δ 8.61 (d, *J* = 9.7 Hz, 1H), 8.48 (d, *J* = 9.9 Hz, 1H), 8.21 (d, *J* = 6.4 Hz, 1H), 8.09 (d, *J* = 8.8 Hz, 1H), 7.92-7.87 (m, 2H), 7.26-7.23 (m, 2H), 7.21-7.18 (m, 3H), 6.78 (bs, 1H), 5.88 (bs, 1H), 5.37 (bs, 2H), 5.29-5.23 (m, 1H), 5.02-5.00 (m, 1H), 4.50-4.47 (m, 1H), 4.38-4.35 (m, 1H), 4.26-4.22 (m, 1H), 4.15-4.10 (m, 1H), 4.08-4.04 (m, 1H), 3.95-3.92 (m, 1H), 3.60-3.56 (m, 1H), 3.52-3.49 (m, 1H), 3.11-3.08 (m, 1H), 3.02-3.01 (m, 1H), 2.93-2.88 (m, 3H), 2.71 (s, 3H), 2.10 (m, 8H), 1.86-1.81 (m, 2H), 1.76-.73 (m, 3H), 1.50 (m, 4H), 1.15 (d, *J* = 6.6 Hz, 3H), 0.88-0.84 (m, 6H), 0.75-0.72 (m, 3H), 0.67-0.64 (m, 3H), 0.52 (d, *J* = 6.7 Hz, 3H).

LC-MS: t_R = 7.77 min (C_{18}), *m/z* = 917.47($M^+ + H^+$, 100%), 917.51 calcd for $C_{43}H_{69}N_{10}O_{12}^+$.

SAR-9:

Yield: 2.70 mg (5.2 µmol, 6.5%) as a white powder.

^{1}H NMR (600 MHz, DMSO-d$_6$) δ 8.62 (d, *J* = 6.6 Hz, 1H), 8.59 (d, *J* = 9.4 Hz, 1H), 8.42 (d, *J* = 9.4 Hz, 1H), 8.31 (d, *J* = 8.6 Hz, 1H), 7.94 (d, *J* = 7.7 Hz, 1H), 7.38 (s, 1H), 7.27-7.25 (m, 3H), 7.21-7.18 (m, 2H), 6.88 (bs, 2H), 5.90 (bs, 1H), 5.09-5.06 (m, 1H), 4.52-4.48 (m, 1H), 4.42-4.39 (m, 1H), 4.35-4.32 (m, 1H), 4.27-4.24 (m, 1H), 4.21-4.19 (m, 1H), 4.08-4.05 (m, 2H), 3.82 (bs, 2H), 3.51 (dd, *J* = 10.8, 4.5 Hz, 1H), 3.43 (dd, *J* = 10.7, 6.8 Hz, 1H), 3.23 (dd, *J* = 14.0, 6.8 Hz, 1H), 3.03- 3.00 (m, 1H), 2.91-2.89 (m, 2H), 2.83 (dd, *J* = 13.9, 7.7 Hz, 1H), 2.72 (s, 3H), 2.16-2.11 (m, 4H), 2.10-2.06 (m, 4H), 1.82-1.77 (m, 2H), 1.74-1.72 (m, 2H), 1.69-1.66 (m, 1H), 1.52-1.47 (m, 4H), 1.13 (d, *J* = 6.3 Hz, 3H), 0.90 (d, *J* = 6.6 Hz, 3H), 0.85-0.82 (m, 3H), 0.67-0.63 (m, 6H), 0.48 (d, *J* = 6.6 Hz, 3H).

LC-MS: t_R = 7.79 min (C_{18}), *m/z* = 917.47($M^+ + H^+$, 100%), 917.51 calcd for $C_{43}H_{69}N_{10}O_{12}^+$.

6.4.4.7 Synthesis of SAR-10, SAR-11 and SAR-12: (Scyptolin A analogs; 10: Ahp→Ser, 11: Ahp→Thr, 12: Ahp→Val)

Loading of Fmoc-Leu-OH onto 2-chlorotrityl resin

2-chlorotrityl resin (1.6 mmol/g, 750 mg, 1.20 mmol) was transferred to a glass solid-phase reactor under an argon atmosphere. To the resin was added a solution of Fmoc-Leu-OH (509 mg, 1.44 mmol, 1.2 eq.) and DIEA (794 µL, 4.80 mmol, 4.0 eq.) in DCM (15 mL) and the resin was shaken gently at RT overnight. The resin was capped using a solution of DCM/MeOH/DIEA (85%/10%/5 %) which was applied 3x for 5 min. The resin was washed with DMF (2x 1 min), alternatingly with MeOH and DCM (3x 1 min), DMF (3x 1 min) and finally with DCM (3x 1 min). After drying under high vacuum, the loading of the resin was determined according to *method F*, revealing a loading of 0.83 mmol/g (52%).

Coupling of Fmoc-Thr-OH, Fmoc-Thr(*t*Bu)-OH, Fmoc-Ala-OH and butyric acid

The dried resin (0.83 mmol/g, 580 mg, 0.48 mmol) was transferred into a solid-phase syringe reactor for the subsequent couplings.
The resin was deprotected prior to every coupling according to *method B*.
The amino acids were coupled using the protocol described in *method D*.
A Kaiser test following the protocol in *method G* was performed after each coupling.
The following amounts of reagents and coupling times were used for the respective couplings:
HOBt: 259 mg, 1.92 mmol
HBTU: 638 mg, 1.68 mmol
DIEA: 238 µL, 1.44 mmol.

Fmoc-Thr-OH*H_2O: 690 mg, 1.92 mmol
The coupling was performed for 2 h; the Kaiser test performed after the coupling remained negative, indicating a complete coupling.

Fmoc-Thr(*t*Bu)-OH: 763 mg, 1.92 mmol
The coupling was performed as an overnight reaction; the Kaiser test performed after this time remained negative.

Fmoc-Ala-OH: 598 mg, 1.92 mmol
The coupling was performed for 3 h; the Kaiser test performed after the coupling remained negative, indicating a complete coupling.

butyric acid: 117.5 µL, 1.28 mmol
The coupling was performed as an overnight reaction, after which the Kaiser test remained negative, thereby indicating a complete coupling.

Esterification with Fmoc-Val-OH

The esterification of the threonine side chain was performed as described in *method E*, using the following amounts of reagents:
Fmoc-Val-OH: 1.63 g, 4.80 mmol
di*iso*propyl carbodiimide: 748 µL, 4.80 mmol
(4-dimethylamino)pyridine: 54 mg, 0.48 mmol.

Coupling of Alloc-(Cl, O(TBDMS))-mTyr-OH, Fmoc-Thr(*t*Bu)-OH and Fmoc-Ser(*t*Bu)-OH (SAR-10), Fmoc-Thr(*t*Bu)-OH (SAR-11) or Fmoc-Val-OH (SAR-12)

The resin was deprotected prior to the coupling according to *method B*.
The coupling with Alloc-(Br,OMe)-mTyr-OH was carried out using the following amounts of reagents and following *method D*:
HOAt: 130 mg, 0.96 mmol, 2.0 eq.
HATU: 800 mg, 2.40 mmol, 5.0 eq.
DIEA: 793 µL, 4.80 mmol, 10 eq.
Alloc-(Cl,O(TBDMS))-mTyr-OH: 532 mg, 1.24 mmol, 2.6 eq.

The Kaiser test performed according to *method G* remained negative after a coupling time of 24 h. The washing and subsequent removal of the Alloc group was carried out as described in *method C*. The following amounts of reagents were used for the deprotection reaction:
morpholine: 1070 µL, 11.5 mmol
$Pd(PPh_3)_4$: 139 mg, 0.12 mmol.

The subsequent coupling with Fmoc-Thr(*t*Bu)-OH was carried out using the following amounts of reagents:
PyBrOP: 1.10 g, 2.35 mmol, 4.9 eq.
DIEA: 793 µL, 4.80 mmol, 10 eq.
Fmoc-Thr(*t*Bu)-OH: 954 mg, 2.40 mmol, 5.0 eq.

The coupling was performed for 24 h; the resin was washed as described in *method D* after the coupling. Additionally, the resin was washed with DCM (3x 1 min) and ether (3x 1 min) and dried under high vacuum for 1 h.

The chloranil test carried out according to the protocol described in *method H* after the 24 h coupling remained negative, thereby indicating a complete coupling.
After drying the resin was divided into three equal portions (0.83 mmol/g, 0.16 mmol each) and transferred to fresh solid-phase syringe reactors.

The coupling with Fmoc-Ser(*t*Bu)-OH, Fmoc-Thr(*t*Bu)-OH or Fmoc-Val-OH was performed as a double coupling as described in *method D* using the following amounts of reagents:
HOBt: 87 mg, 0.64 mmol
HBTU: 213 mg, 0.56 mmol
DIEA: 79 µL, 0.48 mmol.
SAR-10: Fmoc-Ser(*t*Bu)-OH: 245 mg, 0.64 mmol
SAR-11: Fmoc-Ser(*t*Bu)-OH: 254 mg, 0.64 mmol
SAR-11: Fmoc-Val-OH: 217 mg, 0.64 mmol

After a reaction time of 2x 2 h, a Kaiser test performed according to *method G* remained negative for all of the three sequences.
After removal of the Fmoc group according to *method B* the resins were additionally washed with DCM (2x 1 min) and ether (3x 1 min) and dried under high vacuum for 1 h.

Cleavage from the solid phase

The peptides were cleaved from the resins according to *method I*, the ether precipitation yielded 114 mg of crude peptide for **SAR-10**, 136 mg for **SAR-11** and 182 mg for **SAR-12**. An LC-MS control indicated that the TBDMS protection had been cleaved, probably during the cleavage from solid phase.

Cyclization of the linear peptide and removal of the *t*Bu protecting groups

The cyclization was carried out in the same manner for all three peptides, the respective amounts of reagents are given in brackets.
The crude peptide (**SAR-10**: 114 mg, 100 µmol / **SAR-11**: 136 mg, 118 µmol / **SAR-12**: 182 mg, 166 µmol) was dissolved in pre-cooled DMF (90 mL / 110 mL / 160 mL) and cooled to 10 °C. DIEA (99 µL, 600 µmol, / 117 µL, 708 µmol / 165 µL, 996 µmol, 6.0 eq.) was added and the flasks containing the reaction solutions were placed on an orbital shaker and shaken

gently. PyBOP (156 mg, 300 µmol / 184 mg, 354 µmol / 259 mg, 498 µmol, 3.0 eq.) dissolved in pre-cooled DMF (10 mL) was added and the mixture was gently shaken at 10 °C for 2 d. After this time the solvent was removed and the residue was co-evaporated twice with toluene. The remaining crude mixture was dissolved in a minimal amount of ethyl acetate (and optionally a few drops of MeOH to enhance solubility). This solution was added to cold ether, resulting in the precipitation of the crude peptide. The suspension was centrifuged and the pellet was washed once with cold ether and dried subsequently.

The *t*Bu protecting groups were removed as described in *method J*.

The crude peptides were purified by preparative HPLC using a preparative C_{18} column and a linear gradient of acetonitrile in H_2O, starting from 10% acetonitrile.

After the purification the solvent was removed and the products were lyophilized.

SAR-10:

Yield: 2.41 mg (2.5 µmol, 1.6%) as a white powder.

^{1}H NMR (700 MHz, DMSO-d_6) δ 10.01 (s, 1H), 8.45 (d, *J* = 8.1 Hz, 1H), 8.04-8.00 (m, 2H), 7.80 (d, *J* = 4.9 Hz, 1H), 7.72-7.70 (m, 1H), 7.69-7.66 (m, 1H), 7.22 (d, *J* = 2.0 Hz, 1H), 7.16 (s, 1H), 7.09 (s, 1H), 7.02 (s, 1H), 5.30-5.26 (m, 1H), 5.21-5.17 (m, 1H), 4.70-4.66 (m, 1H), 4.64-4.60 (m, 1H), 4.53-4.50 (m, 1H), 4.39-4.35 (m, 3H), 4.31-4.28 (m, 2H), 4.22-4.20 (m, 1H), 4.07 (bs, 1H), 4.01 (bs, 1H), 3.97-3.94 (m, 1H), 3.83-3.80 (m, 1H), 3.79-3.77 (m, 1H), 3.78 (bs, 1H), 3.12-3.11 (m, 1H), 2.70 (s, 3H), 2.41-2.39 (m, 1H), 2.09 (t, *J* = 7.3 Hz, 2H), 2.02-1.97 (m, 1H), 1.85-1.83 (m, 2H), 1.52-1.49 (m, 2H), 1.07 (d, *J* = 6.5 Hz, 3H), 1.01 (d, *J* = 6.2 Hz, 3H), 0.87-0.84 (m, 15H), 0.82 (d, *J* = 7.2 Hz, 3H), 0.75 (d, *J* = 6.5 Hz, 3H).

LC-MS: t_R = 7.12 min (C_{18}), *m/z* = 955.47($M^+ + H^+$, 100%), 945.45 calcd for $C_{43}H_{68}ClN_8O_{14}^+$.

SAR-11:

Yield: 2.23 mg (2.3 µmol, 1.4%) as a white powder.

^{1}H NMR (700 MHz, DMSO-d_6) δ 10.00 (s, 1H), 8.49 (d, *J* = 7.4 Hz, 1H), 8.42 (d, *J* = 6.4 Hz, 1H), 8.01 (d, *J* = 7.5 Hz, 1H), 7.82 (d, *J* = 8.5 Hz, 1H), 7.77 (d, *J* = 8.2 Hz, 1H), 7.25 (d, *J* = 1.8 Hz, 1H), 7.16 (s, 1H), 7.09 (s, 1H), 7.02 (s, 1H), 6.99 (d, *J* = 8.3 Hz, 1H), 5.- 5.22 (m, 1H), 5.21-5.19 (m, 1H), 4.92-4.90 (m, 1H), 4.69-4.66 (m, 1H), 4.62-4.59 (m, 1H), 4.55-4.52 (m, 1H), 4.39-4.35 (m, 2H), 4.34-4.31 (m, 1H), 4.29-4.26 (m, 1H), 4.23-4.20 (m, 1H), 4.18-4.16 (m, 1H), 4.10 (bs, 1H), 3.95 (bs, 1H), 3.86 (bs, 1H), 3.11-3.09 (m, 1H), 3.03-3.00 (m, 1H), 2.70 (s, 3H), 2.41-2.39 (m, 1H), 2.08 (t, *J* = 7.2 Hz, 2H), 1.86-1.85 (m, 2H), 1.74-1.72 (m, 1H), 1.53-1.48 (m, 2H), 1.20 (d, *J* = 7.1 Hz, 3H), 1.01 (d, *J* = 6.3 Hz, 3H), 0.92 (d, *J* = 6.3 Hz, 3H), 0.87-0.83 (m, 15H), 0.79 (d, *J* = 6.6 Hz, 3H), 0.75 (d, *J* = 6.3 Hz, 3H).

LC-MS: t_R = 7.33 min (C_{18}), *m/z* = 969.47($M^+ + H^+$, 100%), 969.47 calcd for $C_{44}H_{70}ClN_8O_{14}^+$.

SAR-12:

Yield: 7.04 mg (7.3 µmol, 4.5%) as a white powder.

^{1}H NMR (700 MHz, DMSO) δ 9.99 (s, 1H), 8.66 (s, 1H), 8.06-8.01 (m, 2H), 7.88 (d, *J* = 8.6 Hz, 1H), 7.76 (d, *J* = 8.1 Hz, 1H), 7.72 (d, *J* = 8.2 Hz, 1H), 7.26 (d, *J* = 1.6 Hz, 1H), 7.22 (s, 1H), 7.14 (s, 1H), 7.07 (s, 1H), 5.18-5.14 (m, 1H), 5.10-5.05 (m, 1H), 4.63-4.59 (m, 1H), 4.59-4.54 (m, 1H), 4.40-4.35 (m, 2H), 4.33-4.30 (m, 1H), 4.27-4.25 (m, 1H), 4.23-4.12 (m, 3H), 4.02 b(s, 1H), 3.93 (bs, 1H), 3.18-3.14 (m, 1H), 3.13-3.09 (m, 1H), 3.06-3.02 (m, 1H), 2.68 (s, 3H), 2.57-2.54 (m, 1H), 2.12-2.07 (m, 3H), 1.88-1.83 (m, 2H), 1.53-1.48 (m, 2H), 1.14 (d, *J* = 6.5 Hz, 3H), 1.08 (d, *J* = 6.0 Hz, 3H), 1.01 (d, *J* = 6.2 Hz, 3H), 0.93 (d, *J* = 6.3 Hz, 3H), 0.88-0.84 (m, 6H), 0.81 (d, *J* = 6.8 Hz, 6H), 0.79 (d, *J* = 6.6 Hz, 3H), 0.76 (d, *J* = 6.1 Hz, 3H), 0.71 (d, *J* = 6.8 Hz, 3H).

LC-MS: t_R = 7.04 min (C_{18}), *m/z* = 967.40($M^+ + H^+$, 100%), 967.49 calcd for $C_{45}H_{72}ClN_8O_{13}^+$.

6.5 Synthesis of symplostatin 4 and analogs

6.5.1 Synthesis of the building blocks for Symplostatin 4 and its derivatives

(*S,E*)-Methyl-4-((*tert*-butoxycarbonyl)amino)pent-2-enoate (37)

N,O-Dimethylhydroxylamine hydrochloride (1.07 g, 11.0 mmol, 1.1 eq.) was suspended in DCM (50 mL). Triethylamine (1.53 mL, 11.0 mmol, 1.1 eq.) and Boc-Ala-OH (1.89 g, 10.0 mmol) were added and the resulting solution was stirred until it became clear. Finally, dicyclohexylcarbodiimide (2.27 g, 11.0 mmol, 1.1 eq.) was added and the reaction mixture was stirred for 1 h. After this period the reaction mixture was filtered through a pad of Celite® and the solvent was removed.

The resulting white solid was suspended in ether (50 mL) and cooled in an ice bath. $LiAlH_4$ (417 mg, 11.0 mmol, 1.1. eq.) was added in one portion and the resulting mixture was stirred for 20 min at 0 °C. The reaction was quenched by addition of 1 M $KHSO_4$ solution, the resulting mixture was filtered through a pad of Celite® and the solvent was removed.

The resulting colorless oil was dissolved in DCM (100 mL) and methyl-2-(triphenylphosphoranylidene)acetate (5.02 g, 15.0 mmol, 1.5 eq.) was added. The reaction mixture was stirred at RT overnight.

The solvent was removed and the crude product was purified by flash column chromatography (33 % ethyl acetate in cyclohexane) yielding (*S,E*)-methyl-4-((*tert*-butoxycarbonyl)amino)pent-2-enoate (**37**).

Yield: 1.35 g (5.88 mmol, 59 %) as a pale yellow oil.

TLC (33 % ethyl acetate in cyclohexane): R_f = 0.47.

^{1}H NMR (500 MHz, $CDCl_3$): δ 6.81 (dd, *J* = 15.70, 4.90 Hz, 1H), 5.83 (dd, *J* = 15.70, 1.70. Hz, 1H), 4.68 (m, 1H), 4.32(bs, 1H), 3.66(s, 3H), 1.37(s, 9H), 1.20(d, *J* = 7.00 Hz, 3H).

^{13}C NMR (126 MHz, $CDCl_3$): δ 166.93, 155.07, 149.90, 119.80, 79.79, 51.68, 47.17, 28.47, 20.35.

LC-MS: t_R = 9.11 min (C_{18}), *m/z* = 229 (M^+, 15 %).

HRMS (ESI)*: m/z* calcd for $C_{11}H_{20}NO_4^+$ $[M + H]^+$ 230.1387, found 230.1388.

(*S*)-Methyl-2-((*S,E*)-4-((*tert*-butoxycarbonyl)amino)pent-2-enamido)propanoate (38)

(*S,E*)-Methyl-4-((*tert*-butoxycarbonyl)amino)pent-2-enoate (**37**, 700 mg, 3.05 mmol) was dissolved in a mixture of THF (5 mL) and MeOH (3 mL), then lithium hydroxide (146 mg, 6.11 mmol, 2.0 eq.) in water (2 mL) was added and the reaction mixture was stirred for 5 h at RT. After this time the reaction mixture was acidified to pH = 4 by addition of 1 N HCl and then diluted by the addition of brine (25 mL) and DCM (25 mL). The phases were separated and the aqueous phase was extracted once with DCM (25 mL). The organic phases were unified and the solvent was evaporated to dryness.

The remaining white solid was suspended in acetonitrile (25 mL) and alanine methylester hydrochloride (482 mg, 3.66 mmol, 1.2 eq.) was added. The suspension was cooled in an ice bath and DIEA (1.60 mL, 9.76 mmol, 3.2 eq.), HOBt (412 mg, 3.05 mmol, 1.0 eq.) and HBTU (1.16 g, 3.05 mmol, 1.0 eq.) were added consecutively. The reaction was allowed to warm to RT and stirred overnight.

The solvent was removed and the residue was taken up in ethyl acetate (100 mL), washed with 0.5 M aq. $KHSO_4$ solution (2x 20 mL), saturated aq. $NaHCO_3$ solution (2x 20 mL) and brine (2x 20 mL), dried over Na_2SO_4 and evaporated to dryness.

The crude product was purified by flash column chromatography (66 % ethyl acetate in cyclohexane, to afford pure (*S*)-methyl-2-((*S,E*)-4-((*tert*-butoxycarbonyl)amino)pent-2-enamido)propanoate (**38**).

Yield: 424 mg (1.41 mmol, 46 %) as white solid.

TLC (50 % ethyl acetate in cyclohexane): R_f = 0.22.

^{1}H NMR (400 MHz, MeOD): δ 6.70 (dd, *J* = 15.50, 5.40 Hz, 1H), 6.04 (dd, *J* = 15.50, 1.40 Hz, 1H), 4.45 (q, *J* = 7.30 Hz, 1H), 4.10 (q, *J* = 7.10 Hz, 1H), 3.71 (s, 3H), 1.44 (s, 3H), 1.39 (d, *J* = 7.30 Hz, 3H), 1.24 (d, *J* = 7.00 Hz, 3H).

^{13}C NMR (101 MHz, MeOD): δ 174.82, 168.10, 157.70, 147.41, 122.90, 80.39, 61.69, 52.89, 28.88, 21.01, 20.48, 17.51, 14.59.

LC-MS: t_R = 8.05 min (C_{18}), *m/z* 600 ($2M^+$, 100 %), ,323 (M^+ +Na^+, 50) 300 (M^+, 60).

HRMS (ESI)*: m/z* calcd for $C_{14}H_{25}N_2O_5^+$ 301.1758, found 301.1758.

***tert*-Butyl((*S,E*)-5-((*S*)-3-methoxy-2-methyl-5-oxo-2,5-dihydro-1*H*-pyrrol-1-yl)-5-oxopent-3-en-2-yl)carbamate (39)**

(*S*)-Methyl-2-((*S,E*)-4-((*tert*-butoxycarbonyl)amino)pent-2-enamido)propanoate (**38**, 250 mg, 0.83 mmol) was dissolved in a mixture of THF (1.7 mL) and MeOH (1 mL) and lithium hydroxide (40 mg, 1.66 mmol, 2.0 eq.) in water (0.65 mL) was added. The resulting reaction mixture was stirred for 5 h at RT. The reaction mixture was acidified to pH = 4 by the addition of 1 N HCl and then diluted by the addition of brine (10 mL) and DCM (10 mL). The phases were allowed to separate and the aqueous phase was extracted once with DCM (10 mL). The organic phases were unified and the solvent was evaporated to dryness.

The resulting white solid was dissolved with 4-(dimethyl)aminopyridine (254 mg, 2.08 mmol, 2.5 eq.) and 2,2-dimethyl-1,3-dioxane-4,6-dione (132 mg, 0.91 mmol, 1.1 eq.) in DCM (10 mL) and the mixture was cooled to -10 °C. 1-Ethyl-3-(3-dimethylaminopropyl)carbodiimide (191 mg, 1.00 mmol, 1.2 eq.) dissolved in DCM (5 mL) was added to the mixture over a period of 30 min and after the complete addition the reaction was allowed to warm to RT and stirred overnight.

The solvent was removed and the residue was taken up in ethyl acetate. The organic phase was washed with 0.5 M $KHSO_4$ solution (2x 10 mL), dried over Na_2SO_4 and evaporated to dryness.

The remaining bright yellow oil was dissolved in acetonitrile (20 mL) and heated to reflux for 1 h. The solvent was evaporated and the resulting yellow oil was dissolved in THF (10 mL). Triphenylphoshine (262 mg, 1.00 mmol, 1.2 eq.) and MeOH (40.5 µL, 1.00 mmol, 1.2 eq.) were added to this solution. Diethylazodicarboxylate (40 % in toluene, 458 µL, 1.00 mmol, 1.2 eq.) was added dropwise to the mixture, which remained light orange after complete addition. The reaction was stirred at RT overnight. The solvent was removed and the crude mixture was purified by flash column chromatography (2 % MeOH in DCM) to afford *tert*-butyl((*S,E*)-5-((*S*)-3-methoxy-2-methyl-5-oxo-2,5-dihydro-1*H*-pyrrol-1-yl)-5-oxopent-3-en-2-yl)carbamate (**39**).

Yield: 240 mg (0.74 mmol, 90 %) as a light yellow solid.

TLC (2 % MeOH in DCM): $R_f = 0.37$.

^{1}H NMR (400 MHz, $CDCl_3$): δ 7.34 (dd, *J* = 15.50, 6.10 Hz, 1H), 6.94 (dd, *J* = 14.80, 5.10 Hz, 1H), 4.97 (s, 1H), 4.69 (m, 1H), 4.39 (m, 1H) 3.80 (s, 3H) , 1.42 (s, 3H) 1.38 (s, 9H) 1.23 (d, *J* = 7.0 Hz, 3H).

^{13}C NMR (101 MHz, $CDCl_3$): δ 180.78, 169.87, 164.45, 155.14, 149.65, 121.87, 93.09, 79.63, 58.85, 55.79, 47.45, 28.48, 20.50, 17.20.

LC-MS: t_R = 9.41 (C_{18}), *m/z* = 671 ($2M^+ + Na^+$, 100 %), 548 ($2M^+$ -Boc, 85), 325 ($M^+ + H^+$, 75).

HRMS (ESI)*: m/z* calcd for $C_{16}H_{25}N_2O_5^+$ 325.1758, found 325.1760.

***tert*-Butyl((*S*)-1-(((*S*,*E*)-5-((*S*)-3-methoxy-2-methyl-5-oxo-2,5-dihydro-1*H*-pyrrol-1-yl)-5-oxopent-3-en-2-yl)amino)-4-methyl-1-oxopentan-2-yl)carbamate (40)**

tert-Butyl((*S,E*)-5-((*S*)-3-methoxy-2-methyl-5-oxo-2,5-dihydro-1*H*-pyrrol-1-yl)-5-oxopent-3-en-2-yl)carbamate (**39**, 390 mg, 1.30 mmol) was dissolved in DCM (3 mL) and trifluoroacetic acid (3 mL) was added. The reaction mixture was stirred for 3 h at RT. The solvent was evaporated and the remaining oil was co-evaporated twice with toluene to remove residual trifluoroacetic acid.

The resulting white solid was suspended in acetonitrile (10 mL) and Boc-Leu-OH (130 mg, 0.61 mmol, 1.1 eq.) was added. The suspension was cooled in an ice bath and DIEA (291 µL, 1.76 mmol, 3.2 eq.), HOBt (82 mg, 0.61 mmol, 1.1 eq.) and HBTU (332 mg, 0.61 mmol, 1.1 eq.) were added successively. The reaction was allowed to warm to RT and then stirred overnight.

The solvent was removed and the residue was taken up in ethyl acetate (40 mL), washed with 0.5 M $KHSO_4$ solution (2x 10 mL), saturated aq. $NaHCO_3$ solution (2x 10 mL) and brine (2x 10 mL). After drying over Na_2SO_4 the solvent was evaporated to dryness.

The crude product was purified by flash column chromatography (66 % ethyl acetate in cyclohexane) affording *tert*-butyl((*S*)-1-(((*S*,*E*)-5-((*S*)-3-methoxy-2-methyl-5-oxo-2,5-dihydro-1*H*-pyrrol-1-yl)-5-oxopent-3-en-2-yl)amino)-4-methyl-1-oxopentan-2-yl)carbamate (**40**).

Yield: 209 mg (0.47 mmol, 85 %) as a white solid.

TLC (66 % MeOH in DCM): R_f = 0.50.

^{1}H NMR (400 MHz, MeOD): δ 7.38 (dd, *J* = 15.6, 2.1 Hz, 1H), 6.96 (dd, *J* = 15.5, 5.2 Hz, 1H), 5.20 (s, 1H), 4.63 (m, 2H), 4.14 (m, 1H), 3.92 (s, 3H), 1.74-1.67 (m, 2H), 1.64-1.40 (m, 2H), 1.44 (s, 9H), 1.31 (d, *J* = 6.9 Hz, 3H), 1.23 (m, 3H), 0.98-0.93 (m, 6H).

^{13}C NMR (101 MHz, MeOD): δ 182.91, 175.08, 171.62, 165.75, 157.77, 150.05, 123.19, 93.77, 80.46, 68.16, 61.57, 59.95, 56.98, 54.46, 28.86, 26.03, 23.68, 17.52, 14.63.

LC-MS: t_R = 9.74 min (C_{18}), *m/z* = 438 (M^+ +H^+, 100 %), 338 (M^+ -Boc, 40).

HRMS (ESI)*: m/z* calcd for $C_{22}H_{36}N_3O_6^+$ 438.2599, found 438.2599.

(6*S*,9*S*,14*S*,*E*)-Methyl-6-*iso*butyl-2,2,9,14-tetramethyl-4,7,12-trioxo-3-oxa-5,8,13-triazapentadec-10-en-15-oate (41)

(*S*)-Methyl-2-((*S,E*)-4-((*tert*-butoxycarbonyl)amino)pent-2-enamido)propanoate (**38**, 390 mg, 1.30 mmol) was dissolved in DCM (5 mL), trifluoroacetic acid (5 mL) was added and the reaction mixture was stirred at RT for 2 h. The solvent was evaporated and the remaining oil was co-evaporated twice with toluene to remove residual trifluoroacetic acid.

The resulting white foamy solid was suspended in acetonitrile (10 mL) and Boc-Leu-OH (292 mg, 1.37 mmol, 1.1 eq.) was added. The suspension was cooled in an ice bath and DIEA (716 µL, 4.33 mmol, 3.3 eq.), HOBt (185 mg, 1.37 mmol, 1.1 eq.) and HBTU (520 mg, 1.37 mmol, 1.1 eq.) were added. The reaction was allowed to warm to RT and stirred overnight.

After this time the solvent was removed and the residue was taken up in ethyl acetate (100 mL), washed with 0.5 M $KHSO_4$ solution (2x 20 mL), saturated $NaHCO_3$ solution (2x 20 mL) and brine (2x 20 mL). After drying over Na_2SO_4 the solvent was removed.

The crude product was purified by flash column chromatography (66 % ethyl acetate in cyclohexane, affording (6*S*,9*S*,14*S*,*E*)-methyl-6-*iso*butyl-2,2,9,14-tetramethyl-4,7,12-trioxo-3-oxa-5,8,13-triazapentadec-10-en-15-oate (**41**).

Yield: 529 mg (1.28 mmol, 99 %) as a white solid.

TLC (66 % MeOH in DCM): R_f = 0.27.

^{1}H NMR (400 MHz, MeOD): δ 6.69 (dd, *J* = 15.4, 5.7 Hz, 1H), 6.06 (t, *J* = 15.7 Hz, 1H), 4.59 (m, 1H), 4.47 (m, 1H), 4.10 (m, 1H), 3.71 (s, 3H), 1.69 (m, 1H), 1.52 (m, 2H), 1.44 (s, 9H), 1.39 (d, *J* = 7.3 Hz, 3H), 1.29 (d, *J* = 6.5 Hz, 3H), 0.94 (m, 6H).

^{13}C NMR (101 MHz, MeOD): δ 175.19, 174.67, 167.82, 157.96, 146.18, 123.64, 80.67, 54.73, 52.88, 47.27, 42.49, 38.78, 28.87, 26.05, 23.68, 22.00, 17.60.

LC-MS: t_R = 9.14 min (C_{18}), *m/z* = 436 (M^+ +Na^+, 40 %), 314 (M^+ -Boc, 40 %).

HRMS (ESI)*: m/z* calcd for $C_{20}H_{36}N_3O_6^+$ 414.2599, found 414.2602.

(2*S*,3*S*)-(*S*)-1-Methoxy-4-methyl-1-oxopentan-2-yl-2-((*tert*-butoxycarbonyl)-(methyl)amino)-3-methylpentanoate (42)

(*S*)-(-)2-Hydroxyisocaproic acid (500 mg, 3.78 mmol) was dissolved in MeOH (20 mL) and cooled in an ice bath. Thionyl chloride (685 µL, 9.45 mmol, 2.5 eq.) was slowly added from a 2 M solution in DCM (4.8 mL). The reaction mixture was allowed to warm to RT and stirred overnight. The solvent was removed carefully due to the high volatility of the intermediate methyl ester.

The remaining light yellow oil was dissolved in DCM (20 mL) and Boc-*N*MeIle-OH (927 mg, 3.78 mmol, 1.0 eq.) and 4-(dimethyl)aminopyridine (46 mg, 0.38 mmol, 0.1 eq.) were added. The mixture was cooled in an ice bath and stirred for 5 min. Dicyclohexylcarbodiimide (840 mg, 4.07 mmol, 1.1 eq.) was added in one portion and the reaction mixture was allowed to warm to RT and stirred overnight.

The urea side product was filtered off and the solvent was removed. The residual solid was taken up in DCM (50 mL) and filtered once again. The organic phase was washed with 0.5 M HCl (2x 25 mL) and saturated aq. $NaHCO_3$ solution (2x 25 mL) and dried over Na_2SO_4.

The solvent was evaporated to dryness and the crude mixture was purified by flash column chromatography (12.5 % ethyl acetate in cyclohexane) to yield (2*S*,3*S*)-(*S*)-1-methoxy-4-methyl-1-oxopentan-2-yl-2-((*tert*-butoxycarbonyl)-(methyl)amino)-3-methylpentanoate (**42**).

Yield: 771 mg (2.06 mmol, 55%) as a colorless oil.

TLC (12.5% ethyl acetate in cyclohexane): R_f = 0.39.

^{1}H NMR (500 MHz, $CDCl_3$): δ 4.48 (m, 1H), 4.17 (m, 1H), 3.63 (s, 3H), 2.75 (s, 3H), 1.91 (m, 1H), 1.39 (s 14H), 1.02 (m, 3H), 0.84 (m, 6H).

^{13}C NMR (126 MHz, $CDCl_3$): δ 173.01, 170.84, 155.70, 79.86, 71.74, 58.04, 52.04, 39.99, 38.24, 28.47, 25.21, 23.10, 21.78, 15.63, 11.71.

(2*S*,3*S*)-(*S*)-1-Methoxy-4-methyl-1-oxopentan-2-yl2-(dimethylamino)-3-methyl-pentanoate (43)

(2*S*,3*S*)-(*S*)-1-Methoxy-4-methyl-1-oxopentan-2-yl-2-((*tert*-butoxycarbonyl)(methyl)-amino)-3-methylpentanoate (**42**, 400 mg, 1.07 mmol) was dissolved in DCM (5 mL) and trifluoroacetic acid was added. The reaction mixture was stirred for 2 h at RT. The solvent was evaporated and the remaining oil was co-evaporated twice with toluene to remove residual trifluoroacetic acid.

The resulting pale yellow oil was dissolved in DMF (5 mL) and methyl iodide (79 µL, 1.26 mmol, 1.2 eq.) and DIEA (531 µL, 3.21 mmol, 3.0 eq.) were added. The reaction mixture was stirred for 2 h, whereupon a TLC indicated a completed reaction.

The reaction mixture was quenched with saturated aq. NH_4Cl solution (5 mL) and extracted with ether (3x 30 mL). The unified organic phases were washed with brine (2x 30 mL) and dried over Na_2SO_4. Removal of the solvent afforded (2*S*,3*S*)-(*S*)-1-methoxy-4-methyl-1-oxopentan-2-yl2-(dimethylamino)-3-methyl-pentanoate (**43**) without further purification.

Yield: 118 mg (0.41 mmol, 38%) as a colorless oil.

^{1}H NMR (400 MHz, $CDCl_3$): δ 5.15 (dd, *J* = 9.1, 4.4 Hz, 1H), 4.52 (s, 1H), 3.73 (s, 3H), 3.61 (s, 6H), 2.35 (dd, *J* = 14.0, 7.0 Hz, 1H), 1.79 (m, 3H), 1.65 (m, 2H), 1.08 (m, 3H), 0.91 (dd, *J* = 14.9, 6.2 Hz, 9H).

^{13}C NMR (101 MHz, $CDCl_3$): δ 169.96, 166.08, 77.75, 72.99, 53.12, 39.70, 33.51, 29.17, 24.64, 23.05, 21.71, 16.65, 12.21.

LC-MS: t_R = 7.93 min, *m/z* = 288 ($M^+ + H^+$, 10 %).

HRMS (ESI)*: m/z* calcd for $C_{15}H_{30}NO_4^+$ 288.2169, found 288.2170.

(2*S*,3*S*)-(*S*)-1-Methoxy-4-methyl-1-oxopentan-2-yl-3-methyl-2-(methyl(prop-2-yn-1-yl)amino)pentanoate (44)

(2*S*,3*S*)-(*S*)-1-Methoxy-4-methyl-1-oxopentan-2-yl-2-((*tert*-butoxycarbonyl)(methyl)-amino)-3-methylpentanoate (**42**, 357 mg, 0.95 mmol) was dissolved in DCM (5 mL) and trifluoroacetic acid was added. The reaction mixture was stirred for 2 h at RT. The solvent was evaporated and the remaining oil was co-evaporated twice with toluene to remove residual trifluoroacetic acid.

The resulting pale yellow oil was dissolved in acetonitrile (10 mL) and propargyl bromide (80%wt in toluene, 125 µL, 1.12 mmol, 1.2 eq.) and DIEA (471 µL, 2.85 mmol, 3.0 eq.) were added. The reaction mixture was heated to 80 °C and stirred at this temperature overnight. The reaction mixture was allowed to cool to RT, quenched with saturated aq. NH_4Cl solution (5 mL) and extracted with ether (3x 30 mL). The unified organic phases were washed with brine (2x 30 mL) and dried over Na_2SO_4. After evaporation to dryness, the crude mixture was purified by flash column chromatography (50 % ethyl acetate in cyclohexane) to afford (2*S*,3*S*)-(*S*)-1-methoxy-4-methyl-1-oxopentan-2-yl-3-methyl-2-(methyl(prop-2-yn-1-yl)amino)pentanoate (**44**).

Yield: 186 mg (0.60 mmol, 63%) as a light yellow oil.
^{1}H NMR (400 MHz, $CDCl_3$): δ 4.97 (dd, *J* = 9.8, 4.0 Hz, 1H), 3.69 (s, 3H), 3.34 (ddd, *J* = 54.4, 16.9, 2.0 Hz, 2H), 3.12 (d, *J* = 9.8 Hz, 1H), 2.37 (s, 3H), 2.18 (t, *J* = 2.3 Hz, 1H), 1.78 (m, 3H), 1.61 (m, 2H), 1.17 (m, 1H), 0.89 (m, 12H).
^{13}C NMR (101 MHz, $CDCl_3$): δ 171.35, 171.26, 80.16, 72.52, 71.04, 70.09, 52.31, 43.46, 40.00, 38.23, 33.65, 25.30, 24.68, 23.28, 21.48, 15.46, 10.65.
LC-MS: t_R =12.49 min *m/z* = 312 ($M^+ + H^+$, 100 %).

6.5.2 Synthesis of symplostatin 4 and derivatives from the *C*-terminal and *N*-terminal peptides

Synthesis of symplostatin 4 (Sym4)

(2*S*,3*S*)-(*S*)-1-Methoxy-4-methyl-1-oxopentan-2-yl2-(dimethylamino)-3-methyl-pentanoate (**43**, 118 mg, 0.41 mmol) was dissolved in a mixture of THF (1.6 mL) and MeOH (1 mL) and lithium hydroxide (20 mg, 0.82 mmol, 2.0 eq.) in water (0.65 mL) was added. The resulting reaction mixture was stirred for 5 h at RT. The reaction mixture was acidified by addition of 1 M aq. HCl to pH 4 and diluted by the addition of DCM (5 mL) and brine (5 mL). The phases were separated and the water phase was extracted with DCM (2x 5 mL). The organic phases were combined and evaporation to dryness yielded the free acid, which was used directly for the following coupling.
To obtain the free amine, *tert*-butyl((S)-1-(((*S*,*E*)-5-((*S*)-3-methoxy-2-methyl-5-oxo-2,5-dihydro-1*H*-pyrrol-1-yl)-5-oxopent-3-en-2-yl)amino)-4-methyl-1-oxopentan-2-yl)carbamate (**40**, 170 mg, 0.39 mmol, 0.95 eq.) was dissolved in DCM (5 mL). trifluoroacetic acid (5 mL)

was added and the reaction mixture was stirred at RT for 2 h. The solvent was evaporated and the resulting oil was co-evaporated twice with toluene to remove residual trifluoroacetic acid.

For the peptide coupling the free acid and the free amine were dissolved separately in acetonitrile (6 mL) and cooled in an ice bath. The solution containing the amine was added to the acid solution and HOBt (55 mg, 0.41 mmol, 1.0 eq.), HBTU (156 mg, 0.41 mmol, 1.0 eq.) and DIEA (214 µL, 1.30 mmol, 3.2 eq.) were added successively. The reaction was allowed to warm to RT and followed by LC-MS analysis. A sample taken after 5 h indicated no further conversion, so the reaction was worked up.

The solvent was removed and the residue was taken up in ethyl acetate (100 mL). The organic phase was washed with 0.5 M aq. $KHSO_4$ solution (2x 10 mL), saturated aq. $NaHCO_3$ solution (2x 10 mL) and brine (2x 10 mL) and dried over Na_2SO_4. After removal of the solvent the crude product was purified by flash column chromatography (50 % ethyl acetate in cyclohexane) yielding symplostatin 4 (**Sym4**).

For a further purification, 96 mg of the pre-purified **Sym4** (210 mg in total, 91 %) were purified by preparative HPLC (0 min / 10% B → 3 min / 10% B → 30 min / 45% B → 32 min / 50% B → 33 min / 100% B → 43 min / 100% B) to afford symplostatin 4 (**Sym4**).

Yield: 48.8 mg (82.3 µmol, 20 %, 51 % in total) as a white powder.

TLC (50% ethyl acetate in cyclohexane): $R_f = 0.24$.

^{1}H NMR (600 MHz, CD_3CN): δ 7.34-7.29 (m, 1H), 6.89-6.85 (m, 1H), 5.09 (s, 1H), 5.08 (m, 1H), 4.59-4.55 (m, 2H), 4.38-4.31 (m, 1H), 3.86 (s, 1H), 3.13-3.08 (s, 1H) 2.91 (s, 6H), 2.18-2.13 (m, 1H), 1.82-1.73 (m, 2H), 1.70-1.64 (m, 1H), 1.63-1.53 (m, 4H), 1.42 (d, *J* = 6.6 Hz, 3H), 1.40-1.36 (m, 1H), 1.24 (d, *J* = 7.0 Hz, 3H), 1.00-0.88 (m, 18H).

^{13}C NMR (151 MHz, CD_3CN): δ 182.25, 172.28, 171.00, 170.19, 166.96, 164.99, 149.49, 123.06, 93.79, 75.83, 72.54, 60.03, 56.57, 52.99, 47.09, 42.05, 41.83, 41.22, 34.41, 27.32, 25.54, 25.29, 23.51, 23.34, 21.97, 21.83, 20.13, 17.44, 14.58, 11.82.

LC-MS: t_R = 7.39 min (C_{18}), *m/z* = 616 ($M^+ + Na^+$, 30 %) 593 ($M^+ + H^+$, 100).

HRMS (ESI)*: m/z* calcd for $C_{31}H_{53}N_4O_7^+$ 593.3909, found 592.3895.

Synthesis of a symplostatin 4 analog lacking the mmp unit (Sym4$^{\text{mmp→Ala}}$)

(2*S*,3*S*)-(*S*)-1-Methoxy-4-methyl-1-oxopentan-2-yl2-(dimethylamino)-3-methyl-pentanoate (**43**, 49 mg, 0.17 mmol) was dissolved in a mixture of THF (1.6 mL) and MeOH (1 mL), then lithium hydroxide (8 mg, 0.34 mmol, 2.0 eq.) dissolved in water (0.65 mL) was added and the reaction mixture was stirred for 5 h at RT. After this time the reaction mixture was acidified by addition of 1 M HCl to pH 4 and diluted with DCM (10 mL) and brine (10 mL). The phases were separated and the organic phase was extracted with DCM (2x 10 mL). Evaporation to dryness afforded the free acid, which was directly used in the following coupling.

To obtain the free amine (6*S*,9*S*,14*S*,*E*)-methyl-6-*iso*butyl-2,2,9,14-tetramethyl-4,7,12-trioxo-3-oxa-5,8,13-triazapentadec-10-en-15-oate (**41**, 78 mg, 0.25 mmol, 1.5 eq.) was dissolved in DCM (3 mL) and trifluoroacetic acid (3 mL) was added. The reaction mixture was stirred for 2 h at RT. The solvent was evaporated and the resulting oil was co-evaporated twice with toluene to remove residual trifluoroacetic acid.

For the peptide coupling the free acid and the free amine were dissolved separately in acetonitrile (5 mL) and cooled in an ice bath. The amine solution was added to the solution containing the acid; then HOBt (24 mg, 0.18 mmol, 1.1 eq.), HBTU (68 mg, 0.18 mmol, 1.1 eq.) and DIEA (93 µL, 0.56 mmol, 3.2 eq.) were added successively. After the addition of the reagents the reaction was allowed to warm to RT and stirred overnight.

The solvent was removed and the residue was taken up in ethyl acetate (50 mL). The organic phase was washed with 0.5 M aq. $KHSO_4$ solution (2x 10 mL), saturated aq. $NaHCO_3$ solution (2x 10 mL) and brine (2x 10 mL) and dried over Na_2SO_4. After evaporation of the solvent the crude product (49 mg) was purified by preparative HPLC (0 min / 10% B → 3 min / 10% B → 32 min / 50% B → 33 min / 100% B → 43 min / 100% B) to afford symplostatin 4 lacking the mmp unit (**Sym4$^{\text{mmp→Ala}}$**).

Yield: 37.5 mg (65.9 µmol, 39 %) as a white powder.

^{1}H NMR (600 MHz, CD_3CN): δ 7.51 (d, *J* = 7.6 Hz, 1H), 7.04 (d, *J* = 6.0 Hz, 1H), 6.79 (d, *J* = 7.9 Hz, 1H) 6.65 (dd, *J* = 15.5, 4.9 Hz, 1H), 5.98 (dd, *J* = 15.5, 1.6 Hz), 5.09-5.07 (m, 1H), 4.54-4.48 (m, 1H), 4.43-4.38 (m, 1H), 4.33-4.28(m, 1H), 3.89-3.87 (m, 1H), 3.66 (s, 3H), 2.91 (s, 6H), 2.18-2.14 (m, 1H), 1.81-1.73 (m, 2H), 1.67-1.54 (m, 5H), 1.42-1.37 (m, 1H), 1.35 (d, *J* = 7.3 Hz, 3H), 1.21 (d, *J* = 7.0 Hz, 3H), 0.98-0.97 (m, 3H), 0.96-0.91 (m, 12H), 0.89 (d, *J* = 6.4 Hz, 3H).

^{13}C NMR (151 MHz, CD_3CN): δ 174.34, 172.16, 170.39, 167.03, 166.15, 145.75, 123.22, 76.09, 72.60, 53.09, 52.84, 49.25, 46.78, 41.75, 41.41, 41.19, 34.43, 27.39, 25.57, 25.31, 23.45, 23.31, 21.86, 20.19, 17.76, 14.48, 11.89.
LC-MS: t_R = 6.68 min (C_{18}) *m/z* = 591 (M^+ +Na^+, 50 %), 569 (M^+ +H^+, 100).
HRMS (ESI)*: m/z* calcd for $C_{29}H_{53}N_4O_7^+$ 569.3909, found 569.3894.

6.5.3 Synthesis of tagged symplostatin 4 derivatives

Synthesis of an alkyne-tagged symplostatin 4 derivative (≡Sym4)

(2*S*,3*S*)-(*S*)-1-Methoxy-4-methyl-1-oxopentan-2-yl-3-methyl-2-(methyl(prop-2-yn-1-yl)amino)pentanoate (**44**, 86 mg, 0.28 mmol) was dissolved in a mixture of THF (1.6 mL) and MeOH (1 mL) and lithium hydroxide (13 mg, 0.55 mmol, 2.0 eq.) in water (0.65 mL) was added. The resulting reaction mixture was stirred for 5 h at RT. After this time the reaction mixture was acidified by addition of 1 M HCl to pH 4 and diluted by the addition of DCM (10 mL) and brine (10 mL). The phases were allowed to separate and the organic phase was extracted with DCM (2x 10 mL). Evaporation to dryness afforded the free acid, which was directly used for the following coupling.

To obtain the free amine *tert*-butyl((S)-1-(((*S*,*E*)-5-((*S*)-3-methoxy-2-methyl-5-oxo-2,5-dihydro-1*H*-pyrrol-1-yl)-5-oxopent-3-en-2-yl)amino)-4-methyl-1-oxopentan-2-yl)carbamate (**40**, 109 mg, 0.25 mmol, 0.9 eq.) was dissolved in DCM (5 mL) and trifluoroacetic acid (5 mL) was added. The resulting reaction mixture was stirred for 2 h at RT. The solvent was removed and the remaining oil was co-evaporated twice with toluene to remove residual trifluoroacetic acid.

For the peptide coupling the free acid and the free amine were dissolved separately in acetonitrile (5 mL) and cooled in an ice bath. The solution containing the amine was added to the acid solution and then HOBt (35 mg, 0.26 mmol, 0.9 eq.), HBTU (99 mg, 0.26 mmol, 0.9 eq.) and DIEA (136 µL, 0.83 mmol, 3.0 eq.) were added successively. The reaction was allowed to warm to RT and stirred overnight.

The solvent was evaporated and the residue was taken up in ethyl acetate (50 mL). The organic phase was washed with 0.5 M aq. $KHSO_4$ solution (2x 10 mL), saturated aq. $NaHCO_3$ solution (2x 10 mL) and brine (2x 10 mL) and dried over Na_2SO_4. After evaporation to dryness the crude product was purified by flash column chromatography (50 % ethyl acetate in cyclohexane) yielding the symplostatin 4 click derivative (**≡Sym4**).

For a further purification, 55 mg of the pre-purified **≡Sym4** (127 mg in total, 82 %) was purified by preparative HPLC (0 min / 10% B → 3 min / 10% B → 13 min / 45% B → 48 min / 85% B → 55 min / 100% B → 63 min / 100% B) to afford symplostatin 4 click derivative (**≡Sym4**).

Yield: 36.2 mg (58.7 µmol, 23 %, 64 % in total) as a white powder.

TLC (50% ethyl acetate in cyclohexane): $R_f = 0.34$.

^{1}H NMR (600 MHz, CD_3CN): δ 7.34-7.29 (m, 1H), 7.11 (d, J = 7.0 Hz, 1H), 6.91-6.86 (m, 1H), 6.81 (d, J = 8.2 Hz, 1H), 5.09 (s, 1H), 5.05-5.03 (m, 1H), 4.59-4.56 (m, 2H), 4.38-4.32 (m, 1H), 3.86 (s, 3H), 3.81 (s, 2H), 3.62-3.59 (m, 1H), 2.77 (s, 1H), 2.69 (s, 1H), 2.05-1.99 (m, 1H), 1.79-1.74 (m, 2H), 1.70-1.65 (m, 1H), 1.63-1.55 (m, 4H),1.42 (d, J = 6.6 Hz, 3H), 1.32-1.27 (m, 1H), 1.24 (d, J = 7.0 Hz, 3H), 0.95-0.88 (m, 18H).

^{13}C NMR (151 MHz, CD_3CN): δ 182.24, 172.23, 170.95, 170.64, 168.86, 164.91, 149.47, 123.06, 93.78, 77.89, 74.85, 70.61, 60.03, 56.56, 52.82, 52.64, 47.08, 44.90, 42.08, 41.45, 39.45, 34.32, 26.82, 25.56, 25.28, 23.52, 21.93, 21.88, 20.16, 20.05, 17.43, 15.32, 11.38.

LC-MS: t_R = 10.76 min, *m/z* = 639 ($M^+ + Na^+$, 100 %), 617 ($M^+ + H^+$, 30 %).

HRMS (ESI)*: m/z* calcd for $C_{33}H_{53}N_4O_7^+$ 617.3909, found 617.3896.

Synthesis of a alkyne-tagged Sym4$^{mmp\rightarrow Ala}$ derivative (≡Sym4$^{mmp\rightarrow Ala}$)

(2*S*,3*S*)-(*S*)-1-Methoxy-4-methyl-1-oxopentan-2-yl-3-methyl-2-(methyl(prop-2-yn-1-yl)amino)pentanoate (**44**, 100 mg, 0.32 mmol) was dissolved in a mixture of THF (1.6 mL) and MeOH (1 mL) and lithium hydroxide (15 mg, 0.64 mmol, 2.0 eq.) in water (0.65 mL) was added. The reaction mixture was stirred for 5 h at RT and the reaction mixture was acidified by addition of 1 M HCl to pH 4. DCM (10 mL) and brine (10 mL) were added, the phases were separated and the organic phase was extracted with DCM (2x 10 mL). Evaporation to dryness afforded the free acid, which was used directly for the following coupling.

To obtain the free amine (6*S*,9*S*,14*S*,*E*)-methyl-6-*iso*butyl-2,2,9,14-tetramethyl-4,7,12-trioxo-3-oxa-5,8,13-triazapentadec-10-en-15-oate (**41**, 100 mg, 0.32 mmol, 1.0 eq.) was dissolved in DCM (3 mL) and trifluoroacetic acid (3 mL) was added. The resulting reaction mixture was stirred for 2 h at RT. The solvent was evaporated and the resulting oil was co-evaporated twice with toluene to remove residual trifluoroacetic acid.

For the peptide coupling the free acid and the free amine were dissolved separately in acetonitrile (5 mL) and cooled in an ice bath. The amine solution was added to the solution containing the acid; then HOBt (43 mg, 0.32 mmol, 1.0 eq.), HBTU (121 mg, 0.32 mmol, 1.0 eq.) and DIEA (131 µL, 1.01 mmol, 3.2 eq.) were added successively. The reaction mixture was warmed to RT and then stirred for further 5 h.

The solvent was removed and the residue was taken up in ethyl acetate (50 mL). The organic phase was washed with 0.5 M aq. $KHSO_4$ solution (2x 10 mL), saturated aq. $NaHCO_3$ solution (2x 10 mL) and brine (2x 10 mL) and dried over Na_2SO_4. The solvent was removed and the crude product was purified by flash column chromatography (50 % ethyl acetate in cyclohexane) yielding the **Sym4**$^{\mathbf{mmp \rightarrow Ala}}$ click derivative (**≡Sym4**$^{\mathbf{mmp \rightarrow Ala}}$).

For a further purification, 66 mg of the pre-purified **≡Sym4**$^{\mathbf{mmp \rightarrow Ala}}$ (139 mg in total, 73 %) was purified by preparative HPLC (0 min / 10% B → 3 min / 10% B → 13 min / 45% B → 48 min / 85% B → 55 min / 100% B → 63 min / 100% B) to afford the **Sym4**$^{\mathbf{mmp \rightarrow Ala}}$ click derivative (**≡Sym4**$^{\mathbf{mmp \rightarrow Ala}}$).

Yield: 35.2 mg (59.5 µmol, 19 %, 53 % in total) as a white powder.

TLC (50% ethyl acetate in cyclohexane): R_f = 0.14.

^{1}H NMR (600 MHz, CD_3CN): δ 7.15 (bs, 1H), 6.95 (bs, 1H), 6.76 (bs, 1H), 6.66-6.61 (m, 1H), 5.96-5.91 (m, 1H), 5.03-5.01(m, 1H), 4.54-4.48 (m, 1H), 4.43-4.39 (m, 1H), 4.34-4.30 (m, 1H), 3.76 (s, 2H), 3.66 (s, 3H), 3.56-3.54 (m, 1H), 2.74 (s, 1H), 2.65 (s, 3H), 2.01-1.99 (m, 1H), 1.79-1.74 (m, 2H), 1.69-1.65 (m, 1H), 1.64-1.58 (m, 2H), 1.57-1.53 (m, 2H), 1.35 (d, *J* = 7.3 Hz, 3H), 1.30-1.25 (m,, 1H), 1.22-1.20 (m, 3H), 0.94-0.91 (m, 15H), 0.89 (d, *J* = 6.5 Hz, 3H).

^{13}C NMR (151 MHz, CD_3CN): δ 173.33, 171.21, 169.94, 168.41, 165.01, 144.71, 144.63, 122.23, 80.56, 76.43, 73.74, 69.64, 57.89, 51.85, 48.21, 45.79, 43.85, 40.84, 40.70, 40.41, 40.39, 38.41, 33.33, 25.73, 24.57, 24.31, 22.55, 22.43, 20.93, 19.21, 16.87, 16.80, 14.46, 10.31.

LC-MS: t_R = 9.87 min, *m/z* = 615 (M^+ +Na^+, 100 %), 593 (M^+ +H^+, 50).

HRMS (ESI)*: m/z* calcd for $C_{31}H_{53}N_4O_7^+$ 593.3909, found 593.3895.

Synthesis of a rhodamine-labeled symplostatin 4 derivative (Rh-Sym4)

≡Sym4 (1.14 mg, 1.85 µmol) and rhodamine azide (1 mg, 1.85 µmol, 1.0 eq.) were dissolved in water (400 µL) and *tris*(2-carboxyethyl)phosphine (TCEP, 100 mM aq. solution, 4.6 µL, 0.46 µmol, 0.25 eq.), *tris*[(1-benzyl-1*H*-1,2,3-triazol-4-yl)methyl]amine (TBTA, 100 mM solution in DMSO, 9.3 µL, 0.93 µmol, 0.5 eq.) and $CuSO_4$ (5 mM aq. solution, 92 µL, 0.46 µmol, 0.25 eq.) were added subsequently. The resulting reaction solution was stirred at RT overnight under exclusion of light.

The solvent was removed in a nitrogen stream and the crude product was purified by column chromatography (AluOx, 12.5 % MeOH in chloroform). This work-up yielded impure **Rh-Sym4**, and was purified further by a second chromatographic purification (AluOx, 12.5 % MeOH in chloroform) to yield pure **Rh-Sym4**.

Yield: 0.5 mg (0.43 µmol, 23 %) as a pink solid.

LC-MS: t_R = 8.55 min, *m/z* = 1157 (M^+ +H^+, 100 %), 1179 (M^+ +Na^+, 80).

HRMS (ESI)*: m/z* calcd for $C_{63}H_{85}N_{10}O_{11}^+$ 1157.6394, found 1157.6411.

Synthesis of a rhodamine-labeled symplostatin 4 derivative lacking the mmp unit (Rh-Sym4$^{mmp\rightarrow Ala}$)

≡Sym4$^{mmp\rightarrow Ala}$ (1.30 mg, 1.85 µmol) and rhodamine azide (1 mg, 1.85 µmol, 1.0 eq.) were dissolved in water (400 µL) and *tris*(2-carboxyethyl)phosphine (TCEP, 100 mM aq. solution, 4.6 µL, 0.46 µmol, 0.25 eq.), *tris*[(1-benzyl-1*H*-1,2,3-triazol-4-yl)methyl]amine (TBTA, 100 mM solution in DMSO, 9.3 µL, 0.93 µmol, 0.5 eq.) and $CuSO_4$ (5 mM aq. solution, 92 µL, 0.46 µmol, 0.25 eq.) were added subsequently. The reaction solution was stirred at RT overnight under exclusion of light.

The solvent was removed in a nitrogen stream and the crude product was purified by column chromatography (AluOx, 12.5 % MeOH in chloroform to yield pure **Rh-Sym4$^{mmp\rightarrow Ala}$**.

Yield: 1.4 mg (1.24 µmol, 67 %) as a pink solid.

LC-MS: t_R = 8.55 min, *m/z* = 1133 (M^+ +H^+, 30 %), 1155 (M^+ +Na^+, 75).

HRMS (ESI)*: m/z* calcd for $C_{61}H_{85}N_{10}O_{11}^+$ 1133.6394, found 1157.6404.

Synthesis of a trifunctional symplostatin 4 derivative (Tri-Sym4)

≡Sym4 (1.4 mg, 1.95 µmol, 1.05 eq.) and “Tri-azide” (2 mg, 1.85 µmol, 1.0 eq.) were dissolved in water (400 µL), then *tris*(2-carboxyethyl)phosphine (TCEP, 100 mM aq. solution, 4.6 µL, 0.46 µmol, 0.25 eq.), *tris*[(1-benzyl-1*H*-1,2,3-triazol-4-yl)methyl]amine (TBTA, 100 mM solution in DMSO, 9.3 µL, 0.93 µmol, 0.5 eq.) and $CuSO_4$ (5 mM aq. solution, 92 µL, 0.46 µmol, 0.25 eq.) were added successively. The reaction solution was stirred at RT overnight under exclusion of light. A LC-MS control performed after this time indicated that only a small amount of product had formed; consequently, the same amounts of the click reagents (TCEP, TBTA and $CuSO_4$) were added again to the solution which was then stirred for further 24 h. Although product had formed, a large quantity of starting material was still present. Thus, another 100 µL of a 1 M $CuSO_4$ solution and 10 µL of the TCEP solution were added and the reaction was stirred for another 24 h. After this time, the LC-MS control indicated a complete reaction.

The solvent was removed in a nitrogen stream and the crude product was purified by column chromatography (C_{18} silica gel, gradient starting from 30 % acetonitrile in H_2O) to yield pure **Tri-Sym4**.

Yield: 0.92 mg (0.54 µmol, 29 %) as a pink solid.

LC-MS: t_R = 8.21 min, *m/z* calcd for $C_{89}H_{128}N_{15}O_{16}S^+$ 1696.12, found 848.87 (100%, M^{2+}).

Synthesis of a trifunctional symplostatin 4 derivative lacking the mmp unit (Tri-Sym4$^{mmp\rightarrow Ala}$)

≡Sym4$^{mmp\rightarrow Ala}$ (1.4 mg, 1.95 µmol, 1.05 eq.) and “Tri-azide” (2 mg, 1.85 µmol, 1.0 eq.) were dissolved in water (400 µL), then *tris*(2-carboxyethyl)phosphine (TCEP, 100 mM aq. solution, 4.6 µL, 0.46 µmol, 0.25 eq.), *tris*[(1-benzyl-1*H*-1,2,3-triazol-4-yl)methyl]amine (TBTA, 100 mM solution in DMSO, 9.3 µL, 0.93 µmol, 0.5 eq.) and $CuSO_4$ (5 mM aq. solution, 92 µL, 0.46 µmol, 0.25 eq.) were added successively. The reaction solution was stirred at RT overnight under exclusion of light. A LC-MS control performed after this time indicated that only a small amount of product had formed; consequently, the same amounts of the click reagents (TCEP, TBTA and $CuSO_4$) were added again to the solution and the resulting mixture was stirred for further 24 h. Although the desired product was formed, a large quantity of starting material was still present. To overcome this, 100 µL of a 1 M $CuSO_4$ solution and

10 µL of the TCEP solution were added again and the reaction was stirred for another 24 h. After this time, the LC-MS control indicated a complete reaction.

The solvent was removed in a nitrogen stream and the crude product was purified by column chromatography (C_{18} silica gel, gradient starting from 30 % acetonitrile in H_2O) to yield pure **Tri- Sym4$^{\mathbf{mmp \rightarrow Ala}}$**.

Yield: 1.41 mg (0.84 µmol, 45 %) as a pink solid.

LC-MS: t_R = 8.43 min, *m/z* calcd for $C_{86}H_{178}N_{16}O_{16}S^+$ 1673.09, found 837.07 (100%, M^{2+}).

Synthesis of a biotinylated symplostatin 4 derivative (biotin-Sym4)

≡Sym4 (2.2 mg, 2.96 µmol, 1.05 eq.) and biotin azide (1 mg, 2.82 µmol, 1.0 eq.) were dissolved in water (500 µL), then *tris*[(1-benzyl-1*H*-1,2,3-triazol-4-yl)methyl]amine (TBTA, 100 mM solution in DMSO, 14.1 µL, 1.41 µmol, 0.5 eq.), *tris*(2-carboxyethyl)phosphine (TCEP, 100 mM aq. solution, 7.1 µL, 0.71 µmol, 0.25 eq.), and $CuSO_4$ (1 M solution, 141 µL, 141 µmol, 50 eq.) were added successively. The resulting reaction solution was stirred at RT for 3 d. A LC-MS control performed after this time indicated a complete reaction.

The solvent was removed in a nitrogen stream and the crude product was purified by column chromatography (C_{18} silica gel, gradient starting from 30 % acetonitrile in H_2O) to afford pure **biotin-Sym4**.

Yield: 0.67 mg (0.69 µmol, 24 %) as a white solid.

LC-MS: t_R = 9.21 min, *m/z* calcd for $C_{48}H_{79}N_{10}O_9S^+$ 971.57, found 971.53 (100%).

Synthesis of a biotinylated symplostatin 4 derivative lacking the mmp unit (biotin-Sym4$^{mmp\rightarrow Ala}$)

≡Sym4$^{mmp\rightarrow Ala}$ (2.1 mg, 2.96 µmol, 1.05 eq.) and biotin azide (1 mg, 2.82 µmol, 1.0 eq.) were dissolved in water (500 µL), then *tris*[(1-benzyl-1*H*-1,2,3-triazol-4-yl)methyl]amine (TBTA, 100 mM solution in DMSO, 14.1 µL, 1.41 µmol, 0.5 eq.), *tris*(2-carboxyethyl)phosphine (TCEP, 100 mM aq. solution, 7.1 µL, 0.71 µmol, 0.25 eq.), and $CuSO_4$ (1 M solution, 141 µL, 141 µmol, 50 eq.) were added successively. The resulting reaction solution was stirred at RT for 3 d. A LC-MS control performed after this time indicated a complete reaction.

The solvent was removed in a nitrogen stream and the crude product was purified by column chromatography (C_{18} silica gel, gradient starting from 30 % acetonitrile in H_2O) to afford pure **biotin-Sym4**.

Yield: 1.22 mg (1.29 µmol, 46 %) as a white solid.

LC-MS: t_R = 8.93 min, *m/z* calcd for $C_{46}H_{49}N_{10}O_9S^+$ 947.57, found 947.24 (100%).

6.6 Activity-based protein profiling experiments

6.6.1 General methods

Plant material

Arabidopsis thaliana ecotype Columbia plants were grown in a growth chamber at 24 °C (day)/20 °C (night) under a 12-h light regime. For the manufacturing of leaf extracts 4 to 6 week old rosette leaves were chosen.[156]

Protein extraction from A. thaliana leaves

Two rosette leaves were transferred into a 1.5 mL Eppendorf tube and 100 µL of water were added. The leaves were grinded and the grinder was rinsed with water (900 µL in total). The extract was then cleared by centrifugation (1 min at 16000 *g*).[156]

Labeling of A. thaliana leaf extracts

The labeling was carried out with 100 µL of leaf extract. 8 µL of buffer (50 mM sodium acetate for pH<6.5 and 50 mM 2-amino-2-(hydroxymethyl)-1,3-propandiol for pH>6.5) and 2 µL of 100 mM DTT (2 mM final concentration) were added. This solution was then incubated with 4.5 µL of the respective probe solution (100 mM stock in DMSO for 5 µM final concentration, 200 mM stock in DMSO for 10 µM final concentration) for 3 h under the exclusion of light with gentle agitation.

The labeling was stopped by the addition of 4X SDS-PAGE loading buffer (20 µL) and heating of the sample to 95 °C for 5 min. The proteins were separated by SDS-PAGE and visualized using a Typhoon scanner in case of the fluorescent probes. For the Western blotting of the biotinylated probes, the proteins were transferred onto polyvinylidene fluoride membranes after SDS-PAGE separation and detected using streptavidin-horseradish-peroxidase (HRP).

For competitive ABPP experiments, the protein extract was pre-incubated with competitor (11 µM) for 30 min, then the probe (5 µM) was added and the labeling was carried out as described.

In vivo labeling of A. thaliana cell culture

The cell cultures (*A. thaliana*,ecotype Landsberg[157]) were weekly subcultured in medium (3% w/v sucrose, 0.5 mg/L naphthalene acetic acid, 0.05 mg/L 6-benzylaminopurine (BAP)) and 4.4 g MS Gamborg B5 vitamins (Duchefa, http://www.duchefa.com), pH 5.7. Before the labeling experiment, the medium of a 7-day old cell culture was replaced by fresh medium.[149]

Labeling experiments were carried out using 300 µL of cell culture solution for each experiment; the solution was transferred to a 24-well microtiter plate. To this solution was added DTT (6 µL, 2 mM final concentration). In case of a competitive experiment, the cell culture was pre-incubated with competitor (15 µL, 25 µM final concentration) for 30 min, then the probe (13.5 µL, 5 µM final concentration (100 µM stock) or 13.5 µL, 10 µM final concentration (200 µM stock)) was added and the labeling was carried out for 1 h under the exclusion of light with gentle agitation. After the labeling, the cells were washed 3 - 5 times with medium that was carefully removed after each washing step, avoiding to remove cells as well. After the final washing step, 150 µL cell-containing solution were removed and transferred to a 1.5 mL Eppendorf tube where the cells were grinded. The solution was cleared by centrifugation (5 min at 16000 *g*), then 100 µL of the supernatant were transferred to a fresh Eppendorf tube and the reaction was stopped by addition of 20 µL 4X SDS-PAGE loading buffer and heating the sample to 95 °C for 5 min. The proteins were separated by SDS-PAGE and visualized using a Typhoon scanner in case of the fluorescent probes. For the Western blotting of the biotinylated probes, the proteins were transferred onto polyvinylidene fluoride membrane after SDS-PAGE separation and detected using streptavidin-horseradish-peroxidase (HRP).

6.6.2 Infiltration experiments

Infiltration of *A. thaliana* leaves *via* their petioles

The infiltration experiments were carried out in 24-well microtiter plates. Each well was filled with 500 µL of probe solution (2 µM/water), then three leaves with intact petioles were carefully inserted into the well with the leaves leaning against the walls of the well. The incubation was carried out at ambient temperature for 1 h; subsequently, the leaves were removed from the well. The petioles were detached and the leaves were transferred into an

Eppendorf tube containing a metal bead, then 300 µL of water were added and the leaves were grinded. After addition of 200 µL of water the extract was cleared by centrifugation (5 min at 16000 *g*) and 100 µL of supernatant were transferred to a fresh Eppendorf tube. The reaction was stopped by addition of 20 µL of 4X SDS-PAGE loading buffer and heating to 95 °C for 5 min.

The proteins were separated by SDS-PAGE and visualized using a Typhoon scanner in case of the fluorescent probes. For the Western blotting of the biotinylated probes, the proteins were transferred onto polyvinylidene fluoride membrane after SDS-PAGE separation and detected using streptavidin-horseradish-peroxidase (HRP).

Infiltration of *A. thaliana* leaves *via* their stomata

The infiltration of *A. thaliana* leaves *via* the stomata on the reverse side of the leaf was carried out while the leaves were still attached to the plant. To achieve the infiltration, the probe solution (2 µM/water, 500 µL per sample) was carefully applied by pressing a syringe (without a cannula) to the reverse side of a detached leaf and pressing down the plunger; a successful infiltration is visualized by the slight darkening of the leaves resulting from the uptake of the liquid into the vascular system. After the infiltration the infiltrated leaf was detached and incubated on a damp blotting paper in a petri dish. Each experiment was carried out with three leaves that were combined in the latter extraction. The infiltrated leaves were incubated for 2 h under the exclusion of light.

After this time, the leaves were transferred into an Eppendorf tube containing a metal bead, then 300 µL of water were added and the leaves were grinded. After addition of 200 µL of water, the extract was cleared by centrifugation (5 min at 16000 *g*) and 100 µL of supernatant were transferred to a fresh Eppendorf tube, the reaction was stopped by addition of 20 µL of 4X SDS-PAGE loading buffer and heating to 95 °C for 5 min.

The proteins were separated by SDS-PAGE and visualized using a Typhoon scanner in case of the fluorescent probes. For the Western blotting of the biotinylated probes, the proteins were transferred onto polyvinylidene fluoride membrane after SDS-PAGE separation and detected using streptavidin-horseradish-peroxidase (HRP).

7 References

[1] Koehn, F. E.; Carter, G. T. *Nat. Rev. Drug Disc.* **2005**, *4*, 206.

[2] Newman, D. J.; Cragg, G. M. *J. Nat. Prod.* **2007**, *70*, 461.

[3] Breinbauer, R.; Vetter, I. R.; Waldmann, H. *Angew. Chem. Int. Ed.* **2002**, *41*, 2878.

[4] Wetzel, S.; Bon, R. S.; Kumar, K.; Waldmann, H. *Angew. Chem. Int. Ed.* **2011**, *50*, 10800.

[5] Berg, J.; Tymoczko, J.; Stryer, L. *Biochemie*; Spektrum, 2007.

[6] Neurath, H. *Science* **1984**, *224*, 350.

[7] López-Otín, C.; Bond, J. S. *J. Biol. Chem.* **2008**, *283*, 30433.

[8] Schechter, I.; Berger, A. *Biochem. Biophys. Res. Commun.* **1967**, *27*, 157.

[9] Turk, B. *Nat. Rev. Drug Discov.* **2006**, *5*, 785.

[10] Drag, M.; Salvesen, G. S. *Nat. Rev. Drug Discov.* **2010**, *9*, 690.

[11] Rawlings, N. D.; Barrett, A. J.; Bateman, A. *Nucl. Acids Res.* **2012**, *40*, D343.

[12] Di Cera, E. *IUBMB Life* **2009**, *61*, 510.

[13] Southan, C. *Drug Discov. Today* **2001**, *6*, 1029.

[14] Page, M.; Di Cera, E. *Cell. Mol. Life Sci.* **2008**, *65*, 1220.

[15] Voet, D.; Voet, J. G.; Pratt, C. W. *Lehrbuch der Biochemie*; Wiley-VCH, 2002.

[16] Page, M. J.; Di Cera, E. *J. Biol. Chem.* **2008**, *283*, 30010.

[17] Bode, W.; Huber, R. *Curr. Opin. Struct. Biol.* **1991**, *1*, 45.

[18] Brauer, A. B. E.; McBride, J. D.; Kelly, G.; Matthews, S. J.; Leatherbarrow, R. J. *Bioorg. Med. Chem.* **2007**, *15*, 4618.

[19] Bode, W.; Huber, R. *Eur. J. Biochem.* **1992**, *204*, 433.

[20] McBride, J. D.; Watson, E. M.; Brauer, A. B. E.; Jaulent, A. M.; Leatherbarrow, R. J. *Peptide Sci.* **2002**, *66*, 79.

[21] Descours, A.; Moehle, K.; Renard, A.; Robinson, J. A. *ChemBioChem* **2002**, *3*, 318.

[22] Brauer, A. B. E.; Leatherbarrow, R. J. *Biochem. Biophys. Res. Commun.* **2003**, *308*, 300.

[23] Brauer, A. B. E.; Domingo, G. J.; Cooke, R. M.; Matthews, S. J.; Leatherbarrow, R. J. *Biochemistry* **2002**, *41*, 10608.

[24] Linington, R. G.; Edwards, D. J.; Shuman, C. F.; McPhail, K. L.; Matainaho, T.; Gerwick, W. H. *J. Nat. Prod.* **2007**, *71*, 22.

[25] Radau, G. *Curr. Enzyme Inhib.* **2005**, *1*, 295.

[26] Lee, A. Y.; Smitka, T. A.; Bonjouklian, R.; Clardy, J. *Chem. Biol.* **1994**, *1*, 113.

[27] Matern, U.; Oberer, L.; Falchetto, R. A.; Erhard, M.; König, W. A.; Herdman, M.; Weckesser, J. *Phytochemistry* **2001**, *58*, 1087.

[28] Matern, U.; Schleberger, C.; Jelakovic, S.; Weckesser, J.; Schulz, G. E. *Chem. Biol.* **2003**, *10*, 997.

[29] McDonough, M. A.; Schofield, C. J. *Chem. Biol.* **2003**, *10*, 898.

[30] *The Global Malaria Action Plan*, Roll Back Malaria Partnership, Geneva, 2008.

[31] *World Malaria Report 2010*, World Health Organization, Geneva, 2011.

[32] World Health Organization *Malaria, Fact sheet No. 94, October 2011*,accessed online: 24.11.2011.

[33] Wells, T. N. C.; Alonso, P. L.; Gutteridge, W. E. *Nat. Rev. Drug Discov.* **2009**, *8*, 879.

[34] Chen, Q.; Schlichtherle, M.; Wahlgren, M. *Clin. Microbiol. Rev.* **2000**, *13*, 439.

[35] Anstey, N. M.; Russell, B.; Yeo, T. W.; Price, R. N. *Trends Parasitol.* **2009**, *25*, 220.

[36] Parroche, P.; Lauw, F. N.; Goutagny, N.; Latz, E.; Monks, B. G.; Visintin, A.; Halmen, K. A.; Lamphier, M.; Olivier, M.; Bartholomeu, D. C.; Gazzinelli, R. T.; Golenbock, D. T. *Proc. Natl. Acad. Sci. U. S. A.* **2007**, *104*, 1919.

[37] Talisuna, A. O.; Bloland, P.; D'Alessandro, U. *Clin. Microbiol. Rev.* **2004**, *17*, 235.

[38] Sullivan, D. J.; Matile, H.; Ridley, R. G.; Goldberg, D. E. *J. Biol. Chem.* **1998**, *273*, 31103.

[39] Hempelmann, E. *Parasitol. Res.* **2007**, *100*, 671.

[40] Olliaro, P. L.; Yuthavong, Y. *Pharmacol. Ther.* **1999**, *81*, 91.

[41] Pandey, A. V.; Bisht, H.; Babbarwal, V. K.; Srivastava, J.; Pandey, K. C.; Chauhan, V. S. *Biochem. J.* **2001**, *355*, 333.

[42] Mendis, K.; Sina, B.; Marchesini, P.; Carter, R. *Am. J. Trop. Med. Hyg.* **2001**, *64*, 97.

[43] Farooq, U.; Mahajan, R. C. *J. Vect. Borne Dis.* **2004**, *41*, 45.

[44] Dondorp, A. M.; Yeung, S.; White, L.; Nguon, C.; Day, N. P. J.; Socheat, D.; von Seidlein, L. *Nat. Rev. Microbiol.* **2010**, *8*, 272.

[45] Meshnick, S. R.; Taylor, T. E.; Kamchonwongpaisan, S. *Microbiol. Rev.* **1996**, *60*, 301.

[46] Otto, H.-H.; Schirmeister, T. *Chem. Rev.* **1997**, *97*, 133.

[47] Turk, B.; Turk, D.; Turk, V. *Biochim. Biophys. Acta* **2000**, *1477*, 98.

[48] Dubin, G. *Cell. Mol. Life Sci.* **2005**, *62*, 653.

[49] Wegscheid-Gerlach, C.; Gerber, H.-D.; Diederich, W. E. *Curr. Top. Med.l Chem.* **2010**, *10*, 346.

[50] Rosenthal, P. J. In *Cysteine Proteases of Pathogenic Organisms*; Robinson, M. W., Dalton, J. P., Eds.; Springer US: 2011; Vol. 712, p 30-48.

[51] Kerr, I. D.; Lee, J. H.; Pandey, K. C.; Harrison, A.; Sajid, M.; Rosenthal, P. J.; Brinen, L. S. *J. Med. Chem.* **2009**, *52*, 852.

[52] Sijwali, P. S.; Rosenthal, P. J. *Proc. Natl. Acad. Sci. U. S. A.* **2004**, *101*, 4384.

[53] Sijwali, P. S.; Koo, J.; Singh, N.; Rosenthal, P. J. *Mol. Biochem. Parasitol.* **2006**, *150*, 96.

[54] Sijwali, P. S.; Shenai, B. R.; Gut, J.; Singh, A.; Rosenthal, P. J. *Biochem. J.* **2001**, *360*, 481.

[55] Ettari, R.; Bova, F.; Zappalà, M.; Grasso, S.; Micale, N. *Med. Res. Rev.* **2010**, *30*, 136.

[56] Wasinger, V. C.; Cordwell, S. J.; Cerpa-Poljak, A.; Yan, J. X.; Gooley, A. A.; Wilkins, M. R.; Duncan, M. W.; Harris, R.; Williams, K. L.; Humphery-Smith, I. *Electrophoresis* **1995**, *16*, 1090.

[57] Blackstock, W. P.; Weir, M. P. *Trends Biotechnol.* **1999**, *17*, 121.

[58] Patterson, S. D.; Aebersold, R. H. *Nat. Genet.* **2003**, *33*, 311.

[59] Mishra, N. C. *Introduction to Proteomics: Principles and Applications*; John Wiley & Sons, 2010, p 16.

[60] Tyers, M.; Mann, M. *Nature* **2003**, *422*, 193.

[61] Aebersold, R.; Mann, M. *Nature* **2003**, *422*, 198.

[62] Shiio, Y.; Aebersold, R. *Nat. Protoc.* **2006**, *1*, 139.

[63] Cravatt, B. F.; Wright, A. T.; Kozarich, J. W. *Annu. Rev. Biochem.* **2008**, *77*, 383.

[64] Adam, G. C.; Sorensen, E. J.; Cravatt, B. F. *Mol. Cell. Proteomics* **2002**, *1*, 828.

[65] Nicolaou, K. C. *Proc. Natl. Acad. Sci. U. S. A.* **2004**, *101*, 11928.

[66] Nicolaou, K. C.; Snyder, S. A. *Proc. Natl. Acad. Sci. U. S. A.* **2004**, *101*, 11929.

[67] Groner, B. In *Peptides as Drugs: Discovery and Development*; Groner, B., Ed.; Wiley-VCH: 2009, p 1-8.

[68] Kimmerlin, T.; Seebach, D. *J. Pept. Res.* **2005**, *65*, 229.

[69] El-Faham, A.; Albericio, F. *Chem. Rev.* **2011**, *111*, 6557.

[70] Dettner, F.; Hanchen, A.; Schols, D.; Toti, L.; Nusser, A.; Sussmuth, R. D. *Angew. Chem. Int. Ed.* **2009**, *48*, 1856.

[71] Seto, H.; Fujioka, T.; Furihata, K.; Kaneko, I.; Takahashi, S. *Tetrahedron Lett.* **1989**, *30*, 4987.

[72] Matsuzaki, K.; Ikeda, H.; Ogino, T.; Matsumoto, A.; Woodruff, H. B.; Tanaka, H.; Omura, S. *J. Antibiot. (Tokyo)* **1994**, *47*, 1173.

[73] Snapper, M. L.; Deng, H. B.; Jung, J. K.; Liu, T.; Kuntz, K. W.; Hoveyda, A. H. *J. Am. Chem. Soc.* **2003**, *125*, 9032.

[74] Krueger, C. A.; Kuntz, K. W.; Dzierba, C. D.; Wirschun, W. G.; Gleason, J. D.; Snapper, M. L.; Hoveyda, A. H. *J. Am. Chem. Soc.* **1999**, *121*, 4284.

[75] Shinohara, T.; Deng, H. B.; Snapper, M. L.; Hoveyda, A. H. *J. Am. Chem. Soc.* **2005**, *127*, 7334.

[76] Garfunkle, J.; Kimball, F. S.; Trzupek, J. D.; Takizawa, S.; Shimamura, H.; Tomishima, M.; Boger, D. L. *J. Am. Chem. Soc.* **2009**, *131*, 16036.

[77] Shimamura, H.; Breazzano, S. P.; Garfunkle, J.; Kimball, F. S.; Trzupek, J. D.; Boger, D. L. *J. Am. Chem. Soc.* **2010**, *132*, 7776.

[78] Newhouse, T.; Lewis, C. A.; Baran, P. S. *J. Am. Chem. Soc.* **2009**, *131*, 6360.

[79] Newhouse, T.; Lewis, C. A.; Eastman, K. J.; Baran, P. S. *J. Am. Chem. Soc.* **2010**, *132*, 7119.

[80] Rainier, J. D.; Espejo, V. R. *Org. Lett.* **2010**, *12*, 2154.

[81] Espejo, V. R.; Rainier, J. D. *J. Am. Chem. Soc.* **2008**, *130*, 12894.

[82] Herzner, H.; Rück-Braun, K. In *Organic Synthesis Highlights IV*; Schmalz, H. G., Ed.; Wiley-VCH: 2000, p 281-289.

[83] Peltier, H. M.; McMahon, J. P.; Patterson, A. W.; Ellman, J. A. *J. Am. Chem. Soc.* **2006**, *128*, 16018.

[84] Li, K. W.; Wu, J.; Xing, W. N.; Simon, J. A. *J. Am. Chem. Soc.* **1996**, *118*, 7237.

[85] Greshock, T. J.; Johns, D. M.; Noguchi, Y.; Williams, R. M. *Org. Lett.* **2008**, *10*, 613.

[86] Wen, S.; Packham, G.; Ganesan, A. *J. Org. Chem.* **2008**, *73*, 9353.

[87] Waldmann, H.; Hu, T. S.; Renner, S.; Menninger, S.; Tannert, R.; Oda, T.; Arndt, H. D. *Angew. Chem. Int. Ed.* **2008**, *47*, 6473.

[88] Clerc, J.; Groll, M.; Illich, D. J.; Bachmann, A. S.; Huber, R.; Schellenberg, B.; Dudler, R.; Kaiser, M. *Proc. Natl. Acad. Sci. U. S. A.* **2009**, *106*, 6507.

[89] Clerc, J.; Schellenberg, B.; Groll, M.; Bachmann, A. S.; Huber, R.; Dudler, R.; Kaiser, M. *Eur. J. Org. Chem.* **2010**, 3991.

[90] Tulla-Puche, J.; Bayo-Puxan, N.; Moreno, J. A.; Francesch, A. M.; Cuevas, C.; Alvarez, M.; Albericio, F. *J. Am. Chem. Soc.* **2007**, *129*, 5322.

[91] Bayo-Puxan, N.; Fernandez, A.; Tulla-Puche, J.; Riego, E.; Cuevas, C.; Alvarez, M.; Albericio, F. *Chem. Eur. J.* **2006**, *12*, 9001.

[92] Evans, D. A.; Wood, M. R.; Trotter, B. W.; Richardson, T. I.; Barrow, J. C.; Katz, J. L. *Angew. Chem. Int. Ed.* **1998**, *37*, 2700.

[93] Nicolaou, K. C.; Natarajan, S.; Li, H.; Jain, N. F.; Hughes, R.; Solomon, M. E.; Ramanjulu, J. M.; Boddy, C. N. C.; Takayanagi, M. *Angew. Chem. Int. Ed.* **1998**, *37*, 2708.

[94] Nicolaou, K. C.; Jain, N. F.; Natarajan, S.; Hughes, R.; Solomon, M. E.; Li, H.; Ramanjulu, J. M.; Takayanagi, M.; Koumbis, A. E.; Bando, T. *Angew. Chem. Int. Ed.* **1998**, *37*, 2714.

[95] Nicolaou, K. C.; Takayanagi, M.; Jain, N. F.; Natarajan, S.; Koumbis, A. E.; Bando, T.; Ramanjulu, J. M. *Angew. Chem. Int. Ed.* **1998**, *37*, 2717.

[96] Nicolaou, K. C.; Mitchell, H. J.; Jain, N. F.; Winssinger, N.; Hughes, R.; Bando, T. *Angew. Chem. Int. Ed.* **1999**, *38*, 240.

[97] Zolova, O. E.; Mady, A. S. A.; Garneau-Tsodikova, S. *Biopolymers* **2010**, *93*, 777.

[98] Romero, F.; Espliego, F.; Perez Baz, J.; Garcia de Quesada, T.; Gravalos, D.; de la Calle, F.; Fernandez-Puentes, J. L. *J. Antibiot. (Tokyo)* **1997**, *50*, 734.

[99] Perez Baz, J.; Canedo, L. M.; Fernandez Puentes, J. L.; Silva Elipe, M. V. *J. Antibiot. (Tokyo)* **1997**, *50*, 738.

[100] Yokokawa, F.; Inaizumi, A.; Shioiri, T. *Tetrahedron Lett.* **2001**, *42*, 5903.

[101] Yokokawa, F.; Inaizumi, A.; Shioiri, T. *Tetrahedron* **2005**, *61*, 1459.

[102] Yokokawa, F.; Shioiri, T. *Tetrahedron Lett.* **2002**, *43*, 8673.

[103] Taori, K.; Liu, Y. X.; Paul, V. J.; Luesch, H. *ChemBioChem* **2009**, *10*, 1634.

[104] Linington, R. G.; Clark, B. R.; Trimble, E. E.; Almanza, A.; Urena, L. D.; Kyle, D. E.; Gerwick, W. H. *J. Nat. Prod.* **2009**, *72*, 14.

[105] Vaz, E.; Brunsveld, L. *Org. Lett.* **2006**, *8*, 4199.

[106] Le Quement, S. T.; Nielsen, T. E.; Meldal, M. *J. Comb. Chem.* **2007**, *9*, 1060.

[107] Nielsen, T. E.; Le Quement, S. T.; Meldal, M. *Org. Lett.* **2007**, *9*, 2469.

[108] Nielsen, T. E.; Meldal, M. *Org. Lett.* **2005**, *7*, 2695.

[109] Zhu, J. P.; Jia, Y. X. *J. Org. Chem.* **2006**, *71*, 7826.

[110] Kokotos, G.; Padron, J. M.; Martin, T.; Gibbons, W. A.; Martin, V. S. *J. Org. Chem.* **1998**, *63*, 3741.

[111] Padrón, J. M.; Kokotos, G.; Martín, T.; Markidis, T.; Gibbons, W. A.; Martín, V. c. S. *Tetrahedron: Asymmetry* **1998**, *9*, 3381.

[112] Englund, E. A.; Gopi, H. N.; Appella, D. H. *Org. Lett.* **2004**, *6*, 213.

[113] Coleman, R. S.; Shah, J. A. *Synthesis* **1999**, *1999*, 1399.

[114] Kunz, H.; Waldmann, H.; Unverzagt, C. *Int. J. Pept. Protein Res.* **1985**, *26*, 493.

[115] Stolze, S. C.; Meltzer, M.; Ehrmann, M.; Kaiser, M. *Eur. J. Org. Chem.* **2012**, *2012*, 1616.

[116] Kishore Kumar, G. D.; Baskaran, S. *J. Org. Chem.* **2005**, *70*, 4520.

[117] Tan, Z. P.; Wang, L.; Wang, J. B. *Chin. Chem. Lett.* **2000**, *11*, 753.

[118] Stolze, S. C.; Meltzer, M.; Ehrmann, M.; Kaiser, M. *Chem. Commun.* **2010**, *46*, 8857.

[119] Kessler, H.; Becker, G.; Kogler, H.; Wolff, M. *Tetrahedron Lett.* **1984**, *25*, 3971.

[120] Kunz, H.; Kneip, M. *Angew. Chem.* **1984**, *96*, 702.

[121] Yu, C.; Taylor, J. W. *Tetrahedron Lett.* **1996**, *37*, 1731.

[122] Piettre, S. R.; Baltzer, S. *Tetrahedron Lett.* **1997**, *38*, 1197.

[123] Chamoin, S.; Houldsworth, S.; Kruse, C. G.; Iwema Bakker, W.; Snieckus, V. *Tetrahedron Lett.* **1998**, *39*, 4179.

[124] Hayashi, K.; Kim, S.; Kono, Y.; Tamura, M.; Chiba, K. *Tetrahedron Lett.* **2006**, *47*, 171.

[125] Prieto, M.; Mayor, S.; Rodriguez, K.; Lloyd-Williams, P.; Giralt, E. *J. Org. Chem.* **2007**, *72*, 1047.

[126] Hauske, P.; Meltzer, M.; Ottmann, C.; Krojer, T.; Clausen, T.; Ehrmann, M.; Kaiser, M. *Bioorg. Med. Chem.* **2009**, *17*, 2920.

[127] Meltzer, M.; Hasenbein, S.; Hauske, P.; Kucz, N.; Merdanovic, M.; Grau, S.; Beil, A.; Jones, D.; Krojer, T.; Clausen, T.; Ehrmann, M.; Kaiser, M. *Angew. Chem.* **2008**, *120*, 1352.

[128] Meltzer, M.; Hasenbein, S.; Hauske, P.; Kucz, N.; Merdanovic, M.; Grau, S.; Beil, A.; Jones, D.; Krojer, T.; Clausen, T.; Ehrmann, M.; Kaiser, M. *Angew. Chem. Int. Ed.* **2008**, *47*, 1332.

[129] Krowarsch, D.; Cierpicki, T.; Jelen, F.; Otlewski, J. *Cell. Mol. Life Sci.* **2003**, *60*, 2427.

[130] Novabiochem technical notes: *Fmoc-resin cleavage and deprotection*; Novabiochem, Merck KgAa, Darmstadt, Germany, 2007.

[131] López-Macià, À.; Jiménez, J. C.; Royo, M.; Giralt, E.; Albericio, F. *J. Am. Chem. Soc.* **2001**, *123*, 11398.

[132] Hamada, Y.; Kondo, Y.; Shibata, M.; Shioiri, T. *J. Am. Chem. Soc.* **1989**, *111*, 669.

[133] Lin, G.; Bode, W.; Huber, R.; Chi, C.; Engh, R. A. *Eur. J. Biochem.* **1993**, *212*, 549.

[134] Radisky, E. S.; Lee, J. M.; Lu, C.-J. K.; Koshland, D. E. *Proc. Natl. Acad. Sci. U. S. A.* **2006**, *103*, 6835.

[135] Fodor, K.; Harmat, V.; Neutze, R.; Szilágyi, L.; Gráf, L.; Katona, G. *Biochemistry* **2006**, *45*, 2114.

[136] Topf, M.; Richards, W. G. *J. Am. Chem. Soc.* **2004**, *126*, 14631.

[137] Topf, M.; Várnai, P.; Richards, W. G. *J. Am. Chem. Soc.* **2002**, *124*, 14780.

[138] Liu, B.; Schofield, C. J.; Wilmouth, R. C. *J. Biol. Chem.* **2006**, *281*, 24024.

[139] Speers, A. E.; Adam, G. C.; Cravatt, B. F. *J. Am. Chem. Soc.* **2003**, *125*, 4686.

[140] Speers, A. E.; Cravatt, B. F. *Chem. Biol.* **2004**, *11*, 535.

[141] Hosseini, M.; Kringelum, H.; Murray, A.; Tonder, J. E. *Org. Lett.* **2006**, *8*, 2103.

[142] Patino, N.; Frerot, E.; Galeotti, N.; Poncet, J.; Coste, J.; Dufour, M. N.; Jouin, P. *Tetrahedron* **1992**, *48*, 4115.

[143] Guerlavais, V.; Boeglin, D.; Mousseaux, D.; Oiry, C.; Heitz, A.; Deghenghi, R.; Locatelli, V.; Torsello, A.; Ghé, C.; Catapano, F.; Muccioli, G.; Galleyrand, J.-C.; Fehrentz, J.-A.; Martinez, J. *J. Med. Chem.* **2003**, *46*, 1191.

[144] Pine, S. H.; Sanchez, B. L. *J. Org. Chem.* **1971**, *36*, 829.

[145] Da, C. S.; Ni, M.; Han, Z. J.; Yang, F.; Wang, R. *J. Mol. Catal. A: Chem.* **2006**, *245*, 1.

[146] Schmidt, S.; Teich, L.; Khodja, M.; Sicker, D. *Lett. Org. Chem.* **2005**, *2*, 165.

[147] Benetti, S.; De Risi, C.; Marchetti, P.; Pollini, G. P.; Zanirato, V. *Synthesis* **2002**, *2002*, 331.

[148] Jou, G.; Gonzalez, I.; Albericio, F.; Lloyd-Williams, P.; Giralt, E. *J. Org. Chem.* **1997**, *62*, 354.

[149] Kaschani, F.; Verhelst, S. H. L.; Van Swieten, P. F.; Verdoes, M.; Wong, C.-S.; Wang, Z.; Kaiser, M.; Overkleeft, H. S.; Bogyo, M.; Van Der Hoorn, R. A. L. *Plant J.* **2009**, *57*, 373.

[150] Shindo, T.; Misas-Villamil, J. C.; Hörger, A. C.; Song, J.; van der Hoorn, R. A. L. *PLoS One* **2012**, *7*, e29317.

[151] Rosenthal, P. J. *Int. J. Parasitol.* **2004**, *34*, 1489.

[152] Wang, F.; Krai, P.; Deu, E.; Bibb, B.; Lauritzen, C.; Pedersen, J.; Bogyo, M.; Klemba, M. *Mol. Biochem. Parasitol.* **2011**, *175*, 10.

[153] Greenbaum, D. C.; Baruch, A.; Grainger, M.; Bozdech, Z.; Medzihradszky, K. F.; Engel, J.; DeRisi, J.; Holder, A. A.; Bogyo, M. *Science* **2002**, *298*, 2002.

[154] Pandey, K. C.; Singh, N.; Arastu-Kapur, S.; Bogyo, M.; Rosenthal, P. J. *PLoS Pathog.* **2006**, *2*, e117.

[155] Teixeira, C.; R.B. Gomes, J.; Gomes, P. *Curr. Med. Chem.* **2011**, *18*, 1555.

[156] Gu, C.; Kolodziejek, I.; Misas-Villamil, J.; Shindo, T.; Colby, T.; Verdoes, M.; Richau, K. H.; Schmidt, J.; Overkleeft, H. S.; Van Der Hoorn, R. A. L. *Plant J.* **2010**, *62*, 160.

[157] May, M. J.; Leaver, C. J. *Plant Physiol.* **1993**, *103*, 621.

8 Appendix

Abbreviations

The amino acids were abbreviated according to the 1-letter or 3-letter code recommended by the IUPAC-IUB joint commission on biochemical nomenclature (compare: *Pure Appl. Chem.* **1984**, *56*, 595-624.)

A. thaliana	*Arabidopsis thaliana*
aa	amino acid(s)
ABP	activity-based probe
ABPP	activity-based protein profiling
Ac	acyl-
Acm	acetamidomethyl-
AcOH	acetic acid
ACT	artemisinin combination therapy
Ahp	3-amino-6-hydroxy-2-piperidone
AIDS	acquired immunodeficiency syndrome
Alloc	allyloxycarbonyl-
aq.	aqueous
ASPP	active site peptide profiling
b	broad signal (NMR)
BBI	Bowman-Birk inhibitor
Bn	benzyl-
Boc	*tert*-butoxycarbonyl-
Bz/Bzl	benzyl-
Cbz	benzyloxylcarbonyl-
CID	collision-induced dissociation
Cit	citrulline
d	doublet
Da	Dalton
DABCO	1,4-Diazobicyclo[2.2.2]octane
DCC	*N,N′*-Dicyclohexyl carbodiimide
DCM	dichloromethane
dd	doublet of doublets
Ddm	4,4-dimethoxydiphenylmethyl-

DEAD	Diethyl azodicarboxylate
DHA	dihydroartemisinin
DHFR	dihydrofolate reductase
DHPS	dihydropteroate synthetase
DIAD	di*iso*-propyl azodicarboxylate
DIBAL-H	diiso-butyl aluminum hydride
DIC/DIPCDI	*N,N'*-Diisopropyl carbodiimide
DIEA	*N,N'*-Diisopropylethylamine
DMAP	4-Dimethylamino pyridine
DMF	dimethyl formamide
DMPU	1,3-Dimethyltetrahydropyrimidin-2(1*H*)-one
DMSO	dimethyl sulfoxide
DNA	deoxyribonucleic acid
DPPA	Diphenylphosphorylazide
dr	diastereomeric ratio
dt	doublet of triplets
EDC	1-Ethyl-3-(3'-dimethylaminopropyl)carbodiimide
eq.	equivalent(s)
ESI	electrospray ionization
Et	ethyl-
EtOAc	ethyl acetate
EtOH	ethanol
FDPP	Pentafluorophenyl diphenylphosphinate
Fmoc	9-fluorenylmethoxy carbonyl-
FP-1/-2/-3	falcipain-1/-2/-3
h	hour(s)
HATU	2-(1*H*-Azabenzotriazole-1-yl)1,1,3,3-tetramethylaminium hexafluorophosphate
HBTU	2-(1*H*-Benzotriazole-1-yl)1,1,3,3-tetramethylaminium hexafluorophosphate
HIV	human immunodeficiency virus
HOAt	1-Hydroxy-7-azabenzotriazole
HOBt	*N*-Hydroxybenzotriazole
HOSu	*N*-Hydroxysuccinimide
HPLC	high pressure liquid chromatography
HRMS	high resolution mass spectrometry
HRP	horseradish peroxidase

Hse	homoserine
Hz	Hertz
*i*Bu	*iso*-butyl-
ICAT	isotope-coded affinity tags
*i*Pr	*iso*-propyl-
IRS	indoor residual spraying
ITN	insecticide-treated net
J	coupling constant
k	kilo-
KHMDS	Potassium bis(trimethylsilyl)amide
K_i	dissociation constant
k_i	rate of inactivation
KO	knock-out
LC-MS	liquid chromatography mass spectrometry
LHMDS	Lithium bis(trimethylsilyl)amide
m	multiplet
M	molar
MALDI	matrix-assisted laser desorption ionization
Me	methyl-
MeOH	methanol
MHz	Megahertz
min	minute(s)
mL	milliliter(s)
mRNA	messenger ribonucleic acid
Ms	mesyl-
MS	mass spectrometry
Mu	morpholine urea
MudPIT	multidimensional protein identification technology
N	normal
NaHMDS	Sodium bis(trimethylsilyl)amide
nm	nanometer
NMP	*N*-Methylpyrrolidone
NMR	nuclear magnetic resonance
N-Pipu	*N*-Methylpiperazyl urea
o/n	overnight

P. falciparum	*Plasmodium falciparum*
PCR	polymerase chain reaction
PEG	polyethylene glycol
Pet	2-(pyridyl)ethyl-
Piv	pivaloyl-
PLCP	papain-like cysteine protease
*p*NZ	*para*-nitrobenzyloxycarbonyl-
ppm	parts per million
Py	pyrrole-
PyBOP	Benzotriazole-1-yl-oxy-tris-pyrrolidino-phosphonium hexafluorophosphate
PyBrOP	Bromo-tris-pyrrolidino-phosphonium hexafluorophosphate
quant.	quantitative
RBC	red blood cell
RCM	ring closing metathesis
rt/RT	room temperature
s	singlet
SAR	structure-activity relationship
SDS-PAGE	sodium dodecylsulfate polyacrylamide gel eletrophoresis
Sharpless AA	Sharpless asymmetric aminohydroxylation
Sharpless AD	Sharpless asymmetric dihydroxylation
SP	sulfadoxine-pyrimethamine
sp.	species
spp.	species pluralis
SPPS	solid-phase peptide synthesis
t	triplet
TBS/TBDMS	*tert*-butyl dimethylsilyl-
TBTA	Tris[(1-benzyl-1*H*-1,2,3-triazol-4-yl)methyl]amine
*t*Bu	*tert*-butyl
*t*BuOH	*tert*-butanol
TCEP	Tris(2-chloroethyl)phosphate
TEA	triethylamine
Tf	triflyl-
Tfa	trifluoroacetyl-
TFA	Trifluoroacetic acid
TFE	Trifluoro ethanol

THF	tetrahydrofuran
TIS	Triisopropyl silane
TLC	thin layer chromatography
TLR9	toll-like receptor 9
TMSE	trimethylsilyl ethyl-
TNF-α	tumor necrosis factor α
TOF	time of flight
Trt	trityl-, triphenylmethyl-
Ts	tosyl-
UNDP	United Nations Development Program
UNICEF	United Nations (International) Children’s (Emergency) Fund
UV	ultraviolet
WHO	World Health Organizaztion
WT	wild-type
Z	benzyloxylcarbonyl-
°C	degrees Celsius
2DE	2-dimensional gel electrophoresis
δ	chemical shift
ε	extinction coefficient
µ	micro-

Hiermit erkläre ich an Eides statt, dass ich die vorliegende Dissertation selbständig verfasst habe und alle dafür verwendeten Quellen und Hilfen kenntlich gemacht habe. Darüber hinaus wurden keine weiteren Quellen oder Hilfsmittel verwendet.

Zudem erkläre ich, dass diese Dissertation weder in der gegenwärtigen noch in einer anderen Form an der Technischen Universität Dortmund oder an einer anderen Hochschule im Zusammenhang mit einer staatlichen oder akademischen Prüfung bereits vorgelegt worden ist.

Ort, Datum

Sara Christina Stolze

Lebenslauf Sara Christina Stolze

Persönliche Daten

Geburtsdatum und-ort:	21/12/1982 in Dortmund
Eltern:	Prof. Dr. Joachim Stolze, Physiker Angelika Stolze, Lehrerin
Geschwister:	Jan-Christoph Stolze
Familienstand:	ledig

Ausbildung

seit 06/2011	Promotion in Chemie an der TU Dortmund, Zentrum für Medizinsche Biotechnologie, Universität Duisburg-Essen
10/2007 - 06/2011	Promotion in Chemie an der TU Dortmund, Chemical Genomics Centre der Max-Planck-Gesellschaft Arbeitsgruppe Prof. Dr. M. Kaiser (Universität Duisburg-Essen) Betreuer: Prof. Dr. H. Waldmann (TU Dortmund) Dissertation: “Chemistry and Biology of Natural Product-derived Protease Inhibitors”
04/2007 - 10/2007	Diplomarbeit, TU Dortmund, Chemical Genomics Centre der Max-Planck-Gesellschaft Arbeitsgruppe Dr. M. Kaiser Betreuer: Prof. Dr. H. Waldmann Diplomarbeit “Festphasen-Synthese von Cyanopeptolin-Analoga” Abschluss: Diplom-Chemikerin
10/2002 - 04/2007	Diplomstudium in Chemie, TU Dortmund
10/1993 - 05/2002	Käthe-Kollwitz-Gymnasium, Dortmund Abschluss: Abitur
09/1992 - 09/1993	West Kingston Elementary School, West Kingston, R. I., USA
08/1989 - 09/1992	Reichshof Grundschule, Dortmund-Brackel

Wissenschaftliche Arbeit

seit 04/2007	Chemische Synthese am Chemical Genomics Centre der Max-Planck-Gesellschaft, Dortmund und am Zentrum für Medizinische Biotechnologie, Universität Duisburg-Essen
Juni 2010	Forschungsaufenthalt im Plant Chemetics Labor, Dr. R. van der Hoorn, MPI für Pflanzenzüchtungsforschung, Köln
Oktober 2011	Teilnehmerin am ZMB Mentoring Programm, Mentor: Prof. Dr. Dr. hc. mult. Kurt Wüthrich
10/2006 - 12/2006	Praktikum in bio-anorganischer Chemie, AG Dr. J. Müller, TU Dortmund
08/2005 - 10/2005	Praktikum in bio-organischer Chemie, Prof. Dr. R. Breinbauer, TU Dortmund

Publikationen

Solid-Phase Total Synthesis of the 3-Amino-6-Hydroxy-2-Piperidone (Ahp) Cyclodepsipeptide and Protease Inhibitor Symplocamide A, Stolze, S. C.; Meltzer, M.; Ehrmann, M.; Kaiser, M. *Chem. Commun.* **2010**, *46*, 8857-8859.
Highlighted in: *Synfacts* **2011**, *2*, 233.

Development of a Solid-Phase Approach to the Natural Product Class of Ahp-Containing Cyclodepsipeptides, Stolze, S. C.; Meltzer, M.; Ehrmann, M.; Kaiser, M. *Eur. J. Org. Chem.* **2012**, 1616-1625.

Challenges in the Syntheses of Peptidic Natural Products, Stolze, S. C.; Kaiser, M. *Synthesis* **2012**, *44*, 1755-1777.

CV Sara Christina Stolze

Personal Data

Date and place of birth: 12/21/1982 in Dortmund, Germany
Parents: Prof. Dr. Joachim Stolze, physicist
Angelika Stolze, teacher
Siblings: Jan-Christoph Stolze
Marital status: unmarried

Education

since 06/2011	PhD student in Chemistry, TU Dortmund University, Zentrum für Medizinische Biotechnologie, University of Duisburg-Essen
10/2007 - 06/2011	PhD student in Chemistry, TU Dortmund University, Chemical Genomics Centre of the Max Planck Society research group Prof. Dr. M. Kaiser (University of Duisburg-Essen) Supervisor: Prof. Dr. H. Waldmann (TU Dortmund) Title of thesis: “Chemistry and Biology of Natural Product-derived Protease Inhibitors”
04/2007 - 10/2007	Graduate student, TU Dortmund University, Chemical Genomics Centre of the Max Planck Society, research group Dr. M. Kaiser Supervisor: Prof. Dr. H. Waldmann Title of thesis “Solid-Phase Synthesis of Cyanopeptolin Analogs” Degree: Diplom (diploma)
10/2002 - 04/2007	undergraduate student in Chemistry, TU Dortmund University
10/1993 - 05/2002	Käthe-Kollwitz-Gymnasium, Dortmund Degree: Abitur (high school diploma)
09/1992 - 09/1993	West Kingston Elementary School, West Kingston, R. I., USA
08/1989 - 09/1992	Reichshof Grundschule, Dortmund-Brackel

Scientific experience

since 04/2007	Chemical synthesis at the Chemical Genomics Center of the Max Planck Society, Dortmund and at the Zentrum für Medizinische Biotechnologie, University of Duisburg-Essen
June 2010	visiting researcher in the Plant Chemetics lab, Dr. R. van der Hoorn, MPI for Plant breeding research, Cologne, Germany
October 2011	participant of the ZMB Mentoring Program, Mentor: Prof. Dr. Dr. hc. mult. Kurt Wüthrich
10/2006 - 12/2006	internship in bio-inorganic chemistry, Dr. J. Müller, TU Dortmund University
08/2005 - 10/2005	internship in bio-organic chemistry, Prof. Dr. R. Breinbauer, TU Dortmund University

Publications

Solid-Phase Total Synthesis of the 3-Amino-6-Hydroxy-2-Piperidone (Ahp) Cyclodepsipeptide and Protease Inhibitor Symplocamide A, Stolze, S. C.; Meltzer, M.; Ehrmann, M.; Kaiser, M. *Chem. Commun.* **2010**, *46*, 8857-8859.
Highlighted in: *Synfacts* **2011**, *2*, 233.

Development of a Solid-Phase Approach to the Natural Product Class of Ahp-Containing Cyclodepsipeptides, Stolze, S. C.; Meltzer, M.; Ehrmann, M.; Kaiser, M. *Eur. J. Org. Chem.* **2012**, 1616-1625.

Challenges in the Syntheses of Peptidic Natural Products, Stolze, S. C.; Kaiser, M. *Synthesis* **2012**, *44*, 1755-1777.

Acknowledgement/Danksagung

Ich bedanke mich bei Prof. Dr. Herbert Waldmann dafür, dass er mir ermöglich hat, meine Promotion unter den exzellenten Arbeitsbedingungen am Chemical Genomics Centre der Max-Planck-Gesellschaft und in seiner Arbeitsgruppe am Max-Planck-Institut für Molekulare Physiologie durchzuführen. Desweiteren möchte ich Prof. Waldmann für die Übernahme des ersten Gutachtens danken.

Meinem Doktorvater Prof. Dr. Markus Kaiser möchte ich für die fruchtbare Zusammenarbeit in den letzten fünf Jahren danken. Du hast mir immer die Freiheit gelassen eigene Ideen zu verwirklichen und meine Forschungsarbeit eigenständig durchzuführen. Du hattest immer ein offenes Ohr und deine Denkanstöße haben sehr zum Gelingen meiner Arbeit beigetragen. Ich danke dir für die Übernahme des Zweitgutachtens.

Bei den aktuellen und ehemaligen Mitgliedern der Arbeitsgruppe Kaiser möchte ich mich für die sehr angenehme Arbeitsatmosphäre und die kollegiale Zusammenarbeit bedanken:

Sabrina Nickel und Philipp Kuhenne, euch danke ich für die jahrelange tolle und im wahrsten Sinne des Wortes enge Zusammenarbeit am CGC. Hätten wir 3 uns nicht so gut verstanden, hätten wir kaum mit drei Personen in 2 Abzügen arbeiten können. Ich wünsche euch beiden alles Gute für eure gemeinsame Zukunft!

Timon Mönig, dir danke ich für unsere langjährige Freundschaft, die schon seit dem ersten Vorkurs währt. Unsere gemeinsame Leidenschaft für den BVB hat uns immer verbunden, wir haben gelitten aber in der letzten Zeit auch viel gejubelt. Hoffen wir, dass es noch lange so bleibt! Heja BVB!

Bei Julian Oeljeklaus, Daniel Krahn und Patrick Hauske möchte ich mich für die kollegiale Zusammenarbeit und die stetige Diskussionsbereitschaft über eine Vielzahl von Themen bedanken. Bei allen technischen Fragen oder Problemen hattet ihr immer ein offenes Ohr und habt nach allen Kräften geholfen!

Yvonne Blass und Marija Mamic ihr habt mit eurer fröhlichen und aufgeschlossenen Art die Gruppe bereichert und ich danke euch für die gute Zusammenarbeit.

Bei Dr. Farnusch Kaschani bedanke ich mich für die kollegiale Zusammenarbeit und das Interesse an meiner Arbeit. Vielen Dank für den Impuls, den du dem Symplostatin-Projekt gegeben hast.
I would like to thank the former lab members Dr. Rama Krishna Reddy Narayana, Dr. Jerôme Clerc, Dr. Zheming Wang and Marius Löhken; it was a pleasure to work with you.

A very special thanks goes to my two great office mates Dr. Vijay Pawar and Prof. Willem van Otterlo. I enjoyed the time I shared with you greatly, thanks for the scientific discussions, your interest in my work; and the insights you guys gave me to Indian and Southafrican culture!

A “Thank you” to all colleagues at the CGC, the MPI and the University of Duisburg-Essen!

Ich danke der Max-Planck-Gesellschaft für die Gewährung eines Promotionsstipendiums für die Zeit am Chemical Genomics Centre.

Ich möchte mich beim NMR-Team der der Fakultät Chemie der TU Dortmund, speziell bei Dr. Bernhard Griewel und auch beim Team der Massenspektrometrie für die durchgeführten Messungen bedanken. Ich danke auch Heinz Bandmann vom NMR-Zentrum der Universität Duisburg-Essen für die sehr gute und unkomplizierte Zusammenarbeit.

I would also like to thank Dr. Renier van der Hoorn and the whole Plant Chemetics group at the MPI in Cologne for hosting me and providing such a wonderful working atmosphere. Especially, I would like to thank Dr. Kerstin Richau who introduced me to the major ABPP working techniques, thanks for the good time we had together!

Mein Dank gilt Dr. Michael Meltzer und Prof. Michael Ehrmann für die ausgezeichnete Zusammenarbeit im Serin-Proteaseinhibitoren-Projekt. Ich danke Michael Meltzer für die schnelle Durchführung aller Enzymassays und die anregenden Diskussionen.

I would like to thank Prof. Matthew Bogyo and Dr. Edgar Deu Sandoval for the fruitful collaboration in the symplostatin project.

Mein größter Dank gilt meiner Familie, ohne euch wäre all das nicht möglich gewesen!
Ich danke meinem Vater für seinen wissenschaftlichen Beistand, ein offenes Ohr in allen Lebenslagen und natürlich fürs Korrekturlesen! Meiner Mutter danke ich für ihre bedingungslose Unterstützung und die vielen kleinen Dinge, die nicht immer selbstverständlich sind. Meinem Bruder Jan danke für seinen Beistand, seine Freundschaft und natürlich die vielen Spiele auf der Südtribüne und die großartigen Momente, die wir gemeinsam mit der Borussia erlebt haben! Wir halten fest und treu zusammen!

Ich danke allen Mitgliedern des Takemusu Aikido Dortmund. Das Training mit euch ist immer ein Ausgleich zum hektischen Alltag, bei euch habe ich meine innere Mitte gefunden. Domo arigato!

Von all den Freunden die mich über die Jahre begleitet und unterstützt haben möchte ich speziell Saskia Baumann mit meinem Patenkind Lukas, sowie Manuel Wagner danken: bei euch bin ich immer auf Verständnis gestoßen und ihr wart in jeder Lebenslage für mich da!

Summary

The objective of this dissertation was the synthesis and biological evaluation of natural product protease inhibitors as well as derivatives thereof.

For the natural product class of 3-amino-6-hydroxy-2-piperidone(Ahp) cyclodepsipeptides that are known as non-covalent inhibitors of serine proteases, a solid-phase synthesis could be developed. The established solid-phase strategy thereby enables the synthesis of tailor-made Ahp cyclodepsipeptides. The synthesis is based on the use of a general Ahp precursor molecule, which was generated by a solution phase synthesis. It furthermore includes an esterification on solid phase, as well as a solid-phase macrolactamization and features a novel protocol for the generation of an aldehyde upon cleavage from the solid support. As a proof-of-principle for the synthesis strategy, the chymotrypsin inhibitor symplocamide A was synthesized successfully and was then analyzed regarding its biological activity.

Next, simplified analogs of Ahp cyclodepsipeptides in which the Ahp residue was mimicked by other amino acids were synthesized, using symplocamide A as the lead structure. These studies aimed to investigate if a mimicry of the Ahp unit under retention of the canonical conformation is possible. The canonical conformation was first discovered and studied for proteinaceous serine protease inhibitors. Only recently, peptidic analogs of these inhibitors were examined for the adoption of the canonical inhibition. In this context, the Ahp cyclodepsipeptides were also suggested to mediate inhibition by the adoption of a canonical conformation.

In this dissertation, it could firstly be demonstrated that the Ahp unit can be replaced by commercially available amino acid under retention of the biological activity. Furthermore, the critical determinants for the adoption of the canonical conformation could be defined and an insight into the molecular basis of an efficient inhibition was gained.

In an alternative project, a convergent solution synthesis for the natural product symplostatin 4 was developed, enabling a flexible access to modified derivatives. Especially the synthesis of probes for the examination of symplostatin 4 by activity-based protein profiling was possible in a simplified manner by a 1,3-dipolar Huisgen cycloaddition of propargyl-modified derivatives with azide-modified reporter molecules.

By the use of the chemical biology methodology of activity-based protein profiling, the direct targets of symplostatin 4 in the model plant *Arabidopsis thaliana* were identified, being the cysteine proteases RD21A and RD21B. In addition, the direct target being responsible for the antimalarial activity of symplostatin 4 was investigated. Experiments with the malaria parasite *Plasmodium falciparum* then distinguished symplostatin 4 as a nanomolar inhibitor of the parasital cysteine proteases falcipain 2 and 3 that are responsible for the hemoglobin digestion and have been recognized as target enzymes for alternative malaria chemotherapy.

technische universität
dortmund

fakultät
chemie

Max-Planck-Institut
für molekulare Physiologie

mpi

CGC
Chemical Genomics Centre
of the Max Planck Society

UNIVERSITÄT
DUISBURG
ESSEN

ZMB